Republic of Iraq
Ministry of Higher Education and Scientific Research
Middle Technical University
Engineering Technical College- Baghdad

Performance Enhancement of Compact Thermal Battery System for Refrigeration Applications

A Dissertation Submitted to
the Council of the Engineering Technical
College-Baghdad in a Partial Fulfillment
of the Requirements for the Degree of
Doctor of Philosophy (Ph.D.) in Thermal Engineering

By
Fadhil Abdulrazzaq Kareem
B.Sc. 2012
M.Sc. 2015

Supervisor
Dr. Abdul Hadi N. Khalifa
Professor

Supervisor
Dr. Ahmed J. Hamad
Professor

April 2024 Shawwal 1445

بِسْمِ اللَّهِ الرَّحْمَٰنِ الرَّحِيمِ

﴿ يَا أَيُّهَا الَّذِينَ آمَنُوا إِذَا قِيلَ لَكُمْ تَفَسَّحُوا فِي الْمَجَالِسِ فَافْسَحُوا يَفْسَحِ اللَّهُ لَكُمْ ۖ وَإِذَا قِيلَ انشُزُوا فَانشُزُوا يَرْفَعِ اللَّهُ الَّذِينَ آمَنُوا مِنكُمْ وَالَّذِينَ أُوتُوا الْعِلْمَ دَرَجَاتٍ ۚ وَاللَّهُ بِمَا تَعْمَلُونَ خَبِيرٌ ﴾

صدق الله العظيم

سورة المجادلة

الاية: 11

Supervisors Certification

We certify that this dissertation was prepared under our supervision as a partial fulfillment of requirements for the degree of Doctor of Philosophy in Thermal Engineering Technology.

Signature:
Name: Dr. Abdul Hadi N. Khalifa
Title: Professor
(Supervisor)
Date: / / 2024

Signature:
Name: Dr. Ahmed J. Hamad
Title: Professor
(Supervisor)
Date: / / 2024

Linguistic Certification

I certify that I have read this dissertation entitled **"Performance Enhancement of Compact Thermal Battery System for Refrigeration Applications",** and I examined the language of the dissertation in my opinion, it's adequate as a dissertation for degree Doctor of Philosophy in Thermal Engineering Technology.

Signature:
Name: Dr. Mouayed Hassan Ziada Al-Toki
Title: Lecturer
Date: / / 2024

Signature:
Name: Dr. Hamid Ali Hussein
Title: Professor
Head of Engineering Power Mechanics Department
Date: / / 2024

In view of the available recommendation, I forward this dissertation for debating by the examining committee.

Signature:
Name: Dr. Sabah Khammass Hussein
Title: Professor
(Deputy Dean for Scientific Affairs,
Students and Postgraduates Studies)
Date: / / 2024

Certification

We are the members of the Examining Committee certify that after reading this dissertation, **"Performance Enhancement of Compact Thermal Battery System for Refrigeration Applications,"** and examining the student "**Fadhil Abdulrazzaq Kareem**" in its contents. We think it is adequate for the award of the *Doctor of Philosophy in Thermal Engineering Technology.*

Signature:
Name: Dr. Musaab K. Rasheed
Title: Assistant Professor
(Member)
Date: / / 2024

Signature:
Name: Dr. Johain J. Faraj
Title: Assistant Professor
(Member)
Date: / / 2024

Signature:
Name: Dr. Kifah H. Hilal
Title: Assistant Professor
(Member)
Date: / / 2024

Signature:
Name: Dr. Ahmed Q. Ahmed
Title: Assistant Professor
(Member)
Date: / / 2024

Signature:
Name: Dr. Raheek I. Ibrahim
Title: Professor
(Chairman)
Date: / / 2024

Signature:
Name: Dr. Abdul Hadi N. Khalifa
Title: Professor
(Supervisor)
Date: / / 2024

Signature:
Name: Dr. Ahmed J. Hamad
Title: Professor
(Supervisor)
Date: / / 2024

Signature:
Name: Dr. Nabil J. Yasin
Title: Professor
(Dean)
Date: / / 2024

Dedication

To My Homeland

To My Family

To My Supervisors

To My Teachers

To My friends

With Respect

Fadhil Abdulrazzaq Kareem
2024

ACKNOWLEDGMENTS

In the name of Allah, the Beneficent, the Merciful

All praise is to Allah, the Sustainer of the entire world and Origin of science, wisdom, mercy, and peace be upon our leader, the Prophet Mohammad, his family, and companions. I want to thank my esteemed supervisors, Prof. Dr. Abdul Hadi N. Khalifa and Prof. Dr. Ahmed J Hamad, for their invaluable supervision, support, and tutelage during the course of my PhD study. Their immense knowledge and plentiful experience have encouraged me all the time in my academic research and daily life. My gratitude extends to the Middle Technical University / Institute of Technology - Baghdad for the funding opportunity to undertake my PhD study. I want to thank all the members of the Middle Technical University Engineering / Technical College-Baghdad /Department of Engineering Power Mechanics.

Also, I would like to thank my esteemed Dr. Hassan J. Dakkama / Dean of Computer Center / Middle Technical University; Dr. Saja Mohsen / Nanotechnology and Advanced Materials Research Center, University of Technology; Dr. Murtadha Sabah Al-Eissa / Ministry of Environment, engineer Nadim Abd Ibrahim / electrical engineer- Al Nadir Trading Company, and engineer Abass A. Kareem/ Technical Instructors Training Institute for his encouragement and support throughout my studies and without whom I would not have been able to complete this research.

I want to thank the following friends who have helped me with patience and encouragement to undertake this research: Ms. Doaa Z. Khalaf, engineer Thabet Jamel, engineer Maula Twoma, engineer Ammar Kareem, engineer Rafid Wissam, engineer Haroon Aziz, and Mohammed Ali Oudah.

I am so grateful to have you both as my parents, my brothers, and my sisters. I am thankful to my parents for always supporting me, guiding me, and pushing me to do my best in life. And my most enormous thanks to my family for all the support you have shown me through this research. Thanks to my lovely kid, Yahya, and my beautiful wife, Manar, for all your support. My appreciation also goes out to my friends for their encouragement and support throughout my studies.

Fadhil Abdulrazzaq Kareem
2024

List of Contents

Chapter One: Introduction

Chapter Two: Literature Review

Chapter Three: Theoretical Analysis and Numerical Modelling of Two-bed ATB

Chapter Four: Experimental Work

Chapter Five: Results and Discussion

Chapter Six: Conclusions and Recommendations

References

List of Figures

List of Tables

List of Appendices

List of Symbols

Symbol	Definition	Unit
A_{ABU}	Heat transfer area of ABU	m^2
A_{ECU}	Heat transfer area of ECU	m^2
A_f	Fin surface area	m^2
BET	Specific surface area	m^2/g
C_f	Coefficient of friction	-
Cp_{ads}	Specific heat for adsorbent material	kJ/kg.K
$Cp_{HE,ABU}$	Specific heat for heat exchanger for ABU	kJ/kg.K
$Cp_{ref,cond}$	Specific heat of liquid refrigerant for ECU/condenser	kJ/kg.K
$Cp_{ref,liquid}$	Specific heat for liquid refrigerant	kJ/kg.K
$Cp_{ref,v}$	Specific heat for vapor refrigerant	kJ/kg.K
D_f	Fin diameter	m

ID	Inner tube diameter	m
OD	Outer tube diameter	m
dq_{ads}/dt	Instantaneous adsorption uptake during the charging process	$kg_{ref}/kg_{ads}.s$
D_{so}	Diffusion coefficient	m^2 / s
dT_{ads}/dt	Temperature gradient with time during the charge	K/s
dT_{cond}/dt	Change in the condenser temperature with time	K/s
dT_{des}/dt	Temperature changes with time during the discharge process	K/s
dT_{evap}/dt	Evaporator temperature changes with time	K/s
Ea	Activation energy	kJ/ kg
g	Gravitational acceleration	m/s^2
h_{ads}	Heat of adsorption	kJ/kg
HCR_{sg}	Heat capacity ratio of silica gel RD	-
$h_{fg,\ ref}$	Latent heat enthalpy of refrigerant	kJ/kg
$h_{fg,ref}$	Refrigerant latent heat of vaporization	kJ/kg
K	Thermal conductivity	W/m.K
K^*	Langmuir coefficient	-
K_{ads}	Adsorption rate coefficient	1/s
K_{des}	Desorption rate coefficient	1/s
k_o	Empirical constant	1/s
k_w	Water's thermal conductivity	W/mK
LMDT	Logarithmic mean temperature differences	K
L_t	Length of the tube	m
m^*	Heterogeneity parameter	-
$m.Cp_{ch}$	Heat capacity for chilled water flow in ECU	kW/K
$m.Cp_{cw}$	Heat capacity for cooled coolant flow in ABU	kW/K
$m.Cp_{cw,cond}$	Heat capacity of the cooling water flow in ECU during condensation	kW/K
$m.Cp_{hw}$	Heat capacity for hot coolant flow in ABU	kW/K
M_{ABU}	Mass of heat exchanger	kg
M_{ads}	Mass of adsorbent	kg
M_f	Mass of fins	kg
$M_{HE,ABU}$	Mass of heat exchanger in the ABU	kg
M_{ref}	Refrigerant mass in the ECU	kg
M_{sg}	Mass of silica gel RD	Kg
M_t	Mass of tubes	kg
N_f	Number of fins	-
N_t	Number of tubes	-

Nu	Nusselt number	-
P	Pressure	kPa
Pr_{liq}	The Prandtl number for liquid refrigerant	-
P_s	Saturated pressure	kPa
q^*	Amount of water vapor uptake	kg_{ref}/kg_{ads}
Q_{ch}	Heat supply to the evaporator	kW
Q_{cw}	Heat rejected from ABU by cooling water	kW
$Q_{cw,cond}$	Heat rejected from ECU/condenser	kW
Q_e	Heat supply to the ABU by electric heater	kW
Q_{hw}	Heat supply to the ABU by heating water	kW
q^o	Limiting uptake	kg_{ref}/kg_{ads}
R_{axi}	Axial thermal resistance between solid adsorbents	K/W
R_{cond}	Conduction thermal resistance in the tube wall	K/W
R_{cont1}	Contact thermal resistance between the outer tube and adsorbent	K/W
$R_{contact}$	Contact thermal resistance	m^2K/W
R_{conv}	Convective thermal resistance for the inlet coolant fluid	K/W
R_p	The radius of the solid adsorbent particle	m
R_{rad}	Radial thermal resistance between solid adsorbents	K/W
R_u	Universal gas constant	kJ/kg K
S	Fin space	m
T_{ads}	ABU temperature during adsorption	K
t_{ads}	Diffusion time for adsorption	s
$T_{ch,in}$	Inlet chilled temperature to ECU during the evaporation process	K
$T_{ch,out}$	Outlet chilled temperature from ECU during evaporation	K
T_{cond}	ECU/ condenser temperature	K
$T_{cw,cond,in}$	Inlet-cooled water temperature to ECU during the condensation	K
$T_{cw,cond,out}$	Outlet-cooled water temperature from ECU during the condensation	K
$T_{cw,in}$	Inlet-cooled water temperature from coolant unit to ABU	K
$T_{cw,out}$	Outlet cooled water temperature from coolant unit to ABU	K
T_{des}	ABU temperature during desorption	K
t_{des}	Diffusion time for desorption	s
T_{evap}	ECU/ evaporator temperature	K

$T_{hw,in}$	Hot water inlet temperature from the heating unit to the ABU	K
$T_{hw,out}$	Hot water outlet temperature from ABU to heating unit	K
$U_{ABU,ads}$	Overall heat transfer coefficient for ABU during adsorption	kW/m^2K
$U_{ABU,des}$	Overall heat transfer coefficient for ABU during desorption	kW/m^2K
$U_{ECU,\ evap}$	Overall heat transfer coefficient in ECU	kW/m^2K
$U_{ECU,cond}$	Overall heat transfer coefficient for ECU/condenser	kW/m^2K
V_f	Fin volume	m^3
V_{er}	Vapor phase velocity in radial direction	m/s
V_{ez}	Vapor phase velocity in an axial direction	m/s

List of Greek letters

Greek letters	Definition	Unit
α_v	Fluid-solid specific surface area per unit volume	1/m
ε_v	Vapor porosity	-
μ_{ref}	Dynamic viscosity of refrigerant	Pa.s
$\rho_{ref,liq}$	Density of liquid refrigerant	kg/m^3
$\rho_{ref,vap}$	Density of vapor refrigerant	kg/m^3
σ	Surface tension for refrigerant	N/m
ε_b	Bed porosity	-
ε_p	Particle porosity	-
ε_t	Total porosity	-
ρ_s	Density of solid phase	kg/m^3

List of Abbreviations

Abbreviations	Definition
ABU	Adsorber Bed Unit
ARS	Adsorption Refrigeration Systems
ATB	Adsorption Thermophysical Battery
CFD	Computational Fluid Dynamics
COP	Coefficient of Performance
ECU	Evaporator/Condenser Unit
EES	Engineering Equation Solver
HMTM	The Heat and Mass Transfer Mode
HTF	Heat Transfer Fluid
LPM	Lumped Parameter Predicting Model
MCM	Mobil Composition of Matter

MOF	Metal-Organic Frameworks
RD	Regular Density
SCP	Specific Cooling Power

List of Subscripts

Subscripts	Definition
ads	Adsorption
ch	Chilled
co	Cooling water
cond	Condenser
dse	Desorption
evap	Evaporator
HE	Heat exchanger
hw	Heating water
ref	Refrigerant
sg	Silica gel
w	Water

Abstract

The Adsorption Thermophysical Battery (ATB) is emerging as a sustainable alternative to electrical-powered vapor-compression systems in the field of cooling technology. The primary purpose of this study was to examine and evaluate the performance of the developed two-bed ATB under different operating conditions. The present study was divided into theoretical, experimental, and numerical analysis.

The theoretical study dealt with solving the Lumped Parameter Predicting Model (LPM), modified Freundlich adsorption, and kinetic equilibrium equations to evaluate the performance of Metal-Organic Frameworks adsorbent (MOF-801) and RD-silica gel. MATLAB-19 software and engineering equation solver (EES) were used to solve and analyze the theoretical study. Conversely, in the experimental part, a test rig of a two-bed ATB system with mass recovery was fabricated and examined. The ATB unit has two Adsorber Bed Units (ABU), each 24 cm in diameter and 30 cm in height, manufactured for semi-continuous operation and refrigeration. Each ABU can function as either an adsorption or desorption medium.

In addition, the design integrates the evaporator and condenser into a single heat exchanger called the Evaporator-Condenser Unit (ECU), which has dimensions of 22 cm in length, 14 cm in width, and 12 cm in height. This unit reduces the overall size and costs of the ATB. Furthermore, the ATB utilized Mobil Composition of Matter (MCM-41) and Regular Density (RD) silica gel as adsorbent materials. At the same time, the numerical part dealt with solving the transient three-dimensional local thermal non-equilibrium model using COMSOL-6 software to analyze Heat and Mass Transfer (HMTM) inside the adsorbent-packed bed.

The theoretical results concluded that the coefficient of performance (COP) of the ATB when using MOF 801 outperforms silica gel RD and enhancement by 20 % when the cycle time is set at 1000 s. Also, the COP and the specific cooling

power (SCP) of the ATB were improved by about 25 % and 39 % for Metal-Organic Frameworks (MOF 801) compared with silica gel at the entire mass of the adsorbent 10 kg, respectively. The COP of the ATB was reduced by 31.6 % when the hot water temperature increased from 343 to 363 K. It increased by 5% when the cooled coolant temperature dropped from 313 to 303 K for MOF-801. Also, it can be concluded that the COP was directly proportional to the chilled and cooled water flow rate and inversely to the hot water flow rate. Next, the experimental results showed that the COP and refrigeration capacity (RC) of the two-bed ATB were improved by 14 and 8% when using mass recovery, respectively, compared with the system without mass recovery. Also, the investigation revealed an enhancement in RC and COP using MCM-41 by 11.1% for RC and 10.5 % for COP compared with silica gel-RD for the same operation conditions. The COP of the two-bed mass recovery ATB was improved by 14% and 8.6 % for RD-silica gel and MCM-41, respectively, compared with single-bed ATB. Finally, the numerical results summarized that the temperature of the solid adsorbent increased gradually during the discharge process and decreased gradually during the charge process over time. Also, the thinner layer can be cooled faster than the thicker layers. As predicted, the temperature and uptake distribution for the smaller layer thickness of 2 mm were better than those of the 4 mm and 6 mm.

Chapter One

Introduction

Chapter One

Introduction

1.1 Introduction

In many developing countries with limited access to electricity, there is a growing interest in cooling and heating demand. According to the International Institution of Refrigeration (IIR), refrigeration and air-conditioning applications consume roughly 15% of total electrical power [1]. Refrigeration and air-conditioning systems are divided into two main types. The first operates with high-grade energy, which is electrical energy. This type of system is called the vapor compression system, which has a high Coefficient of Performance (COP). The second type is the thermally driven system, which operates with low grade- energy. Such systems are absorption and adsorption systems characterized by a COP of no more than unity. High-quality energy from gas or steam power plants leads to an increase in global warming effect and environmental pollution. Therefore, the current circumstance calls for developing a thermally driven cooling and heating system using low-grade energy such as waste heat or renewable energy sources. The absorption and adsorption systems have been studied since the 1970s [2].

In recent years, there has been a growing interest in using waste heat to offset rising energy demand while preserving the environment. Solar energy, power plants, commercial and industrial manufacturers, and other waste heat sources are available in many areas worldwide [3], where 72 % of the initial energy is released as waste heat. Working with a thermal energy source, especially waste heat, is the first advantage the adsorption system offers. Adsorption systems use low-temperature heat sources from 60 to 120°C to generate a cooling effect without potentially hazardous environmental impact. The solar adsorption system with a cooling capacity of 528 kW was deployed in an Indian government building. As well as in

2018, Fahrenheit (a German company) successfully installed several innovative adsorption units in numerous countries, such as Germany, Austria, Netherlands, Spain, and Saudi Arabia [4]. The second advantage of an adsorption system is that it is significant for various applications, including thermal batteries, dehumidification, and drinking water delivery. The third benefit of the system is that it has no moving parts other than a few valves, which minimizes maintenance costs. Most adsorption systems have additional benefits, including long lifespan, low noise and vibration, absence of crystallization, and environmentally friendly operating refrigerant [5].

Furthermore, the adsorption systems employ natural working fluids and adsorbent materials with low global warming and no ozone depletion potential. In recent decades, absorption-cooling and heating systems have been commercially viable due to their susceptibility to corrosion, toxicity, and working fluid crystallization. On the other hand, adsorption cooling and heating systems provide various advantages, including low energy consumption (no circulating pump), low-temperature heat sources, and better operational reliability due to fewer moving parts [5]. The evaluation of the adsorption cooling and heating system depends directly on the amount of water vapor uptake of the adsorbent material, which is affected by the relative pressure and the temperature of the adsorption beds.

1.2 Adsorption and Desorption Phenomena

The adsorption (charging) phenomenon occurs when the adsorbent surface (solid materials) is exposed to a liquid or gas without physically or chemically altering the adsorbent. The solid materials that adsorbed the fluid are known as adsorptive, adsorbed, and adsorbate. Moreover, desorption (discharging) refers to extracting vapor from an adsorbed material and returning it to its original condition. The adsorption and desorption processes can be repeated continuously. Theoretically, a

particular quantity of heat may be stored in an adsorbent matter and then removed later with no losses [6].

1.3 Working pairs

Many adsorbents of different characters and different geometrical surface structures are currently available. Silica gel, Zeolites, activated carbon, and novel adsorbent materials, known as Metal-Organic Frameworks (MOFs) and Mobil Composition of Matter (MCM-41), are formed by combining metal ions with organic linkers. These materials show significant potential as adsorbents and can replace the currently employed adsorbent materials [7]. The properties of the MOF are as follows [8], [9]:

1- They have a high capacity to adsorb molecules, resulting in a great potential for heat and mass transfer.
2- Exhibit thermal stability.
3- Unimpeded water absorption at a high relative pressure level.
4- Excellent energy storage solution for heating and cooling applications.

The MOF has several uses, such as thermal energy storage, Heating, ventilation, and air conditioning (HVAC) systems, power production, water desalination, and moisture removal [10], [11]. MOFs are the most prevalent and widely utilized adsorbents. [12].

Mobil Composition of Matter No. 41 (MCM-41) is a mesoporous material developed by the Mobil Oil Corporation. MCM-41 is part of a family of silicate and alum-silicate solids that are well-suited for use as catalysts and catalytic supports. Silica mesostructured (MCM-41) is a part of low a density-organized mesoporous silicate system that has a 2D hexagonal phase (MCM-41) that can be prepared in the presence of quaternary ammonium halide surfactant. It has ordered and large pores with a diameter in the range of 1.5 -10 nm and a specific surface area of 1500 m^2/g.

The water uptake for different materials at various ranges of P/P_0 values in the five consecutive cycles is plotted in Figure 1.1. Furthermore, the uptake capacities for the first and fifth cycles for zirconium MOFs and other porous solids are also compared in the figure. The adsorbents MOF-801-P, MOF-802, MOF-841, UiO66, CAU-10, and MCM-41 exhibit the best and closest to the ideal cycling performance [13].

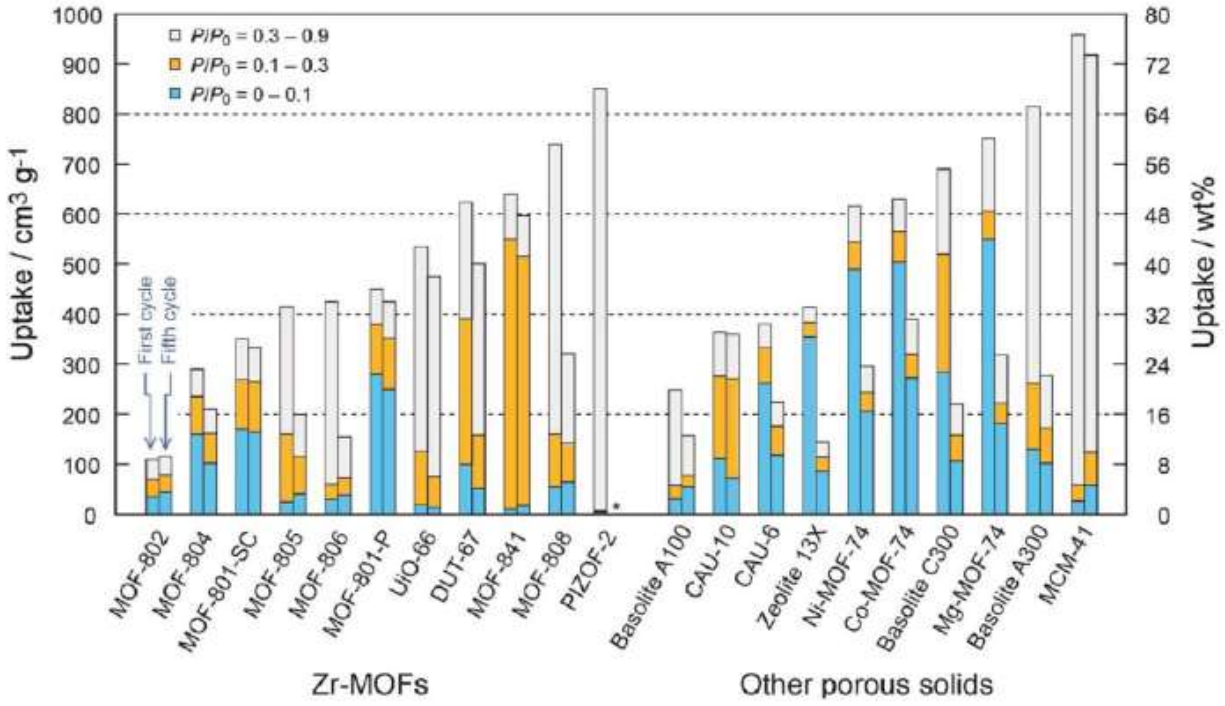

Figure (1.1) Water uptake capacity of zirconium MOFs (left) and other representative porous materials (right) in different pressure ranges [13].

Numerous commonly employed adsorbates can be combined with the adsorbent to establish an effective adsorption pairing that can be used in the heat pump system. Water, ammonia, methanol, and refrigerants like R-134a are among the most significant and often employed types of adsorbates. The unique characteristics of working pairs should be considered when dealing with specific physical adsorbents and adsorbates, such as rapid water uptake and considerable changes in adsorbate concentration. The latent heat of vaporization exhibits a

significant magnitude, indicating a substantial amount of energy required for the phase transition from liquid to vapor. Additionally, the substance demonstrates a high thermal conductivity, implying its ability to transfer heat efficiently. Conversely, the specific volume is deficient, indicating a relatively compact arrangement of nontoxic, nonflammable, and noncorrosive particles that exhibit cycle stability [14].

1.4 Adsorption Heat Pump's Thermodynamic Cycle

The simple adsorption refrigeration system consists of a generator (adsorbent vessel) containing the adsorbent and adsorbant together, a condenser, an expansion valve, an evaporator, and several water pumps. The adsorption cycle is similar to the vapor compression cycle in the presence of an evaporator, condenser, and expansion valve, while the generator works like a compressor in the compression cycle, as shown in Figure (1.2).

Figure (1.3) shows the adsorption-based heat pump's thermodynamic cycle, where T_{evap}, P_{evap}, T_{cond}, and P_{cond} Indicate the temperature and pressure of the evaporator and condenser, respectively. The pressure in the system throughout the adsorption process is dictated by the saturation temperature of the evaporator unless there is a significant drop in pressure between the adsorbent and the evaporator. Moreover, the condenser saturation temperature determines the pressure at the desorption process unless a significant pressure decrease exists between the adsorbent and the condenser. During the operational phase, the term (Q_{evap}) represents the amount of heat absorbed by the evaporator, whereas (Q_{cond}) refers to the quantity of heat released from the condenser during the regeneration process. Q_{adsorb} represents the heat emitted from the generator during adsorption, whereas Q_{desorb} denotes the heat provided to the generator during the regeneration process

[15]. The detailed working operations of physical adsorbents in the adsorption system are:

1- **a-b:** When the adsorbent bed is in operation, both the adsorber and the adsorbent experience a temperature rise, going from the initial ambient temperature (T_a) to the higher temperature of the generator or bed (T_b). Furthermore, the refrigerant's pressure increases from P_e to P_c within the adsorption bed throughout this operation. The process being examined is defined by isosteric heating, where the volume remains constant. Hence, the mass of the refrigerant contained in the bed's mass transfer channels and the adsorbent's micropores is insignificant compared to the refrigerant's mass. Furthermore, the heat absorbed by the refrigerant gas in the adsorbent layer is commonly disregarded throughout the heating process.

2- **b-c:** The temperature of the adsorbent within the bed gradually rises until it approaches the upper limit known as the maximum desorption temperature, denoted as T_c. Simultaneous desorption of the adsorbed refrigerant occurs. The process mentioned above can be classified as an isobaric process.

3- **c-d:** It is similar to the process denoted as a-b. Once the adsorbent within the bed has undergone complete desorption, the bed's temperature experiences a cooling effect, transitioning from T_c to desorption temperature (T_d). Furthermore, the refrigerant experiences a decrease in pressure from P_c to P_e. The procedure is called the isosteric heating process due to the absence of any volume change.

4- **d-a:** The adsorption temperature is reduced to the T_a level, enabling the adsorption of the refrigerant by the adsorbent within the evaporator. The pressure regulation for this process is achieved by controlling evaporating pressure, while an isobaric process can be employed to investigate this process.

In an isobaric process, the refrigerant gas released from the adsorbent bed is condensed in the condenser. As it enters the condenser, the temperature of the refrigerant gas should be identical to its exit from the bed. In addition, during an isobaric procedure, the evaporator evaporates the refrigerant gas that the adsorbent has adsorbed. The temperature of the refrigerant gas before entering the bed should be equal to its temperature once exiting the evaporator. The line a-b-c denote the desorption process, while the line c-d-a denote the adsorption process.

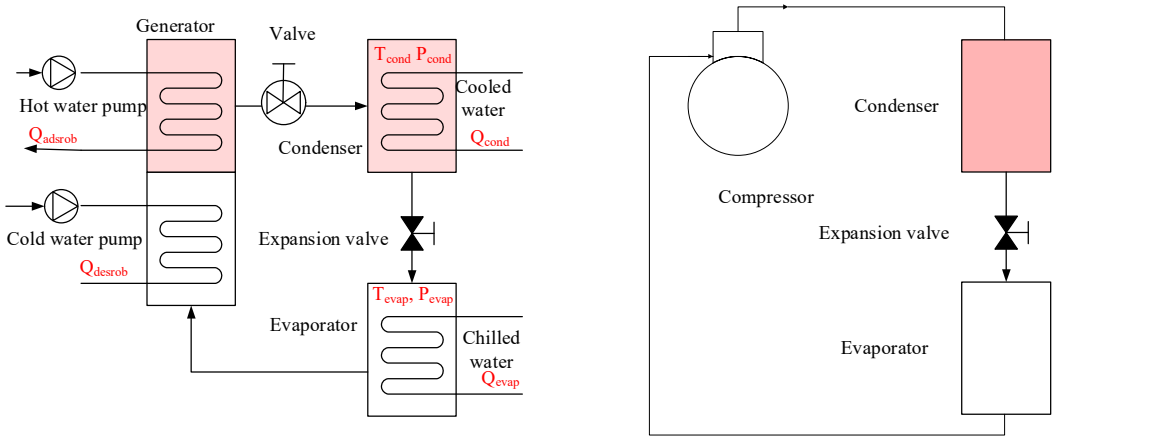

a. Simple adsorption cycle b. Simple vapor compression cycle

Figure (1.2) Simple adsorption and vapor compression cycles.

1.5 Semi Continuous Adsorption System

A semi-continuous refrigeration cycle involving at least two beds is utilized for adsorption refrigeration. A continuous and uninterrupted cooling and adsorption cycle requires a steady and reliable output of cooling power, so there is always at least one adsorbent bed in the cooling and adsorption stage. The two-bed operating system is typically employed when the ideal desorption and adsorption times are the same. Both the adsorption and desorption processes can take a reasonable amount of time as a half-cycle duration. Adopting a multi-bed system is a practical approach when there is a substantial disparity between the ideal duration for adsorption and desorption.

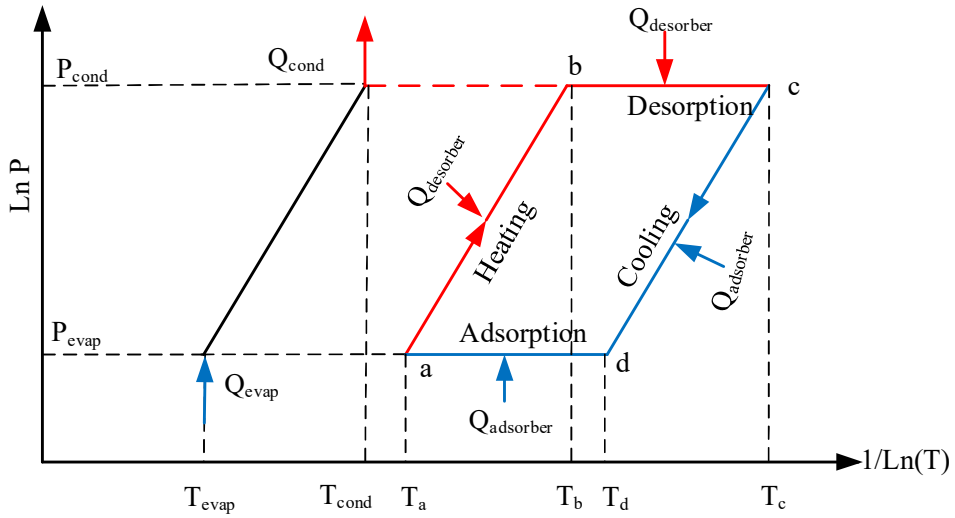

Figure (1.3) Pressure-Temperature-composition diagram illustrating the adsorption heat pump cycle [15].

Utilizing the three-bed system is a viable option when the ideal duration for adsorption is twice as long as the perfect duration for desorption. In this system, it is observed that two beds undergo cooling and adsorption while another bed undergoes heating and desorption. In semi-continuous adsorption systems, various approaches are employed to improve the COP and Specific Cooling Power (SCP), such as mass-recovery technology [16], heat recovery technology [17], and mass-heat recovery technology [18].

Figure (1.4 a) shows that the primary mass recovery cycle comprises four heat exchangers, an evaporator-adsorber, and a condenser-desorber [16]. The cycle demonstrates a fundamental structure that roughly corresponds to the traditional two-bed adsorption cycle. The adsorber and desorber are linked via a pipe, enabling the smooth movement of refrigerant. Due to a non-equilibrium pressure, the refrigerant can move from the desorber to the adsorber. This results in an increase in the mass circulation of refrigerant inside the bed, hence enhancing the cooling capacity. The mass recovery is illustrated in the pressure-temperature-composition (P-T-X) diagram shown in Figure (1.4 b) [19].

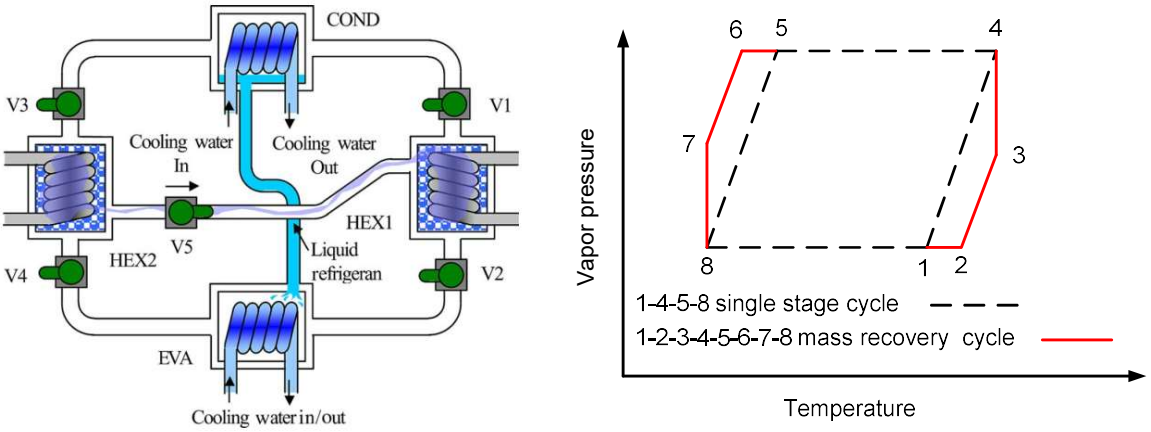

a. Schematic of basic mass recovery adsorption system.

b. P-T-x diagram of the mass recovery adsorption system.

Figure (1.4) Mass recovery adsorption system [19]

1.6 Advanced Adsorption Thermophysical Battery

Two primary components comprise the advanced Adsorption Thermophysical Battery (ATB) system. The initial component is the adsorption bed unit (ABU), which is comprised of adsorbent materials known for their extremely high heat of adsorption, hydrophobicity, and water absorption capacity. The Evaporator/Condenser Unit (ECU) is the second part, which employs a heat exchanger to evaporate and condense vapor at low pressures [20]. Coolant fluid is circulated across the adsorption beds and the ECU to cool and heat the beds. In the ECU, the evaporator produces the vapor, drawing all vapors by the adsorption bed. No compression device is required to transport the vapor between the ECU and the adsorption bed [21]. This process is called the adsorption process, shown in Figure (1.5 a). As shown in Figure (1.5 b), the reverse process is called the desorption process. The desorption can be accomplished by supplying heat energy into the adsorption beds, releasing the vapor from molecules, and returning it to the ECU. Finally, the vapor is condensed in the ECU by condenser coils.

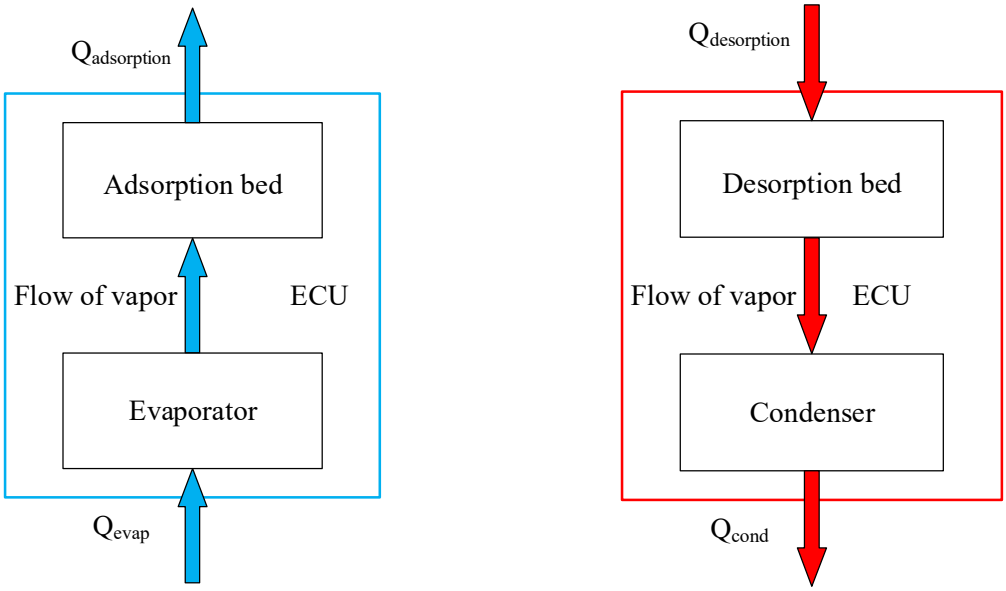

a. charging mode (adsorption) b. discharging mode (desorption)

Figure (1.5) Schematic of ATB operation during the adsorption and desorption process

1.7 Study Objectives

The main objective of this study is to limit environmental impact by using waste heat to operate a thermophysical battery refrigeration unit. It also eliminates carbon dioxide emissions by using waste heat sources instead of conventional energy sources to operate the air conditioning system and minimize power consumption in air-conditioning applications. The following can be used to outline the research's secondary aim and objectives:

1- Investigated the operational efficiency of the ATB system, which is presently employed in air conditioning.
2- Developing and producing two-bed ATB cycles to provide semi-continuous operation with semi-continuous refrigeration.
3- Enhancing the overall COP and SCP of the ATB.
4- Mass recovery technology was used to increase the system's performance.
5- Advanced and effective adsorbent materials with higher vapor uptake are necessary to improve ATB performance.

1.8 Motivation and Originality

The depletion of the ozone layer and the effects of global warming are the two major issues that have recently challenged the world. The potential of these problems can be avoided through various methods, including replacing the refrigeration working substance with a new one with a minimal environmental impact. It also eliminates carbon dioxide emissions by using waste heat sources instead of conventional energy sources to operate the air conditioning system and Minimize power consumption in air-conditioning applications. As a result, a thermophysical battery refrigeration unit that utilizes a thermal energy source, particularly waste heat low-temperature sources, is developed, constructed, and tested. The following present study novelty:

1- The research area of investigating ATB performance and improving the energy density of the ATB system is still attractive and not totally covered by the researchers.
2- Develop a compact ATB system as an applicable cooling unit by designing and developing the evaporator-condenser unit (ECU) and adsorption bed unit (ABU) to improve energy density and ATB performance .
3- Design and manufacture a two-bed ATB with mass recovery technology to obtain semi continue refrigeration effect.
4- Investigating the alternative advanced adsorbent materials with relatively higher adsorption uptake and acceptable cost to enhance the thermal performance of ATB.
5- A theoretical predicting model and numerical analysis were developed to evaluate the performance of the modified compact ATB system under various operating conditions and several adsorption working pairs.

6- Several control strategies are investigated to satisfy conditioning needs for the difficult operation of a two-bed ATB while simultaneously decreasing the cost and complexity of the ATB system.

1.9 Research Methodology

The present study includes three main parts: experimental investigation, theoretical, and numerical analysis (modeling), which is conducted through the following steps:

1. Review literature on thermal battery cooling systems and heat-driven cooling systems for cooling, including absorption and adsorption technologies. To understand the background of these systems and highlight their advantages and disadvantages.
2. A theoretical model based on the Lumped Parameter Predicting Model (LPM) and modified Freundlich adsorption and kinetic equilibrium equations is being developed to simulate the ATB system. This model is being solved using the MATLAB-19 software and the Engineering Equation Solver (EES).
3. Investigate the feasibility of modifying the basic thermal battery cooling system to generate cooling using advanced adsorbent materials and modified adsorption bed heat exchangers.
4. Developing a numerical simulation model based on the Heat and Mass Transfer Modeling (HMTM) inside the adsorbent packed bed using a transient three-dimensional local thermal equilibrium model and solved using COMSOL-6 software .
5. Built and constructed a compact and lightweight two-bed ATB system test rig with mass recovery technology to conduct the experimental work of the present study.

6. Evaluating the energy efficiency of several adsorbents, such as silica gel and advanced adsorbent materials (MOF801 and MCM-41), with water as the refrigerant.
7. ATB thermal performance, including COP, RC, SCP, uptake and offtake adsorption, adsorption isotherm, kinetics, and the change in chilled and coolant fluid temperatures, are evaluated by comparing the data.

1.10 Dissertation Outlines

The previous sections of this chapter disclosed this project's significance and objectives. In addition, this thesis was divided into six technical chapters, each of them is devoted to the description of a specific part of the research activities as follows:

Chapter Two describes surveying the literature review about adsorption systems according to the topic of this thesis. Firstly, this chapter includes short write-ups on the definition and principle operation of adsorption systems and their types. Furthermore, the technologies for improvement of these systems were surveyed and classified according to theoretical, experimental, and numerical studies.

Chapter Three presents the theoretical analysis and numerical modeling for analyzing the performance of each component of the ATB system.

Chapter Four details experimental work, including materials, project description, and experimental procedure.

Chapter Five describes the experimental, theoretical, and numerical results. In addition, the comparisons between the experimental, theoretical, and numerical results are presented.

Chapter Six concludes the results of this study and provides suggestions for future studies to improve and develop the technique of study.

Chapter Two

Literature Review

Chapter Two

Literature Review

2.1 Introduction

The main objectives of this chapter are to provide basic knowledge of modified adsorption systems ATB, valuable guidelines for developing parameters of adsorbent beds, and the system's applicability in air conditioning with an enhancement of COP.

2.2 Experimental Research

In recent decades, authors have constructed and experimentally analyzed the adsorption systems of various methods such as working pairs, ABU sizes, and numbers, developments in ECU, heat and mass recovery and transfer, cycle stage, and number.

In 2002, **M. Tokarev et al.** [22] developed a new selective water sorbents (SWS) material, calcium chloride in the MCM-41, and its application for sorption cooling/heating. The composite material absorbed as much as 0.75 g of H_2O per gram as a dry sorbent. The COP of the single bed adsorption refrigeration unit based on the composite $CaCl_2$– MCM achieves 0.71, whereas pure silica does not surpass 0.6. In 2004, **Y. TASHIRO et al.** [23] analyzed the performance of several materials to identify an acceptable dehumidification component for an adsorptive dehumidification cooling system. MCM-41's highest effective adsorption rate was 0.39 g_{ref}/g_{ads}, compared to the introductory amount of activated carbon, which was 0.18 g_{ref}/g_{ads}; the adequate adsorption amount of activated carbon with silica gel was 0.25 g_{ref}/g_{ads}. **Akira Akahira et al.** [24] **2005** investigated the impacts of operating parameters on mass recovery cycles experimentally utilizing a silica gel–water pair. The results demonstrate that the SCP of the mass recovery cycle is better than that of the traditional cycle and that the mass recovery cycle can be used with a low-

temperature heat source. The COP decreases with the increase in the time of the mass recovery procedure. **Khalifa et al. (2011)** [12] constructed a semi-continuous adsorption-desorption cycle using two generators with mass recovery by employing methanol and active carbon as the working pair. The mass recovery method increases the initial methanol concentration in the desorption generator, enhancing the cycle's COP and SCP. The Thermophysical parameters of six primary activated carbons for use in an adsorption chiller are described experimentally by **S.K. Henninger et al. 2012** [25]; at lower desorption temperature of 95 ºC, CarboTech A35/1 had the highest mass-SCP for evaporation at 7ºC. For higher desorption at 120 ºC and evaporation at (-5 ºC), the coconut-based sample G32-H has the highest mass-SCP. In 2013, **Z. Lu et al.** [26] described a silica gel water solar adsorption air conditioner's adsorption and mass-heat recovery performance. The adsorption cooling efficiency increases with high temperatures of hot water inlet and chilled water. Conversely, as the cooling water input temperature rises, efficiency decreases. By utilizing mass-heat recovery, efficacy can be substantially enhanced. In 2016, **S.W. Du et al.** [27] investigated the heat and mass transfer characteristics of ZSM-5 and SAPO-34 zeolite during an adsorption/desorption procedure utilizing water vapor as the refrigeration medium. The SAPO-34 zeolite outperformed the ZSM-5 zeolite in terms of mass transfer. In terms of refrigeration capacity, the SAPO-34 surpassed the ZSM-5 zeolite. The SAPO-34's COP and SCP are higher than the ZSM-5 zeolite in any cooling mode. The SAPO-34 zeolite is more suited for solar adsorption refrigeration. In 2016, **T.X. Li et al.** [28] investigated a possible portable high-performance single-bed sorption thermal battery that uses Manganese chloride and ammonia sorbent as a working pair for waste heat recovery and mixed cold and heat storage. The cold energy density is 600 kJ/kg, while the heat energy density is 1498 kJ/kg. The sorption thermal battery is a potential compact, high-performance energy storage technology for waste heat recovery and renewable energy usage. In

2016, **Ahmed Elsayed et al.** [29] proposed an experimental work for a single bed TB using CPO-27(Ni) MOF adsorbent material. The performance of CPO-27(Ni) was compared to that of silica gel. The CPO-27(Ni) outperformed silica gel, making it appropriate for energy storage applications. The CPO-27(Ni) was discovered to have an energy density of 170 Wh/kg (discharging temperature of 100 ^{o}C and half cycle duration of 3600 s). In 2016, **Q.W. Pan et al.** [30] presented a silica gel-water adsorption chiller that used efficient and reliable heat and mass recovery technologies. The optimal recovery times for heat, mass, and cooling are 720 seconds, 40 seconds, and 24 seconds, respectively. Standard configurations include an 86°C hot water inlet, a 30°C cooling water inlet, and an 11°C chilled water outlet; the cooling power, COP, and SCP are correspondingly 42.8 kW, 0.51, and 125.0 W/kg. When the chilled water outlet temperature rises, the cooling power, COP, and SCP increase. **E. Elsayed et al. 2016** [31] evaluated various operating parameters for the adsorption single-bed system. Applications requiring low evaporation temperatures were more compatible with the CPO-27(Ni)/water pair; conversely, applications requiring high evaporation temperatures were more compatible with the aluminum fumarate/water pair. It was discovered that raising the regeneration temperature decreased the COP of aluminum fumarate while increasing it for CPO-27(Ni). On the other hand, increasing the condensation temperature reduced the efficiency of the two materials. In 2016, **E. Elsayed et al.** [32] evaluated three MOF materials: aluminum fumarate, CPO-27(Ni), and MIL-101(Cr). The performance of these MOFs in a two-bed adsorption desalination system was predicted using MATLAB/Simulink and varied heat source temperatures. CPO-27(Ni) and aluminum fumarate production at different evaporation temperatures showed significant potential, with MIL-101(Cr) showing a higher water production rate at 20°C. The experiment of single bed adsorption chiller using silica gel and water as the working pair was investigated by **P. J. Vodianitskaia et al.** [33] in 2017. The

adsorbent bed heat exchanger is supplied with free grains of silica gel placed between finned tubes. The system achieved a net cooling power of 143 W, a COP of 0.53, and a SCP of 68 W/kg. The following outcomes were obtained during an 80-minute cycle: 80°C for the heated water, 30°C for the cooled water, and 15°C for the chilled water. A 4 percent reduction in particle diameter from 2 mm to 0.26 mm adversely affected the COP. In 2017, **Q.W. Pan** [34] studied a silica gel-water adsorption refrigeration system with heat recovery between two adsorbers and a mass recovery between two evaporators. Results indicate that the evaporators' and adsorbers' heat transfer fluid significantly affect the heat and mass recovery processes. Heat and mass recovery times should be 25-45 s and 5-50 s, respectively, for best results. **S. Narayanan et al.** [35], in 2017, studied a thermophysical battery that stores thermal energy and subsequently releases it to deliver heating and cooling as required. For heating, a NaX-water pair was utilized; the maximum power density and specific power measured were 103 W/l and 65 W/kg, respectively; for cooling, they were 78 W/l and 49 W/kg. In 2017, **Hassan J. Dakkama et al.** [36] developed a single-bed adsorption system for generating ice, cooling, ice slurry, and potable water, employing CPO-27 (Ni) -water as a working pair. The COP cooling was 0.9, and water desalination was 1.8 tons per day per ton of ads. In 2018, G**. Engela** [37] suggested A thermal energy storage system utilizing SAPO-34 for sorption. The storage system, which holds 2.5 kilograms of adsorbent, delivers an average cooling power of 1 kilowatt for 30 minutes. The results show a power density of 50 watts per kilogram of adsorbent and an energy density of 20 watts per kilogram of adsorbent. A study presented by **Kyung et al.** [38] in 2018 was introduced to modify the surface characteristics of silica and MOF materials. It was shown that both silica (MCM-41) and MOF (MIL-101) demonstrated limited water adsorption capacities. In addition, the MCM-41 and MOF (MIL-101) materials were immersed in calcium chloride ($CaCl_2$), enhancing the adsorption capacity of MCM-41 and MIL-101. In

2019, **Z. Lu** [39] introduced an adsorption system for air conditioning, refrigeration, and heat pumps. This technique employs an improved adsorbent combining Calcium chloride ($CaCl_2$) and activated carbon. The cooling capacity, SCP, COP, and exergy efficiency were estimated to be approximately 0.91 kW, 456.9 W/kg, 0.24, and 0.12, respectively. In 2019 **Q. Pan et al.** [40] Designed and constructed a 3 kW adsorption refrigeration system (ARS) utilizing a silica gel-water working pair. The cooling power and the COP were 3.98 kW and 0.632, respectively. The most efficient duration for each half-cycle of ARS was found to be 750 seconds. The COP of an adsorption air-conditioner is often higher than that of an adsorption chiller that produces chilled water because of the elevated evaporation temperature. **Abd-Elhady et al.** [41] 2020 assessed the efficiency of a two-bed adsorption chiller that incorporates heat and mass recovery cycles. The working pair consisted of RD silica gel water. A small fin spacing has a better specific cooling capacity (SCC) and COP than wider fin spacing. In greater detail, by lowering fin thickness to 50% of its base value, COP rises by an average of 9.4 %. In 2020, **B. Han and A. Chakraborty** [42] presented the parent MOF-801 and CH_3 ligand MOF-801 (Zr) adsorbents and their surface characterization processes with water uptake/offtake rates experimentally. The SCP and COP of CH_3 ligand MOF-801 (Zr) are found to be 30 and 40% greater than the parent MOF-801 (Zr) under chiller working conditions, respectively. Furthermore, in 2021, MOF-801 was compared to silica gel by **M. Rezk et al.** [43] for adsorption cooling and desalination applications. The MOF-801-based system outperformed the silica gel-based system, with a 140 percent improvement in SCP, with maximum SCP mass and SCP of 365 W/kg and 170 kW/m^3 compared to 260 W/kg and 185 kW/m^3 for silica gel at cycle time more significant than 400 s. In 2021, **Y.M. Liu et al.** [44] investigated experimentally the performance of a solar adsorption cooling system that used silica gel water as the working pair. The maximum COP for the silica gel system was 0.258 at an

adsorption time of 45 minutes. The performance of the silica gel system outperformed the zeolite system in terms of the COP and SCP. In 2021, **M. B. Elsheniti et al.** [45] evaluated experimentally a lab-scale two-bed adsorption chiller with silica gel water as a working pair that can be driven by solar energy. With a cycle period of 460 seconds and temperatures of 75°C hot water, 25°C cooling water, and 18°C chilled water, the COP and SCP may reach 0.39 and 74 W/kg, respectively. The COP and SCC increase when the hot water temperature rises, the cooling water temperature falls, and the chilled water temperature increases. In 2021, **I. Jahan et al.** [46] investigated Zirconium fumarate (MOF-801) and Cobalt-doped (Co^{+2}) ions mixed with MOF-801 as an adsorbate for adsorption heat pump (AHP). Cobalt-doped mixed with MOF-801 might be a promising and effective adsorbent for AHP. The Cobalt-doped mixed with MOF-801 has a larger surface area and higher uptake than the pure zirconium fumarate MOF-801. In 2022, Using silica gel-RD, silica gel-blue, and MCM-41 as adsorbents, the single bed ATB was investigated by **A. L. Tarish et al.** [47]. The modified adsorber bed demonstrated a higher COP than the ABU. Specifically, the COP values were 0.28, 0.26, and 0.25 for MCM-41, silica gel-RD, and silica gel-blue, respectively.

2.3 Theoretical Research

Many researchers investigated theoretically using an efficient adsorption bed to improve the performance of ATB. For example, the theoretical study **by K.H. Yeung and K. Sumathy** [48] in 2003 analyzed the operational efficiency of a solar-powered adsorption hybrid system that utilized activated carbon fiber and methanol as the working pair. An evacuated vacuum tube collector supplied the heat required for the cycle. An optimum solar hybrid system with a 2 m^2 solar collector can generate 6.2kg_{ice}/day with a daily system COP of approximately 0.56. In 2004, **Akira Akahira et al.** [49] investigated mass recovery procedures that employed

silica gel and water. At lower supply temperatures, a mass recovery cycle exhibits a higher COP compared to a single-stage cycle. In 2009, **Z. Tamainot-Telto et al.** [50] developed a thermodynamic cycle model to identify the best adsorbent-refrigerant pair. The monolithic carbon KOH-AC exhibits the best thermal performances based on power density in a two-bed cycle, with a driving temperature of 100 °C; the results indicate that the cooling production for the ice production system is around 66 MJ/m^3, with a COP of 0.45. The air conditioning system has a cooling capacity of approximately 151 MJ/m^3 with a COP of 0.61. **Sharafianardakani et al.** [51], in 2012, showed a two-bed ARS cycle with heat recovery. For the zeolite 13X/water pair, the heat recovery cycle in the ARS can increase the system's COP by up to 41%. Additionally, the increase in the regeneration and evaporation temperatures leads to increases in the COP and entropy production of ARS while decreasing these quantities when the condensation temperature increases. In 2013, a group of researchers led **by S. Narayanan et al.** [20] developed a single-bed compact ATB. Zeolite 13X has demonstrated the capability to attain volumetric cooling and heating rates of 0.1 kW/L adsorbent and 0.14 kW/L adsorbent, respectively. Lower heat conductivity might result in unfavorable and suboptimal performance. In 2014, **Pan et al.** [52] suggested the implementation of a double mass recovery cycle (DMRC), a traditional mass recovery cycle between two beds (TBMRC), and a mass recovery cycle between evaporators (TEMRC). Thermodynamic evaluations revealed that the DMRC system exhibited the best performance, with TEMRC and TBMRC systems following suit. Furthermore, it demonstrates that utilizing the mass recovery technique may significantly increase the performance of an adsorption refrigeration system. In 2015, **A .Sharafian and M. Bahrami** [53] investigated the thermodynamic cycle of Adsorption Cooling Systems (ACS) employed in automobile A/C units. The results also show that the mass of the adsorber bed and

its total heat transfer conductance have the biggest and lowest effects on the SCP, respectively. Additionally, research results demonstrate that the SCP and COP are unaffected by changes in the mass flow rates of the cooling and heating fluids, coolant fluid, and chilled water during ACS operation. The effect of evaporator input water temperature and condenser cooling water temperature on a typical 450 kW two-bed adsorption chiller with desalination using silica gel was theoretically investigated by **P.G. Youssef et al.** [54] in 2015; the results showed that with increased evaporator water temperature and decreased condenser cooling water, the cycle COP, performance ratio PR, and overall conversion ratio OCR increased. The Dynamic behavior of a cylindrical adsorbent bed utilizing a silica-gel water pair during adsorption was theoretically investigated by **I. Solmus et al.** [55] in 2015. The system's cooling capacity rises as the evaporator pressure and desorption temperature rise and the condenser pressure and temperature drop. The system's COP and SCP increase as a result of this. To achieve a desirable heat transfer rate and reduce the adsorption process's duration, the adsorbent bed's thickness must be below 0.01 m. The study by **S. Narayanan et al.** [21] in 2015 examined an ATB capable of providing heating and cooling functionalities with NaX zeolite water as an adsorbent-refrigerant combination. The ATB is compact and has a chilling and heating capacity greater than 2.5 kWh, with adsorption stacks less than 1.2 mm thick, and a porosity of 0.5 is preferred. In 2015, **A. Allouhi et al.** [56] studied the efficiency of solar adsorption cooling systems with a single-bed configuration, utilizing silica gel and water as a working pair. At a condenser temperature of 25 ^{o}C Celsius, combining silica gel and water for air cooling can achieve a COP of 0.3843. In 2016, **Chekirou et al.** [57] conducted a study to investigate recovery's influence on the effectiveness of adsorption cooling. As part of their investigation, the scientists employed activated carbon AC-35 in combination with methanol. An adsorption refrigeration unit's COP increased from 0.483 without heat recovery to

0.68 with heat recovery. In 2016, the mathematical models for single, two, and three-stage adsorption cycles were developed by **S.Z. Xu et al.** [58], with an active carbon-ammonia as a working pair. When the heating source temperature is between 69 and 93 ºC, the two-stage cycle has a reasonably high COP and exergetic efficiency. The lowest heating source temperature is necessary to operate a two-stage cycle. In a study conducted in 2016, **S. M. Ali et al.** [59] assessed the effectiveness of a proposed water system that utilized AQSOA-Z02 and silica gel for a two-stage ARS. Utilizing AQSOA-Z02 zeolites as the adsorption beds in the cooling cycle is recommended, while silica gels are the sorption components in the desalination cycle. In 2017, **F. N. Al-Mousawi et al.** [60] developed a multi-bed adsorption system in MATLAB Simulink. Advanced adsorption materials like AQSOA-Z02 and MOF Aluminium-Fumarate are used along with normal Silica-gel. The highest COP for Silica-gel is 0.64. With this study's range of heat source temperatures, a two-bed setup gives the best COP for all adsorption materials. Using temperature–heat (T–Q) graphs, **Xu et al.** [61] 20 enhanced the heat exchange network and design of adsorption refrigeration systems. in 2017. In 2017, **R. H. Mohammed et al.** [62] developed A mathematical model to simulate the adsorbent bed's heat and mass transfer mechanisms. Increasing bed thermal conductivity while reducing particle diameter and adsorbent bed thickness can significantly increase SCP. They mentioned that increasing the adsorption period is not recommended. In 2017, **H.J. Dakkama** [63] investigated a cascaded (two-bed) adsorption system; Simulink/MATLAB software was used to study the performance of various adsorbent/refrigerant working pairs. The combination of Maxsorb/R134a and Maxsorb/propane demonstrates superior performance in both COP with a value of 0.08 and cooling capacity reaching 1.82 kW. A study by **Q.W. Pan** [64] 2018 Introduced a mathematical model for a silica gel-water adsorption chiller powered by solar energy. Employing a silica gel-water adsorption chiller with a flexible cycle

duration can improve a solar cooling system's overall efficiency without reducing cooling capacity. The COP of a silica gel-water adsorption chiller increases as cycle time and hot water temperature increase. SCP increases with increasing hot water temperature and increasing cycle time. In 2018 **L.Q. ZHU et al.** [65] examined the cooling performance of the adsorption cooling system, which uses zeolite 13X as adsorbent materials and involves a mass recovery cycle, estimated using a mathematical model. The calculation has yielded a SCP of 231.4 W/kg and a COP of 0.317. The cascaded mass recovery cycle was proposed and investigated by **Quanwen Pan et al.** [66] in 2018, based on silica gel water. The COP of the cascaded mass recovery cycle surpasses that of the primary or traditional mass recovery cycles. Implementing the cascaded mass recovery cycle can significantly enhance the operational efficiency and effectiveness of the AHP. In 2019, **Papakokkino et al.** [67] examined the performance of a single-bed adsorption system. The data show copper is more effective as a heat exchanger than aluminum. To obtain high SCP, reactors with low fin thickness and low fin length are suggested. In 2019, **Duong et al.** [68] developed a new approach with an entire tube to study the system performance of an ARS chiller made of several serial and parallel configuration modules. The fins and tube are packed with FAM – Z01 grains. The COP and SCP with the highest values were 0.47 and 295.19 W/kg, respectively. An adsorption desalination system was investigated in 2019 by **R. Raj et al.** [69]; the silica gel utilized is Type RD silica gel. Low cooling, condensation, and hot water inlet temperatures improve the system's performance. The COP increases fast as the hot water temperature rises. In addition, when the cooling water temperature drops, the system's COP rises. As the temperature of the condenser rises, the system's COP falls. In a study conducted by **Y. Jiang et al.** [70] in 2019, the theoretical thermodynamics of the AHP cycle was examined. The results showed that MOF 801, with a regeneration temperature of 76 °C, achieved a maximum COP of 1.6.

MOF-801 is a better adsorbent for AHPs than Zeolite 13X because it can be regenerated at a lower temperature and provides heat with a better heating COP. In 2019, **E. Elsayed et al.** [71] studied the potential of MIL-101(Cr)/$CaCl_2$ composites in adsorption cooling applications. The SCP was improved from 168 W/kg for the pure MIL-101(Cr) material to 248 and 388 W/kg for the 1:5 and 1:8 $CaCl_2$ composites. The composites 1:8 outperformed silica gel on a constant volume basis, yielding the greatest SCP. In 2019, **Vivekh et al.** [72] introduced a mathematical model to simulate heat and mass circulation in a coated heat exchanger, utilizing silica gel and composite polymer as the materials under investigation. The tube fin form exhibited a 7% increase in moisture removal capacity, whereas the annular fin form showed a substantial improvement of 40%. In 2021, **A. Amirfakhraei et al.** [73] investigated the adsorption desalination system with an improved heat and mass recovery design. Compared to traditional systems without heat and mass recovery modes, the design exhibited an increased water output of nearly 200% and a system performance of about 51%. The performance of the single bed ATB utilizing silica gel water was assessed by **Tarish et al.** [74] in 2022. Under certain working conditions, the CC, COP, and SCP of the ATB system were found to be 2 kW, 0.3, and 100 W/kg, respectively. The COP, SCP, CC, and adsorption intake increased because of the increase in cold temperatures.

2.4 Numerical Research

Many researchers performed numerical simulation and modeling studies to examine the operating parameters and to evaluate COP, SCP, and cooling capacity for the adsorption system.

In 2004, **K.C. Leong et al.** [75] described a two-dimensional non-equilibrium numerical model for coupled heat and mass transfer in an adsorbent bed. The adsorbent/adsorbate pair was chosen to be zeolite-13X/water. The COP increases as

adsorbent thickness increases, whereas the SCP decreases. The COP rises as the temperature of the generator rises. In 2006, **Y. Liu and K.C. Leong** [76] proposed a cascade adsorption cooling cycle for refrigeration applications. This cycle comprises two zeolite adsorbent beds and one silica gel adsorbent bed. The operating refrigerant for all three adsorbers is water. The numerical results indicate that the COP of the system is 1.35, much higher than the COPs of an intermittent cycle (about 0.5) and a two-bed combined heat and mass recovery cycle (around 0.8). In 2008, **J. Y. San et al.** [77] investigated the performance of the multi-bed adsorption heat pump and compared three adsorption pairs: activated carbon/methanol, silica gel/water, and 13X molecular sieves/water for use as the working substances. The activated carbon/methanol pair has the best SCP, COP, and second-law efficiency among the three adsorption pairs. The performance of a cascade adsorption cycle with a driven heat source was presented by **Aep Saepul Uyun et al.** [78] in 2009. The cycle is made up of four beds that are filled with silica gel. The mass recovery cycle enhances the SCP and COP values over the traditional cascade cycle. Compared to the conventional single-stage cycle, cascading adsorption cycles generate greater COP values but lower SCP values. **A. Alahmer et al.** [79], in 2016, used TRNSYS software to evaluate a solar thermal adsorption cooling system. A conventional two-bed silica gel/water adsorption system was used in their study. It was using real-time weather data from two cities: Perth, Australia, and Amman, Jordan. The average COP of the system was 0.491 and 0.467 for Perth and Amman, respectively. Compared to a traditional vapor compression cooling system, an economic analysis revealed that the solar-driven adsorption cooling system might reduce electricity usage by 34% and 28% in Perth and Amman, respectively. In 2017, **P. Yousef et al.** [80] used Simulink to investigate the ability of a two-bed adsorption desalination/cooling system to make fresh water and cool the air. Compare aluminum fumarate to silica gel and AQSOA-Z02 by using it. It has been

found that as the evaporator temperature increases, all materials produce more water and can cool more. AQSOA-Z02 performed better performance because its adsorption rose quickly at low-pressure ratios. In 2017, **E. Elsayed et al.** [81] presented numerically two-bed adsorption cooling applications that utilized MIL-101(Cr)/graphene oxide composites with 2 and 5 % of GrO Phys. The 2 % Gro synthesis composite had a similar SCP and COP to the MIL101(Cr) system under the tested operating circumstances; in contrast, the Gro Phys, 5 % composite, had a lower SCP and a higher COP. In 2019, **M. B. Elsheniti et al.** [82] constructed a numerical model of two-bed adsorption chiller. The COP increased from 0.55 to 0.59, and the SCC doubled to 305 W/kgads when fins increased from 50 to 30. In 2019, **Pártl and Mikyška** [83] investigated a computational model for humid airflow in a zeolite bed. Because of the variations in the adsorption effects, the results reveal that the sizes of the time steps must be carefully chosen. In 2020, **Pinheiro et al.** [84] introduced a Computational Fluid Dynamics (CFD) simulation to assess the efficacy of the CPO-27(Ni) in AHP that utilizes water as an adsorbate. The output of the MOF was measured against that of the AQSOA FAM-Z02. The MOF adsorbent did perform more effectively than the AQSOA FAM-Z02. The COP of CPO-27(Ni)/copper foam was between 1.16 and 1.39. **A. Hassan et al.** [85]**,** in 2020, studied vacuum multi-effect membrane distillation (VMEMD) and an adsorption (AD) unit to produce distilled water. MOFs such as aluminum fumarate have superior water vapor absorption properties compared to silica gel and zeolite. Nickel salts (CPO-27-Ni) were more suitable for applications with low evaporation temperatures. **N.U. Qadir et al.** [86], in 2021, explored the numerical approach for performance modeling of an adsorption chiller, explicitly focusing on the adsorption/desorption cycle with the heat/mass recovery (HR/MR) cycle. It is anticipated that the adsorption/desorption + (HR/MR) + (desorption/adsorption)

yielded an average COP of about 52 % greater than the COP of the adsorption/desorption cycle.

2.5 Experimental and Numerical Research

In this section, the experimental and numerical technologies for improving the adsorption refrigeration system were covered and reviewed in detail.

In 2009, **T. Miyazaki et al.** [87] conducted a study to examine the effectiveness of two-bed adsorption chillers that use RD-type silica gel-water and CaCl2-in-silica gel-water combinations. The COP chiller was optimized by using an improved cycle through $CaCl_2$. The enhanced cycle time distribution for RD-type silica gel-water and $CaCl_2$-in-silica gel-water-based chiller has resulted in a 6% increase in cooling capacity. The utilization of CPO-27(Ni) in a one-bed adsorption system for water desalination and cooling applications was investigated experimentally and numerically by **P. G. Youssef et al.** [88] in 2017. They found more cooling and water produced as the condenser water inlet temperature decreased. However, increasing desorption temperature enhances cycle outputs as SDWP and SCP increase. The use of modern MOF materials for water desalination and cooling applications has been investigated; in 2017, **N. Ghilen et al.** [89] conducted a numerical analysis of the behavior of silica gel/water pairs in refrigeration systems with mass recovery. The numerical and experimental results exhibit a high degree of similarity. Given a driving source temperature of 85°C and coolant and chilled water input temperatures of 40°C and 15°C, respectively, the simulation calculation suggests a COP value of 0.7. Based on the performance of COP and SCP, the most optimal adsorption-desorption cycle period is around 1240s. In 2019, **H. O. Helaly** [90] conducted a numerical and experimental investigation on the adsorption system, utilizing AA13X and silica gel as adsorbents. Increasing the regeneration temperature above 90 °C has a negligible effect on the storage

density of the system; the energy density does not vary significantly with increasing particle diameter in the adsorbent particle diameters up to 1 mm. In 2020, **J. G. Lee et al.** [91] investigated a two-bed type AD system chosen for the simulation study, and silica-gel, metal-organic frameworks (MOFs), and Ferro-alumina-phosphate (FAPO, FAM-Z01) were used as adsorbents. FAM-Z01 outperformed the other two adsorbents in terms of cooling capacity and COP. The AD system with FAM-Z01 offers much promise for using waste heat and renewable energy sources like solar and geothermal. In 2020, **W.D. Chen et al.** [92] investigated A four-bed, two-evaporator adsorption chiller. The two most important factors that substantially impact the chiller's COP are the mass flow rates of hot and chilled water. The cycle time and cooling water temperature influence the chiller's specific daily water production (SDWP) more than other factors. Instead of typical packing, an aluminum fumarate metal-organic framework (MOF) was used as a coated layer by **E. Elsayed et al.** [93] In 2021 to improve ARS. Using a confirmed COMSOL simulation, the ideal coating thickness was determined to be 0.3 mm. The system with an aluminum fumarate-packed heat exchanger produced roughly 200 W/kg, but the coated one performed better, making 600 W/kg. Heat recovery and two-stage operating techniques were developed in 2021 by **S. Yagnamurthy et al.** [94]. A 23–42% improvement in COP was observed when an optimized passive heat recovery strategy was used. The passive heat recovery approach has a thermal energy savings of 1285.9 kJ.

2.6 Experimental and Theoretical Research

In order to investigate the performance of adsorption thermophysical batteries, some researchers have suggested experimental and theoretical methods for studying the system.

In 2004, **L. Yong et al.** [95] analyzed the performance of a continuous adsorption cycle with a double adsorber and heat recovery. This study utilized Activated carbon and methanol as the adsorbent/adsorbate combination. Suppose the cycle duration is too short, which indicates an inhomogeneous temperature distribution in the bed. The increased adsorbent mass makes the SCP more sensitive and diminishes. Similarly, as long as the adsorbent mass is smaller, the COP rises. In 2007, **X. Wang et al.** [96] investigated the performance of two-bed using silica gel water in adsorption chillers by using the lump-parameter model. This model's predictions are compared to experimental data. As a result, the lump parameter model can be utilized to estimate performance accurately and provide vital information to manufacturers for adsorption chiller design. In 2014, **A. Sadeghlu et al.** [97] investigated a two-bed adsorption refrigeration system. When Zeolite 13X/$CaCl_2$ is used instead of Silica gel/$CaCl_2$ and activated carbon/$CaCl_2$, the cooling capacity is enhanced by 7.7% and 36%, respectively. Increased cooling capacity is achieved by raising the hot water temperature and lowering the cold-water temperature. In 2015, **S. Mitra et al.**[98] , investigated a two-stage, four-bed/stage adsorption cooling-desalination system with silica gel as the adsorbent and water as the refrigerant. The system's COP increases slightly with increasing half-cycle times; as the pressure differential between the evaporator and the condenser decreases, the system's COP improves. In 2016 **B. Shi et al.** [99] investigated the performance of a single ARS examined utilizing silica gel RD-2060, SAPO-34, and CPO-27(Ni) MOF materials. The water vapor uptake of CPO-27(Ni) was 0.41 at a relative pressure of 0.1, which is 86.3 percent greater than SAPO-34 and more than seven times higher than silica gel RD-2060. The performance of CPO-27(Ni) was superior to that of SAPO-34, leading to a 42 % increase in the SCP value. In 2020, **A. Alahmer et al.** [100] presented the performance of a two-bed silica gel-water adsorption refrigeration system powered by solar thermal energy. The chilled water

output temperature ranges from 9 to 12 ºC. The system COP varies between 0.4 and 0.55 between 10:00 and 17:00. It also demonstrates that high COPs are observed in the afternoon. In 2021, **P. Soni et al.**[101] , investigated adsorption refrigeration system (ARS) with two adsorbed beds analytically and experimentally. It operates on a silica-gel/methanol pair and is powered by the exhaust gases of the I.C. engine. There is variation in adsorption uptake of up to 0.12 kg/kg of silica gel. The best cycle duration for the silica-gel/methanol pair was 35 minutes, and the maximum theoretical COP and SCP at 7°C evaporator temperature were 0.5 and 102 W/kg, respectively.

In conclusion, this study aims to solve the problem of a non-continuous ATB system. In addition, it investigates if employing mass recovery technology can increase ATB performance. The research focused on the ATB is summarized in Table (2.1).

Table (2.1) Summary of research Work finding

No.	Author and Year	The aim	Pairs	The results
1	S. Narayanan et al. 2013 [20]	Computational analysis of one-bed ATB	zeolite 13X / water.	The computational study shows that materials with higher adsorption capacities and high thermal conductivity support higher heating or cooling rates.
2	S. Narayanan	Developing one bed ATB	NaX zeolite/water	1- The maximum achievable COP for cooling varies

	et al. 2015 [21]			from 0.23 to 0.28, while the COP for heating is between 0.67 and 0.76. 2- To achieve 2.5 kW h of heating and cooling, the thickness of adsorption should be less than 1.2 mm
3	S. Narayanan et al. et al. 2017 [35]	Investigated a single-bed ATB that stores thermal energy to provide heating Moreover cooling on demand	NaX-zeolite / water.	1- The measured maximum power densities and specific powers for heating were 103 W/l and 65 W/kg, respectively. The observed maximum power densities and specific powers for cooling were 78 W/l and 49 W/kg, respectively. 2- Using advanced adsorbents, such as metal-organic frameworks, can significantly enhance the battery's overall performance.

4	***A. L. Tarish et al.*** 2022 [74]	evaluate the performance of the single bed ATB.	Silica gel/water.	1- Increased cold temperatures enhanced the COP, SCP, CC, and adsorption uptake. 3- The reduced input coolant temperature led to an 11% increase in CC. 4- The ATB system's performance values for CC, COP, and SCP were determined to be 2 kW, 0.3, and 100 W/kg, respectively.
5	***A. L. Tarish et al.*** 2022 [47]	studied an experimental investigation of single-bed ATB.	silica gel-RD, silica gel-blue, and MCM-41 / water	1- The experimental results demonstrated that adsorption uptake increased when the cooled water temperature decreased 2- The modified adsorber bed MABU exhibited the greatest COP, 0.28 for MCM-41, 0.26 for silica gel-RD, and 0.25 for silica gel-blue.

2.7 Summary

While researchers have examined numerous ATB systems, specific demonstrations of these advanced systems are promised and should be investigated. Significant areas of research remain focused on the advancement of adsorbent materials, the development of environmentally friendly refrigerants, the improvement of COP, and the achievement of semi-continuous refrigeration. From the reviewed literature, the available improving methods of the ATB can be concluded as follows:

2.7.1 Two-Bed Adsorption Refrigeration System

1- The mass recovery technique was utilized to enhance the initial concentration of the materials in the desorption generator, hence improving the cycle's COP and SCP.
2- The mass recovery cycle can be used with a low-temperature heat source.
3- The COP decreases with the increase in the time of the mass recovery cycle.
4- The mass recovery cycle enhances the SCP and COP over the traditional cascade cycle.

2.7.2 Adsorption Refrigeration System Geometry

1- Adsorbent beds that meet the following criteria—small area, small volume, low cost, lightweight, and low thermal conductivity—are considered suitable for ATB applications.
2- Increased SCP and COP result from the reduced bed geometry.
3- For a desirable heat transfer rate and a decrease in the duration of the adsorption process, the adsorbent bed's thickness should be below 0.001 m.
4- The adsorber bed geometry, including fin height, thickness, refrigerant channel height, and cycle duration, significantly influences the SCP and COP.

5- Finer fins are favored over thicker fins for the heat exchanger of the adsorber bed. Also, a shorter fin substantially influences the specific cooling capacity, with little effect on COP.

2.7.3 Adsorbents Materials

1- The characteristics of the adsorbent material influence the improvement of water adsorption capacity.
2- By enhancing the heat conductivity of the utilized adsorbent material, the time of the adsorption process can be significantly reduced.
3- High thermal conductivity and water capacity uptake of the adsorbent significantly improve the ATB performance.
4- The MOF adsorbent performance outperformed silica gel, making it appropriate for the adsorption system.

2.7.4 Operation Conditions

1- The lump parameter model can be utilized to estimate the performance accurately and provide important information to manufacturers for adsorption chiller design.
2- A higher COP can be obtained by increasing the evaporation temperature, whereas an unfavorable impact on COP can be observed with increased condensation temperature.
3- Increased hot water temperature has an inverse relation to the COP.

2.8 Scope of the work

The current study presented a detailed investigation of approaches for improving the performance of an ATB. Most features of the adsorption chiller systems were reviewed. All the strategies aimed to enhance the COP, RC, and SCP. The following are some specific aims:

1- All of the studies that have been examined have mainly focused on just testing only single beds for advanced thermophysical batteries; in this study,compact two-bed ATB with mass recovery was tested with modified adsorber beds in order to enhance ATB performance.
2- Little experimental testing has been done to see how MCM-41 can influence ATB performance when used as an adsorption cooling application.
3- It is also discovered that the literature contains only limited information on the experimental test rig for adsorber bed design.
4- All of the studies that have been focused on one or two methods of analysis only (experimental, theoretical, and numerical) in the present study focus on using experimental, numerical, and theoretical analysis.
5- All of the studies that have investigated ATB utilized conventional adsorbates such as (silica gel and zeolite), and the present study used advanced materials such as MOF-801 and MCM-41.
6- The mass recovery technique is used to enhance the initial concentration of the materials in the desorption generator, hence improving the cycle's COP and SCP.
7- Reduced bed geometry and combined condenser with evaporator in a single heat exchanger led to increased SCP and COP.

Chapter Three

Theoretical Analysis and Numerical Modelling of Two-Bed ATB

Chapter Three

Theoretical Analysis and Numerical Modelling of Two-bed ATB

3.1 Introduction

Two methods have been covered in this analysis; the first one is the Lumped Parameter Model (LPM), and the second method is the Heat and Mass Transfer Mode (HMTM). In dynamic models, when parameters like temperature, pressure, and mass change over time, the LPM is employed. The energy, mass, and adsorption kinetic equilibrium equations are all expressed as ordinary differential equations in the LPM, which comprises general equations. Many researchers have conducted thermodynamic [102] - [109] and exergy analysis of ATB [110] - [112], where they depend on the entropy and Maxwell relation of the adsorber phase. The thermodynamic model does not consider the heat and mass transfer for ATB; by neglecting the effect of vapor mass in the ABU and ECU, only the upper limits of the performance for ATB are determined. The LPM is implemented to evaluate the COP, SCP, and the cooling capacity of the ATB at various operation and parameter conditions, such as adsorber bed geometry, bed temperatures, solid adsorbent types, and flow rates for coolant and chilled fluids. A mathematical simulation model of a two-bed ATB system for refrigeration and air condition application was built using MATLAB Simulink software, which solved all the governing equations.

The HMTM is applied to analyze the behavior of the adsorber bed domain with time and space using COMSOL 6 Multiphysics software. Many parameters and variables are investigated for two-adsorber beds, such as the overall heat transfer coefficient and thermal and contact resistances. The design of the heat exchanger in the adsorber bed considers the heat transfer area, the mass of the heat exchanger, and the adsorbent mass ratio. The modified Freundlich model [113], [114] calculates the

adsorption isotherm [115] - [117]. The working pairs and coolant fluid changes with parameters and variables of ATB are illustrated in Figure (3.1).

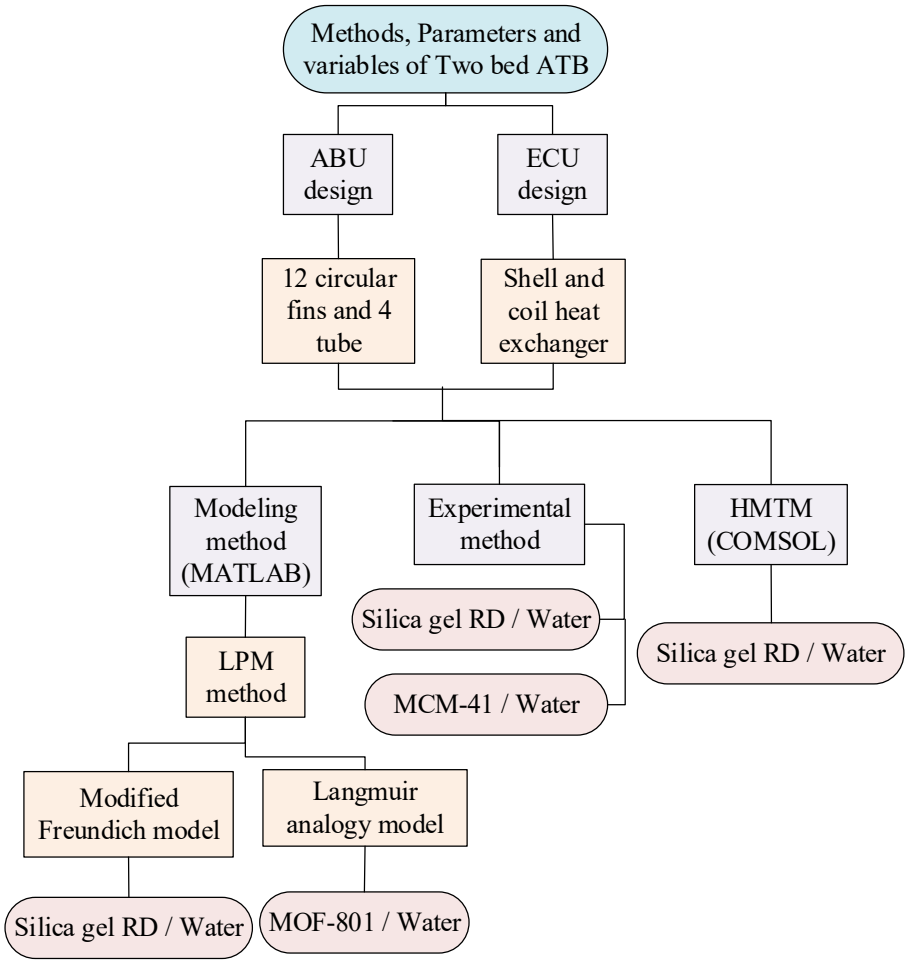

Figure (3.1) Parameters and variables of ATB.

3.2.Working Principle of the Two-bed ATB Cycle

The two-bed ATB system consists of four main parts: two ABUs and two ECUs. It also consists of major parts such as a hot water source, cold water source, chilled storage tank, cooled storage tank, pumps, and valves, as shown in Figure (3.2). The ABU, which contains the adsorbent material and is one of the main components of the ATB system, is where the adsorption/desorption processes take place.

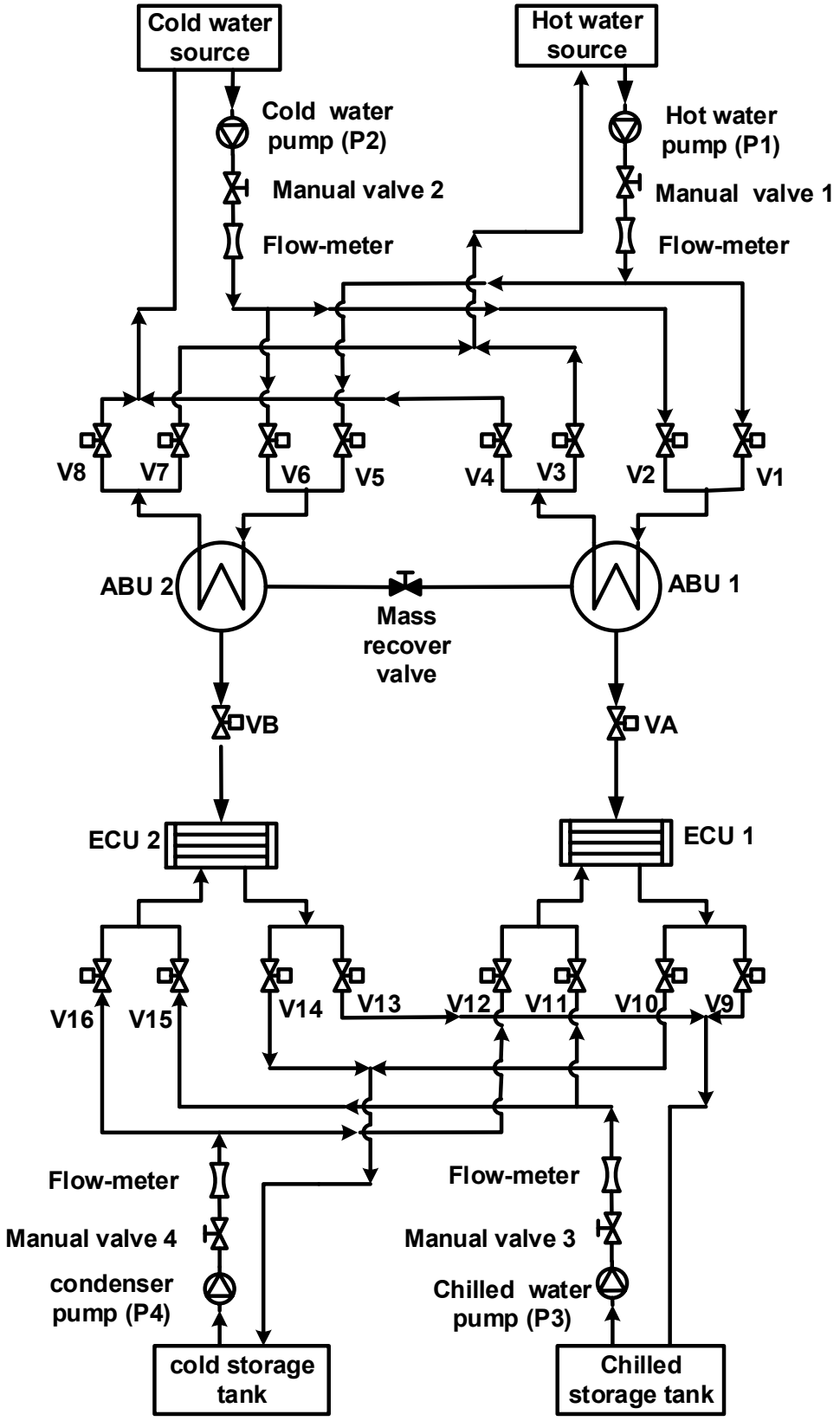

Figure (3.2) Schematic diagram of the Two-bed adsorption thermophysical battery.

The ECU is the secondary component responsible for enabling the processes of refrigerant condensation and evaporation. The operational mechanism of the ATB system includes two primary procedures. Initially, the ATB undergoes discharging by subjecting the ABU to heat, leading to the refrigerant's desorption and subsequent condensation through low-grade heat. During the second process, the ATB undergoes charge through evaporation and refrigerant adsorption. The system shown in Figure (3.2) is divided into ATB_1, consisting (of ABU_1 and ECU_1) and ATB2 (ABU_2 and ECU_2). The processes of the two-bed mass recovery ATB are divided into five steps:

Step one: Preheating/precooling process: all valves of ATB_1 are in a closed position, except for the hot water valves (V_1 and V_3), which are opened to allow the flow of hot water from the hot water source. The hot water pump is also activated, as seen in Figure (3.3 a). The ABU_1 is thermally energized by low-grade heat, such as water from waste heat or solar heaters. The adsorbent materials facilitate the desorption of the refrigerant, resulting in increased pressure within the ABU_1 from the evaporator pressure (point 1) to the condenser pressure (point 2), as depicted in Figure (3.4). In the case of ATB_2, the cooling process of ABU_2 is accomplished by closing all valves except for the cooling water valves (V_6 and V_8), which remain open to allow cold water to flow from the source. This is illustrated in Figure (3.3 a). The pressure of ABU_2 is decreased from the condenser pressure (point 3) to the evaporator pressure (point 4), as shown in Figure (3.4).

Step two Condensation / Evaporation process (refrigeration process 1): The second procedure employed in ATB_1 is referred to as the isobaric process, as indicated by line 2-3 in Figure (3.4). This process occurs when the pressure of ABU_1 reaches the condensing pressure. The valve (V_A) linking ABU_1 to ECU_1, as well as valves (V_{10} and V_{12}) connecting to the cooled storage tank, are opened while valves

(V_1 and V_3) remain open to the hot water source. The condenser and hot water pump are activated according to the diagram provided in Figure (3.3 b). Consequently, the refrigerant undergoes desorption at a constant pressure. The refrigerant vapor transitions from ABU_1 to ECU_1, where it is subjected to condensation through water in the heat exchanger. The condensed refrigerant is subsequently accumulated within the ECU_1. This process continues until the entirety of the refrigerant vapor undergoes condensation. This process depicted in Figure (3.4) is referred to as condensation. The process described in ATB_2 involves a constant pressure process, represented by line (4-1) in Figure (3.4). To initiate this process, The valve (V_B) is opened to establish a connection between the ABU_2 and ECU_2.

Additionally, valves (V_{13} and V_{15}) are opened to allow the flow of chilled storage tank contents. Valves (V_6 and V_8) remain open to facilitate cold water supply from the source. Finally, the chilled and cold-water pumps are activated, as illustrated in Figure (3.3 b). When the valve (V_B) is opened, there is a dramatic decrease in the liquid refrigerant pressure in the ECU_2, causing it to transition from the condenser pressure to the evaporator pressure. This process is related to the throttling of refrigerant in the expansion valve. Consequently, the liquid refrigerant undergoes boiling within ECU_2, followed by evaporation, subsequent movement, and adsorption within the ABU_2. The process depicted in Figure (3.4) is referred to as evaporation.

Step three: Mass recovery process: When refrigeration process 1 is completed, ABU_1 completes desorbing, and ABU_2 completes adsorbing. It can be noticed from Figure (3.4) that the pressure of ABU_1 reaches a condenser pressure (Pc), which is higher than that of ABU_2. The mass recovery valve is turned on to connect the two beds, as shown in Figure (3.3 c). The pressures of ABU_1 and ABU_2 become equal at a medium level, denoted as intermediate pressure (P_m). ABU_1's pressure drop

supports desorption, while ABU_2's pressure rise supports adsorption. As a result, when the mass recovery technique is included, the cycle's refrigeration capacity is enhanced. This process is represented in lines (3-3′, 1-1′) as shown in Figure (3.4).

Step four: Precooling/preheating process: In ATB_1, the cooling of the ABU_1 is accomplished by closing all valves except for the cooling water valves (V_2 and V_4), which are left open to allow the flow of cold water from the source. Additionally, the cold-water pump is activated, as seen in Figure (3.3 d). In this scenario, the ABU_1 pressure decreases from a state of medium pressure (point 3') to the pressure within the evaporator (point 4'), as seen in Figure (3.4). In the ATB_2, it is essential to note that all valves, except for the hot water valves (V_5 and V_7), are in a closed position. These hot water valves are opened and activated to the hot water source, as depicted in Figure (3.3 d). Additionally, the ABU_2 is heated by utilizing low-grade heat, which can be obtained from many sources, such as waste heat or solar energy. The adsorbent materials facilitate the desorption of the refrigerant, resulting in increased pressure within the ABU_2 from medium pressure (point 1') to the condenser pressure (point 2'), as seen in Figure (3.4).

Step five: Condensation/evaporation process (refrigeration process 2): The final step in ATB_1 involves a constant pressure process, represented explicitly by line (4′-1) in Figure (3.4). Valve (VA) establishes a connection between ABU1 and ECU1 during this process. Additionally, valves (V_9 and V_{11}) are opened to allow chilled water to flow into the storage tank. Valves (V_2 and V_4) remain open to enable the water to flow from the source. Furthermore, the chilled and cold-water pumps are activated, as depicted in Figure (3.3 e). When the valve (V_A) is opened, the liquid refrigerant pressure in the ECU_1 suddenly decreases, causing it to transition from condenser pressure to evaporator pressure. This process is similar to the throttling of the refrigerant in the expansion valve.

Consequently, the liquid refrigerant undergoes boiling within the ECU_1, followed by evaporation, subsequent movement, and adsorption within the ABU_1. The process depicted in Figure (3.4) is referred to as evaporation. The final step of ATB_2 includes an isobaric process line (2'-3), as depicted in Figure (3.4), which occurs when the pressure of ABU_2 approaches the condensing pressure. The valve (V_B) that establishes a connection between the ABU_2 and ECU_2 and the valves (V14 and V16) that connect to the hot storage tank are opened. Additionally, valves (V_5 and V_7) are left in an open position, and the condenser pump and hot water pump are activated, as depicted in Figure (3.3 e).

Consequently, the refrigerant undergoes desorption at a constant pressure. The refrigerant vapor changes phase as it transitions from the ABU_2 to the ECU_2. This condensation process occurs through the utilization of water flow within the heat exchanger, resulting in the collection of the condensed refrigerant in the ECU_2. This process continues until the entirety of the refrigerant vapor undergoes condensation. The process depicted in Figure (3.4) is referred to as condensation.

Based on the previous five-step procedure for the ATB system, it can be concluded that the ATB includes three primary procedures. The first involves the discharging of the ATB, wherein heat is introduced to the ABU while simultaneously expelling heat from the ECU into the surrounding environment. The second fundamental procedure involves charging the ATB system, wherein thermal energy is taken from the cold compartment and then released by the working fluid circulating through the ABU. The final is the mass recovery process, in which the pressures of ABU_1 and ABU_2 become equal and support the charging and discharging process.

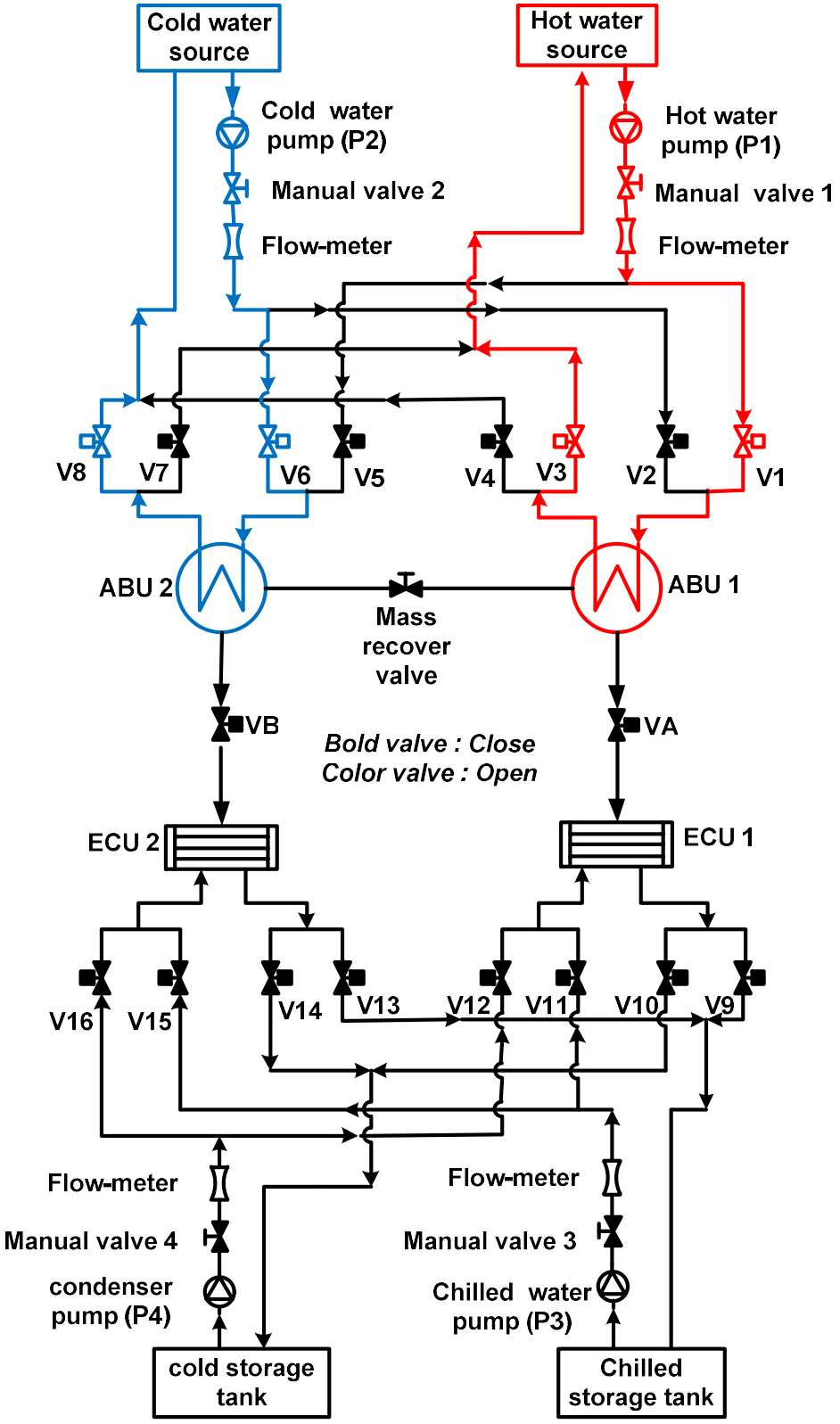

Figure (3.3 a) Heating Bed 1 and cooling bed 2.

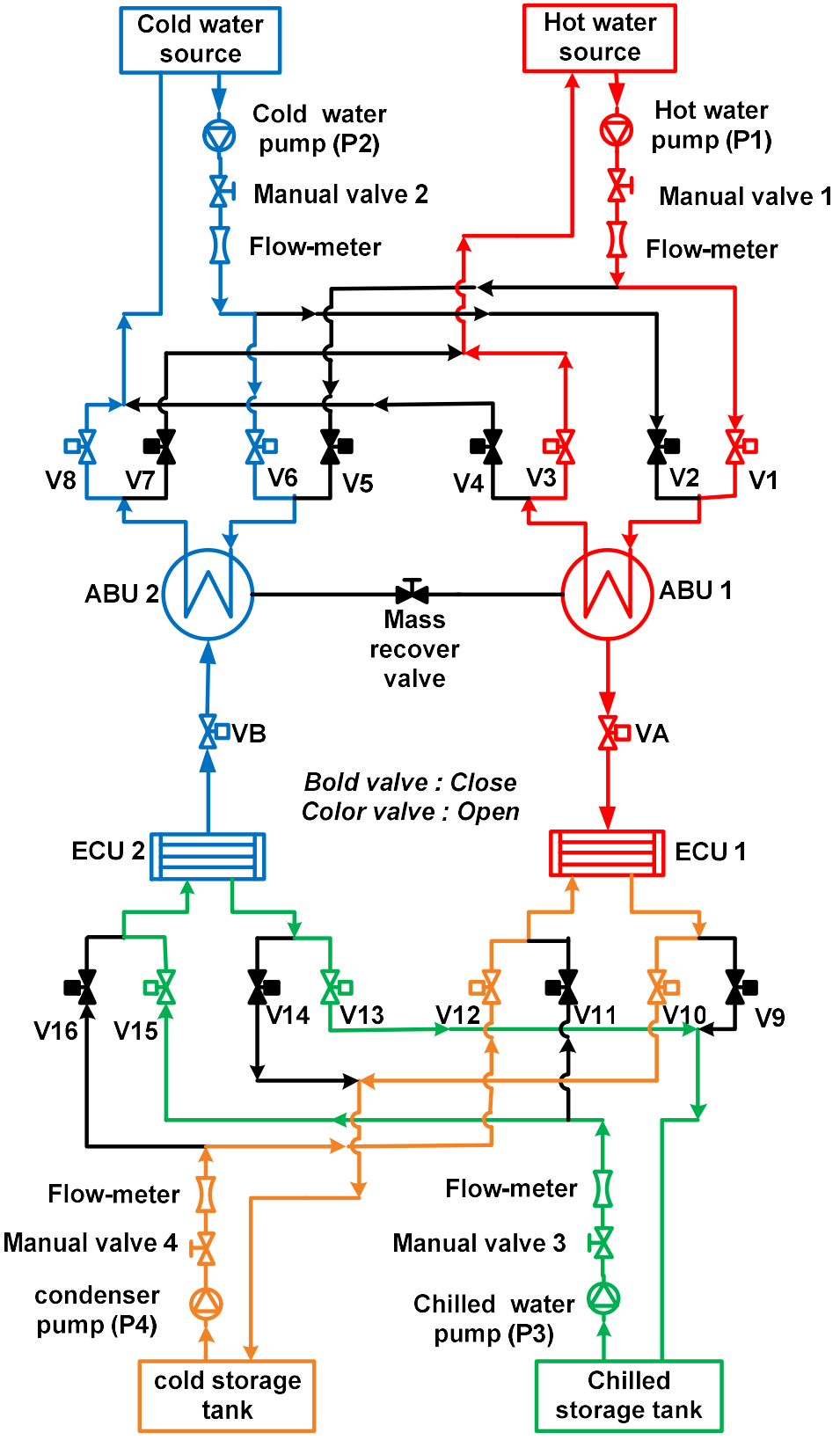

Figure (3.3 b) Chilling water at bed 2 and condensate refrigerant at bed 1.

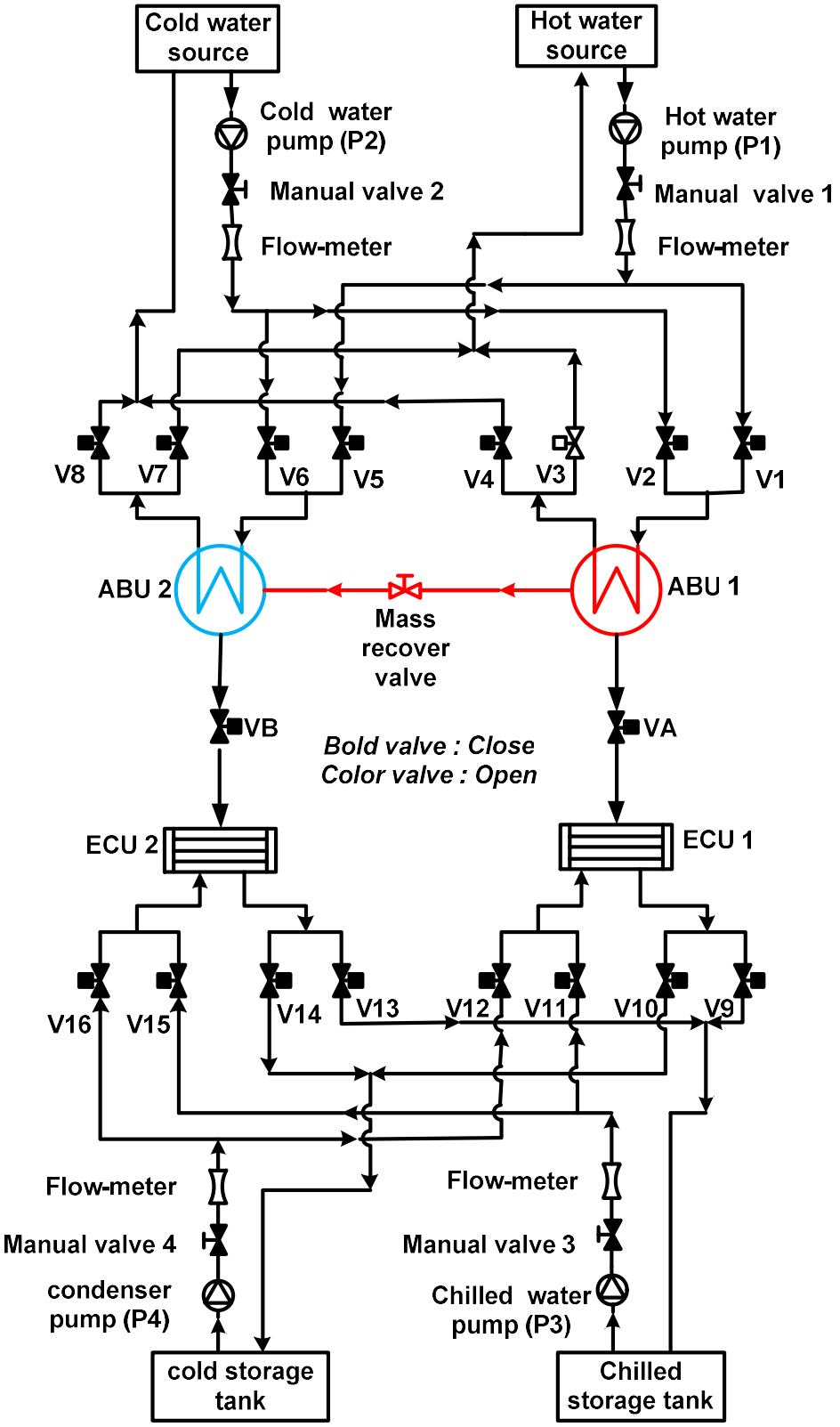

Figure (3.3 c) Mass recovery.

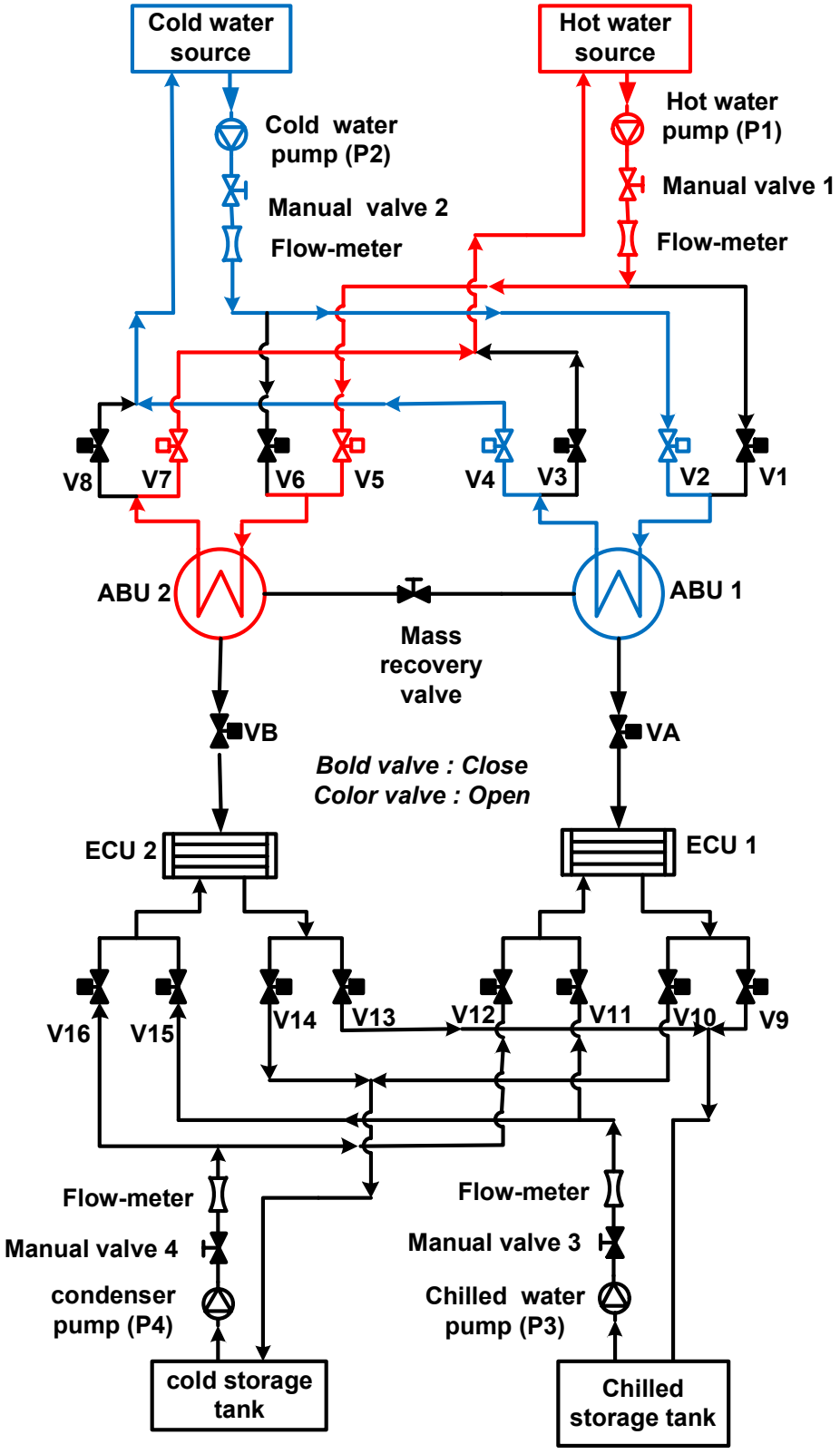

Figure (3.3 d) Heating bed 2 and cooling bed 1.

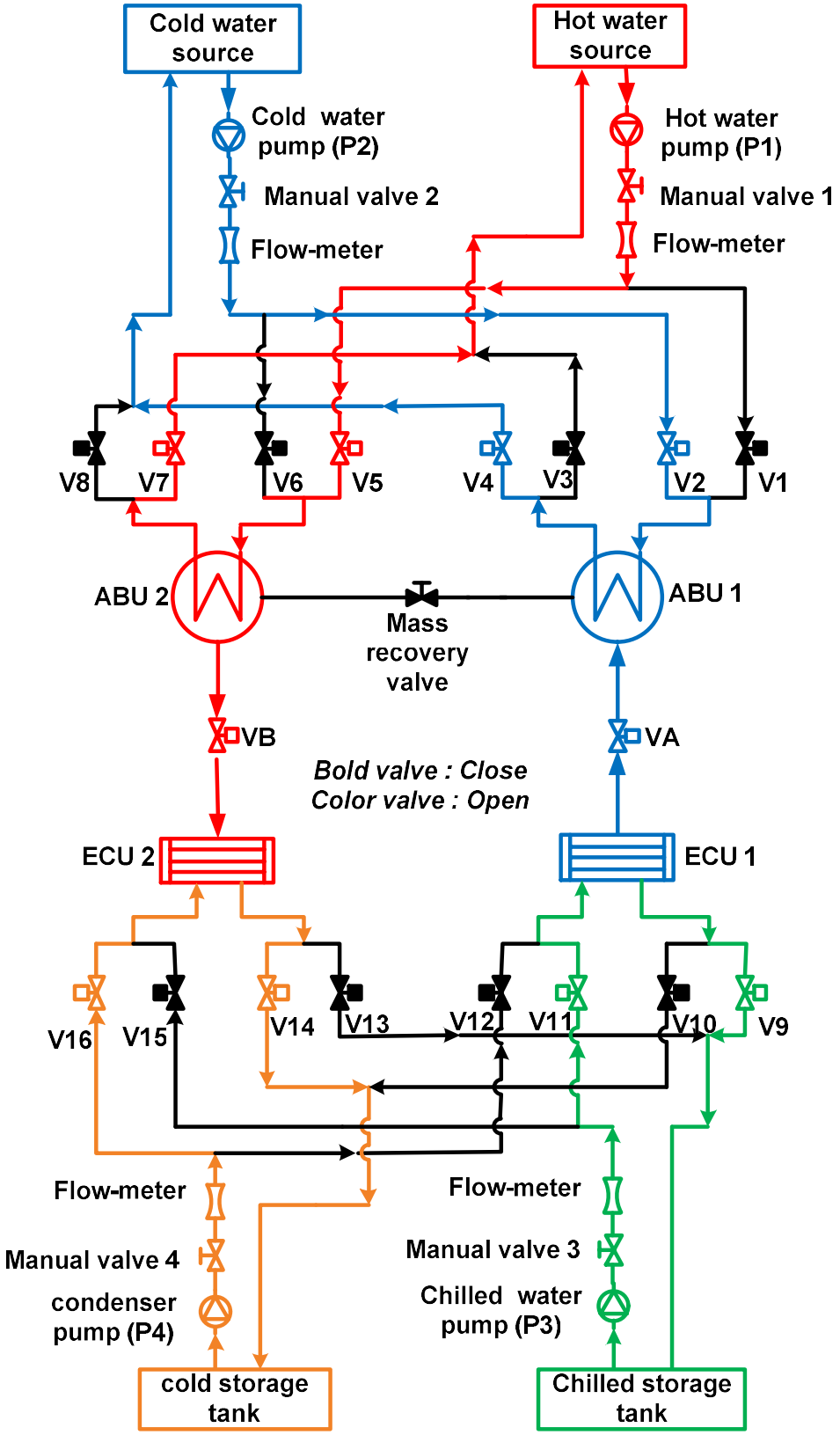

Figure (3.3 e) Chilling water at bed 1 and condensate refrigerant at bed 2.

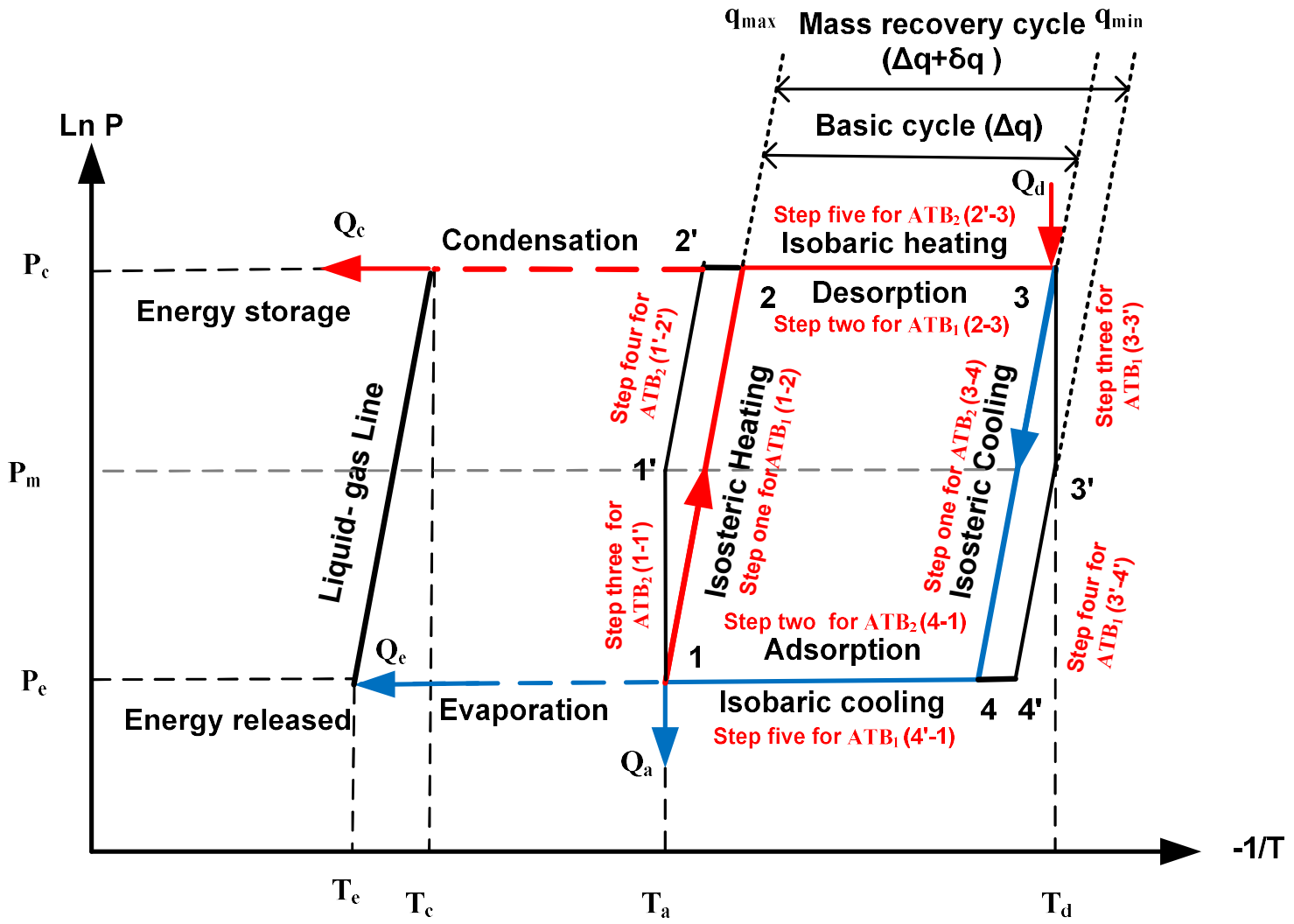

Figure (3.4) Clapeyron diagram (ln P vs. -1/T) of adsorption thermophysical battery with mass recovery.

3.3 Adsorption Uptake Equilibrium

The modeling methodologies for the ATB involve utilizing several parameters such as the charge and discharge processes, working pressure, adsorbent temperature, working pairs, surface area, and reactivity of the adsorbent. The adsorption process is quantitatively explained by many equilibrium equations such as the Dubinin, Langmuir, Freundlich, and others [118].

Equilibrium adsorption uptake refers to the amount of refrigerant accumulated within adsorbent particles once equilibrium has been reached. The determination of the equilibrium adsorption isotherm can be achieved by the utilization of many models, such as the Freundlich model [119], [120] the Dubinin-Astakhov model [121] - [123], and the Modified Freundlich model [124] - [130].

A modified Freundlich model is used to calculate the equilibrium adsorption isotherm. Equilibrium adsorption is the term used to describe the amount of refrigerant stored in solid adsorbent pores at equilibrium. These models account for the effect of the partial pressure between the refrigerant-adsorbent materials and the linked heat exchanger ECU/evaporator or condenser. Freundlich isotherm applies to adsorption processes that occur on heterogonous surfaces. The formula of this isotherm indicates the quantity capacity of surface heterogeneity, the exponential distribution of active sites, and their corresponding energy levels. The adsorption isotherms of the RD silica gel-water pair are shown in the modified Freundlich model by Saha et al. (S-B-K). Modified Freundlich (S-B-K) estimate q^* depending on the temperature for adsorption materials with surface area and pore volume [131].

$$q^* = A(T_{sat}) \left(\frac{P_{sat}(T_{ref})}{P_{sat}(T_{ads})} \right)^{B(T_{ads})} \quad (3\text{-}1)$$

Where

q^*: amount of water vapor uptake (kg_{ref}/kg_{ads})

P_{sat} : saturated vapor pressure (kPa)

T_{ref} : refregerante temperature (K)

T_{ads} : adsorbent temperature (K)

Because the equilibrium uptake q* has dimensions, it follows that the coefficients $A(T_{sat})$, $B(T_{ads})$, A_0, A_1, A_2, A_3, B_0, B_1, B_2, and B_3 are also dimensionless. The constants employed in the S-B-K are as follows:

$$A(T_{sat}) = A_0 + A_1(T_{sat}) + A_2(T_{sat})^2 + A_3(T_{sat})^3 \quad (3\text{-}2)$$

$$B(T_{ads}) = B_0 + B_1(T_{ads}) + B_2(T_{ads})^2 + B_3(T_{ads})^3 \quad (3\text{-}3)$$

$A_0 = -6.5314$, $A_1 = 0.072452$, $A_2 = -0.23951\times10^{-3}$, $A_3 = 0.25493\times10^{-6}$

$B_0 = -15.587$, $B_1 = 0.15915$, $B_2 = -0.50612\times10^{-3}$, $B_3 = 0.5329\times10^{-6}$

The adsorption isotherms of the MOF -801 / water pair are developed by the Langmuir analogy [132]

$$q^* = q^o \frac{K^*(P/P_S)^{m^*}}{1+(K^*-1)(P/P_S)^{m^*}} \quad (3\text{-}4)$$

$$K^* = \alpha * e^{\frac{m^*\left(Q_{st}^*-h_{fg}\right)}{R*T}} \quad (3\text{-}5)$$

Where

K^* : Langmuir coefficient

α: pre-exponential coefficient (isotherm model), $\alpha = 4.54 * 10^{-3}$

m^* : heterogeneity parameter, $m^* = 3.2$

Q_{st}^* : isosteric heat of adsorption in Henry's region, Q_{st}^* =3132.5 (kJ/kg)

h_{fg} : latent heat of vaporization, (kJ/kg)

R: gas constant, (kJ/kgK)

T: temperature, (K)

P: pressure, (kPa)

P_s: saturated pressure, (kPa)

q^o: limiting uptake, $q^o = 0.31$ (kg_{ref}/kg_{ads})

3.4.Adsorption Kinetics and Isotherms

Solid adsorbents like silica gel and MOF undergo time-dependent adsorption and desorption processes. The linear driving force model, initially proposed by Gleuckauf and Coates [133], [134], is a suitable approach for determining the adsorption and desorption rate due to its analytical nature, simplicity, and physical uniformity, as noted by Chihara and Suzuki [135]. The adsorption equilibrium equations were reviewed by Ramy et al. [136], and Wang and Xuan [137] derived the adsorption kinetic solution method. Isotherms and kinetics are the two approaches that are mainly used to calculate the capacity of adsorbent materials. The term "adsorption isotherm" refers to the maximum amount of refrigerant that can be absorbed for each dry kilogram of the solid adsorbent. Kinetics is the rate at which the solid adsorbent will adsorb or desorb the refrigerant at that pressure ratio. The instantaneous adsorption uptake (dynamic adsorption) during the discharge and charge processes for solid adsorbent are as follows [74]:

$$\left(\frac{dq}{dt}\right)_{ads} = \frac{q^* - q}{t_{ads}} \tag{3-6}$$

$$\left(\frac{dq}{dt}\right)_{des} = \frac{q^* - q}{t_{des}} \tag{3-7}$$

The determination of the diffusion time for adsorption and desorption can be accomplished by [74]:

$$t_{ads} = \frac{R_p^2}{15 \ _{so} exp\left(-\frac{E_a}{R_u T_{ads}}\right)} \tag{3-8}$$

$$t_{des} = \frac{R_p^2}{15 \ _{so}exp\left(-\frac{E_a}{R_u T_{des}}\right)} \quad (3\text{-}9)$$

Where:

$\frac{dq}{dt}$: The instantaneous adsorption uptake observed throughout the adsorption and desorption process. (kg_{ref} /kg_{ads} sec).

t_{ads}, t_{des}: Diffusion time for adsorption and desorption (sec).

q^*: Equilibrium uptake (kg_{ref} /kg_{ads}).

D_{so}: Diffusion coefficient (m^2 /sec).

E_a: Activation energy (kJ/ kg).

R_p: Radius of solid adsorbent particle (m).

R_u: Universal gas constant (kJ /kg K).

T: Temperature (K).

k_o: Empirical constant (1/s).

Table (3.1) presents the consistent characteristics of adsorbate materials, whereas the properties of water were approximated using Engineering Equation Solver (EES) software [138].

Table (3.1) Constant properties of adsorbate materials.

Properties \ Materials		Silica gel RD [73], [112], [136], [139], [140]	MOF-801 [132], [141] - [144]
h_{ads}	The heat of adsorption (kJ/kg)	2760	3132.5
Cp	Specific heat (kJ/kg K)	0.924	0.76
K	Thermal conductivity (W/m K)	0.198	0.167
ρ	Density (kg/m^3)	761	1400
E_a	Activation energy (J/kg)	$2.33*10^6$	$3.153*10^4$
D_{so}	Surface specific heat (m^2/s)	$2.54*10^{-4}$	$1.305*10^{-10}$

R_p	The radius of partials (m)	$3*10^{-4}$	$5*10^{-7}$
q_{max}	Maximum uptake (kg_{ref}/kg_{ads})	0.4	0.4
BET	Specific surface area (m^2/g)	720	948

3.5. Overall Heat Transfer Coefficient

The determination of the total heat transfer coefficient (U) in ABU and ECU is dependent upon various factors, including the properties of the adsorbent material, the heat associated with adsorption and desorption processes, the heat involved in evaporation and condensation, the mass flow rate of both the heating and cooling coolants, the logarithmic mean temperature difference (LMTD), and the surface area of both the ABU and ECU [74]. The overall heat transfer coefficient in the ABU/discharge process ($U_{ABU,\ des}$) is greater than that for the ABU/charge process ($U_{ABU,\ ads}$) due to the more minor logarithmic mean temperature differences ($LMTD_{des}$) compared to the logarithmic mean temperature differences ($LMTD_{ads}$). Furthermore, it should be noted that the overall heat transfer coefficient in the ECU/evaporator ($U_{ECU,\ evap}$) is significantly lower than its counterpart in the ECU/condenser ($U_{ECU,\ cond}$) because the logarithmic mean temperature difference in the evaporator ($LMTD_{evap}$) is lower than the logarithmic mean temperature difference in the condenser ($LMTD_{cond}$) [74]. The determination of the overall heat transfer coefficient in ATB involves the utilization of correlations for heat transfer coefficient [145] - [149]. ABU's overall heat transfer coefficient during the charge-adsorption processes is measured using a specific method.

$$U_{ABU,ads} = \frac{Q_{cw}}{A_{ABU} LMTD_{ads}} \tag{3-10}$$

Where:

$$LMTD_{ads} = \frac{\Delta T_1 - \Delta T_2}{ln\frac{\Delta T_1}{\Delta T_2}}, \quad \Delta T_1 = T_{cw,in} - T_{ads}, \ \Delta T_2 = T_{cw,out} - T_{ads}$$

The calculation of the overall heat transfer coefficient in the ABU during the discharge-desorption operations is performed using the following method:

$$U_{ABU,des} = \frac{Q_{hw}}{A_{ABU} LMTD_{des}} \quad (3\text{-}11)$$

Where:

$$LMTD_{des} = \frac{\Delta T_1 - \Delta T_2}{ln\frac{\Delta T_1}{\Delta T_2}}, \quad \Delta T_1 = T_{hw,in} - T_{des}, \ \Delta T_2 = T_{cw,out} - T_{des}$$

The calculation of the overall heat transfer coefficient in the ECU/evaporator is determined by the following method:

$$U_{ECU,evap} = \frac{Q_{ch}}{A_{ECU} LMTD_{evap}} \quad (3\text{-}12)$$

Where:

$$LMTD_{evap} = \frac{\Delta T_1 - \Delta T_2}{ln\frac{\Delta T_1}{\Delta T_2}}, \quad \Delta T_1 = T_{ch,in} - T_{evap}, \ \Delta T_2 = T_{ch,out} - T_{evap}$$

The determination of the overall heat transfer coefficient in the ECU/condenser is accomplished by:

$$U_{ECU,cond} = \frac{Q_{cw,cond}}{A_{ECU} LMTD_{cond}} \quad (3\text{-}13)$$

Where:

$$LMTD_{cond} = \frac{\Delta T_1 - \Delta T_2}{ln\frac{\Delta T_1}{\Delta T_2}}, \Delta T_1 = T_{cw,cond,in} - T_{cond}, \Delta T_2 = T_{cw,cond,out} - T_{cond}$$

3.6.Thermal Resistances Analysis

The temperature difference between the ABU (adsorbent material, heat exchanger fins, and tube) and the coolant fluid is produced by many thermal resistances. These thermal resistances may vary depending on the ABU heat exchanger design and affect the ATB's performance.

3.6.1. Thermal Resistances of ABU

ATB performance is increased by increasing the total heat transfer coefficient and heat transfer area for solid adsorbent materials packed in ABU heat exchangers. Figure (3.5) displays the thermal resistance network of the ABU components. Tables (A-1) and (A-2) in Appendix A show the thermal resistance values for the adsorption and desorption processes. The general formula for the overall heat transfer coefficient of the adsorption and desorption (UA_{ABU}) is given by:

$$UA_{ABU} = \frac{1}{\sum R} \tag{3-14}$$

The convective, conduction, contact, radial, and axial thermal resistances are as follows:

The convective thermal resistance for the inlet coolant fluid:

$$R_{conv} = \frac{1}{h_{in}A_{in}} \tag{3-15}$$

Conduction thermal resistance in the tube wall:

$$R_{cond} = \frac{ln\left(\frac{OD}{ID}\right)}{2\pi K_t L_t} \tag{3-16}$$

Contact thermal resistance between the adsorbent and the outer wall surface of the tube [150] - [153]:

$$R_{cont.} = \frac{R_{contact}}{A_{fin}} \tag{3-17}$$

Where:

h_{in} : inner heat transfer coefficient (W/m^{2}K)

A_{in}: inner heat transfer area (m^2)

ID: inside diameter of the tube (m)

OD: outside diameter of the tube (m)

L_t : length of the tube (m)

k_t: thermal conductivity of tube (W/mK)

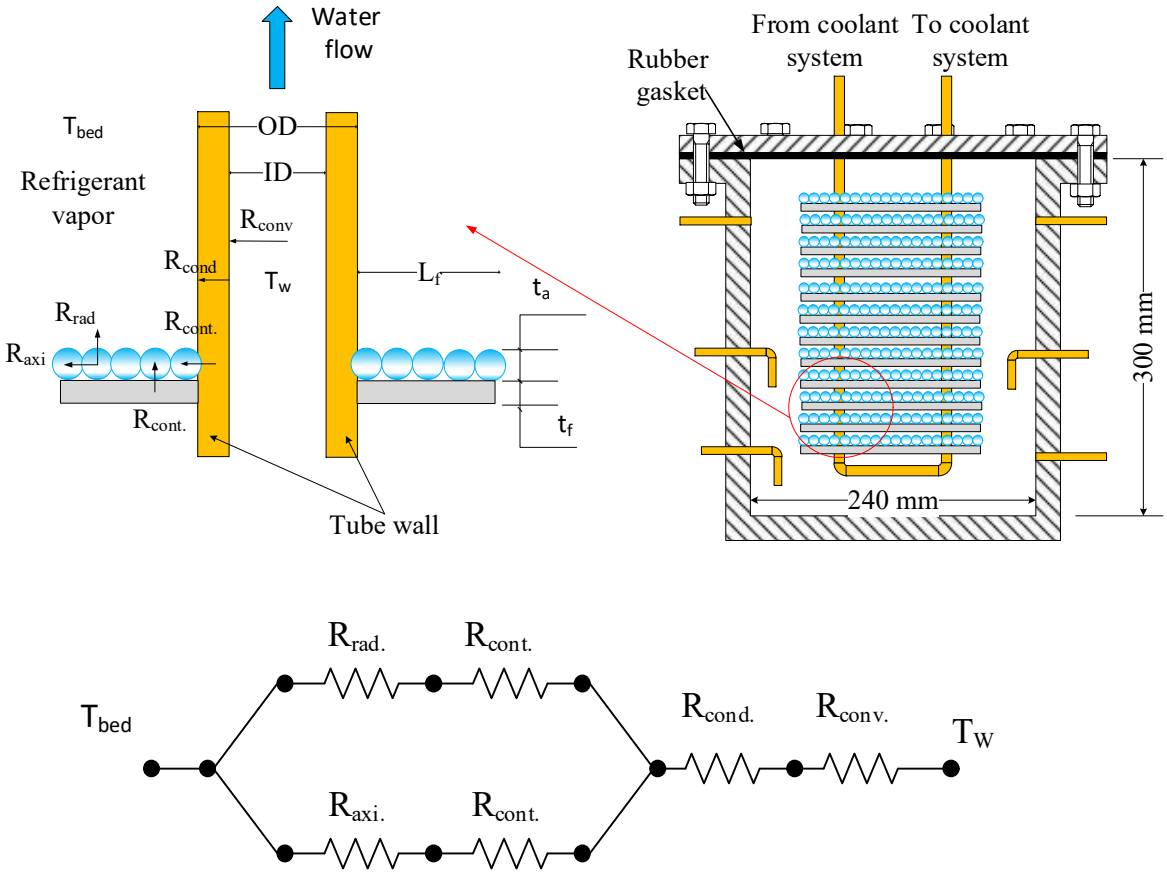

Figure (3.5) Adsorber bed geometry and thermal resistance network.

Thermal contact resistance between solid adsorbent and fin:

$$R_{cont.} = \frac{R_{contact}}{\pi D_{fin}\, t_{ads}} \tag{3-18}$$

Radial and axial thermal resistance between solid adsorbents is as follows:

$$R_{rad} = \frac{x_{ads}}{A_{fin} K_{ads}} \tag{3-19}$$

$$R_{axi} = \frac{ln\left(\frac{D_{fin}}{D_{ads}}\right)}{2\pi K_{ads} L_{fin}} \tag{3-20}$$

The inner and outer surface area of the tube is as follows:

$$A_{in} = \pi . ID . L_t \quad (3\text{-}21)$$

$$A_{out} = \pi . OD . L_t \quad (3\text{-}22)$$

The surface area of the fin, which comes in contact with solid adsorbent, is as follows:

$$A_{fin} = \frac{\pi}{4} D_{fin}^2 \quad (3\text{-}23)$$

The diameter and radius of the solid adsorbent and fin are as follows:

$$D_{ads} = 2R_p\,, \quad D_{fin} = 2\,r_{fin}\,, \quad (3\text{-}24)$$

The contact thermal resistance of the fin at the outer surface of the tube is the following [152], [154]:

$$R_{contact} = \frac{1}{\left[\frac{1}{L_t}\left[\frac{A_c}{A}\frac{(2K_t K_{ads})}{K_t + K_{ads}} + \frac{A_v}{A} K_{fin}\right]\right]} \quad (3\text{-}25)$$

Where:

x_{ads} : thickness of adsorbent (m)

D_{fin}: fin diameter (m)

R_p: The radius of the adsorbent partials (m)

K_{fin} : thermal conductivity of fins (W/mK)

K_{ads} : thermal conductivity of adsorbent (W/mK)

$\frac{A_c}{A}$ is the contact and void area of the fin [151]

3.6.2. Thermal Resistances of ECU/Condensation

Assume laminar layer condensation occurs when the vapor refrigerant condenses across the horizontal tube [146]. Figure (3.6) shows the thermal network resistances in the condenser, and the parameters of the condenser are indicated in Table (A-3) in Appendix A.

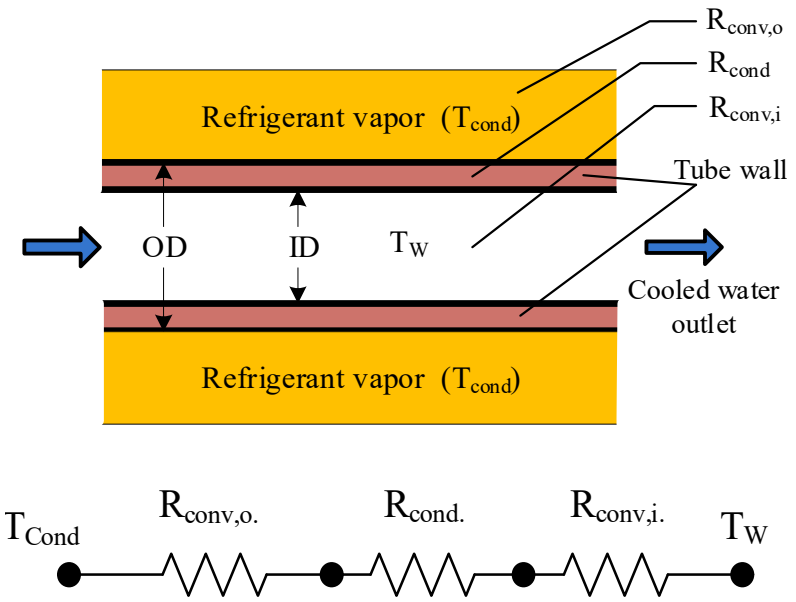

Figure (3.6) Condenser geometry and thermal resistance network.

The overall heat transfer coefficient of the condenser at (UA_{cond}) is calculated by:

$$UA_{cond} = \frac{1}{\sum R} = \frac{1}{R_{conv,i}+R_{cond}+R_{conv,o}} \quad (3\text{-}26)$$

The convective and conduction resistances are as follows:

$$R_{conv,i} = \frac{1}{h_{in}A_{in}} \quad (3\text{-}27)$$

$$R_{cond} = \frac{ln\left(\frac{OD}{ID}\right)}{2\pi K_t L_t} \quad (3\text{-}28)$$

$$R_{conv,o} = \frac{1}{h_{out}A_{out}} \quad (3\text{-}29)$$

The inner and outer surface areas for the tube are determined as follows:

$$A_{in} = \pi . ID . L_t \quad (3\text{-}30)$$

$$A_{out} = \pi . OD . L_t \quad (3\text{-}31)$$

The mean temperature for chilled water is as follows:

$$T_{m,coolant} = \frac{T_{coolant,in}+T_{coolant,out}}{2} \quad (3\text{-}32)$$

The following equation calculates the typical liquid refrigerant heat transfer coefficient; all properties are taken at T_{cond} [155], [156].

$$h_{out} = 0.729 \left[\frac{g\rho_{ref,liq}(\rho_{ref}-\rho_{ref,vap})K^3_{ref,liq}h^-_{ref,fg}}{N_{tube}\mu_{ref}(T_{ref,sat}-T_{m,coolant})OD_{cond}}\right]^{\frac{1}{4}} \quad (3\text{-}33)$$

The modified latent heat $h^-_{ref,fg}$ by Rohsenow equal:

$$h^-_{ref,fg} = h_{fg} + 0.8\, Cp_{vap}\left(T_{ref,sat} - T_{m,coolant}\right) \quad (3\text{-}34)$$

3.6.3. Thermal Resistances of ECU/Evaporation

The liquid refrigerant evaporates at the pool boiling area due to the temperature difference between the tube wall and the refrigerant pool, which is lower than 30 °C. Figure (3.7) shows the resistances in the flooded evaporator, and the parameters of the evaporator are illustrated in Table (A-4) in Appendix A.

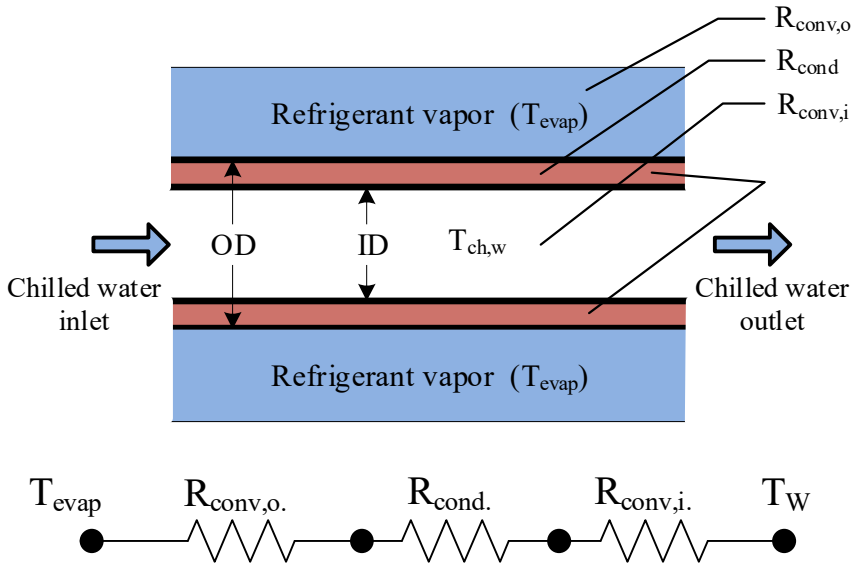

Figure (3.7) Evaporator geometry and thermal resistance network.

The expression indicating the overall heat transfer coefficient of the evaporator, denoted as UA_{evap}, can be stated as follows:

$$UA_{evap} = \frac{1}{\sum R} = \frac{1}{R_{conv,i}+R_{cond}+R_{conv,o}} \quad (3\text{-}35)$$

Convective thermal resistance in the chilled water is as follows:

$$R_{conv,i} = \frac{1}{h_{in}A_{in}} \quad (3\text{-}36)$$

Conduction thermal resistance in the tube wall is as follows:

$$R_{cond} = \frac{ln\left(\frac{OD}{ID}\right)}{2\pi k_t L_t} \quad (3\text{-}37)$$

Convective thermal resistance in the liquid refrigerant is as follows:

$$R_{conv,o} = \frac{1}{h_{out} A_{out}} \quad (3\text{-}38)$$

The inner and outer surface area for the tube is as follows:

$$A_{in} = \pi . ID . L_t \quad (3\text{-}39)$$

$$A_{out} = \pi . OD . L_t \quad (3\text{-}40)$$

The mean temperature for chilled water is as follows:

$$T_{m,ch} = \frac{T_{ch,in} + T_{ch,out}}{2} \quad (3\text{-}41)$$

The average heat transfer coefficient for liquid refrigerant in the evaporator can be calculated by [157]:

$$h_{out} = \frac{\mu_{ref}\, h_{fg,ref}}{\Delta T_{evap}} \left[\frac{g\left(\rho_{ref,liq} - \rho_{ref,vap}\right)}{\sigma}\right]^{\frac{1}{2}} \left[\frac{Ja_{ref}}{C_f Pr_{liq}}\right]^3 \quad (3\text{-}42)$$

Where the Jacquard number Ja_{ref} It is equal to:

$$Ja_{ref} = \frac{Cp_{ref,liq}\, \Delta T_{evap}}{h_{fg,ref}} \quad (3\text{-}43)$$

Where

μ_{ref} : dynamic viscosity of refrigerant (Pa.sec)

$h_{fg,ref}$: enthalpy of refrigerant (kJ/kg)

$\rho_{ref,liq}$: density of liquid refrigerant (kg/m^3)

$\rho_{ref,vap}$: density of vapor refrigerant (kg/m^3)

g gravitational acceleration (9.81m/sec^2)

σ : surface tension for refrigerant (N/m)

Pr_{liq} : Prandtl number for liquid refrigerant

C_f coefficient of friction

All properties are taken at T_{evap}.

3.6.4. Inner Heat Transfer Coefficient

The following equation determines the convective heat transfer coefficient in the heat exchanger between the coolant fluid (water) and the interior tube surface:

$$h_{in} = \frac{Nu.K_w}{ID} \quad (3\text{-}44)$$

Where :

Nu : the Nusselt number

k_w : water's thermal conductivity (W/mK)

ID : the tube's inner diameter (m)

A Nusselt number is a constant number for laminar flow, single-phase, and constant surface temperature (T_s=const) [145].

For laminar flow (Re < 2300)

$$Nu = 3.66 \quad (3\text{-}45)$$

For turbulent flow (Re>3000), Nu can be calculated using Gnielinski modified correlation [152], [153]. This correlation is valid over a wide range of Re ($3000<Re<5*10^6$) and Prandtl number ($0.5\leq Pr\leq 2000$).

$$Nu = \frac{\left(\frac{f}{8}\right)(Re-1000)Pr}{1+12.7\left(\frac{f}{8}\right)^{0.5}\left(Pr^{2/3}-1\right)} \quad (3\text{-}46)$$

$$Re = \frac{4\dot{m}}{\pi.ID.\mu_w} \quad (3\text{-}47)$$

$$Pr = \frac{\mu_w\, Cp_w}{K_w} \quad (3\text{-}48)$$

The Reynolds number and friction factor are inversely related in laminar flow. The Reynolds number and tube roughness determine a tube's friction factor with internal turbulent flow. The explicit representation of the friction factor [146], [152], [153]:

For laminar flow, Re <3000

$$f = \frac{64}{Re} \quad (3\text{-}49)$$

For turbulent flow, Re >3000

$$\frac{1}{\sqrt{f}} = -1.8\ log\left[\frac{6.9}{Re} + \left(\frac{\frac{\varepsilon}{ID}}{3.6}\right)^{1.11}\right] \quad (3\text{-}50)$$

3.7. Modeling of Heat Exchanger in ABU

Many researchers have offered a theoretical analysis to look into the impact of heat exchanger design and adsorber heat exchanger material on the performance of ABU with working pairs of silica gel and MOF-801 with water [158] - [161]. This section will discuss calculating the metal mass of the heat exchanger and the mass ratio of the adsorber and the adsorbent. Figure (3.8) and Table (3.2) show the design parameters of the heat exchanger, while the preliminary design of modeling the heat exchanger is shown in (Appendix B).

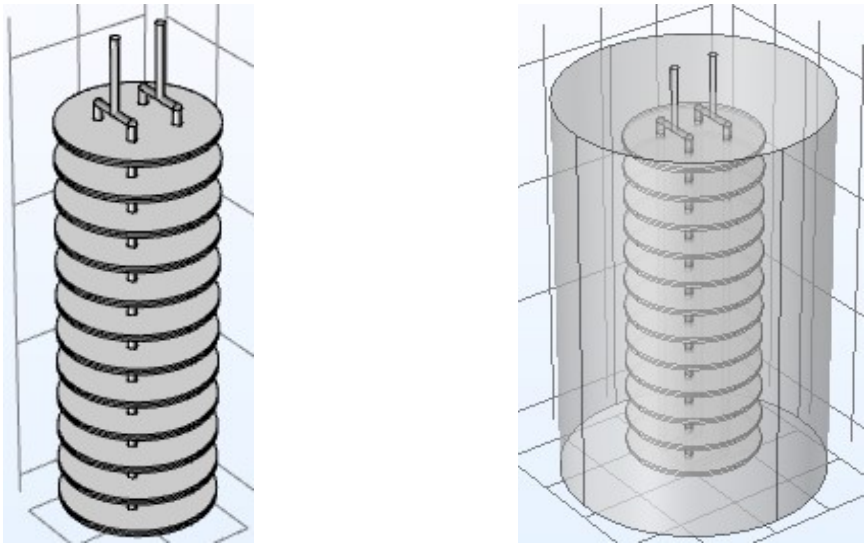

Figure (3.8) Heat exchanger in ABU.

(Table 3.2) Parameter value of ABU heat exchanger

Parameter	symbol	value	unit
Number of fins	N_f	12	-
Fin diameter	D_f	0.1	m

Fin thickness	t_f	0.001	m
Fin space	S	0.02	m
Fin surface area	A_f	0.095	m^2
Fin volume	V_f	0.00018	m^3
Mass of fins	M_f	1.689	kg
Fin material	Copper		
Number of tubes	N_t	4	-
Inner tube diameter	d_i	0.00482	m
Outer tube diameter	d_o	0.00635	m
Length of tubes	L_t	0.264	m
Mass of tubes	M_t	0.1223	kg
Tube material	Copper		
Heat transfer area of ABU	A_{ABU}	0.2135	m^2
Mass of heat exchanger	M_{ABU}	1.811	kg
Layer thickness of the adsorbent	t_{ads}	0.002	m
Silica gel RD density	ρ_{sg}	761	Kg/m^3
Specific heat of Silica gel RD	c_{sg}	0.924	kJ/kgK
Mass of silica gel RD	M_{sg}	0.1315	Kg
Heat capacity ratio of silica gel RD	HCR_{sg}	0.1723	-

3.8. Lumped Parameter Modeling (LPM)

The energy balance equations of the ATB system, including the ABU and ECU, are formulated utilizing the LPM technique as reported in references[139], [162] - [171]. The Log Mean Temperature Difference (LMTD) approach, explained in reference [172], is utilized to calculate the outlet temperatures of the coolant fluid in several heat exchangers, including the adsorber bed, evaporator, and condenser. This approach takes into consideration the following assumptions:

(i) During the desorption and adsorption procedures, the temperature of the working pairs remains constant due to the phase change process.

(ii) It is possible to suppose that the working pairs are uniformly affected by temperature and that average thermophysical characteristics represent effective conductivity.[73],[170].

(iii) The ATB does not lose heat to the surroundings because the ABU and ECU are well insulated.

(iv) The ABU and ECU assume that the metal heat exchanger's thermal characteristics remain constant with temperature due to minimal temperature differences.

(v) The operating conditions of the ABU, including temperature, pressure, and adsorption uptake or desorption offtake, are in an unsteady state due to mass transfer.

3.8.1. ABU's Energy Balance During the Adsorption Processes

During the process of charging, the energy equation for the ABU is as follows:

$$\left(Q_{ads} + Q_{HE} + Q_{ABU,ads}\right)\frac{dT_{ads}}{dt} = Q_{st}\frac{dq_{ads}}{dt} + Q_{cw} \tag{3-51}$$

$$\left[(M_{ads}.Cp_{ads}) + \left(M_{HE,ABU}.Cp_{HE,ABU}\right) + \left(M_{ads}.Cp_{ref,v}\right)q_{ads}\right]\frac{dT_{ads}}{dt} =$$

$$(M_{ads}.H_{st})\frac{dq_{ads}}{dt} + (\dot{m}\,.Cp)_{cw}\left(T_{cw,in} - T_{cw,out}\right) \tag{3-52}$$

The following is an expression for the cooling water outlet temperature from ABU:

$$T_{cw,out} = T_{ads} + \left(T_{cw,in} - T_{ads}\right)exp\left[\frac{-UA_{ABU,ads}}{(\dot{m}\,.Cp)_{cw}}\right]_{ABU,ads} \tag{3-53}$$

The following is an expression that can be used to estimate the rate of heat transfer:

$$Q_{cw} = (\dot{m}\,.Cp)_{cw}\left(T_{cw,in} - T_{cw,out}\right) \tag{3-54}$$

Where:

M_{ads}: Mass of adsorbent material (kg).

Cp_{ads}: Specific heat of adsorbent material (kJ/kg.K).

M_{HE}: Mass of heat exchanger in the ABU (kg).

Cp_{HE}: Specific heat for heat exchanger material in the ABU (kJ/kg.K).

$Cp_{ref,v}$: Specific heat for vapor refrigerant (kJ/kg.k).

q_{ads}: Instantaneous adsorption uptake (kg_{ref}/kg_{ads}).

$\frac{dT_{ads}}{dt}$: Temperature gradient with time during the charging process (K/sec).

H_{st}: Iso-steric heat of adsorption (depend on adsorbent material type) (kJ/kg).

$\frac{dq_{ads}}{dt}$: Instantaneous adsorption uptake during the charge (kg_{ref}/kg_{ads}.sec).

$(\dot{m}\,.\,Cp)_{cw}$: Heat capacity for coolant flow in the heat exchanger in ABU (kW/K).

$T_{cw,\ in}$ and $T_{cw,\ out}$: Inlet and outlet temperatures from coolant unit to ABU (K).

Q_{ads}: Energy capacity of solid adsorbent (kJ/K).

Q_{HE}: Energy capacity of heat exchanger in the ABU (kJ/K).

$Q_{ABU,\ ads}$: Energy capacity of ABU (kJ/K).

Q_{st}: Energy capacity of adsorption heat (kJ/K).

Q_{cw}: Heat was rejected from the heat exchanger in the ABU by cooling coolant (kW).

$U_{ABU,\ ads}$: Overall heat transfer coefficient (kW/m^2 .K).

A_{ABU}: Surface area for ABU (m^2).

T_{ads}: ABU temperature (K).

The subscripts (ads), (des), (HE), (w), (c), and (ref) are adsorption, desorption, heat exchanger, water, cooling, and refrigerant, respectively.

3.8.2. ABU's Energy Balance During the Desorption Processes

During the process of discharging, the energy equation for the ABU is as follows:

$$\left(Q_{ads} + Q_{HE} + Q_{ABU,des}\right)\frac{dT_{des}}{dt} = Q_{hw} \qquad (3\text{-}55)$$

$$\left[(M_{ads}.Cp_{ads}) + (M_{HE}.Cp_{HE,ABU}) + (M_{ads}.Cp_{ref,v})q_{des}\right]\frac{dT_{des}}{dt} = (\dot{m}\,.Cp)_{hw}(T_{hw,in} - T_{hw,out}) \quad (3\text{-}56)$$

The following is an expression for the hot water outlet temperature from ABU:

$$T_{hw,out} = T_{des} + (T_{hw,in} - T_{des})exp\left[\frac{-UA_{ABU,des}}{(\dot{m}\,.Cp)_{hw}}\right]_{ABU,des} \quad (3\text{-}57)$$

The following is an expression that can be used to estimate the rate of heat transfer:

$$Q_{hw} = (\dot{m}\,.Cp)_{hw}(T_{hw,in} - T_{hw,out}) \quad (3\text{-}58)$$

Where:

$\frac{dT_{des}}{dt}$: Temperature changes with time during the discharging process (K/sec).

$(\dot{m}\,.Cp)_{hw}$: Heat capacity for hot coolant flow in the heat exchanger of ABU (kW/K).

$T_{hw,\,in}$ and $T_{hw,\,out}$ Inlet and outlet water temperatures from the heating unit to ABU (K).

$Q_{ABU,\,des}$: Energy capacity of ABU during discharge process (kJ/K).

Q_{hw}: Heat supply to the heat exchanger of ABU by heating coolant (kJ/K).

Q_{eh}: Heat is added to the heat exchanger of ABU by an electric heater (kJ/K).

The heater aims to keep the coolant temperature constant during the discharging period.

$U_{ABU,\,des}$: Overall heat transfer coefficient (kW/m^2.K).

The subscript (h) is heating.

3.8.3 ECU's Energy Balance During the Condensation Processes

During the process of condensation, the energy equation for the ECU is as follows:

$$(Q_{cond} + Q_{HE,cond})\frac{dT_{cond}}{dt} = -(Q_{fg,cond} + Q_{des,cond})\frac{dq_{ads}}{dt} + Q_{cw,cond} \quad (3\text{-}59)$$

$$\left[\left(M_{ref}.Cp_{ref}\right)_{cond}+\left(M_{HE,ECU}.Cp_{HE,ECU}\right)\right]\frac{dT_{cond}}{dt}=-\left[M_{sg}.h_{fg,ref}+\left(M_{ads}.Cp_{ref,v}(T_{des}-T_{cond})\right)\right]\frac{dq_{des}}{dt}+(\dot{m}\,.Cp)_{cw,cond}\left(T_{cw,cond,in}-T_{cw,cond,out}\right) \quad (3.60)$$

The following is an expression for the cooled water outlet temperature from ECU:

$$T_{cw,cond,out}=T_{cond}+\left(T_{cw,cond,in}-T_{cond}\right)exp\left[\frac{-UA_{ECU,cond}}{(\dot{m}\,.Cp)_{cw,cond}}\right]_{ECU,des} \quad (3\text{-}61)$$

The following is an expression that can be used to estimate the rate of heat transfer:

$$Q_{cw,cond}=(\dot{m}\,.Cp)_{cw,cond}\left(T_{cw,cond,in}-T_{cw,cond,out}\right) \quad (3\text{-}62)$$

Where:

$M_{ref,\,cond}$: mass of the refrigerant condensate (kg).

$Cp_{ref,\,cond}$: Specific heat of the condenser's refrigerant (kJ/kg.K).

$Cp_{ref,v}$: Specific heat for vapor refrigerant (kJ/kg.K).

T_{des}: Desorption temperature (K).

$\frac{dT_{cond}}{dt}$: Change the condenser temperature with time during the discharge (K/sec).

$(\dot{m}\,.Cp)_{cw,cond}$: Heat capacity of the cooling water flow in the heat exchanger of ECU during the condensation process (kW/K).

$T_{cw,\,cond,\,in}$ and $T_{cw,\,cond,\,out}$ Inlet and outlet temperatures from cooling unit to heat exchanger in ECU during condensation (K).

Q_{cond}: Energy capacity of the condenser (kJ/K).

$Q_{fg,\,cond}$: Capacity of the condensation (kJ/K).

$Q_{des,cond}$: Capacity of ECU/condenser (desorption and condenser) (kJ/K)

$Q_{cw,\,cond}$: Heat rejected from the condenser (kJ/K).

U_{cond}: Overall heat transfer coefficient for the condenser (kW/m^2.K).

A_{ECU}: ECU surface area (m^2).

3.8.4. ECU's Energy Balance During the Evaporation Processes

During the process of evaporation, the energy equation for the ECU is as follows:

$$\left(Q_{evap} + Q_{HE,evap}\right)\frac{dT_{evap}}{dt} = -\left(Q_{fg,evap} + Q_{ECU}\right)\frac{dq_{ads}}{dt} + Q_{ch} \quad (3\text{-}63)$$

$$\left[\left(M_{ref}.Cp_{ref}\right)_{evap} + (M.Cp)_{HE,ECU}\right]\frac{dT_{evap}}{dt} = -\left[M_{ads}.h_{fg,ref} + \left(M_{ads}.Cp_{ref,liquid}\left(T_{cond} - T_{evap}\right)\right)\right]\frac{dq_{ads}}{dt} + (\dot{m}\,.Cp)_{ch,w}\left(T_{ch,in} - T_{ch,out}\right) \quad (3\text{-}64)$$

The following is an expression for the chilled water outlet temperature from ECU:

$$T_{ch,out} = T_{evap} + \left(T_{ch,in} - T_{evap}\right)exp\left[\frac{-UA_{ECU,evap}}{(\dot{m}\,.Cp)_{ch}}\right]_{ECU,ads} \quad (3\text{-}65)$$

The following is an expression that can be used to estimate the rate of heat transfer:

$$Q_{ch} = (\dot{m}\,.Cp)_{ch}\left(T_{ch,in} - T_{ch,out}\right) \quad (3\text{-}66)$$

Where:

$M_{ref,evap}$: Refrigerant mass in the ECU/evaporator (kg).

$h_{fg,\,ref}$: Vaporization latent refrigerant heat (kJ/kg).

$Cp_{ref,\,liquid}$: Liquid refrigerant specific heat (water liquid) (kJ/kg.K).

T_{evap}: Temperature of evaporator (K).

$\frac{dT_{evap}}{dt}$: Evaporator temperature changes with time during the charge (K/sec).

$(m.Cp)_{ch,w}$: Chilled water heat capacity in ECU during evaporation (kW/K).

During the evaporation process, Tch, in, and Tch, out Inlet and outlet temperatures from the chiller unit to the heat exchanger in ECU (K).

Q_{evap}: Energy capacity of the evaporator (kJ/K).

$Q_{HE,evap}$: Energy capacity of heat exchanger in the ECU/evaporator (kJ/K).

$Q_{fg,evap}$: Energy capacity of evaporation (kJ/K).

Q_{ECU}: Energy capacity of ECU (kJ/K).

Q_{ch}: Heat is added to the evaporator (capacity of the ATB) (kW).

$U_{ECU,evap}$: Overall heat transfer coefficient for ECU/ evaporator ($kW/m^2.K$).

3.9 ATB Performance

The performance of the ATB system, which includes cooling refrigeration capacity, COP, and SCP [173] - [178] are described as follows; the variation in RC with time can be expressed as the following [47]:

$$RC = \frac{(\dot{m}.Cp)_{ch}}{t_{cycle}} \int_0^{t_{cycle}} \left(T_{ch,in} - T_{ch,out}\right) dt \quad (3\text{-}67)$$

The COP of the ATB can be expressed by:

$$COP = \frac{(\dot{m}.Cp)_{ch,w} \int_0^{t_{cycle}} (T_{ch,in} - T_{ch,out}) dt}{(\dot{m}.Cp)_{he,w} \int_0^{t_{cycle}} (T_{hw,in} - T_{hw,out}) dt} \quad (3\text{-}68)$$

The SCP of the ATB can be expressed by:

$$SCP = \frac{(\dot{m}.Cp)_{ch,w} \int_0^{t_{cycle}} (T_{ch,in} - T_{ch,out}) dt}{M_{ads}.t_{cycle}} \quad (3\text{-}69)$$

3.10 Solution Procedure for LPM

The adsorption thermophysical battery system comprises two adsorbent bed units and two evaporator/condenser units. A two-bed adsorption thermophysical battery system is a mathematical simulation model for refrigeration and air condition applications. Furthermore, the MATLAB Simulink software solves all of the governing ODE equations of LPM that were previously presented. A customizable set of block libraries and an interactive graphical interface are provided by integrating Simulink with MATLAB to design, simulate, implement, and test various time-varying systems by dragging and dropping blocks from the library browser into the graphical editor and linking them with lines that generate a mathematical relationship between the blocks. It can update the state of each model block at each time step during the evaluation process. Table (3.3) illustrates the features of the two-bed ATB and the physical specifications, characteristics, and operating variables for the LPM. Figure (3.9) presents the model's flow chart; the

model built in Simulink for the two-bed adsorption thermophysical battery system is shown in Figure (3.10) and Appendix C.

(Table 3.3) Operation condition of ATB

Parameter	Value	Unit	Parameter	Value	Unit
M_{ads}	5 - 60 Interval 5	kg	$\dot{m}_{CW,\ ABU}$	0.2 – 2 Interval 0.2	kg/s
M_{ref}	1	L	$\dot{m}_{CW,\ ECU}$	0.2 – 2 Interval 0.2	kg/s
M_{ABU}	1.811	kg	$\dot{m}_{CHW}$	0.1 –1 Interval 0.1	kg/s
M_{ECU}	1.004	kg	$\dot{m}_{HW}$	0.2- 2 Interval 0.2	kg/s
A_{ABU}	0.2135	m^2	$T_{CW,\ in}$	303, 308 and 313	K
A_{ECU}	0.09927	m^2	$T_{HW,\ in}$	343, 353 and 363	K
$UA_{ABU,ads}$	1060	W/m^2K	$T_{CW,cond,in}$	303, 308 and 313	K
$UA_{ABU,\ des}$	1438	W/m^2K	$T_{CH,in}$	288, 293 and 298	K
$UA_{ECU,\ cond}$	5642	W/m^2K	Half cycle time	250 -3000 Interval 250	sec
$UA_{ECU,evap}$	1638	W/m^2K	Switch time	10 – 100 Interval 10	sec
Fin thickness	0.5 – 5 Interval 0.5	mm			

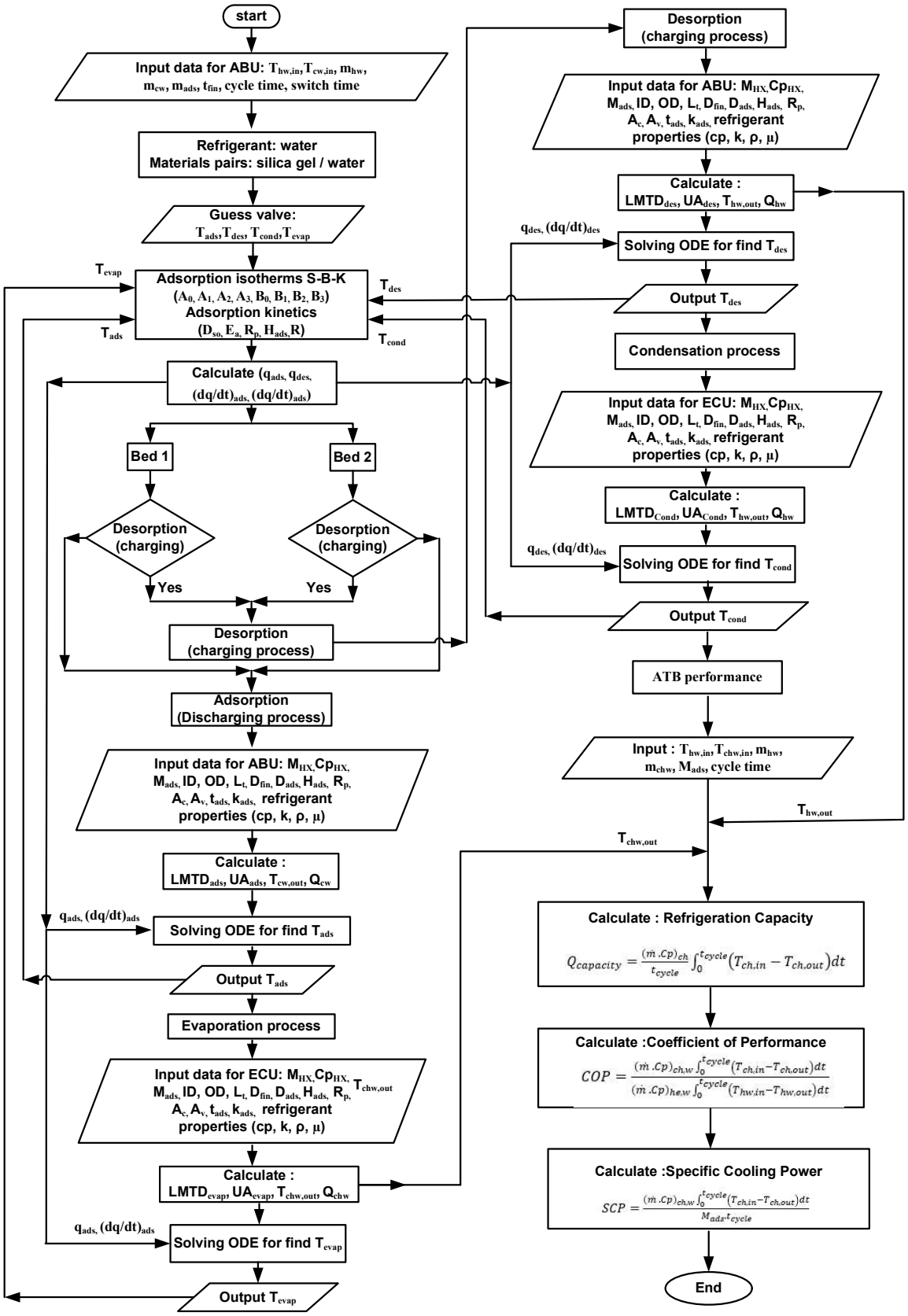

Figure (3.9) Flow chart of the model.

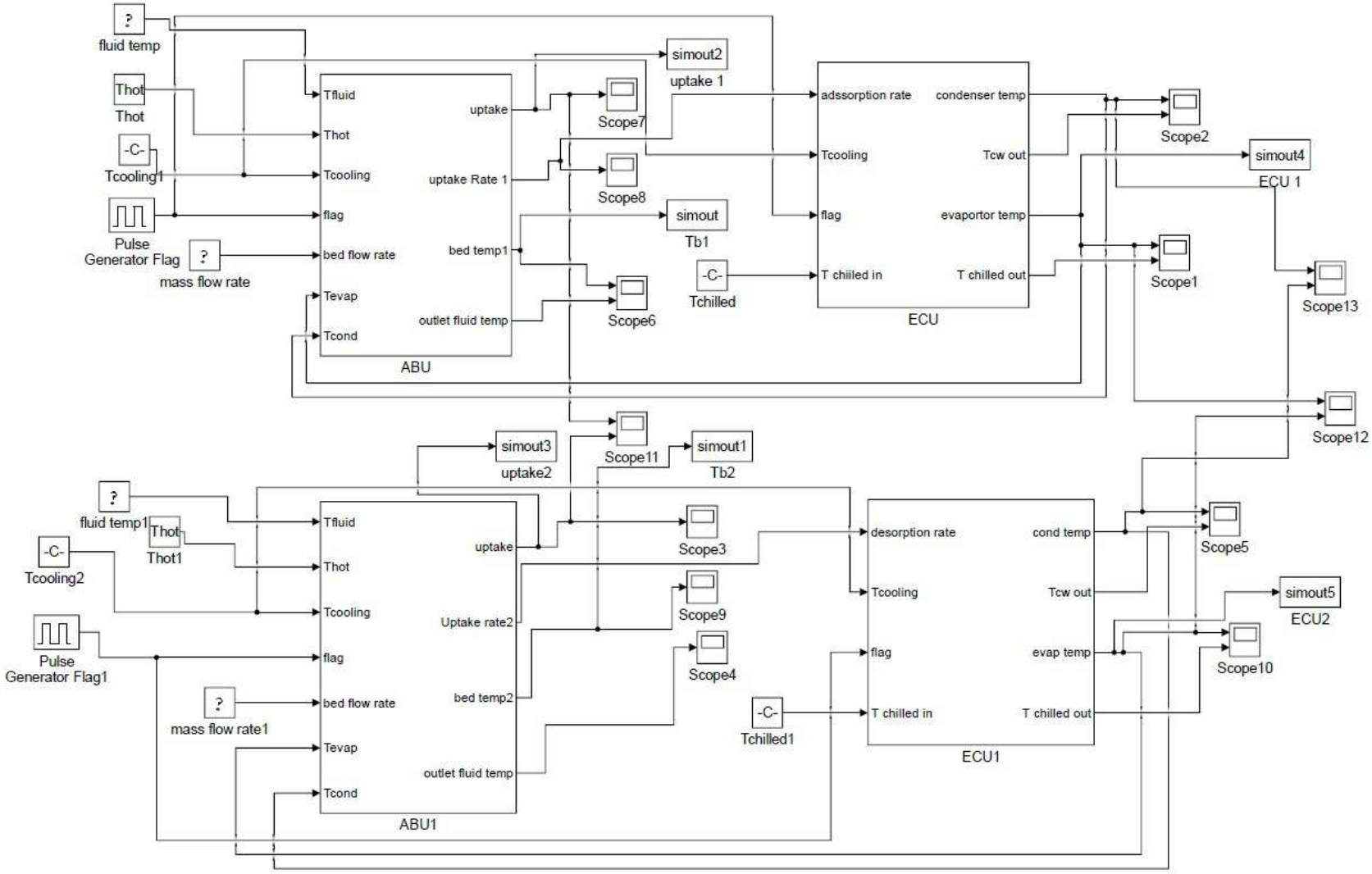

Figure (3.10) Model built in Simulink for the two-bed adsorption thermophysical battery system.

3.11 Numerical Analysis

The heat and mass transfer process within an adsorbent-packed bed is investigated using a transient local thermal equilibrium model. Refrigerant vapor flow in the ABU's heat exchanger, heat transfer from the coolant fluid to the heat exchanger fins and adsorbent, and vapor mass transfer to the adsorbent during the charging process are numerically examined in this study. The heat exchanger with adsorbent material considered in this numerical analysis is illustrated in Figure (3.11). The flow, heat, and mass transfer in the ABU are simulated using a mathematical model based on conservation equations and solved using COMSOL Multiphysics 6 software.

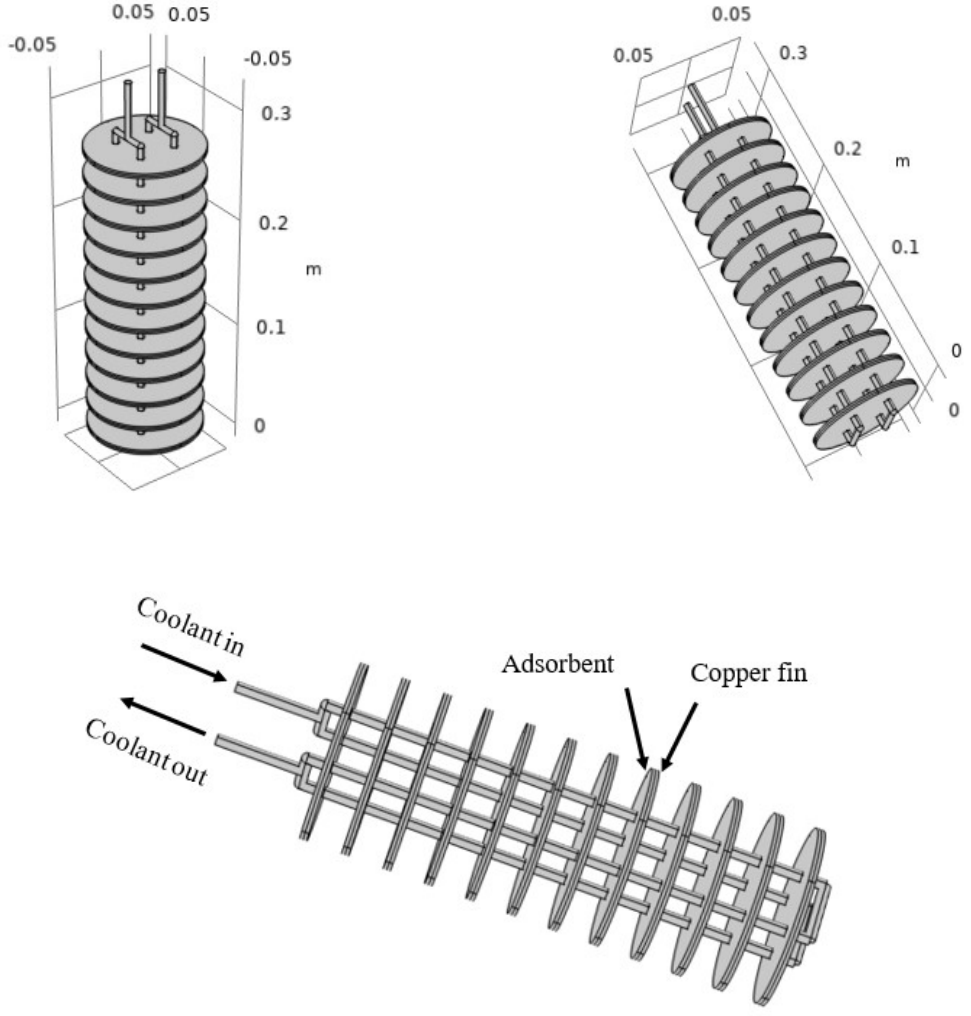

Figure (3.11) Heat exchanger geometry.

3.11.1 Assumptions

The simulation model of ABU has been solved numerically based on the following assumptions:

1- The computational domain is considered symmetrical with a uniform circular section of copper fins in the ABU's heat exchanger; therefore, 3D geometry can be reduced to a 2D symmetric geometry.
2- The working fluid is water, with incompressible flow inside the tubes.
3- An unsteady state is considered for adsorption bed operation.
4- Thermal conductivity and porosity of the solid adsorbent are constant.
5- A thermal equilibrium is assumed for the adsorbent and adsorbate phases.
6- The water vapor (adsorbate) is assumed to be an ideal gas.

3.11.2 Governing Equations

3.11.2.1 Mass Conservation Equation

The mass of refrigerant vapor can be expressed by [179], [180]

$$\varepsilon_t \frac{\partial \rho_v}{\partial t} + \frac{1}{r}\frac{\partial (r \rho_v V e_r)}{\partial r} + \frac{\partial (\rho_g V e_z)}{\partial z} + (1-\varepsilon_t)\rho_s \frac{\partial q}{\partial t} = 0 \quad (3\text{-}70)$$

The total porosity (ε_t) is equal to:

$$\varepsilon_t = \varepsilon_b + (1-\varepsilon_b)\varepsilon_p \quad (3\text{-}71)$$

Where

ε_b : the bed porosity

ε_p : the particle porosity

ρ_v : the density of vapor phase (kg/m^3)

ρ_s : the density of solid phase (kg/m^3)

r : the radius coordinate (m)

z : the axial coordinate (m)

V_{er} : the vapor phase velocity in the radial direction (m/sec)

V_{ez} : the vapor phase velocity in axial direction (m/sec)

(dq/dt) : the rate of uptake is calculated using the LPM model.

3.11.2.2 Momentum Conservation Equation

The velocity distribution of the vapor refrigerant in the ABU computational domain was determined using Darcy's equation as expressed by equation (3-72), [181], [182], [183]:

$$Ve = -\frac{k * \nabla P}{\mu_v} \tag{3-72}$$

$$K = \frac{d_p^2 * \varepsilon_b^3}{150(1-\varepsilon_b)^2} \tag{3-73}$$

Where

K : the permeability (empirical Blank-kozeny equation)

μ_v : the viscosity of the vapor phase (Pa.sec)

P is pressure (kPa)

d_p : the average diameter of adsorbent particles (m).

3.11.2.3 Energy Conservation Equation

The temperature distribution of the vapor and solid phases in the ABU is calculated based on the following energy equations [184], [185]:

For the vapor phase:

$$Cp_v\rho_v\left[\varepsilon_v\frac{\partial T_v}{\partial t} + Ve_r\frac{\partial T_v}{\partial t} + Ve_z\frac{\partial T_v}{\partial t}\right] + (1-\varepsilon_t)\rho_s\frac{\partial q}{\partial t}Cp_v(T_s - T_v) =$$

$$\frac{1}{r}\frac{\partial}{\partial r}\left(rK_{vef}\frac{\partial T_v}{\partial r}\right) + \frac{\partial}{\partial z}\left(K_{vef}\frac{\partial T_v}{\partial z}\right) + \alpha_v h_{fg}(T_s - T_v) \tag{3-74}$$

For the solid phase:

$$\rho_v(1-\varepsilon_t)(Cp_s - qCp_w)\frac{\partial T_s}{\partial t} - (1-\varepsilon_t)\rho_s\frac{\partial q}{\partial t}Q_{ads} = \frac{1}{r}\frac{\partial}{\partial r}\left(rK_{se}\frac{\partial T_s}{\partial r}\right) +$$

$$\frac{\partial}{\partial z}\left(K_{se}\frac{\partial T_s}{\partial z}\right) + \alpha_v h_{vs}(T_s - T_v) \tag{3-75}$$

For copper tube:

$$\frac{\partial T_{cu}}{\partial t} = \alpha_{cu} \nabla^2 T_{cu} \quad (3\text{-}76)$$

The fluid-solid specific surface area for spherical particles is equal to the following:

$$\alpha_{cu} = \frac{6(1-\varepsilon_t)}{d_p} \quad (3\text{-}77)$$

The interfacial heat transfer coefficient (h_{gs}) is determined by:

$$Nu_d = 2 + 1.8 Pr^{0.33} Re_d^{0.5} \quad (3\text{-}78)$$

$$Nu_d = \frac{h_{gs} d_p}{K_v} \quad (3\text{-}79)$$

$$Re_d = \frac{\rho_v Ve\, d_p}{\mu_v} \quad (3\text{-}80)$$

$$Pr = \frac{\mu_v Cp_v}{k_v} \quad (3\text{-}81)$$

Where

Cp_v : the specific heat of the vapor phase (J/kg. K)

ε_v : the vapor porosity

T_v : the temperature of vapor (K)

T_s : the temperature of solid (K)

k_{vef} : the effective thermal conductivity of vapor phase (W/(m.K)

α_v : the fluid-solid specific surface area per unit volume (1/m)

h_{vs} : the convective heat transfer coefficient ($W/m^2.K$)

Cp_s : the specific heat of solid phase (J/kg. K)

Cp_w : the specific heat of refrigerant (J/kg. K)

Q_{ad} is the heat of adsorption (J/kg)

k_{se} : the effective thermal conductivity of solid phase (W/m.K)

d_p : the average diameter of adsorbent (m).

The dimensions of the heat exchanger in an adsorber bed unit (HEABU), which consists of five domains (water vapor, coolant fluid, metal tube, fins, and solid adsorbent), are shown in Figure (3.12). The partial differential equations of heat and mass transfer with time for HEABU are evaluated and solved using the finite element method of the COMSOL-6 Multiphysics with a relative tolerance of 10^{-5}.

The fluid flow physics of the water coolant is computed using the HMTM to address heat transport in the tubes, fins, and adsorbents coupled with mass transfer of refrigerant flow in ABU to predict the values of variables such as velocity and pressure. The physically controlled mesh is utilized with the COMSOL Multiphysics program with the extra acceptable item size option of tube length of 244 mm to estimate heat and mass transfer features precisely. The initial boundary conditions at the charge and discharge of ATB are established during cycle time. The coolant water domain is considered at the inlet of cold and hot water with a zero-gauge pressure at the output. The inlet water vapor temperature represents the ECU's saturation temperature. The charge and discharge processes take about 10^{3} seconds for each cycle.

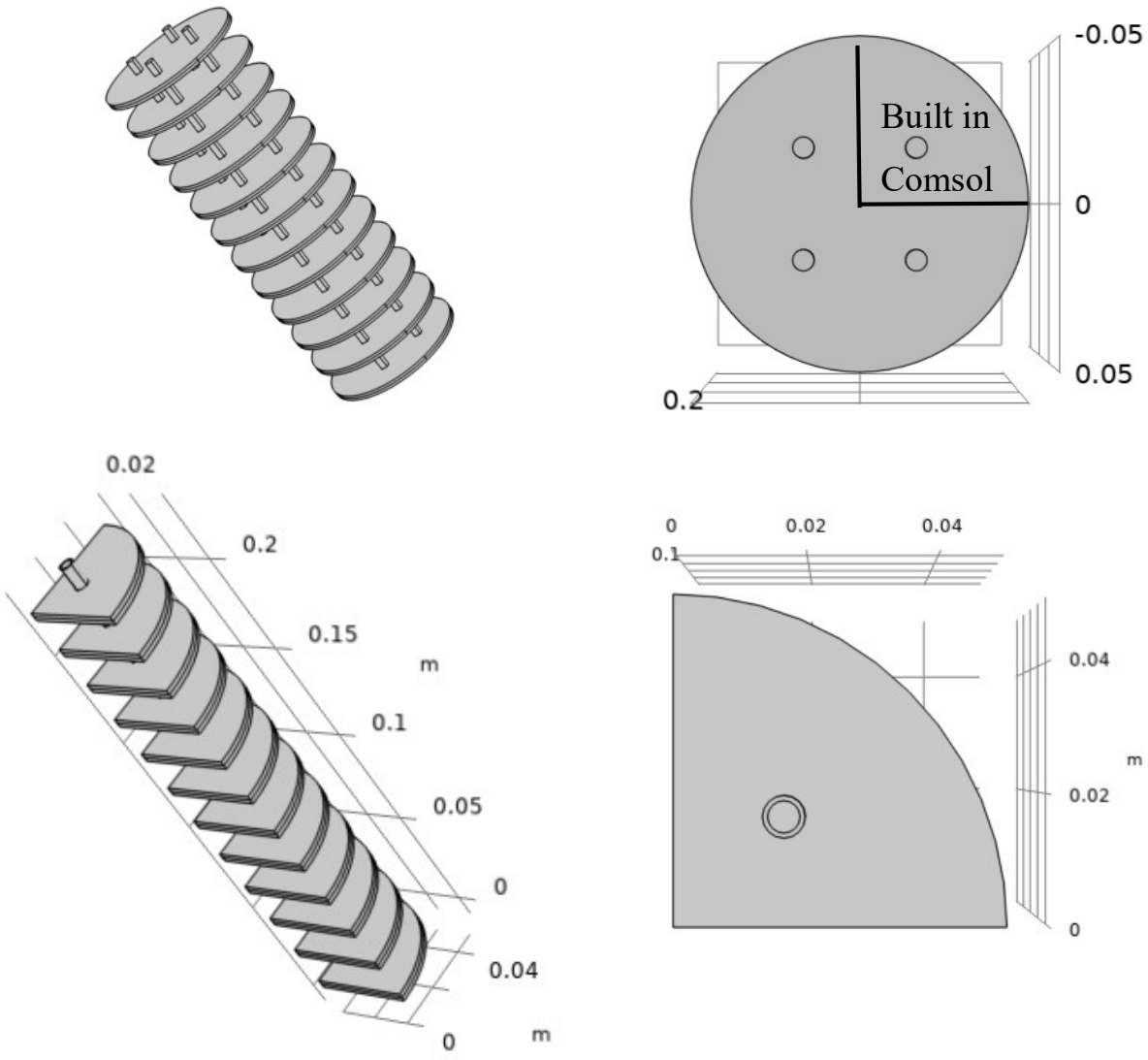

Figure (3.12) Built-in model of HEABU.

3.11.3 Boundary Conditions

The initial and boundary conditions considered in the HMTM numerical solution are illustrated in Table (3.4) and Figure (3.13), respectively.

Table (3.4) Initial conditions of charge and discharge processes of ATB.

Variables	Initial adsorption conditions	Initial desorption conditions
T_{ABU}	353 K	303 K
T_{ECU}	288 K (evaporator)	313 K (condenser)
$T_{cw,\,in}$ (adsorption) $T_{hw,\,in}$ (desorption)	303 K	353 K
Coolant flow rate	1 kg/sec	1 kg/sec
Uptake /offtake	0.02 kg_{ref}/kg_{ads}	0.3 kg_{ref}/kg_{ads}
Cycle time	1000 sec	1000 sec

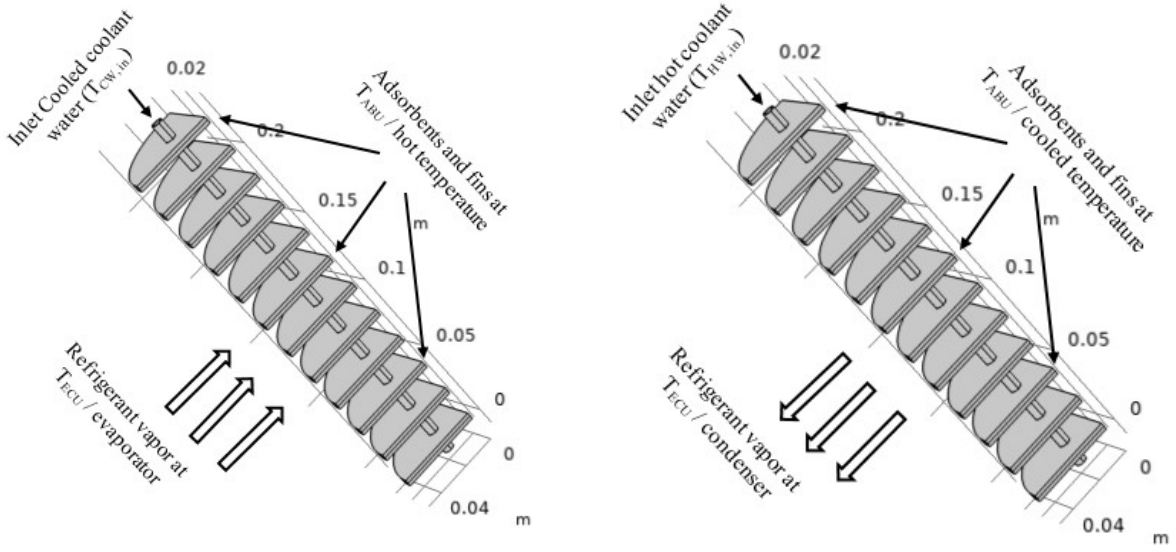

a. Adsorption b. Desorption

Figure (3.13) Boundary conditions on the heat exchanger.

3.11.4 Mesh Independence

The COMSOL software offers several formats for mesh production to specify the geometry, as demonstrated in Figure (3.14). The standard method for determining if a mesh is sensitivity-independent is to increase the resolution and run the simulation three times with the same boundary conditions. The initial mesh is probably sufficient if the data do not change considerably. Figure (3.15) shows the mesh grid

for a 3-D ABU heat exchanger for three types of mesh with the total number of cells in each type. The most effective way to choose an appropriate number of cells and confirm a mesh-independent approach is to plot a diagram of the outcome measured data, such as temperature distribution in the ABU versus the number of elements in the numerical simulation, as shown in Figure (3.16), that illustrates the maximum fluctuations in ABU temperature throughout those three types of mesh are about 8%, indicating that meshing size does not significantly affect the precision of finite element modeling predictions.

Subsequently, the computations for the adsorption cooling bed scenarios were executed using an extra fine mesh. The geometry consisted of approximately 804190 domain elements, 104576 boundary elements, and 7396 edge elements. This mesh size was considered satisfactory in terms of both accuracy and efficiency. A personal computer equipped with dual Xeon processors with 2.4 GHz (Cora i7) and a total memory capacity of 32 GB (RAM) was utilized to complete the assigned task. The duration of the computation varied between 6 and 8 hours, depending on the specific case. The flowchart of the numerical solution steps implemented by COMSOL software is shown in Figure (3.17).

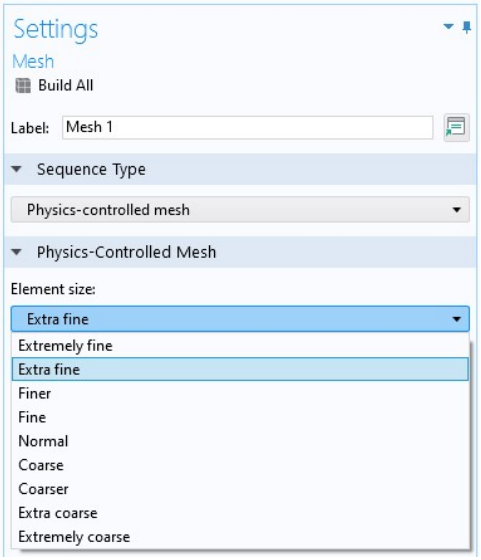

Figure (3.14) Mesh type in COMSOL software.

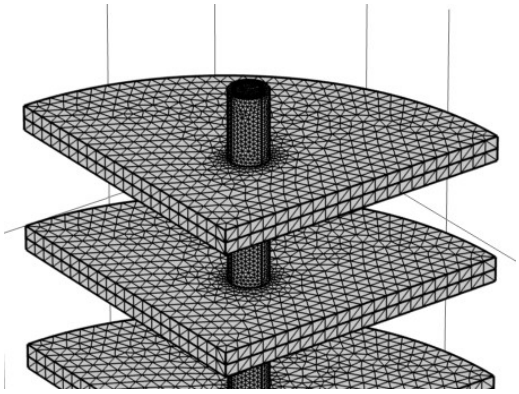

(a) Extra fine: Complete mesh consists of 804190 domain elements, 104576 boundary elements, and 7396 edge elements.

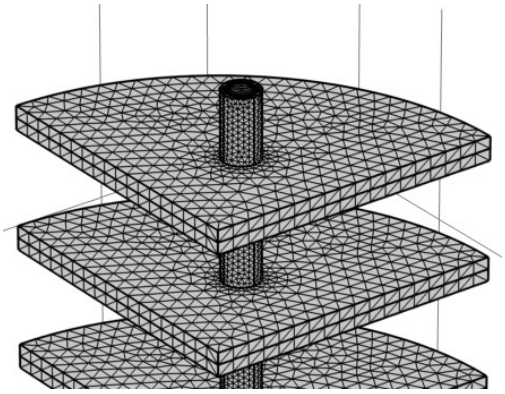

(b) Finer: Complete mesh consists of 270516 domain elements, 59150 boundary elements, and 5528 edge elements.

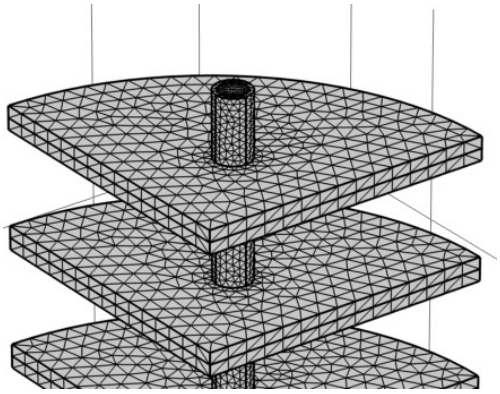

(c) Fine: Complete mesh consists of 143589 domain elements, 39568 boundary elements, and 4460 edge elements.

Figure (3.15) Computational mesh size (3-D), (a) Extra fine, (b) Finer, (c) Fine.

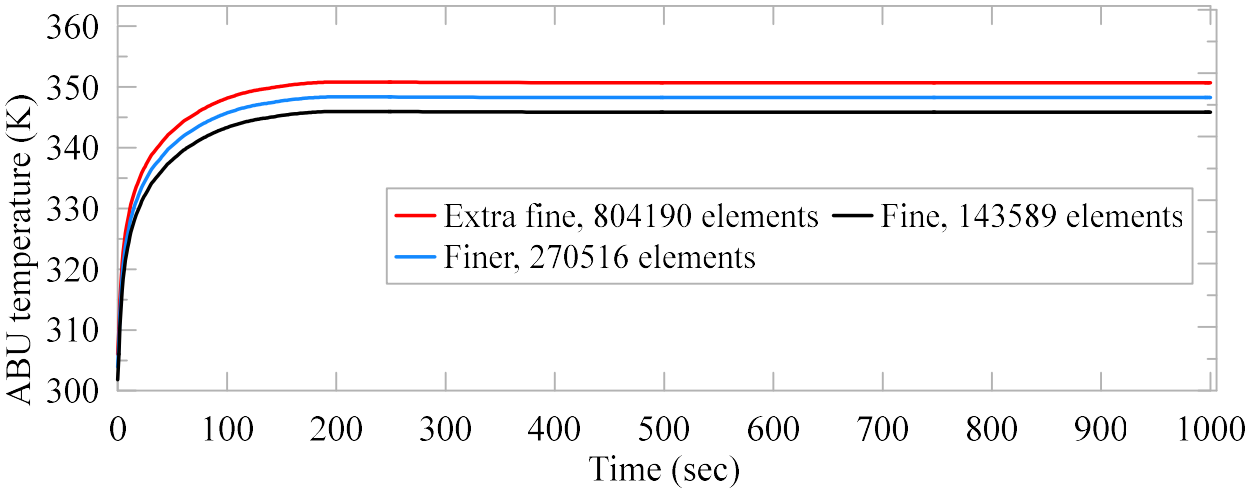

Figure (3.16) Variation of ABU temperature with mesh elements number.

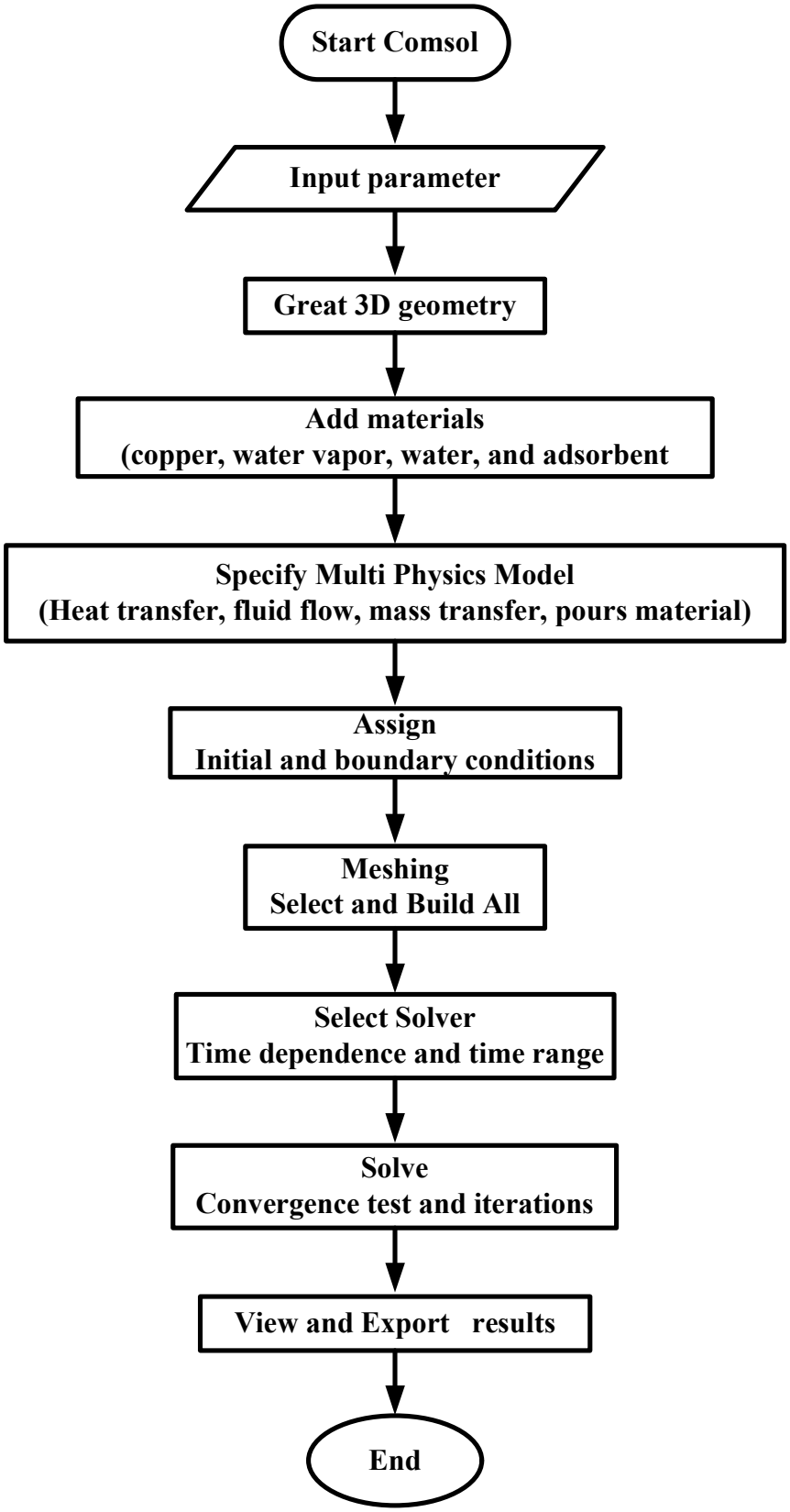

Figure (3.17) Flow chart illustrating the numerical solution.

Chapter Four

Experimental Work

Chapter Four

Experimental Work

4.1 Introduction

This chapter presented the details of the experimental work done to accomplish the main objectives of the present investigation. It includes the experimental setup, test rig construction, measurements, and experimental process. The components of the ATB system were manufactured in the welding workshop at the technical college in Baghdad. Several adsorbent materials should be investigated with a two-bed adsorption thermo-physical battery in this study to evaluate ATB performance. Furthermore, the effects of adsorbent materials and mass recovery time on the operation of the ATB system are evaluated in this research. Silica gel-RD and MCM-41 are the two adsorbent materials examined in the present investigation. The aim is to increase the surface area available for heat exchange between the adsorbent and the refrigerant (water) throughout the cycles of desorption and adsorption. A new configuration of a heat exchanger for the adsorber has been utilized to achieve previous aims. However, to optimize the system's performance, it is crucial to implement a control system that effectively regulates the hot and cold-water supply to the bed and the chilled and condensing water.

4.2 ATB Test Rig

Figures (4.1) and (4.2) describe the construction of an ATB test rig based on a two-adsorber bed cycle. The rig is made up of the following components: Two Adsorber Bed Units (ABU1 and ABU2), Two Evaporator and Condenser Units (ECU1 and ECU2), the Coolant Circulation Unit (CCU), which contain cooling and heating coolants (such as water), the Chilled Unit (CHU), the Condensing Unit (CU), several

valves, pumps, and connections. The mode of operation of the valves and pumps are shown in Table (4.1).

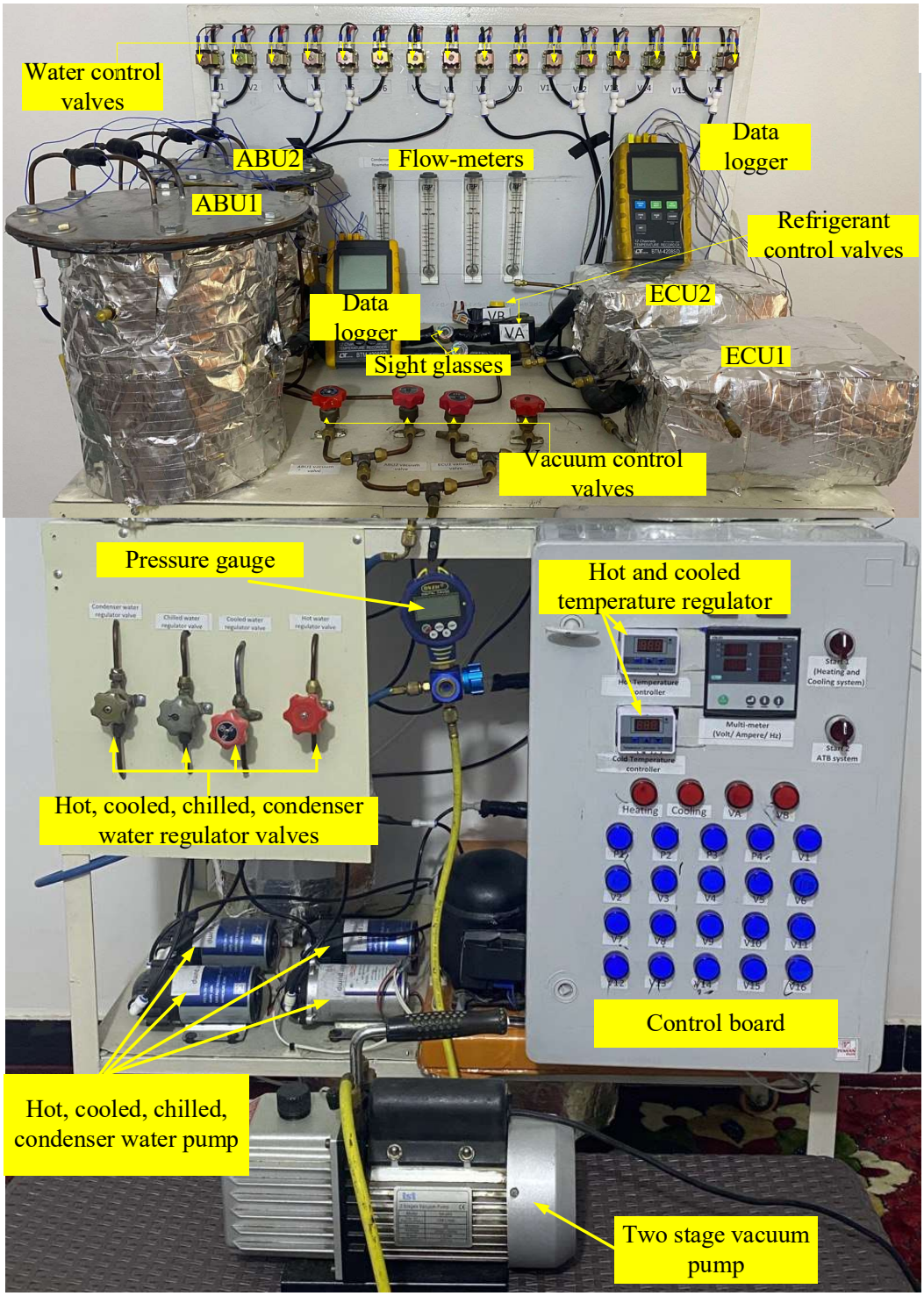

Figure (4.1) ATB Test rig.

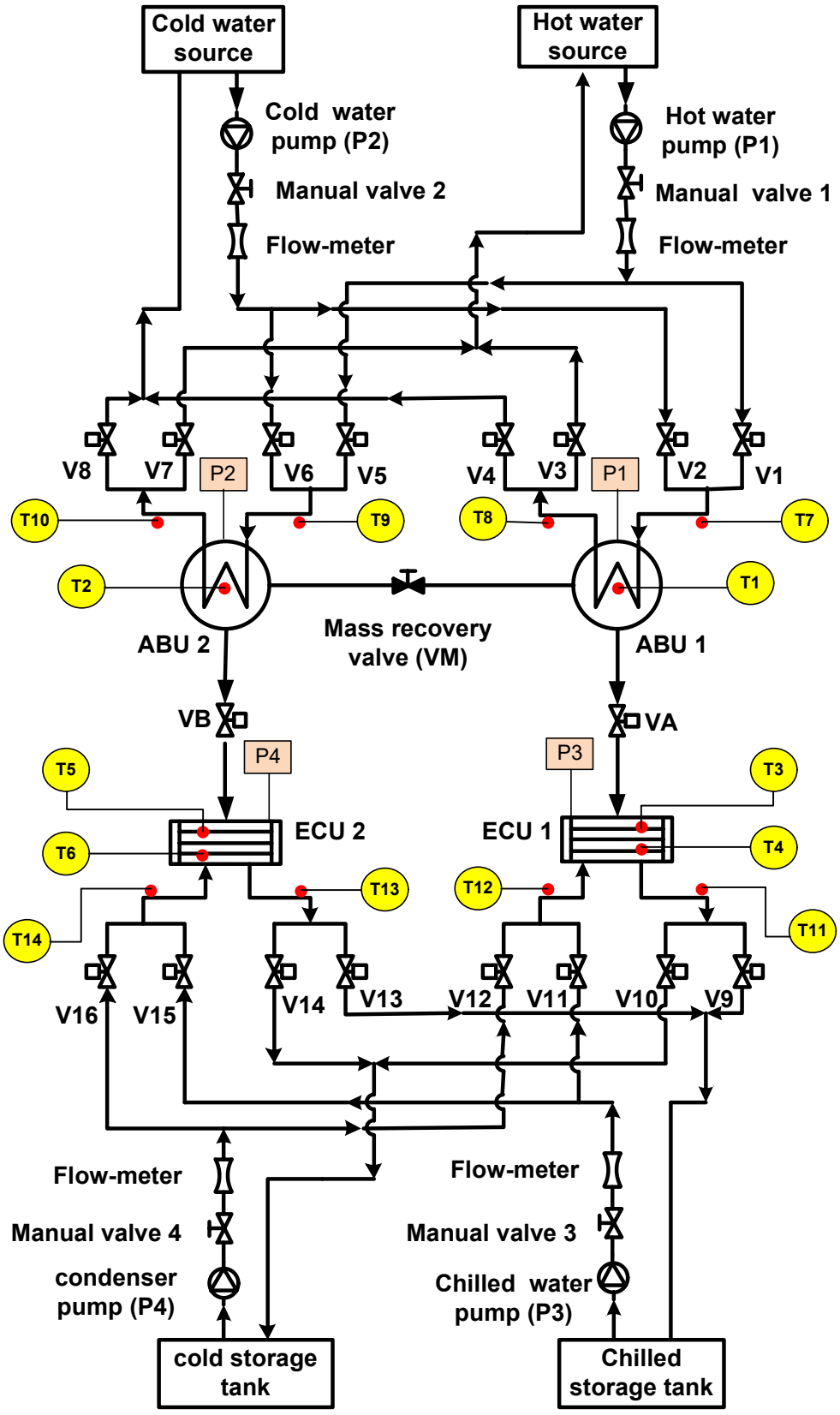

Figure (4.2) Schematic representation of the ATB experimental equipment.

Table (4.1) Valve and pump modes for two-bed ATB units

Step 1		Step 2		Step 3		Step 4		Step 5	
Preheating for ABU1 / precooling for ABU2		Refrigeration process 1		Mass recovery process		Preheating for ABU2 / precooling for ABU1		Refrigeration process 2	
Valve and pump	State	Valve and pump	State	Valve and pump	State	Valve and pump	State	Valve and pump	State
VM	OFF	VM	OFF	VM	ON	VM	OFF	VM	OFF
P1	ON	P1	ON	P1	OFF	P1	ON	P1	ON
P2	ON	P2	ON	P2	OFF	P2	ON	P2	ON
P3	OFF	P3	ON	P3	OFF	P3	OFF	P3	ON
P4	OFF	P4	ON	P4	OFF	P4	OFF	P4	ON
VA	OFF	VA	ON	VA	OFF	VA	OFF	VA	ON
VB	OFF	VB	ON	VB	OFF	VB	OFF	VB	ON
V1	ON	V1	ON	V1	OFF	V1	OFF	V1	OFF
V2	OFF	V2	OFF	V2	OFF	V2	ON	V2	ON
V3	ON	V3	ON	V3	OFF	V3	OFF	V3	OFF
V4	OFF	V4	OFF	V4	OFF	V4	ON	V4	ON
V5	OFF	V5	OFF	V5	OFF	V5	ON	V5	ON
V6	ON	V6	ON	V6	OFF	V6	OFF	V6	OFF
V7	OFF	V7	OFF	V7	OFF	V7	ON	V7	ON
V8	ON	V8	ON	V8	OFF	V8	OFF	V8	OFF
V9	OFF	V9	OFF	V9	OFF	V9	OFF	V9	ON
V10	OFF	V10	ON	V10	OFF	V10	OFF	V10	OFF
V11	OFF	V11	OFF	V11	OFF	V11	OFF	V11	ON
V12	OFF	V12	ON	V12	OFF	V12	OFF	V12	OFF
V13	OFF	V13	ON	V13	OFF	V13	OFF	V13	OFF
V14	OFF	V14	OFF	V14	OFF	V14	OFF	V14	ON
V15	OFF	V15	ON	V15	OFF	V15	OFF	V15	OFF
V16	OFF	V16	OFF	V16	OFF	V16	OFF	V16	ON

4.3 Adsorber Bed Unit

The adsorber represents the heart of the ATB system; two ABUs were designed and manufactured to build and evaluate the performance of ATB, which consists of two parts, a heat exchanger and an adsorber shell (container), as shown in Figure (4.3). The cylindrical-shaped container adsorber shall be made from galvanized steel material with a diameter of 24 cm and a height of 30 cm, and it is provided with two flanges with a thickness of 5 mm to prevent leakage. The adsorber shell has a thickness of 3 mm. In order to prevent entering ambient air, the flange is welded to the upper portion of the adsorber shell, mounted with twenty fasteners, equipped with a rubber gasket, and sealed using thermal silicon. A thermally insulating layer of glass wool, measuring 5 cm in thickness with a thermal conductivity of 0.25 W/mK, is employed to reduce heat loss between the environment and the adsorber bed. The adsorber shell is equipped with eight-port holes, each having a diameter of 6.35 mm (1/4 in.). These port holes serve many purposes, including installing a pressure gauge, thermocouples, connection with the ECU, vacuum, the inlet and outflow of the heat exchanger, and the final port for mass recovery, as shown in Figure (4.3). Also, ABU is fitted with an electric heater that keeps the adsorbent material's temperature at the prescribed value for preparation and discharge processes. The heat exchanger used in the test rig system is provided with 12 circular fins of 10 cm in diameter and a thickness of 1 mm, as shown in appendix B. It is installed on four copper tubes with a 6.35 mm (1/4 in.) diameter, as shown in figure (4.4). The solid adsorbent is inserted between the copper fins.

The heat exchanger module is placed in the ABU, and U-bends connect the tubes with one end. The heat exchanger fins are enveloped by a stainless-steel mesh with a diameter of 0.1 mm. This mesh keeps the adsorbents within the heat exchanger and prevents them from falling out. The heat exchanger's inlet and outlet

are installed onto the flange of the adsorber shell. as shown in Figure (4.3). The primary design specifications of the ABU are presented in Appendix B.

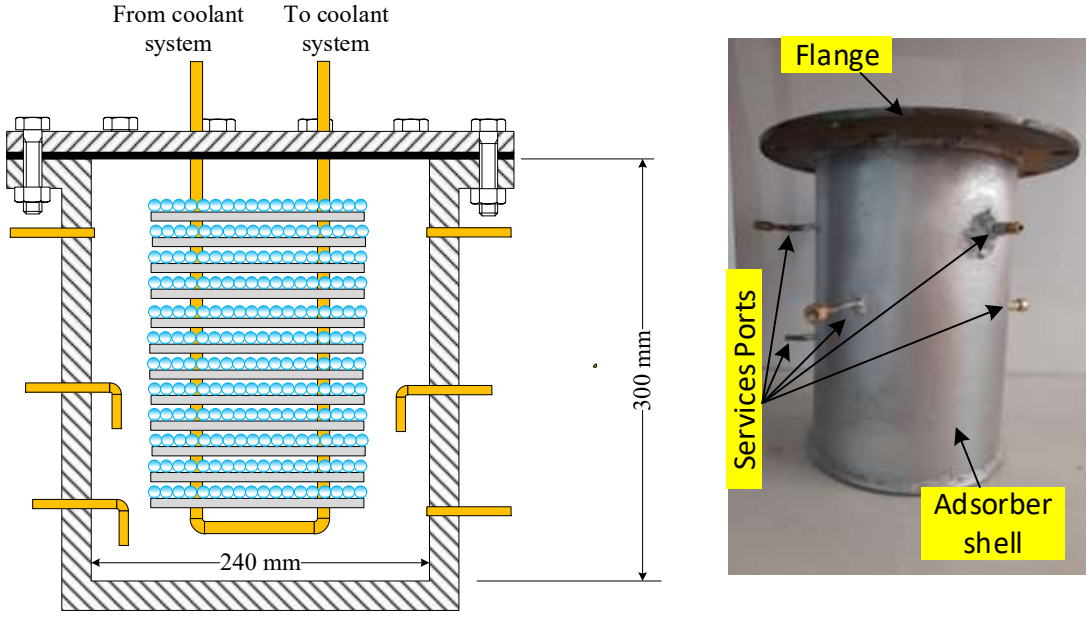

Figure (4.3) ABU geometry and dimension.

4.4 Evaporator/Condenser Unit (ECU)

The ECU is an integrated container within the test apparatus system that accommodates the evaporator and condenser components. The evaporator is connected to ABU during the charging process, while the condenser is connected to ABU during the discharging process. Two ECUs were designed and manufactured to build and evaluate the performance of ATB. The ECU consists of a rectangular tank made of galvanized steel material with a 4 mm thickness, length of 22 cm, width of 14 cm, and height of 12 cm, as shown in Figure (4.5). The ECU shell has seven circular ports, each measuring 6.35 mm (1/4 in.) in diameter. Two of these ports are the entry and exit points for the cooling water circulation connected to the heat exchanger.

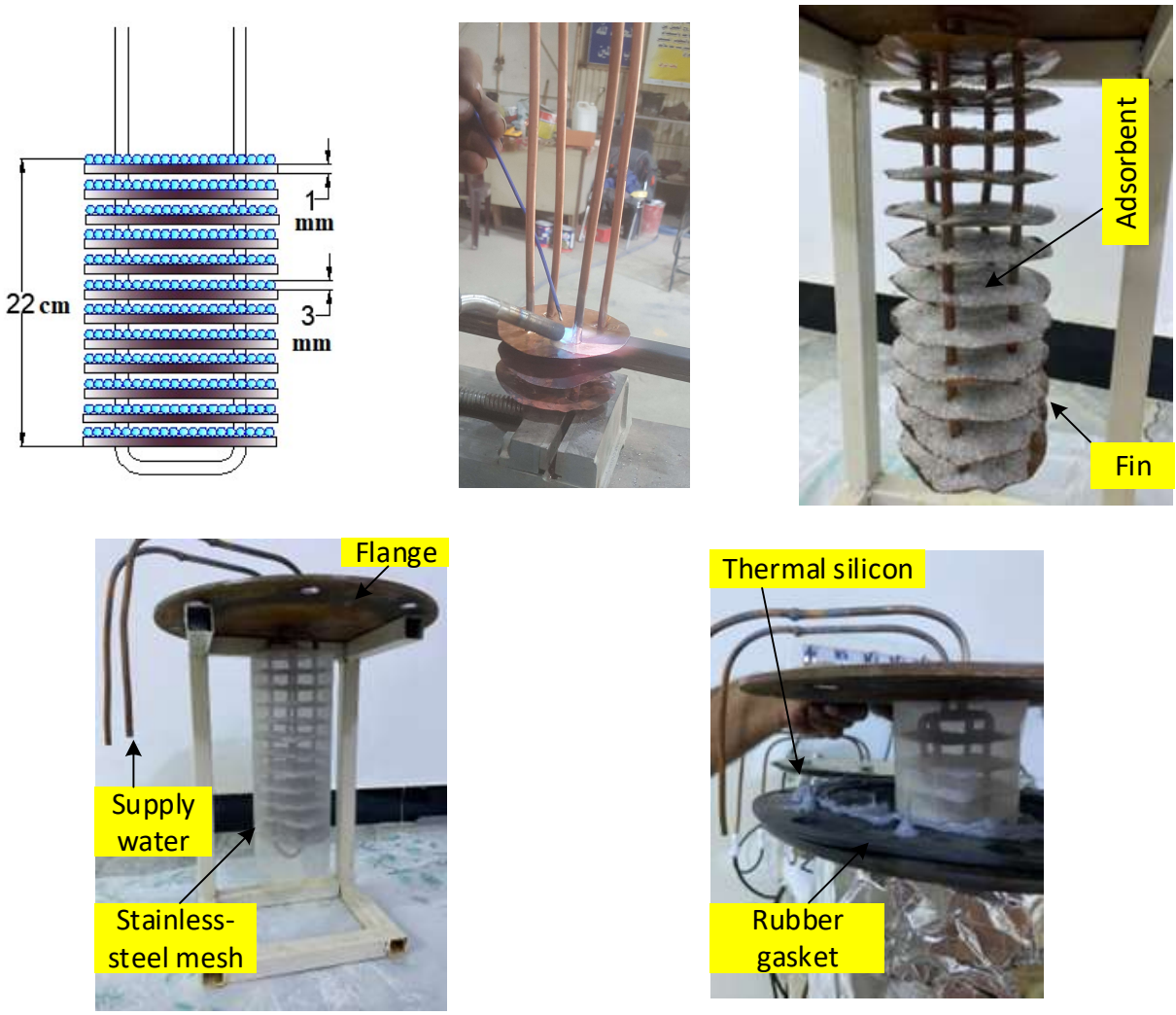

Figure (4.4) Heat exchanger geometry and dimension.

Thermocouples have been carefully installed within the ECU wall, with two holes designated for this purpose. These thermocouples serve the purpose of detecting the temperature of the refrigerant's vapor and liquid phases. One thermocouple is placed at the top of the ECU to monitor vapor temperature, while another is positioned at the bottom to measure liquid temperature. Two holes at the ECU wall are used to install the pressure gauge and vacuum, and the last one is used to connect to the ABU. A ten-copper tube with a 20 cm length and a 1.5 cm (5/8 in) diameter is utilized to construct the heat exchanger. The heat exchanger is positioned

within the ECU, with U-shaped bends linking the tubes at one end, as illustrated in Figure (4.6). The heat exchanger facilitates the requisite heat transmission for the evaporation of the liquid refrigerant throughout the adsorption process by being submerged in the refrigerant liquid within the ECU. The upper portion of the heat exchanger functions as a condenser, facilitating the condensation of the vaporized refrigerant flowing from the ABU. This is achieved by transferring the heat of the vapor to the cold coolant, transforming the vapor into a liquid state.

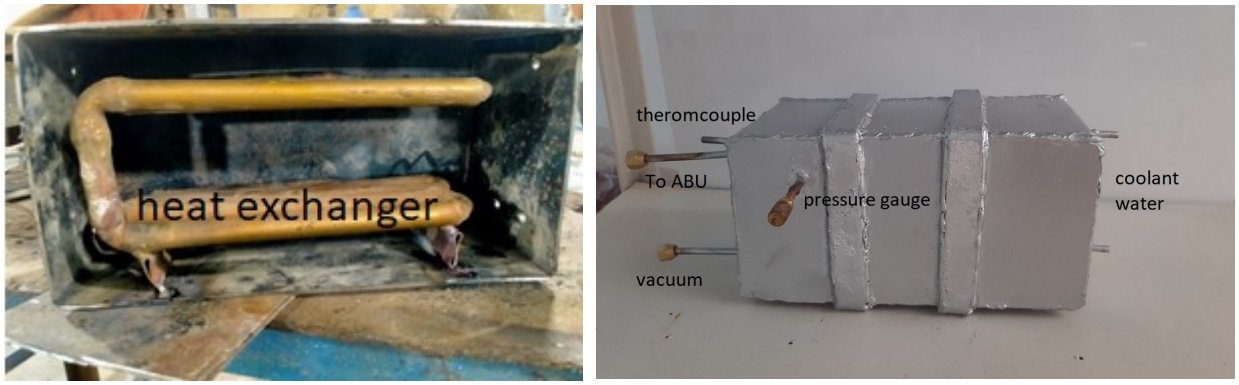

Figure (4.5) ECU geometry and main parts.

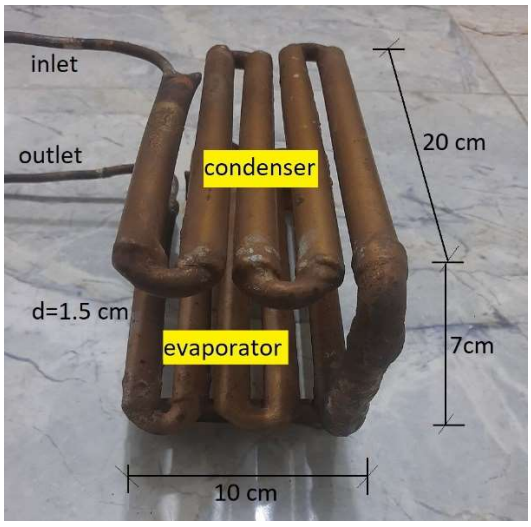

Figure (4.6) ECU heat exchanger.

4.5 Coolant Circulating Unit (CCU)

Two separate coolant circuits compose the CCU: the cooling and heating coolant circuits. In the ABU, the working coolant, water, is utilized to provide heat and cooled water for the adsorption and desorption of the refrigerant. The cooling system of CCU was a vapor compression refrigeration system with R-134a, as shown in Figure (4.7a). It consists of the reciprocated compressor (1/4 hp), air-cooled condenser, capillary tube, shell, and coil heat exchanger. The shell dimension is 25 cm in diameter and 30 cm in length, covered by insulation to prevent heat losses. The coil is made from 9.53 mm (3/8 in.) copper pipe with 6 m length, ten coil turn, 20 cm coil diameter, and 20 cm coil height. Table 4.2 shows the specification of the compressor. The heating system of CCU, as shown in Figure (4.7b), consists of electric heating (250 W) and a shell covered by insulation to prevent heat losses; the shell diameter is 20 cm, and the height is 30 cm.

Throughout the ATB preparation, discharge, and charge procedures, the heat and cooled water were supplied to the heat exchanger fins coated with a solid adsorbent. Two methods supply the heat rate to the ABU during the preparation and desorption processes. The initial approach involves the utilization of an electrical heater that is introduced within the ABU to provide the necessary heat. The second methodology required providing heat using hot water sourced from the heated coolant tank within the CCU. Utilizing these two methodologies offers the benefit of covering an extensive range of temperatures to evaluate the ATB system. However, the ABU can be supplied with heat from other sources, such as waste heat or solar energy. The cooling and heating systems utilize two intelligent controllers to effectively regulate the temperature of the cold and hot water, respectively. This is depicted in Figure (4.14). The (CCU) is equipped with a thermostat that regulates the temperature of the coolant as it enters the heat exchanger.

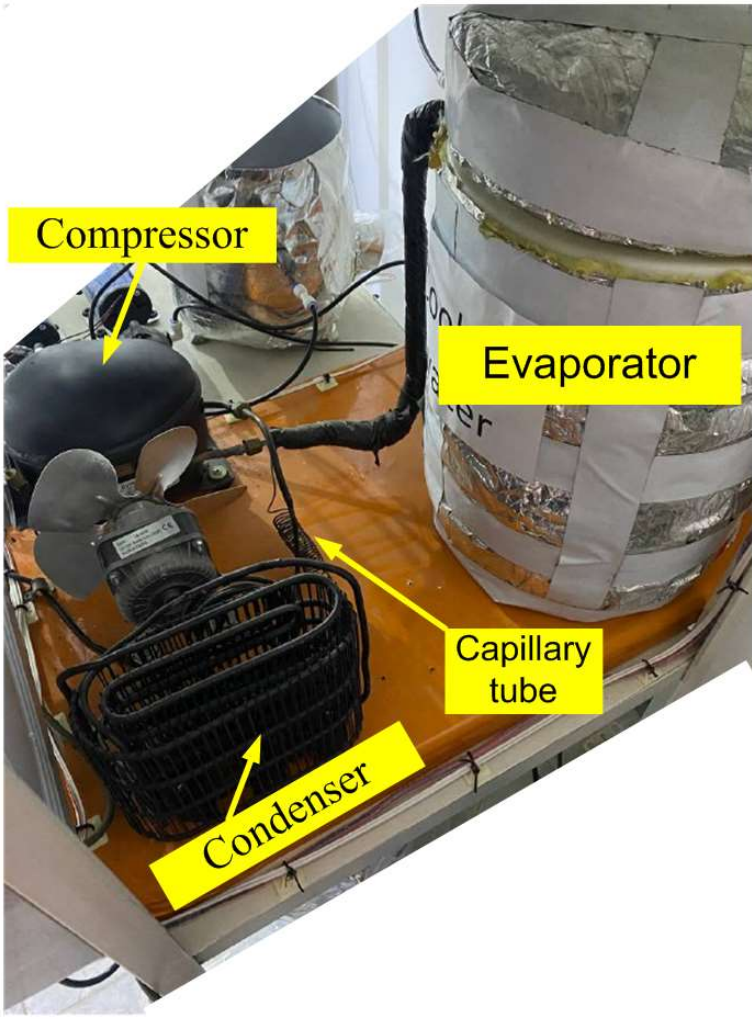

a. cooling system

b. shell and coil evaporator

c. heating system

Figure (4.7) Coolant circulating unit.

Table 4.2 Specification of the compressor

Compressor type	Reciprocated
Model No.	GVY61AA
Capacity	¼ hp
Refrigerant	R-134a
Voltage	220-240 V

4.6 Water Pump

The ATB system employs four water pumps to facilitate the circulation and delivery of water for both ABU and ECU, as depicted in Figure (4.8). Table 4.3 shows the specifications of the compressor. The chilled water pump connects the chilled tank and heat exchanger within the ECU1 and ECU2 systems. Its main objective is to facilitate the circulation of coolant water during the charge phase, which involves the conversion of liquid refrigerant into a vapor in the ECU. The condenser water pump connects the condenser tank and the heat exchanger of ECU1 and ECU2. Its primary function is to facilitate the circulation of coolant water during the discharging process, specifically the condensation of vapor refrigerant. In Both ABU1 and ABU2, the hot water pump is an interface connecting the heat exchanger and the CCU-heating system. Its primary function is to facilitate the flow of hot water during the discharging process. The cooled water pump functions as a connection point from the CCU-cooling system to the heat exchanger in the ABU1 and ABU2. Its primary function is to facilitate a cold-water flow during the charging process.

Table 4.3 Specification of the water pump

Pump type	Diaphragm pump
Model No.	AQ-75GPD
Voltage	24 V DC
Working pressure	80 psi
Working flow	≥ 0.75 LPM

Figure (4.8) Water Pump.

4.7 Vacuum Pump

Before starting the experimental tests, a two-stage vacuum pump (tst-245) removes the air and moisture from ABU and ECU. In addition, it satisfies the required pressure levels for the refrigerant in the evaporator. The vacuum pump can provide a minimum pressure of -30 psi, as illustrated in Figure (4.9). Table 4.4 shows the specification of the compressor.

Table 4.4 Specification of the vacuum pump

Vacuum pump type	Two-stage vacuum pumps
Model No.	tst-245
Capacity	½ hp, 3.5 CFM
Flow rate	100 l/min
Oil capacity	330 ml

Figure (4.9) Vacuum pump.

4.8 Measurements and Instrumentations

The following instrumentations were used in this work:

4.8.1 Temperature Measurements

Fourteen type K thermocouples with a temperature range of -50°C to 300°C and a temperature reader (Model BTM-4208SD) with an accuracy of 0.025°C were employed to measure and record temperatures at different locations within the ATB test system, as depicted in Figure (4.1). These thermocouples and the temperature reader are shown in Figure (4.10). The thermocouples were calibrated by freezing and boiling water to ensure that the thermocouples read the exact temperature at the first step, as shown in **Appendix D**. The second step is thermally insulating the thermocouple junction to reduce the effect of ambient conditions on the reading.

a b

Figure (4.10) a-Thermocouple. b- Temperature Reader.

4.8.2 Pressure measurements

The ABU and ECU pressure was measured using a digital vacuum pressure gauge (DSZH type) with a precision of ± 0.01kPa, as depicted in Figure (4.11), were used to measure the pressure ABU1, ABU2, ECU1, and ECU2 in the ATB test system as illustrated in Figure (4.1).

Figure (4.11) Digital vacuum pressure gauges.

4.8.3 Flow-rate Measurement

Figure (4.12) illustrates the utilization of four flow meters to quantify the coolant flow rate in the heat exchangers for both ABU and ECU. The coolant flow rates range from 0.5 to 5 L/min, with an accuracy of ± 0.01 L/min. The flow meters were calibrated to ensure that the flow meters read the exact flow rate, as shown in **Appendix D.**

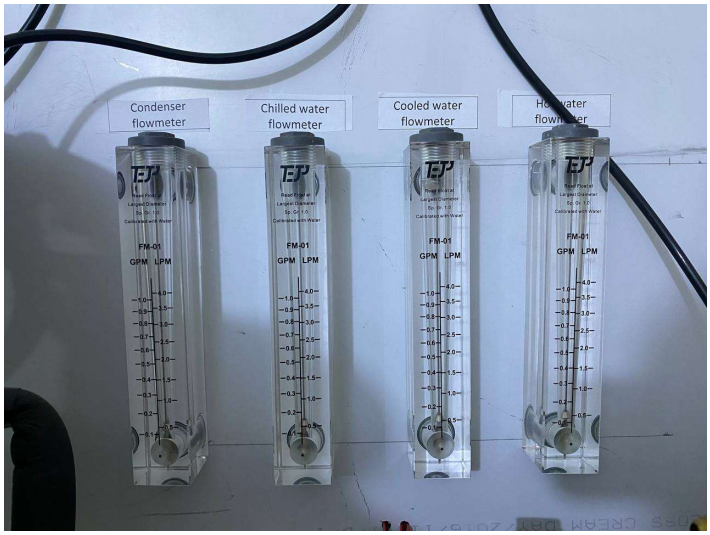

Figure (4.12) Flow meters.

4.9 Sight Glass

Sight glass views the refrigerant state (vapor or liquid) through adsorption and desorption. It is also used to view the refrigerant flow in the tubes. The dimensions of the sight glasses used in the test rig are 10 cm in length and 3 cm in diameter, as shown in Figure (4.13).

Figure (4.13) Sight glass

4.10 Control system

The following electronic components were implemented to control the electric parts of the system, as shown in Figure (4.14), and the wiring schematic of the electronic control circuit is shown in Figure (4.15).

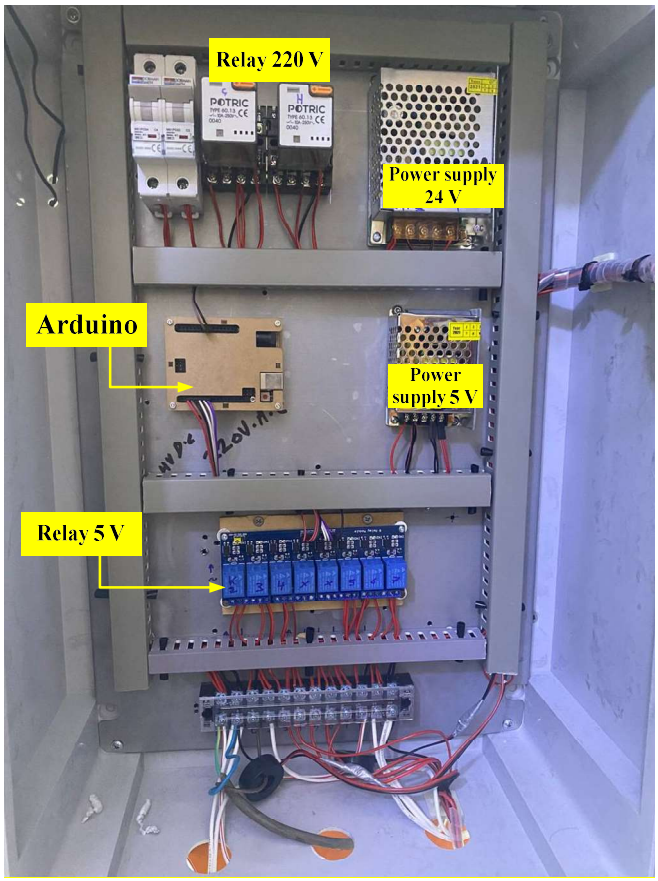

Figure (4.14) Control system for ATB.

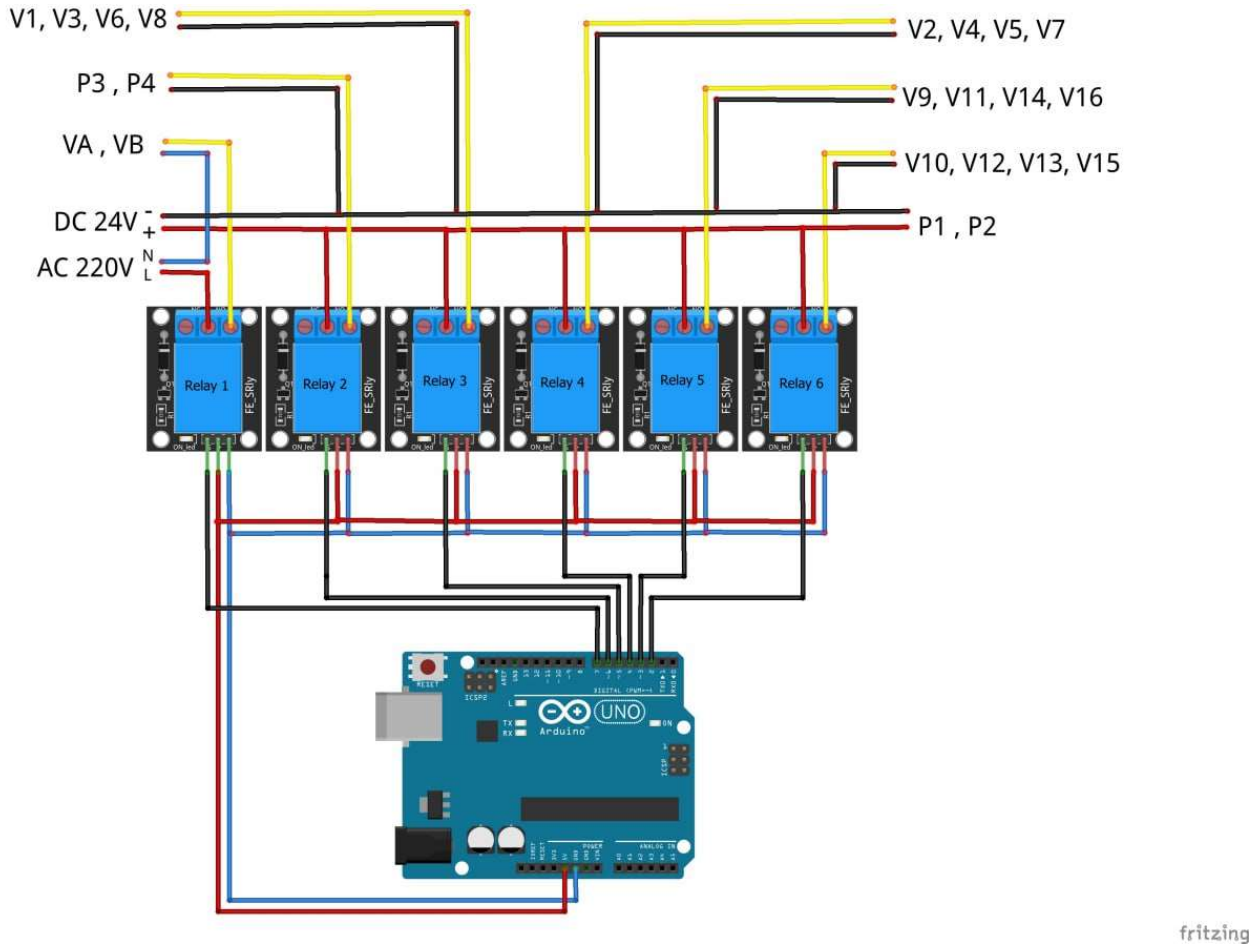

Figure (4.15) Wiring Diagram of the Electronic Control Circuit

4.10.1 Arduino for control

Figure (4.14) shows that one Arduino board was used. Arduino UNO was used as the main microcontroller to control the system parts. Arduino UNO was programmed using Arduino IDE 2.0.4 software. The software used a USB bus to communicate with the development boards. The communication involved uploading the codes; it was used as a controller. The software's front panels and the Arduino coding are shown in Appendix E.

4.10.2 Relay

A relay is a switch that is operated by electricity. Many relays employ an electromagnet to physically activate the switch and provide electrical separation between two circuits. Relays are suitable for driving high-power electronic devices such as lights, electric fans, and air conditioning with a low voltage by connecting them to a microcontroller. A 5-channel 5 Volts low-level trigger relay module, as shown in Figure (4.14), was used and applied to Arduino to control the electric parts of the system through 16 water valves (24 volts), four water pumps (24 volts), and two solenoid valves (220 volts). Also, two relays of 220 Volts, as shown in Figure (4.14), were used to control the operation of CCU.

4.10.3 Valves

The valve is the last part of the control system, which receives a signal from the relay to transform from normally closed (NC) to normally open (NO). There are 27 valves in the system, as shown in Figure (4.2): 16 valves (24 volts) to control the (hot, cold, chilled, and condenser) water flow to the ABU and ECU, two valves (220 volts) to control the refrigerant flow between ABU1 and ABU2 to ECU1 and ECU2, four regulator manual valve to regulate the water (hot, cold, chilled and condenser) flow rate, four manual valves connect to the vacuum pump, and finally, one valve for mass recovery process.

4.10.4 Power Supplies

Two switching mode power supplies were used in the electronic circuit. The first one is the S-15-5 of 5 V, which supplies power to the Arduino. The other one is S-120-24 of 24 V, which powers the water valves, as shown in Figure (4.14).

4.11 Thermophysical Characteristics of the Adsorbents and Water

Two types of adsorbent materials, RD-silica gel and MCM-41, were used in this work, as shown in Figure (4.16). Silica gel-RD, an adsorbent, is commonly used in adsorption applications, such as ATB, because of its exceptional ability to absorb refrigerants, especially water. The ATB system is powered by low-grade heat due to using silica gel, which is environmentally safe. The composition of silica gel consists of partially dehydrated mesoporous polymeric aqueous silicic acid [136], [186], [187]. Mesoporous material MCM-41, which contains a hierarchical structure and large pores, was developed by Mobil Oil Corporation [188] - [190]. The properties of the adsorbent materials utilized as working pairs when combined with deionized water (as the refrigerant) are detailed in Table (4.5). The refrigerant utilized in the ATB system consists of deionized water that has undergone a chemical process to eliminate all mineral ions present.

Silica gel RD MCM-41

Figure (4.16) Experimental samples of the adsorbent materials utilized.

Table (4.5) Properties of the adsorbent materials.

Adsorbent properties	Silica gel -RD	MCM-41
Shape of particle	Spherical	Powder
Density (kg/m^3)	700	250-400

Average pore diameter (mm)	3.24	3.8×10^{-6}
Surface area (m^2/kg)	827.5	1000
Adsorptive capacity (kg_{ref}/kg_{ads})	0.4	0.960

4.12 Experimental Procedure

The two-bed ATB system has four thermal components. The operational mechanisms of the two ABU systems are charge/adsorption and discharge/desorption. Conversely, when the process is discharged (desorption), the two ECUs operate in condensation mode while in evaporation mode during the discharge (desorption) process. It is critical to describe the distinct functions of the four varieties of water utilized by the system. Throughout the charging and discharge processes, the first fluid, the refrigerant, circulates between the ABU and ECU within the ECU case. Chilled fluid, which functions as an air conditioning chilling fluid, constitutes the second fluid within the device. The coolant circulation unit (CCU) makes use of the third fluid. Facilitating the cooling and heating processes of the ABU during both charge and discharge operations, this fluid functions as a heat transfer substrate. The fourth fluid is a condensing fluid within the cold tank unit. This fluid is a heat transfer substance that cools the ECU during condensation.

4.12.1 Leakage Test

Sub-atmospheric pressure was a factor in the design of the system. Hence, a thorough strategy has been established to complete leakage testing to confirm the absence of any leakage via several connections on the refrigeration flow circuit. Upon completion of the leakage problem, the ECU and ABU were subsequently linked to vacuum pumps and evacuated to a pressure of 2 kPa. The pressure was then monitored for 24 hours to maintain steady pressure within the ATB.

4.12.2 Test Rig Preparation Process

In advance of conducting the ATB system test for the test system setup process, as depicted in Figure (4.1), it is necessary to follow the subsequent steps:

a- Fill water into the heating and cooling tanks and allow the water to level off to the desired level.

b- One liter of refrigerant (deionized water) should be added to each ECU.

c- Employ the power controller to stabilize the temperature at a specific point by adjusting the heating and cooling systems.

d- Adjust the hot water coolant and electric heater to maintain the ABU temperature at approximately 80°C while in CCU-heating mode.

e- Adjust the cooled water coolant to maintain the ABU temperature at approximately 30°C while the CCU is cooling.

4.12.3 The Adsorption and Desorption Process

The ATB_1 test rig is initially subjected to a discharging process in which a hot coolant heats the ABU_1. On the other hand, the ATB_2 test rig is initially subjected to a charging process in which the ABU_2 is cooled by cold coolant water. As depicted in Figure (4.1), the experimental tests are carried out following the subsequent steps:

a- For ATB1: To initiate the desorption process in the ABU_1 unit, it is recommended that the ABU1 be heated to approximately 80°C. Additionally, the hot water pump and electric heater should be activated, as depicted in **Figure (3.3 a)**

For ATB2: To initiate the adsorption process in the ABU_2 unit, it is recommended to cool the ABU_2 to around 30 °C. Additionally, the cold-water pump should be activated as depicted in **Figure (3.3 a)**

b- For ATB1: The valve V_A opens when the ABU's pressure reaches the condenser pressure. The condensation process is sustained by the circulation

of water at around 30 °C through the condenser coil within the ECU unit, as seen in **Figure (3.3 b)**

For ATB2: The valve V_B opens when the ABU's pressure reaches the evaporator's pressure. The evaporation process is sustained by water flow through the ECU unit's evaporator coil, as shown in **Figure (3.3 b)**

c- At the end of the desorption and adsorption process for ATB_1 and ATB_2, the mass recovery valve is opened to equalize the pressure and vapor concentration between ABU_1 and ABU_2, as shown in **Figure (3.3 c)**

d- For ATB1: To initiate the adsorption process in the ABU_1 unit, it is recommended to cool the ABU_1 to around 30 °C, as depicted in **Figure (3.3 d)**

For ATB2: To initiate the desorption process in the ABU_2 unit, it is recommended to heat the ABU_2 to approximately 80°C, as depicted in **Figure (3.3 d)**

e- For ATB1: The valve V_A opens when the ABU's pressure reaches the evaporator's pressure, as shown in **Figure (3.3 e)**

For ATB2: The valve V_B opens when the ABU's pressure reaches the condenser pressure, as seen in **Figure (3.3 e)**

f- All parameters, including temperature, pressure, water flow rate, and power consumption, are continuously monitored and recorded.

4.13 Adsorption Uptake and ATB Performance Analysis

The variation in the mass of the ABU throughout the charging and discharging processes is employed to determine the quantity of refrigerant vapor that has been adsorbed. The adsorbed refrigerant vapor ($M_{w,J}$) In the silica gel, it may be achieved at various temperatures ranging from 303 to 310 K through the utilization of equation (4.1) [47].

$$M_{w,J} = M_{ads,(T_j)} - M_{ads,(T_i)} \quad (4.1)$$

Where $M_{ads,(T_i)}$ and $M_{ads,(T_j)}$ The mass of the adsorbent at temperatures T_i and T_j, respectively. The evaluation process involves utilizing an accurate digital balance while maintaining equilibrium conditions.

Equation (4.2) represents the formulation for the adsorption uptake q_j, while the change in $M_{w,J}$takes place over time throughout the adsorption process [47]

$$q_j = \frac{M_{ads,(T_j)} - M_{ads,(T_i)}}{M_{ads}} \quad (4.2)$$

Equation (4.3) expresses the variation in adsorption over time (Δq) [47].

$$\Delta q = \frac{M_{ads,(T_{j,t\to\infty})} - M_{ads,(T_i)}}{M_{ads}} \quad (4.3)$$

The error computation can be calculated from equation (4.4) [191]

$$error = \sqrt{\frac{\sum X^2 - n*\bar{X}}{n-1}} \quad (4.4)$$

Where

X is the absolute relative error

$\bar{X}$ is the average value of absolute relative error

n number of comparison results

4.14 Uncertainty Propagation

The Root Sum Square (RSS) approach for uncertainty propagation assumes that the data follow a normal distribution, are independent, and have no systematic errors [191]. The uncertainties of the measurement variables have been determined, as illustrated in Table (4.6). The uncertainty of measurement variables was analyzed using Engineering Equation Solver (EES) software, as Appendix D shows.

Table (4.6) Absolute accuracy of measurements

Variables	Accuracy
T_1= inside ABU_1	± 0.2563
T_2= inside ABU_2	± 0.3526
T_3=inlet water to ABU_1 heat exchanger.	± 0.1168
T_4=outlet water from ABU_1 heat exchanger.	± 0.1058
T_5=inlet water to ABU_2 heat exchanger.	± 0.3025
T_6=outlet water from ABU_2 heat exchanger.	± 0.2098
T_7= ECU_1 vapor temperature	± 0.1895
T_8= ECU_1 liquid temperature	± 0.3256
T_9= ECU_2 vapor temperature	± 0.2856
T_{10}= ECU_2 liquid temperature	± 0.2796
T_{11}=inlet water to ECU_1 heat exchanger.	± 0.3658
T_{12}=outlet water from ECU_1 heat exchanger.	± 0.3025
T_{13}=inlet water to ECU_2 heat exchanger.	± 0.1065
T_{14}=outlet water from ECU_2 heat exchanger.	± 0.1135

Chapter Five

Results and Discussion

Chapter Five

Results and discussion

5.1 Introduction

This chapter presents the results of theoretical, experimental, and numerical investigations to evaluate the performance of a two-bed Adsorption Thermo-Physical Battery System (ATB) with mass recovery. The Simulink MATLAB-19 software is used to solve the Lumped Parameter Method (LPM) model, which is the focus of the theoretical results for MOF-801 and silica gel RD. The performance metrics evaluated for the ATB system include RC, COP, and SCP. Also, the study investigates the experimental suitability of two commercially available adsorbent materials, specifically silica gel-RD and MCM-41, combined with water refrigerant for implementation in a two-bed ATB system with mass recovery. Finally, the numerical solution is based on the heat and mass transfer modeling (HMTM) solved by COMSOL-6 software.

5.2 Two-bed ATB Theoretical Model Results

The primary purpose of the theoretical model was to investigate the enhancement of ATB performance by utilizing a unique adsorbent-water combination, specifically involving MOF 801 and water. Furthermore, the investigation compared the performance improvement achieved using RD-silica gel and water with ATB.

5.2.1 Adsorption and Desorption Temperature Profiles of ATB

Figure (5.1) shows the time-dependent temperature and water uptake-offtake during the adsorption and desorption of the two beds ATB for silica gel RD during four cycles. Firstly, the process for ATB1 is desorption and condensation, while the process for ATB2 is adsorption and evaporation. The temperature of ABU1 increases while ABU2 decreases due to heat exchange between ABU and the heating/CCU and cooling/CCU for desorption and adsorption, respectively. The

temperature of ABU2 dropped from 353 K to 305 K after 350 s of adsorption period. Meanwhile, ABU1 was the reverse of ABU2, where the temperature increased in ABU1. Subsequently, the adsorption process begins at a uniform thermal potential for ABU2, wherein the refrigerant vapor is transferred from ECU2 to ABU2. Conversely, the desorption process occurs at a constant thermal potential for ABU1, whereby the refrigerant vapor is released from adsorbent materials and transferred from ABU1 to ECU1. The vapor form of the refrigerant (water) was desorbed from the ABU1 adsorbents and subsequently transferred to the ECU1/condenser, where it completed a phase change to become liquid refrigerant at a temperature of 305 K. The ECU/condenser temperature decreased from an initial value of 305 K to around 290 K. whereas the refrigerant vapor is transported from ABU1 to ECU1 through desorption. The ECU/evaporator temperature decreased from 288 K to 280 K in the ECU2/evaporator during the initial phase of the adsorption period. Subsequently, there is a slight increase in temperature until the completion of the adsorption process at 1000 sec.

Clearly, during the initial stages of the adsorption process, the temperature of the ECU was observed to decrease due to the rapid and significant adsorption uptake occurring at that moment. The refrigerant vapor was transported continuously from the ECU to the ABU, resulting in a continuous heat transfer from the evaporator to the chilled water. Consequently, this led to slightly increased refrigerant temperature in the ECU.

Also, the figure demonstrates the fluctuations of uptake and offtake rates as a function of cycle time throughout ATB's adsorption and desorption processes for silica gel RD. During the desorption phase for ATB1, from 0 to 1000 seconds, the water vapor desorption rate indicated a drop from 0.32 to slightly about 0.008 kg_w/kg_{ads}. Throughout this particular procedure, the ABU's temperature experienced an elevation due to heat transfer from the heated coolant fluid to the ABU. During

the adsorption process for ATB1, during the 1000 to 2000 seconds, the mass of the adsorbed water raised to 0.32 kg_w/kg_{ads} because the coolant water cooled ABU. In contrast, ABU2 was a reverse of ABU1. In addition, it is interesting to observe that the relationship between adsorption uptake and cycle time is close to an exponential trend, as shown in Figure (5.1).

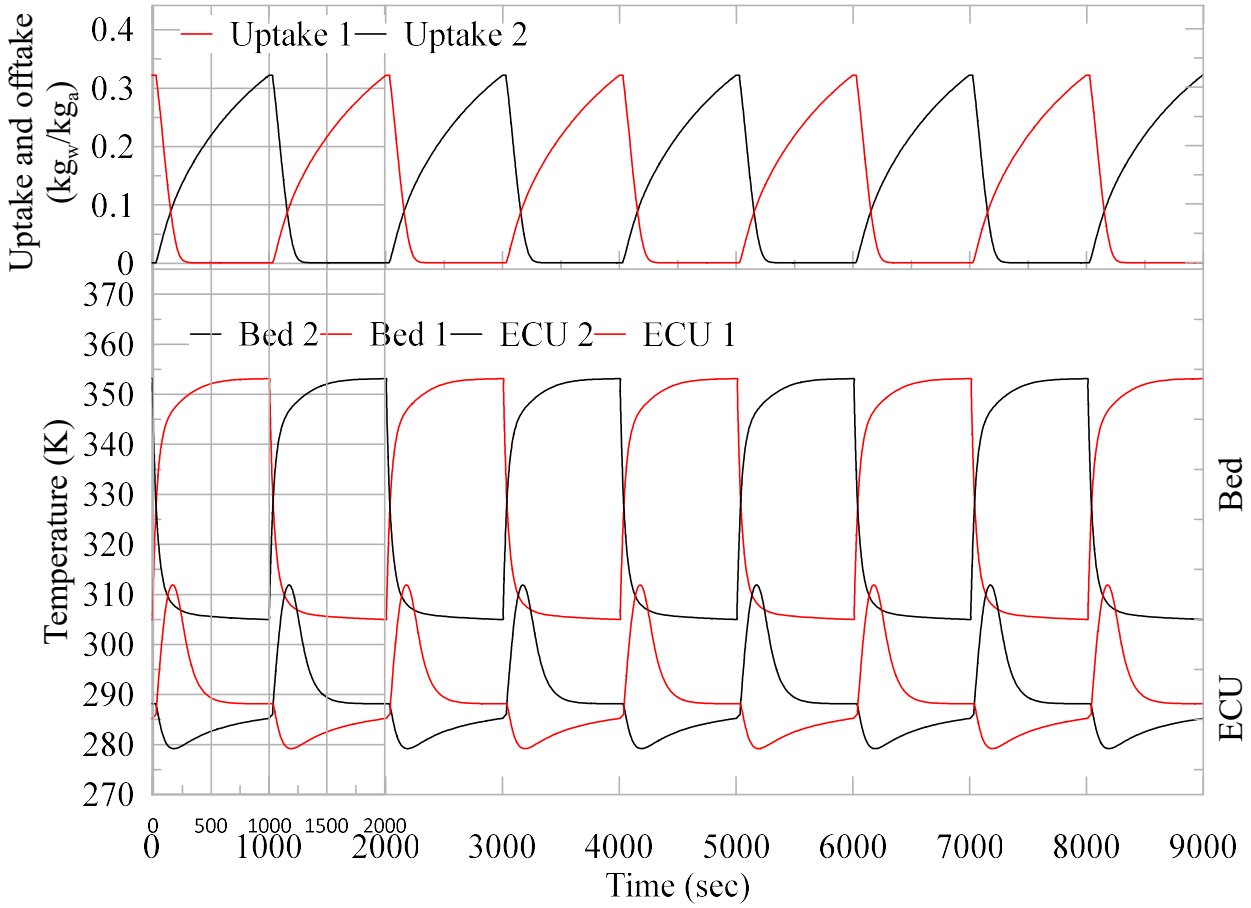

Figure (5.1) Variation of temperature and water uptake with time during the adsorption and desorption of the two beds ATB for four cycles.

A comparison of the time-dependent temperature and water uptake-offtake during the adsorption and desorption of the two beds ATB between MOF-801 and silica gel RD is shown in Figure (5.2). This comparison was made during one cycle. The temperature of ABU1 was increased from 305 to 353 K for MOF 801 and silica gel RD after 450 and 350 s of the adsorption period, respectively. Meanwhile, ABU2

was the reverse of ABU1, which dropped in temperature from 353 to 305K for the same adsorbents and time.

The ECU/condenser temperature decreased from an initial value of 305 to around 290 K. whereas the refrigerant vapor is transported from ABU1 to ECU1 through desorption. The ECU/evaporator temperature decreased from 288 to 278 K for MOF 801 and from 288 to 280 K for silica gel RD in the ECU2/evaporator during the initial phase of the adsorption period.

Also, the figure demonstrates the desorption phase for ATB1; from 0 to 1000 seconds, the water vapor desorption rate indicated a drop from 0.44 to slightly about 0.008 kg_w/kg_{ads} for MOF 801 and from 0.32 to slightly about 0.008 kg_w/kg_{ads} for silica gel. Meanwhile, during the adsorption process for ATB1, during the time interval of 1000 to 2000 seconds, the mass of adsorbed water raised to 0.44 kg_w/kg_{ads} and 0.32 kg_w/kg_{ads} for MOF 801 and silica gel, respectively. MOF 801 required more time than silica gel to complete the adsorption process because it is a more hydrophilic, porous material.

Due to its improved dynamic adsorption capabilities compared to silica gel, MOF 801 gradually decreases evaporator temperature until it exceeds the corresponding value for silica gel. In addition, this figure illustrates that MOF 801 has a higher water absorption than silica gel RD; consequently, it is predicted that MOF 801 will demonstrate better results.

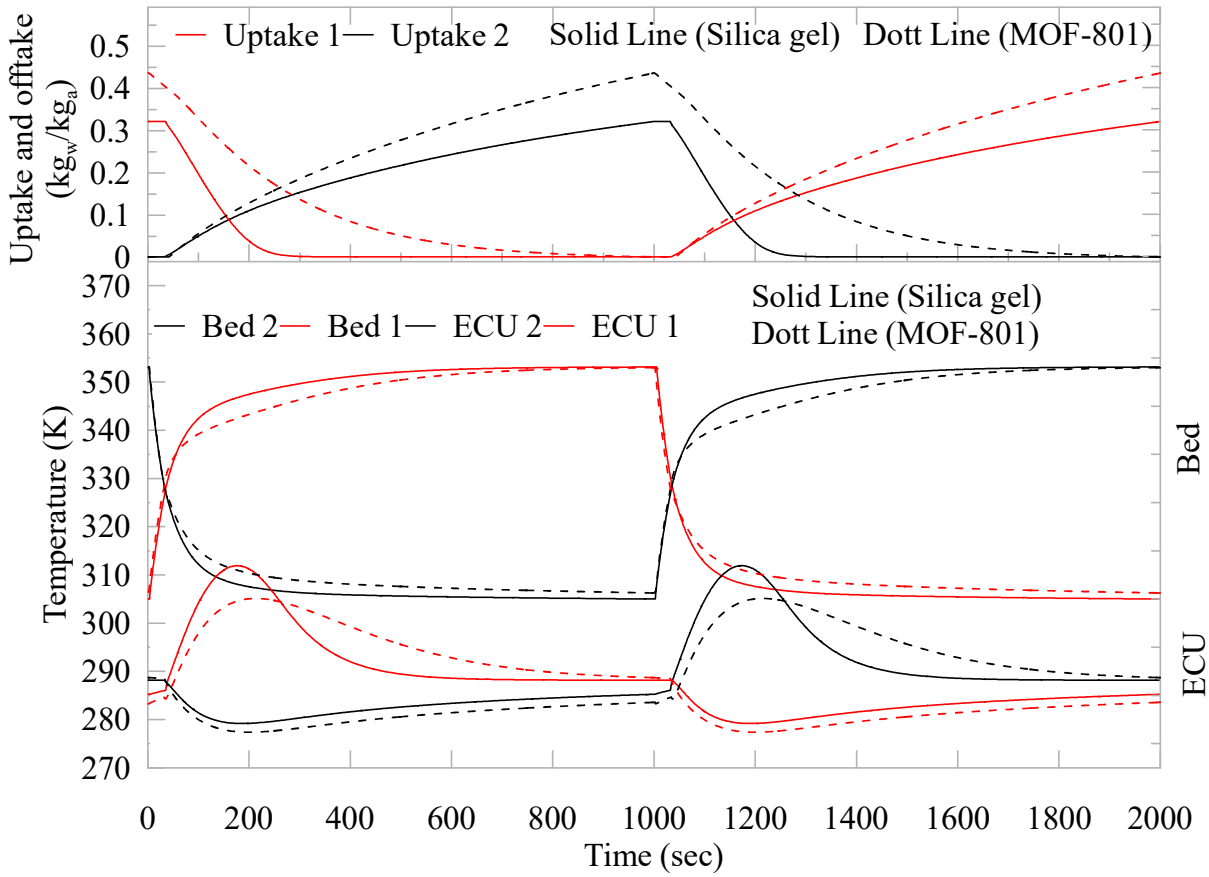

Figure (5.2) Variation of temperature and water uptake with time during the adsorption and desorption of the two beds ATB for one cycle for MOF-801 and silica gel RD

5.2.2 Effect of the Half Cycle and Switching Time

The impact of cycle time on the RC and COP of the ATB under the rated operating conditions is illustrated in Figure (5.3). The RC of the ATB has been increasing in correlation with cycle time, reaching its peak value of 2.7 kW and 4.8 kW when the cycle time is set at 1000 s for silica gel and MOF-801, respectively. The COP of the ATB has reached its peak value of 0.25 and 0.3 when the cycle time is set at 1000 s for silica gel and MOF-801, respectively. When the cycle duration is reduced, the cooling capability reduces due to insufficient time for satisfactory adsorption or desorption. In contrast, for cycle periods above 1000s, the cooling capacity

experiences a slight reduction for both silica gel and MOF 801. This reduction in RC after 1000 s can be attributed to refrigerant exhaustion in the ATB, which causes excessive heating, negatively affecting the RC and performance.

The data presented in Figure (5.4) demonstrates that both the RC and COP of the ATB show a rising trend with an increase in switching time, reaching their optimal values at approximately 30 seconds. When the value is beyond the ideal limits, the cooling performance experiences a drop as the switching time rises. Therefore, a longer switching time is not beneficial. A similar behavior was identified in the outcomes of the research study [173], wherein the COP and RC displayed a rising trend with cycle time. In contrast, they decreased with an increase in switching time.

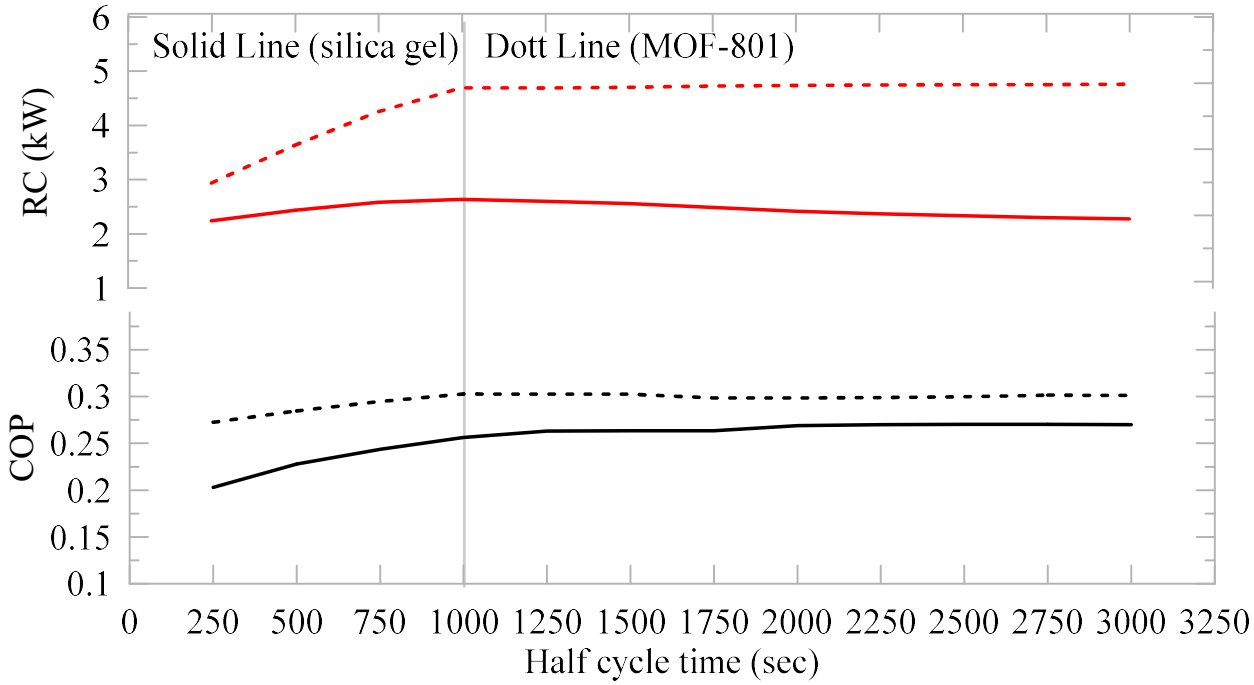

Figure (5.3) Variation of average COP and average RC as a function of half cycle time for MOF-801 and silica gel RD.

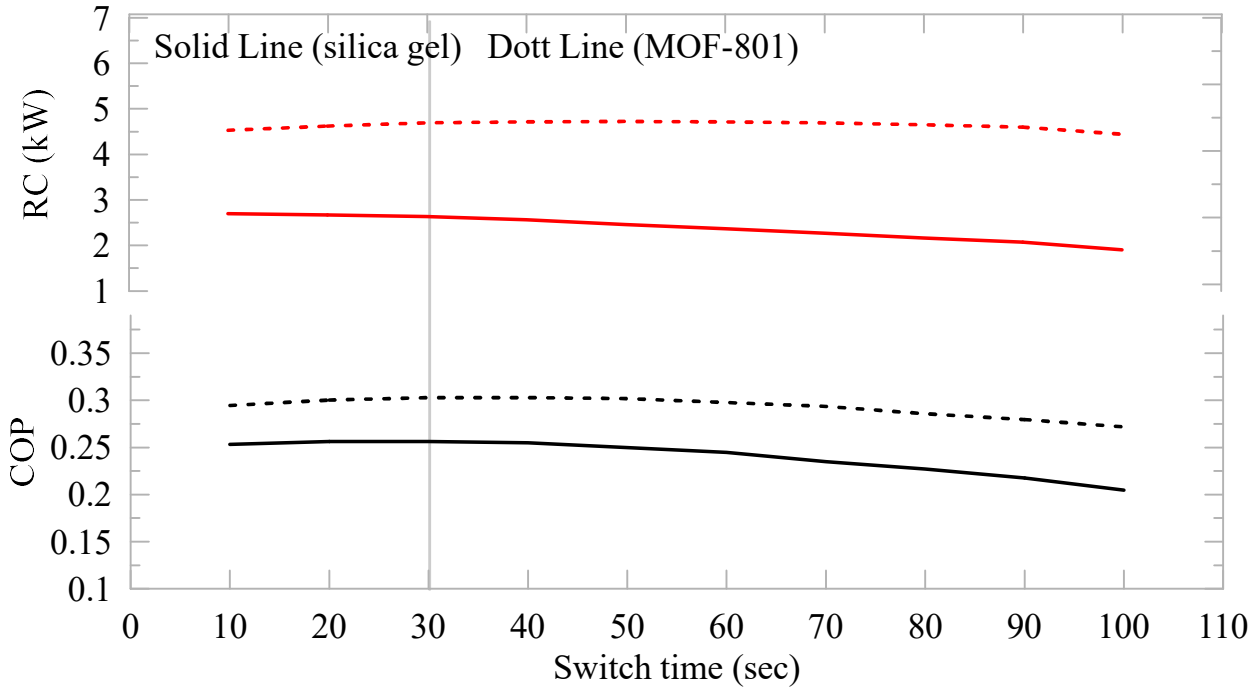

Figure (5.4) Variation of average COP and average RC as a function of switching time for MOF-801 and silica gel RD.

5.2.3 Effect of Adsorbent Mass

The influence of adsorbent mass on the SCP and the COP of the ATB is depicted in Figure (5.5). The COP of the ATB demonstrates an upward trend until the entire mass of the adsorbent reaches 10 kg. In contrast, it is shown that for adsorbent masses exceeding 10 kg, the COP remains constant for both silica gel and MOF 801. This can be attributed to a larger adsorbent mass, allowing for more significant initial adsorption of refrigerant. Therefore, in desorption, more refrigerant vapor is released, leading to an increased cooling impact and consequently yielding a higher COP.

In contrast, when the mass of the adsorbent exceeds 10 kg, there is minimal variation in the COP. At the same time, the SCP continues to decrease with increasing adsorbent mass. The increasing mass of the adsorbent results in a

reduction in heat transfer rates and incomplete desorption, leading to a fall in the chiller's SCP.

Figures (5.3), (5.4), and (5.5) provide conclusive evidence demonstrating that MOF 801 outperforms silica gel RD for COP, RE, and SCP; therefore, the focus of the research is on the performance of the ATB when MOF 801 and water are used as adsorbent pair.

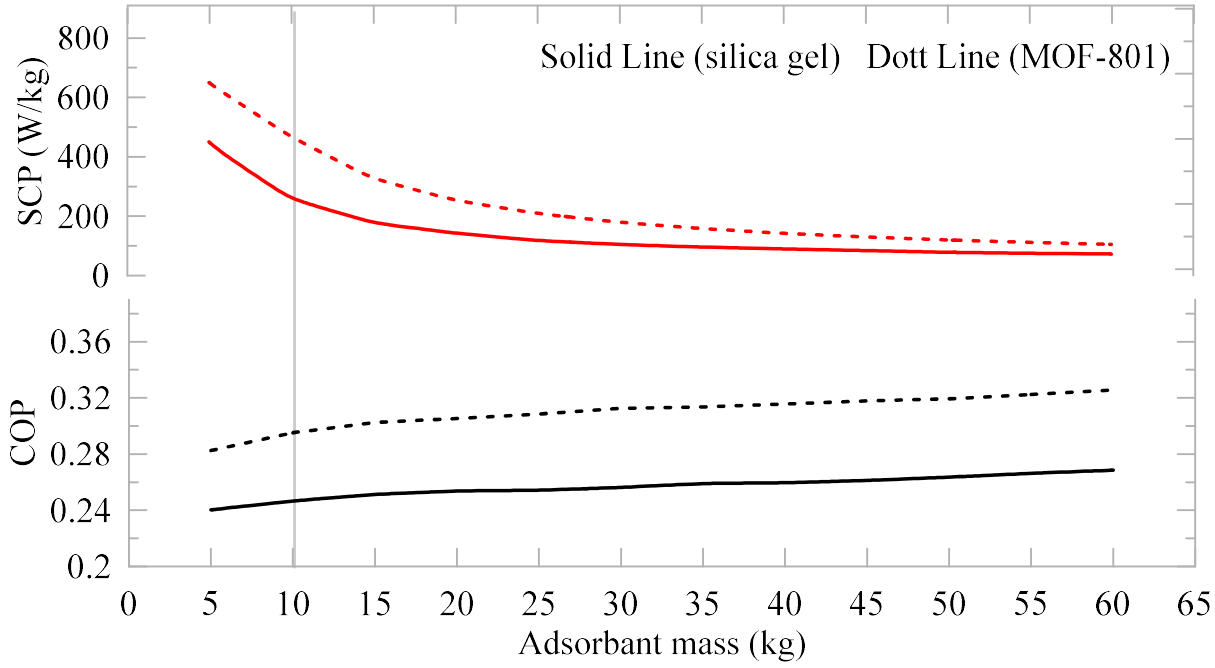

Figure (5.5) Variation of average COP and average SCP as a function of adsorbent mass for MOF-801 and silica gel RD.

5.2.4 Effect of Fin Thickness

The thickness of the fin is a significant parameter that substantially impacts the performance of the ATB cycle. Figure (5.6) illustrates the impact of fin thickness on the COP and RC for MOF 801. The increase in fin thickness is related to a drop in the COP and RC. The heat capacity ratio between the metal fins and the adsorbent is increased for a substantial thickness. Consequently, the rise in heat input to the metal fins and tubes decreased the COP. The study's results indicated a decrease in the COP by 23% when the thickness of the fins was increased from 0.5 to 5 mm.

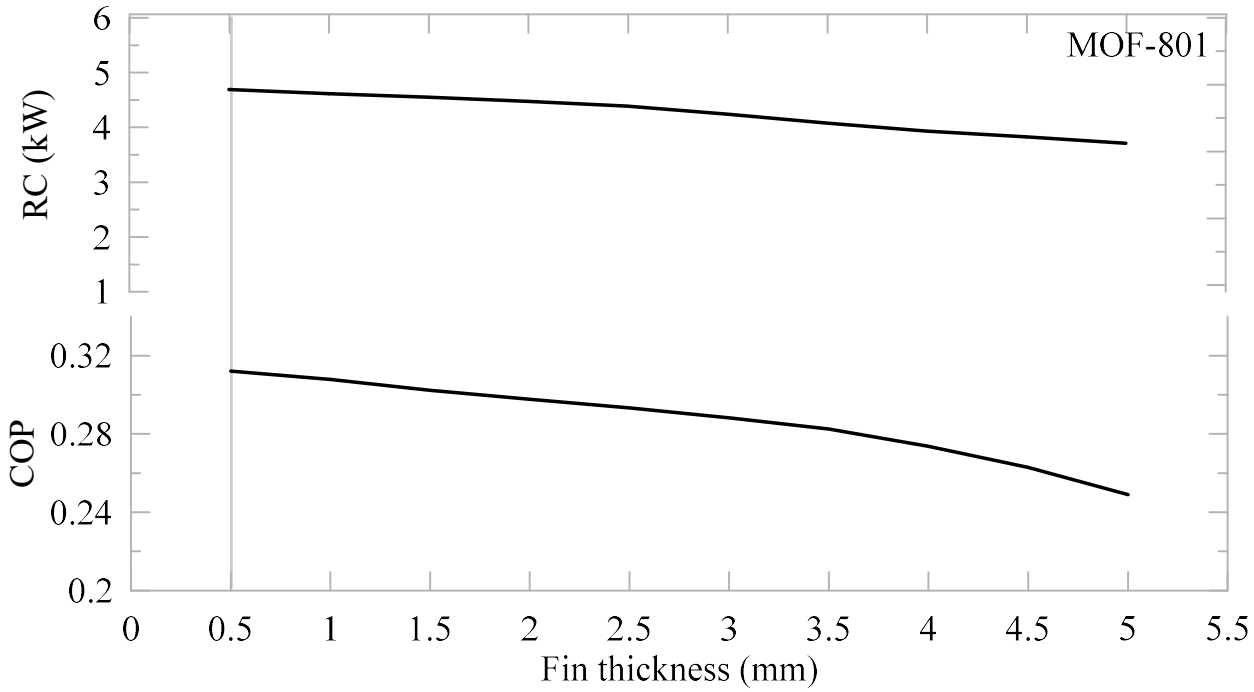

Figure (5.6) Variation of average COP and average RC as a function of adsorbent bed thickness for MOF-801.

5.2.5 Effect of the Hot, Cooled, and Chilled Mass Flow-rate on ATB Performance

The heat energy supplied to ATB by hot coolant during the desorption process is determined by the heat transfer fluid (coolant) mass flow rate and the driving temperature. Figure (5.7) shows the variation of RC and COP with a hot, cooled, and chilled coolant flow rate for MOF 801 adsorbent. It can be observed that the COP drops from 0.37 to 0.28 with a hot coolant mass flow rate increasing from 0.2 – 2 kg/sec. The findings revealed that increasing the hot coolant mass flow rate from 0.2 to 2 kg/sec decreased the COP by 24%.

It can be observed from the figure that the RC raised a maximum value of 4.8 kW for MOF 801 at a mass flow rate of 1 kg/s. It can be concluded that the hot water flow rate was directly proportional to the RE and inversely to COP.

The cooling supplied to ATB by cold water during adsorption is determined by the heat transfer fluid (coolant) mass flow rate and the cooled water temperature.

It can be observed that the COP reaches a maximum value of 0.3 with a cooled coolant mass flow rate of 1 kg/sec. Also, it can be observed from the Figure that the RC raised from 2.1 kW to 4.6 kW. It can be concluded that the cooled water flow rate was directly proportional to the RE and COP.

With the chilled mass flow rate increasing, the COP improved steadily due to the cooling capacity improvements in the heat transfer rate between the chilled coolant and evaporator. Increasing the chilled coolant mass flow rate from 0.2 to 2 kg/sec resulted in an enhancement in the COP by about 26 % and an enhancement in the RC by about 56 %. The figure shows that 1 kg/s is the best flow rate for chilled, hot, and coolant water. Finally, an approximately similar trend was observed in the reported research work result [192], [193]. It can be concluded from the research that the COP was directly proportional to the chilled and cooled water flow rate and inversely to the hot water flow rate.

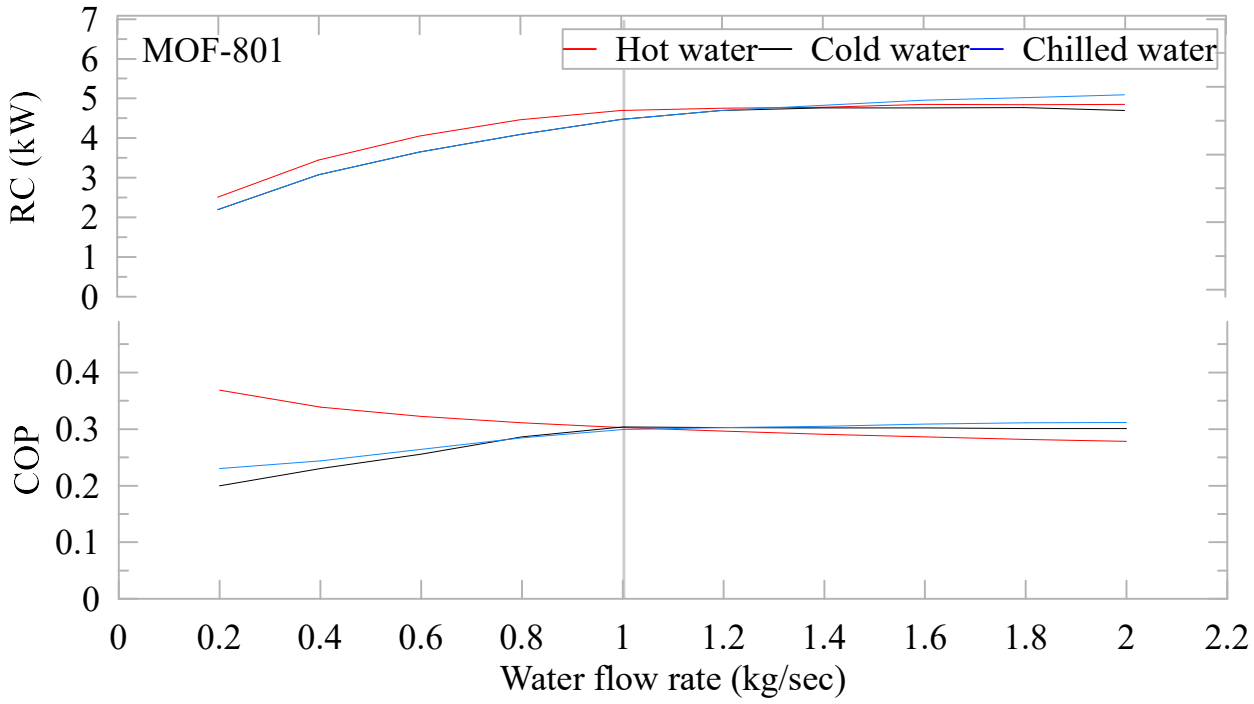

Figure (5.7) Variation of average COP and average RC as a function of hot, cooled, and chilled water mass flow rate for MOF-801.

5.2.6. Effect of Hot Coolant Inlet Temperature

Figure (5.8) consists of three subfigures: the upper one is for the offtake of adsorbent, the middle is for the ABU desorption process, and the lower is for condensation of refrigerant in the ECU. Three temperatures of the hot water are examined: 343, 353, and 363 K. As can be seen from the figure, the hot water temperature increases and the ABU temperature increases during the desorption process, as it is expected that the refrigerant is desorbed at the higher temperature. Also, the condensed refrigerant in ECU is achieved at higher temperatures, as shown in Figure 5.8. However, the amount of desorb refrigerant showed an insignificant improvement. The effect of hot water temperature on the ECU vanishes after about 400 seconds because the condensation process is achieved during the first 400 seconds.

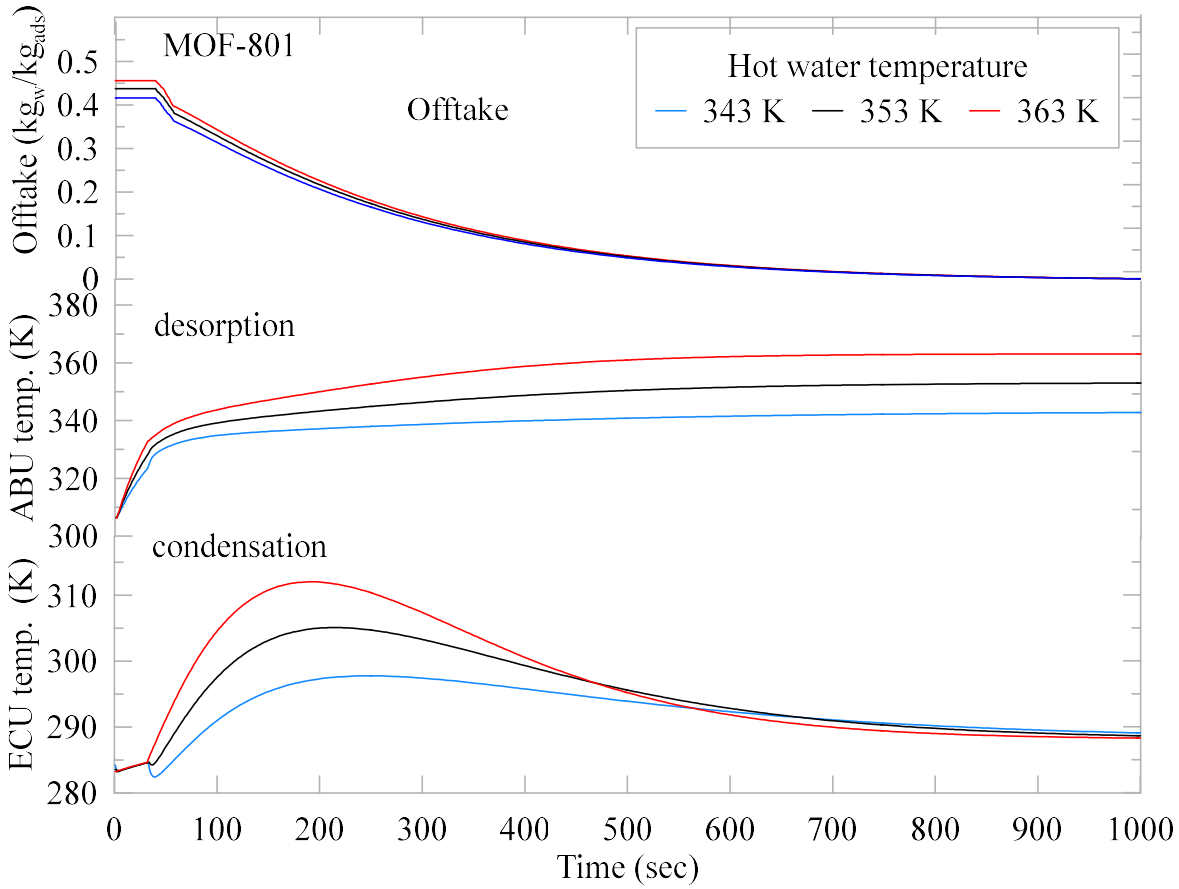

Figure (5.8) Variation of temperature and water offtake with time during the desorption of the two beds ATB at different hot water temperatures for MOF-801.

The insignificant increase in the desorb refrigeration due to the increase in hot water temperature led to a slight rise in SCP and RC, as shown in Figure (5.9). However, this increase is not proportional to the increase in energy consumed for heating water, so the decrease in the desorb refrigeration negatively impacted the system's COP. Based on the figure, the minimum hot water temperature gives a COP of about 0.4 and 0.28 for the higher water temperature. So, the COP was reduced by 31.6 % as the hot water temperature increased from 343 to 363 K.

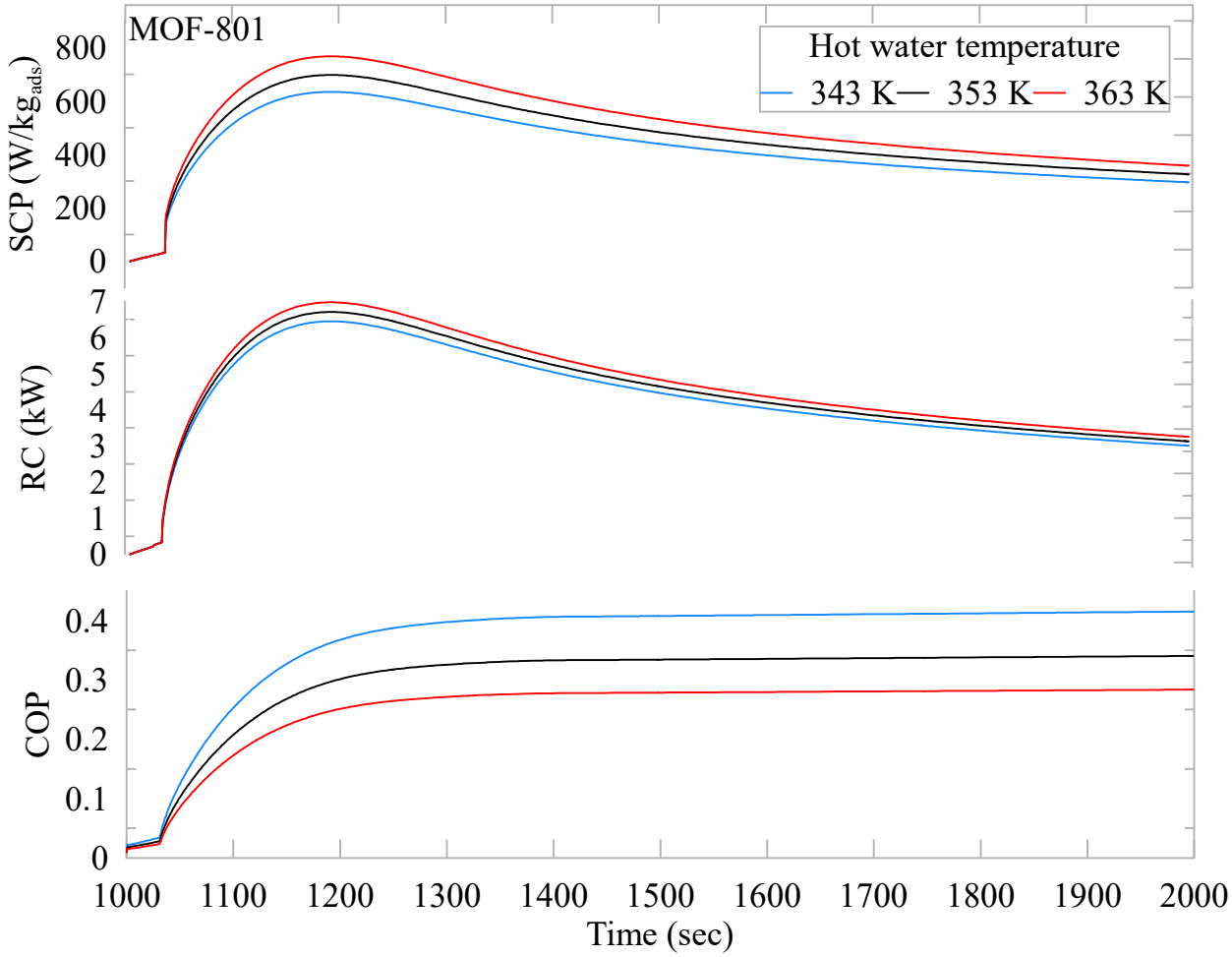

Figure (5.9) Variation of SCP, RE, and COP with time during the adsorption of the two beds ATB at different hot water temperatures for MOF-801.

5.2.7. Effect of Cooled Coolant Inlet Temperature

The next step following the desorption process is the adsorption of refrigerant in the ABU by utilizing cooled water supplied by the CCU. Figure (5.10) consists of three subfigures: the upper one is for the uptake of adsorbent, the middle is for the adsorption process in the ABU, and the lower is for evaporation of refrigerant in the ECU. Three temperatures of the cooled water are 303, 308, and 313 K. It is noticeable that the temperature of the ABU approached the temperature of the cold inlet coolant towards the end of the adsorption process. The decrease in coolant inlet temperature resulted in a reduction of the ABU temperature, causing an increase in the uptake of the adsorbent. At the beginning of the evaporation process, the refrigerant liquid contained within the ECU changed from liquid to vapor, and afterward, it was adsorbed by MOF 801. The Figure illustrates a progressive decrease in the ECU/evaporator temperature as the inlet-cooled temperature is reduced.

The variations of RC, SCP, and COP for the ATB with cycle time at various cooled coolant temperatures of 303 K, 308 K, and 313 K are illustrated in Figure (5.11). Throughout the adsorption process, the quantity of water vapor adsorbed by the adsorbent increased until the adsorbent became saturated with water vapor. As a result, the cooling capacity generated diminished with time. It can be observed that the RC increases with a reduction in coolant temperatures. This behavior is attributed to increased vapor uptake with a decrease in coolant temperature during adsorption and has an insignificant impact on the system's COP. The maximum COP at an inlet coolant temperature of 303 K was 0.34. As the coolant temperature decreased from 313 K to 303 K, the COP increased by 5%. It is believed that the system COP is unaffected by the coolant temperature variation because the energy spent on cooling the water is not included in the COP equation.

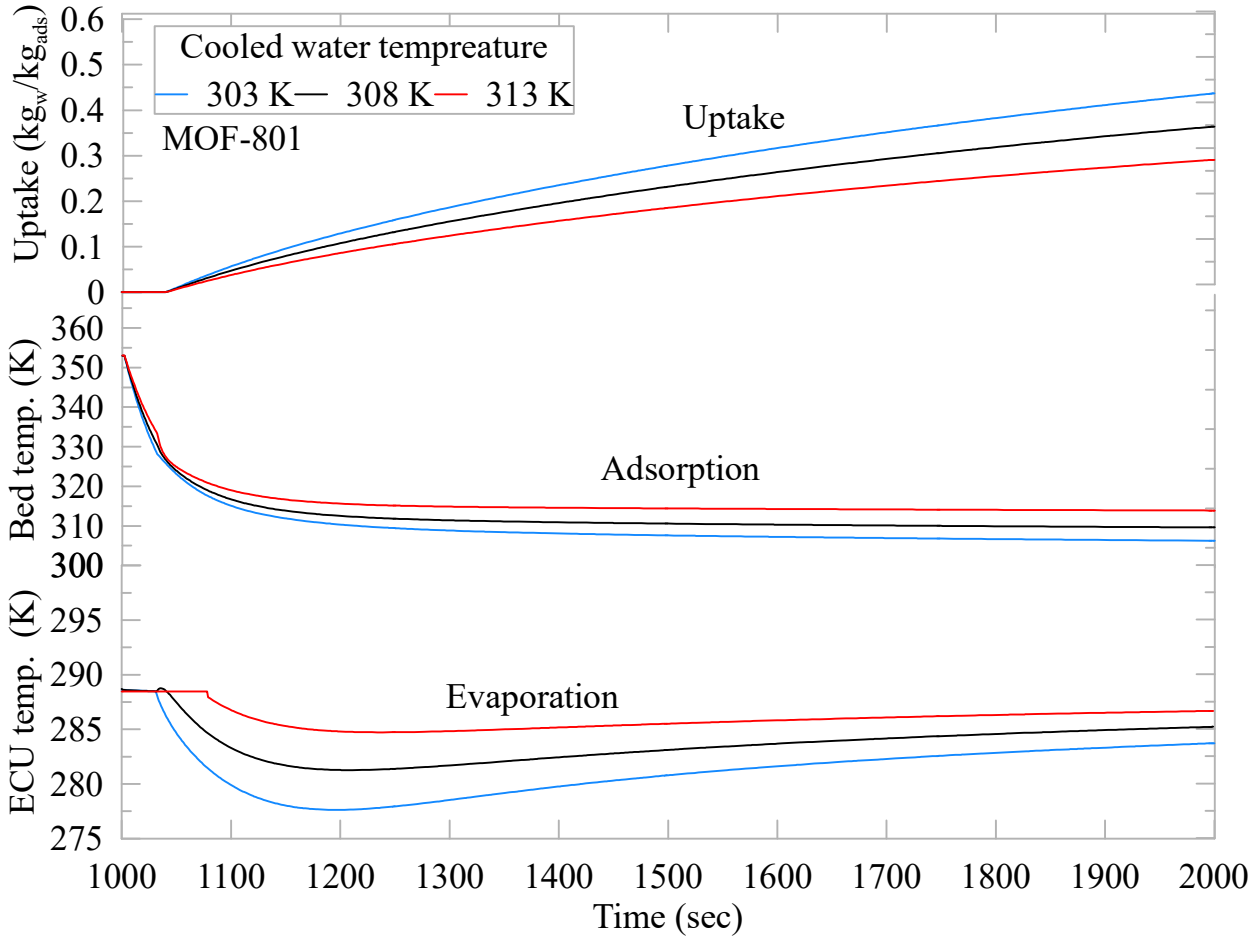

Figure (5.10) Variation of temperature and water uptake with time during the adsorption of the two beds ATB at different cooled water temperatures for MOF-801.

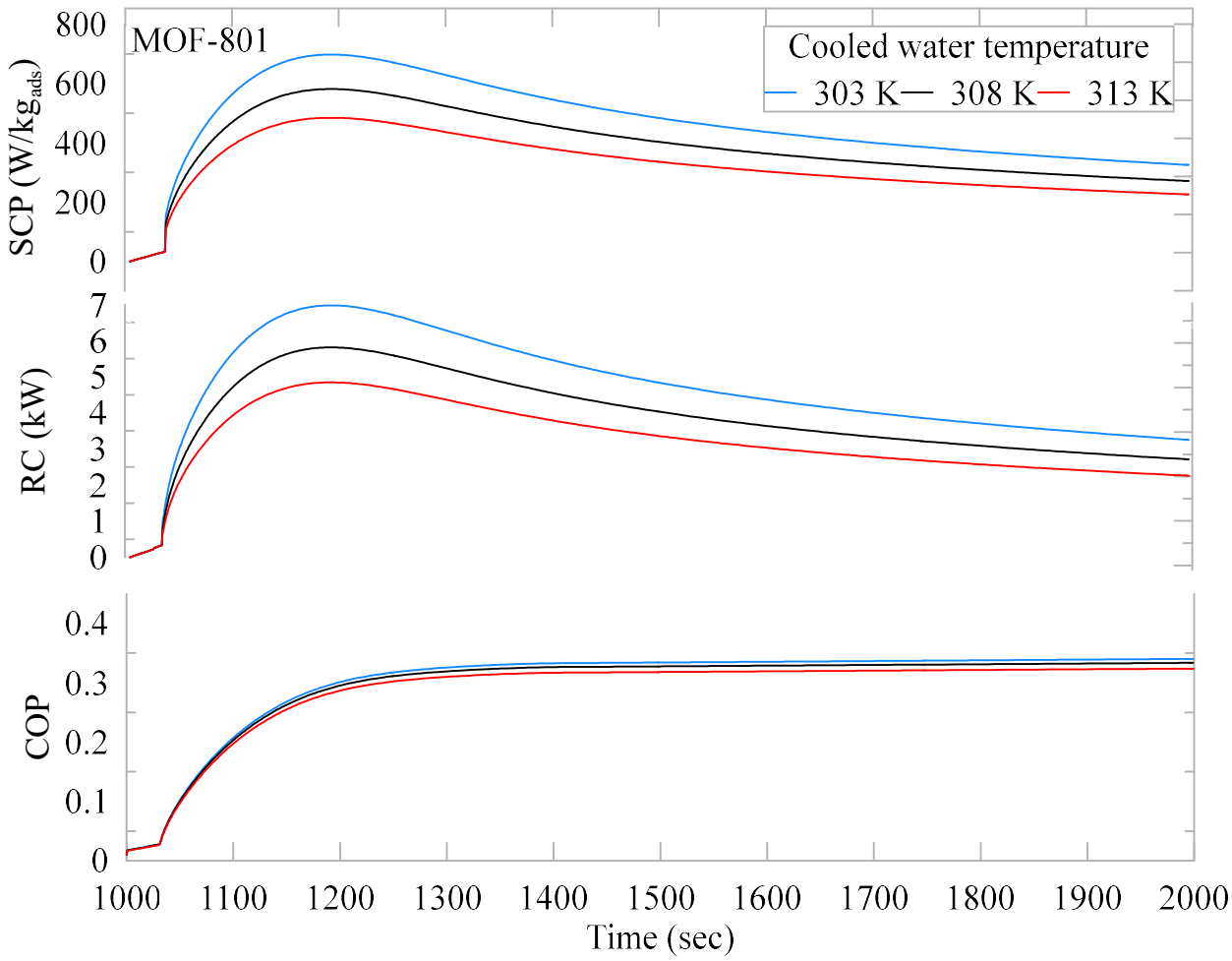

Figure (5.11) Variation of SCP, RE, and COP with time during the adsorption of the two beds ATB at different cooled water temperatures for MOF-801

5.2.8 Theoretical Results Validation with Other Work

The variation of the single-bed system COP with time for the present work was validated with A. L. Tarish [74] and B. B Saha's [194] results, as shown in Figure (5.12). It is observed that the deviation of the present work for Ali Latif's work is +4%, while it is -11% for B. B Saha's, by using equation (4.4). The comparison was based on a chilled coolant temperature of 285 K, an inlet-cooled coolant temperature of 303 K, and a driving temperature of 323 K. Figure (5.12) also shows that the double-bed cycle produces a higher COP than the single-bed cycle by about 17 %.

Thus, the cooling power increased using a double bed system without increasing the driving force's temperature.

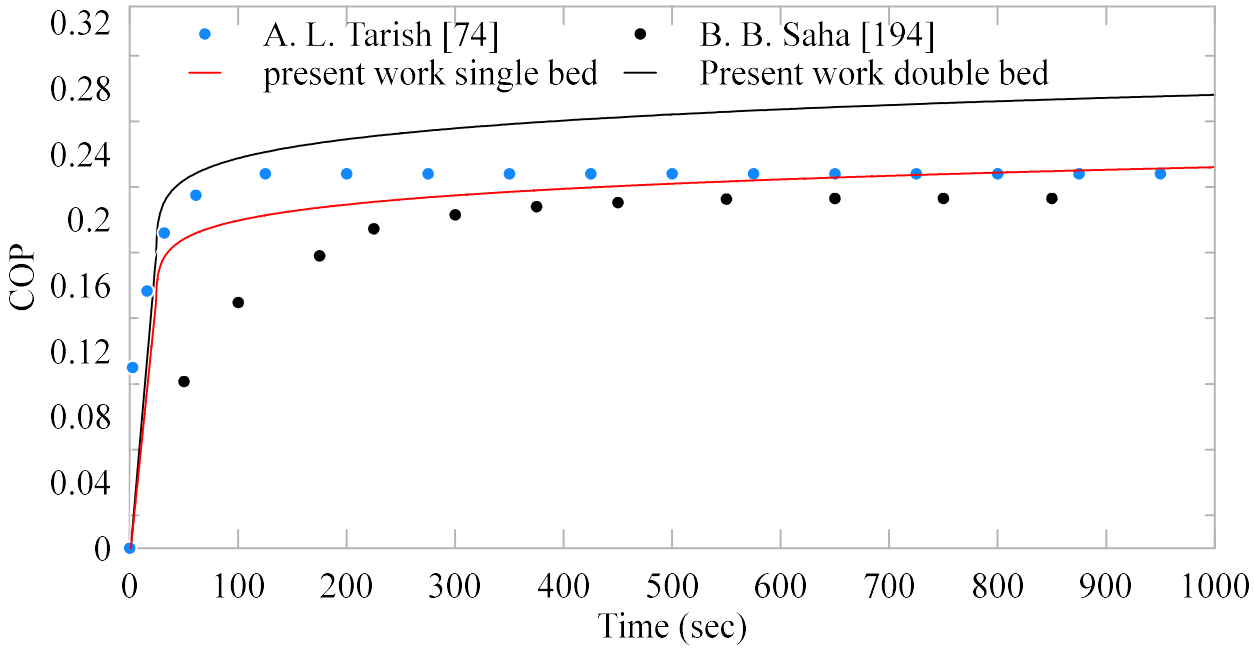

Figure (5.12) Validation of the present work COP with previous works.

5.3. Experimental Results

This part presents the experimental research results that assess the impact of adsorbent materials, coolant temperature, coolant flow rate, and mass recovery time on the air conditioning system's performance using the two-bed ATB with mass recovery technology. MOF 801 costs around 400 to 500 $/g, so it is excluded from the experimental work, and Mobil Composition of Matter No. 41 (MCM-41) is used instead of MOF 801, as the uptake is compared in Figure 1.1. The adsorbents MOF-801 and MCM-41 exhibit the best and closest to the ideal cycling performance. Regular density (RD) silica gel is a reference point, with water refrigerant as a working pair. Several performance criteria were assessed by experimental evaluation conducted under varied operating conditions.

5.3.1 Effect of Duration of Mass Recovery

The ATB was tested without and with mass recovery; the duration of mass recovery was 30, 60, and 90 seconds. Figure (5.13) illustrates the temperature of the ABU and ECU throughout the mass recovery procedure. It was observed from the Figure that the ABU temperature responded to the mass recovery time before switching between two beds for the silica gel RD/water pairs. Also, it can be noticed that there is an improvement in evaporated temperature in the first ATB after mass recovery. The average minimum temperature was 282.3 for no mass recovery and 282.1, 281.1, and 281.8 K for mass recovery times 30, 60, and 90 sec respectively.

Figure (5.14) shows the performance of ECU 1 and ECU2; it can be seen from the figure that the operating time of ECU2 is from 200 to 1000 s. After that, the refrigerant vapor produced from ECU1 is adsorbed by ABU1 during the time extended from 1300 to 2000 s. Meanwhile, the ECU1 and ABU1 exchange the time with the ECU2 and ABU2 to obtain a semi-continuous refrigeration cycle. The figure shows three periods; period one starts after opening the ECU2 valve and continues to about 1000s, where the recovery mass valve is open to enter period 2 from about 1000 to 1300s. The second refrigeration effect occurs when the ECU1 valve is opened and extended to time about 2000s.

As shown in Figure (5.14), the mass recovery is for the third period, i.e., for ECU 1. It can be seen from the figure that when there is no mass recovery, both the RC and SCP are at the minimum; as the mass recovery started for 30 seconds, the RC and SCP increased slightly. The maximum RC, SCP, and COP is when the mass recovery time is 60s. As the period of mass recovery rises more than 60 s, the RC, SCP, and COP deteriorate.

The mass recovery works to transfer the remaining refrigerant mass from the ABU1 to the ECU2 to increase the capacity of the evaporator. However, when the mass is transferred, the pressure in the ECU2 rises slightly, which leads to a partial

decrease in the capacity of the evaporator and is compensated for by the recovered mass. Opening the evaporator to the refrigerator for an extended period may increase the mass of the refrigerant fluid. However, it raises the evaporator pressure significantly, which leads to the loss of the effect of the recovered refrigerant mass, as when the mass recovery time is 90s.

The average SCP, RC, and COP are 386 W/kg, 135 W, 0.2 for no mass recovery, 391 W/kg,136 W, 0.209 for mass recover 30 sec, 409 W/kg, 143 W, 0.228 for mass recovery 60 sec, and 400 W/kg, 140 W, 0.216 for mass recovery 90 sec. Figure (5.15) shows that the COP exhibited its best value following the completion of the mass recovery process, precisely when the mass recovery time was set to 60 seconds.

The COP of the process exhibited a more significant value when mass recovery was implemented than when it was not. Mass recovery facilitated a greater desorption of water vapor from ABU 1 and increased water vapor adsorption by ABU 2. The RC of the circulation system with mass recovery was greater than that of the system without mass recovery. In the case of the ATB2, the COP for the process involving mass recovery over 60 seconds was determined to be 0.228. Conversely, the COP for the process without mass recovery was 0.2. Indicates that mass recovery resulted in a 14% increase in COP.

In the mass recovery process, it is seen that the adsorbers are not physically linked to the evaporator and condenser units. Only the mass recovery valve is activated during the initial phase of the mass recovery procedure. The desorber operates under elevated pressure conditions, whereas the adsorber operates under reduced pressure conditions. The desorbed water vapor is directed from the high-pressure heated desorber to the low-pressure cooled adsorber by connecting the two adsorbers. Mass recovery can further dehydrate the desorber after desorption, diminishing the internal pressure. The dryer adsorber can adsorb a more significant

amount of water vapor during the subsequent adsorption phase. This approach results in an enhancement of the performance provided by the ATB.

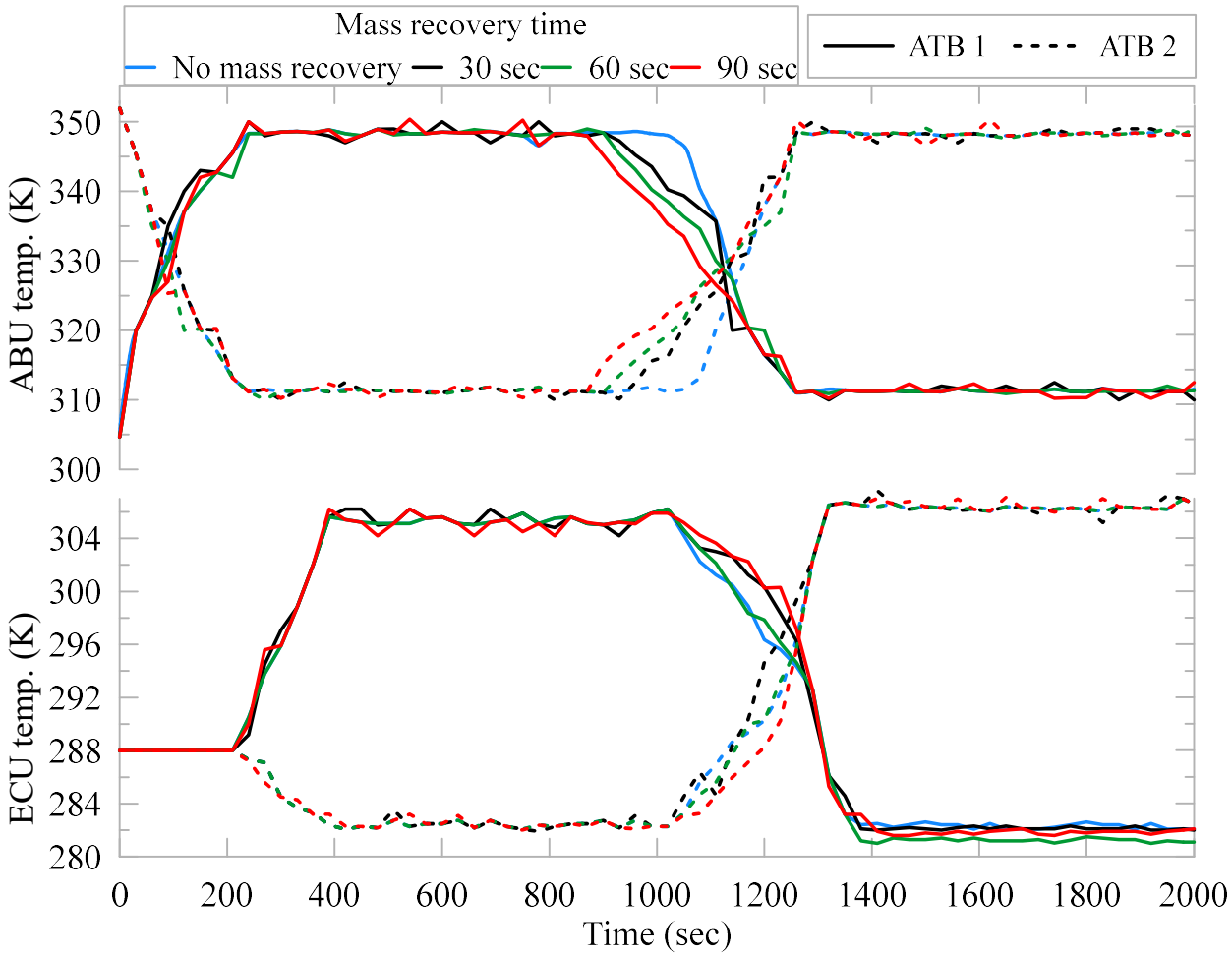

Figure (5.13) Variation in the temperature of the ABU and ECU with time as a function of the mass recovery period.

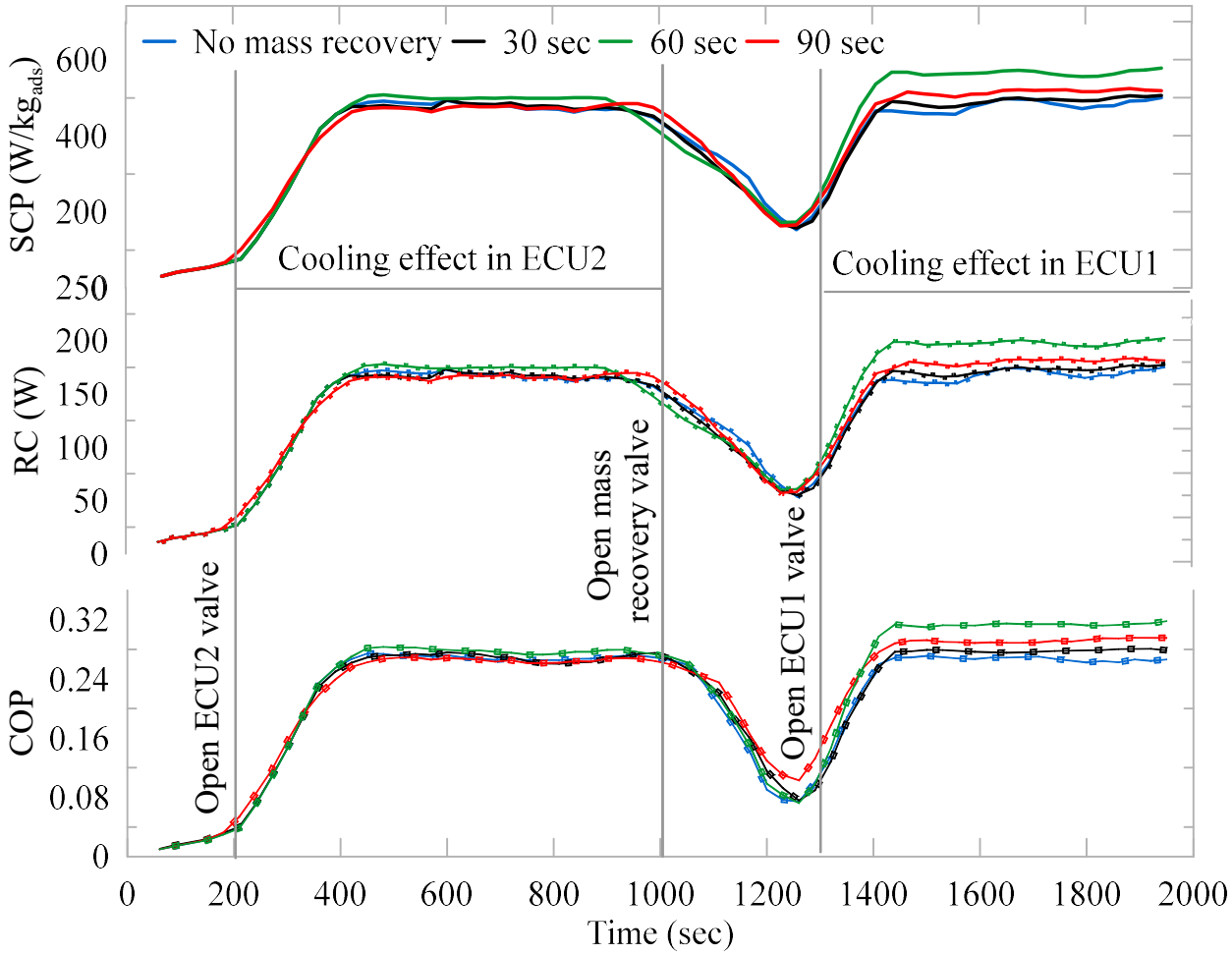

Figure (5.14) Variation of the SCP, RC, and COP with time as a function of the mass recovery period.

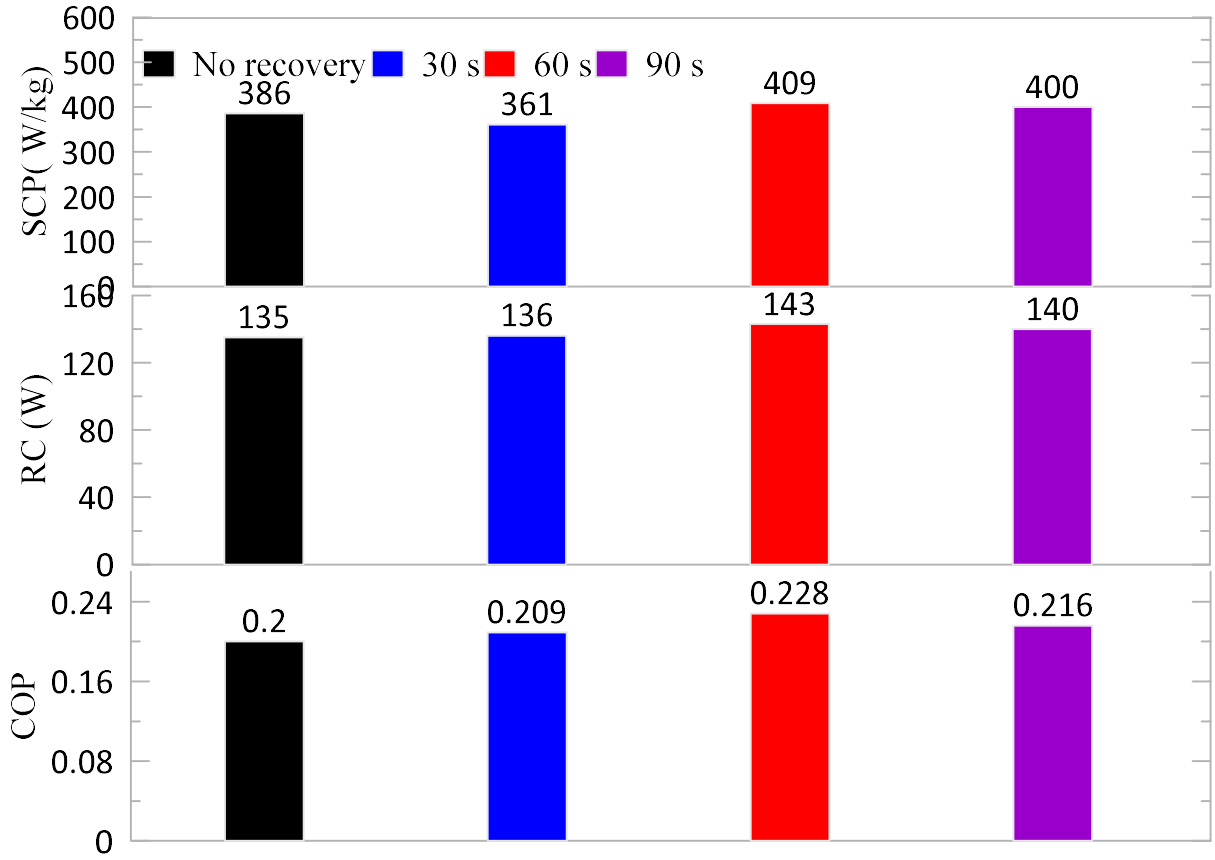

Figure (5.15) Effect of mass recovery on the system performance

5.3.2 Effect of Hot, Cooled, and Chilled Mass Flow-rate

Figure (5.16) illustrates the relationship between the SCP, RC, and COP with the flow rate of hot water, cooled coolant, and chilled water for the silica gel RD/water pair. The figure shows that the SCP and RC have the same trend. The decrease in SCP and RC can be detected when the chilled mass flow rate increases from 0.5 to 1.5 LPM while the COP has an approximately stable value. The reduction in the COP was around 2 % when the mass flow rate of chilled coolant was raised from 0.5 to 0.15 LPM. The study's results indicated that when the hot and cooled coolant flow rate was increased from 0.5 to 1 LPM, there was a corresponding increase in the RC, SCP, and COP, which decreased after the flow rate rose more than 1 LPM.

It can be concluded that the best mass flow rate for the hot cooled was 1 LPM, while the best mass flow rate for chilled water was 0.5 LPM to operate the ATB system for optimum cycle performance.

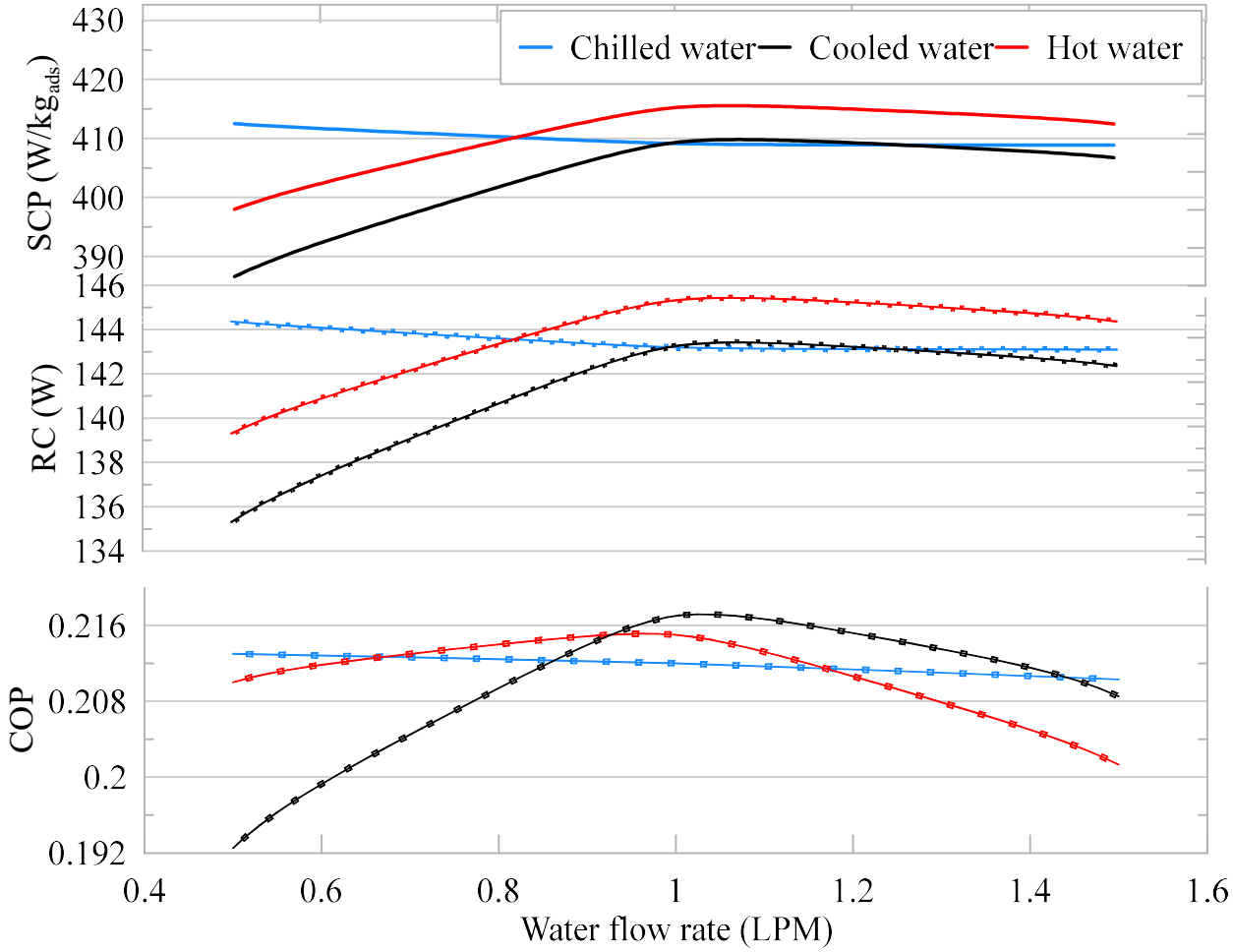

Figure (5.16) Variation of the SCP, RC, and COP with time as a function of the hot, cooled, and chilled water flow rate

5.3.3 Pressure Distribution

Figure (5.17) displays the pressure fluctuations observed in the two adsorbers equipped with mass recovery mechanisms. The pressure of ABU1 rapidly increased until it reached a condenser pressure after 400 seconds, which is attributed to the process of water vapor desorption. In the time between 400 seconds and 940 seconds, the pressure of ABU1 remains consistent due to its connection with ECU1.

Additionally, the water vapor desorbed from ABU1 undergoes condensation in the water condenser.

The pressure of ABU2 gradually decreases over roughly 400 seconds due to refrigerant vapor's adsorption caused by the bed's cooling. The pressure of ABU2 remains consistent between 400 and 940 s due to its connection with ECU2. Additionally, the water evaporated in the ECU is absorbed by ABU2.

The mass recovery process occurred between the time intervals of 940 seconds and 1000 seconds. The pressure equilibrium between the two adsorbers was achieved due to the interconnection between ABU1 and ABU2. However, after 1000 sec, the pressure of ABU 1 decreases to the evaporator pressure because it is connected to the ECU2/evaporator, and the pressure of ABU 2 increases to the condenser pressure because it is connected to the ECU1/condenser.

The pressure of the ECU/condenser and ECU/evaporator remain constant at the first 400 sec because they are isolated from ABU1 and ABU2 after 400 sec. When the ABU1 reaches condenser pressure, it is connected with the ECU/condenser, and when the ABU2 reaches evaporator pressure, it is connected with the ECU/evaporator. The findings of this study also demonstrated that the adsorption process with mass recovery exhibited greater intensity than the adsorption process without mass recovery. The system's RC was enhanced due to mass recovery.

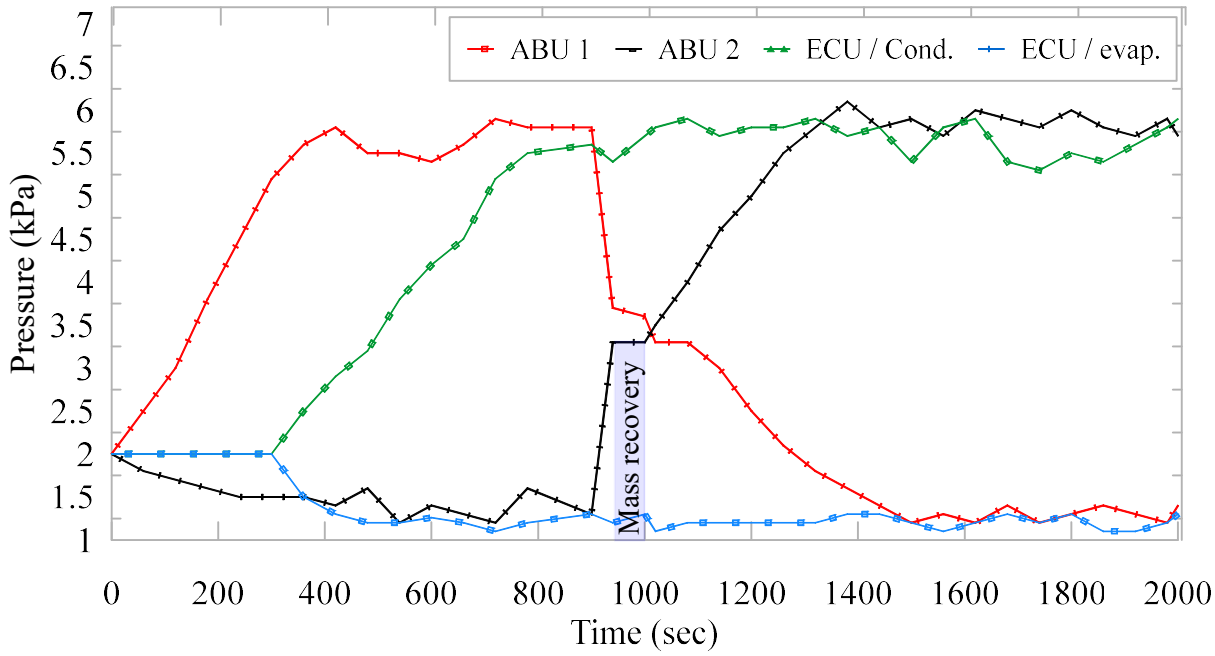

Figure (5.17) Variation of ABU and ECU pressure with time during the adsorption and desorption process of the two beds ATB for silica gel RD/water.

5.3.4 Comparison of Adsorbent Materials (MCM-41 and Silica Gel RD)

The performance operation of a two-bed ATB with mass recovery such as SCP, RC, and COP of the ATB was investigated at a mass recovery time of 60 s, hot and cooled mass flow rate of 1 LPM, chilled water flow rate of 0.5 LPM, hot water temperature is 353 K, cooled water temperatures 308 K. The ABUs heat exchanger was equipped with 350 g of silica gel-RD and 200 g of MCM-41. Figure (5.18) illustrates the time-dependent evolution of the performance of ATB. The results of the investigation revealed an enhancement in SCP, RE, and COP using MCM-41 by 48.5 %, 11.1%, and 10.5 %, respectively, compared with silica gel-RD for the same operation. This improvement is caused by the increased refrigerant uptake, leading to improved system performance with MCM-41. Finally, the figure provides conclusive evidence demonstrating that MCM-41 outperforms silica gel RD for COP, RE, and SCP; therefore, the focus of the experimental work is on the performance of the ATB when MCM-41 and water are used as adsorbent pair.

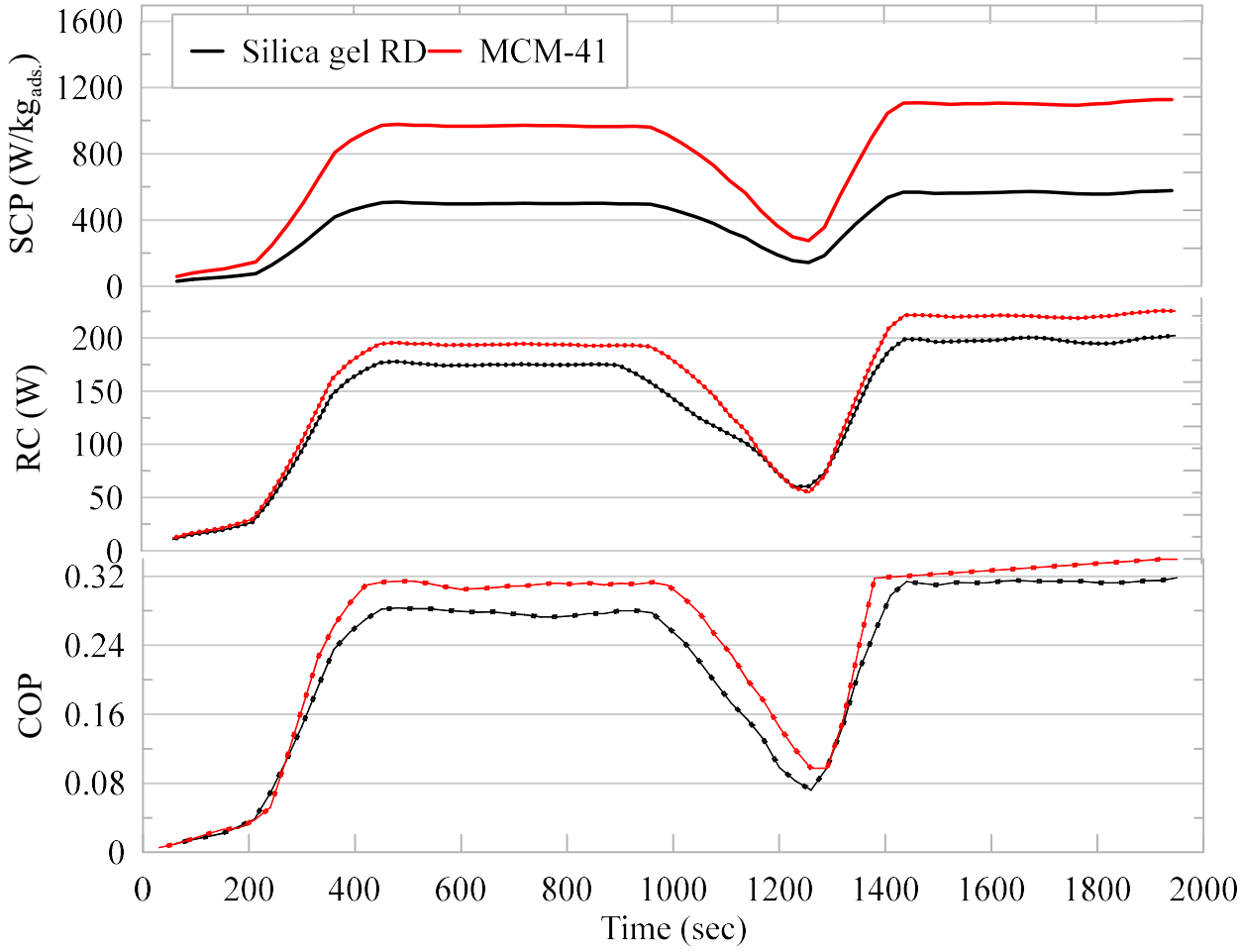

Figure (5.18) Variation of SCP, RC, and COP with time of the two beds ATB for MCM-41 and silica gel RD.

5.3.5 Effect of Hot Water Temperature

Figure (5.19) shows the relation between the hot water temperature and the desorption and condensation processes when the adsorption pair is MCM- 41 and water. The figure shows that after about 200 s of heating, the refrigerant vapor is still in the ABU due to the closed ABU valves. After the first 200 s, the valve is opened, and the refrigerant vapor is released to the ECU to condense. It can be seen from the figure that as the hot water temperature increases, the refrigerant vapor leaving ABU increases and condenses at a high temperature in ECU. The maximum desorption temperature is about 359 K, while it is 304 K for condensation of the refrigerant

vapor. As discussed, increasing the hot water flow rate or hot water temperature increases the desorbed refrigerant vapor, thus increasing both SCP and RC but not necessarily increasing the COP. It can be seen from Figure (5.20) that the maximum COP is for a lower hot water temperature because the energy consumed to increase the refrigerant desorption is not proportional to the increase in the refrigeration effect.

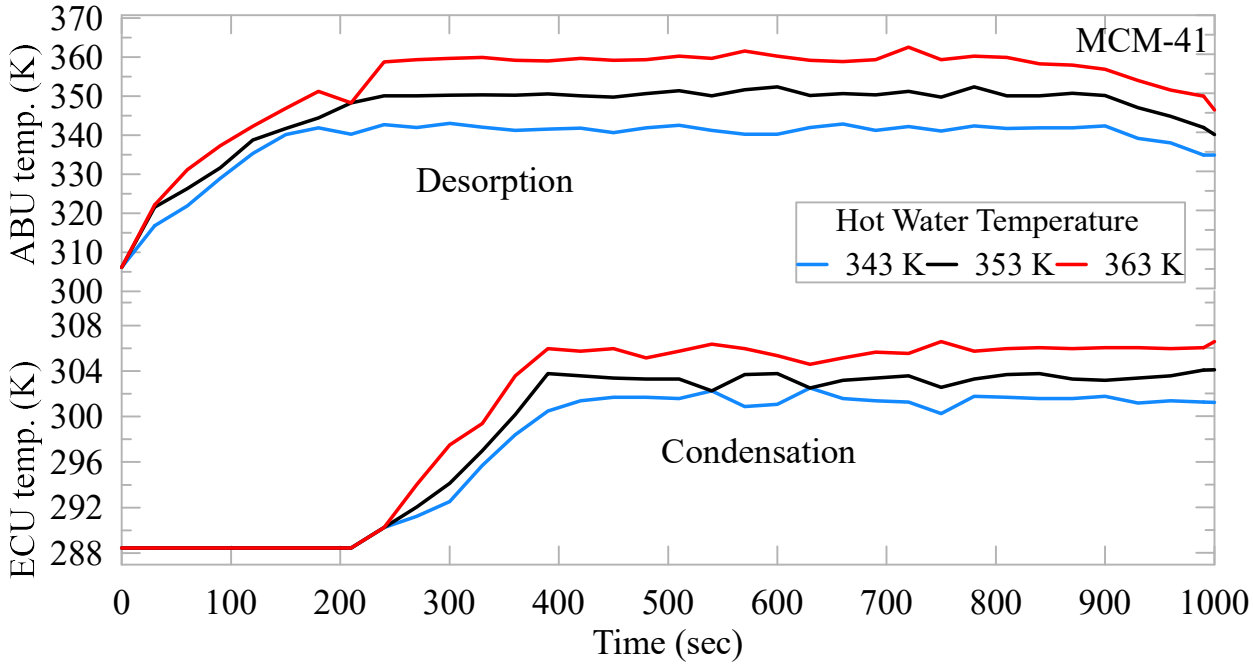

Figure (5.19) Variation of ABU and ECU temperature with time during the desorption of the two beds ATB at different hot water temperatures for MCM-41.

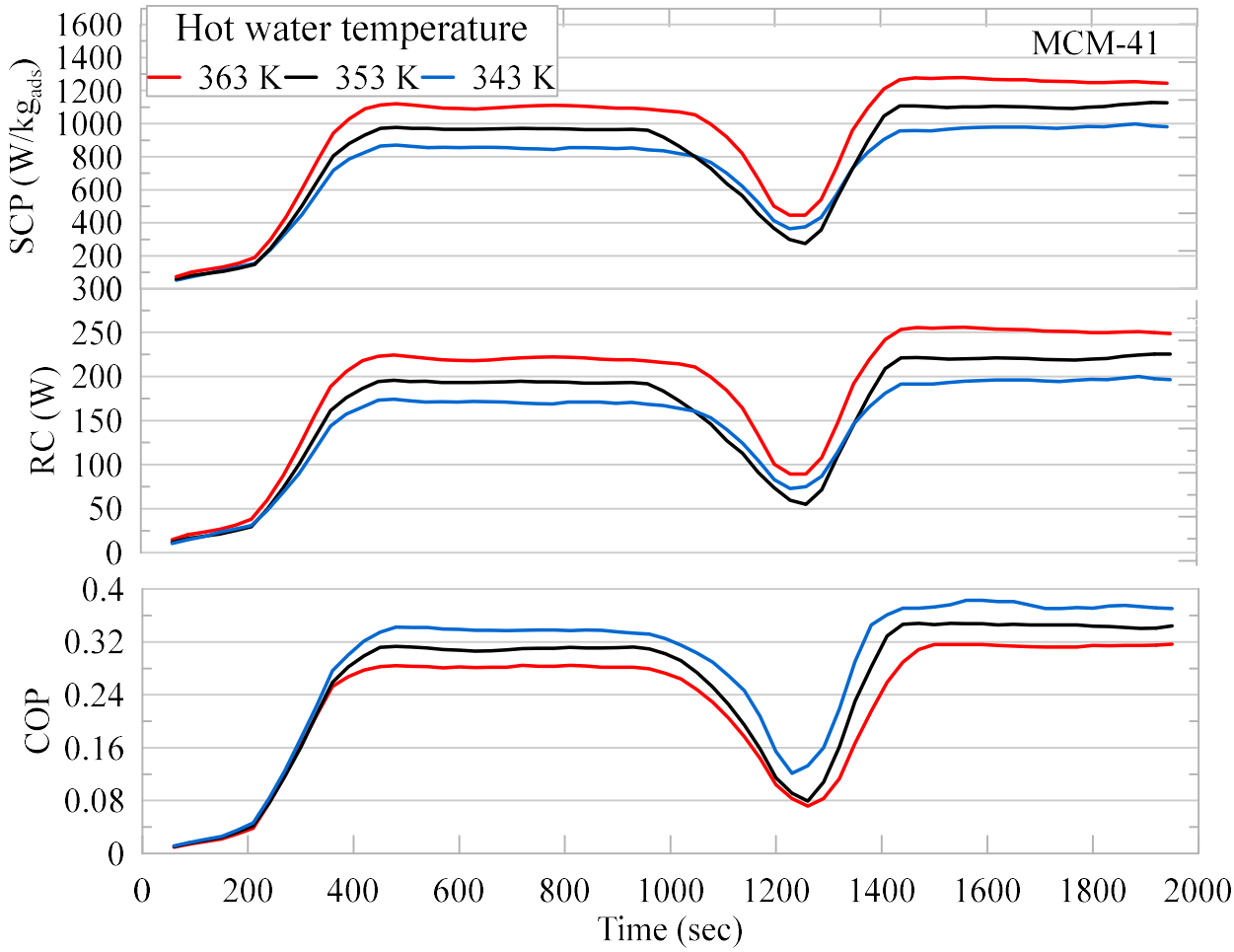

Figure (5.20) Variation of SCP, RC, and COP with time of the two beds ATB at different hot water temperatures for MCM-41.

5.3.6 Effect of Cooled Water Temperature

Figure (5.21) shows the effect of coolant water temperature on the water uptake, ABU, and ECU temperatures. The coolant water temperatures under study are 303 K, 308 K, and 313 K. During the cooling effect in the ECU, the refrigerant vapor is generated and flows to the ABU to adsorb; the fast adsorption of refrigerant vapor in the ABU leads to lower refrigerant vapor pressure in the ECU. In other words, as the temperature of the water that cools the ABU decreases, more refrigerant vapor is desorbed. The pressure in the ECU falls, and thus, the refrigerant evaporates at a lower temperature, as shown in the figure. The temperature of the adsorbent dropped

gradually to 306 K, 311 K, and 315 K, respectively, after roughly 200 seconds of the adsorption period, as seen in Figure (5.21).

As the evaporation temperature decreases due to the lowering coolant temperature, SCP, RC, and COP are improved, as shown in Figure (5.22). It can be seen from the figure that the maximum SCP, RC, and COP are 1200 W/kg, 240W, and 0.38 when the coolant temperature is 303 K. The figure shows that the SCP, RC, and COP of the right cycle are more than that of the left cycle due to the mass recovery at the right cycle. Also, it is evident from the figure that the decrease in COP occurred as the coolant water temperature rose from 303K to 313 K. The maximum COPs for the cycle without mass recovery are 0.343, 0.31, 0.279, and for the mass recovery cycle are 0.382, 0.345, and 0.314 as cooled water temperature variations 303, 308, and 313 K, respectively, as shown in Figure (5.23).

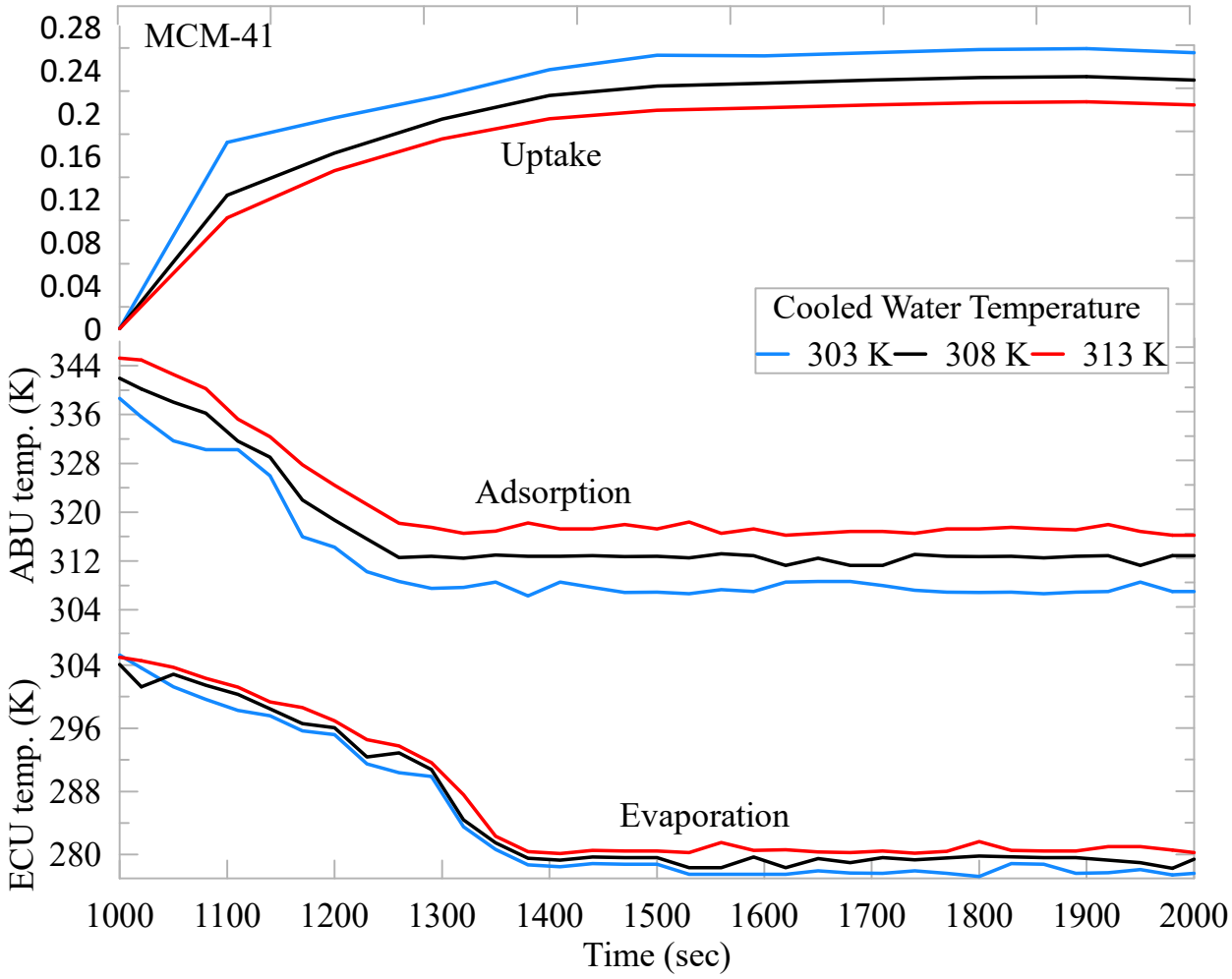

Figure (5.21) Variation of uptake, ABU, and ECU temperature with time during the adsorption of the two beds ATB at different cooled water temperatures for MCM-41.

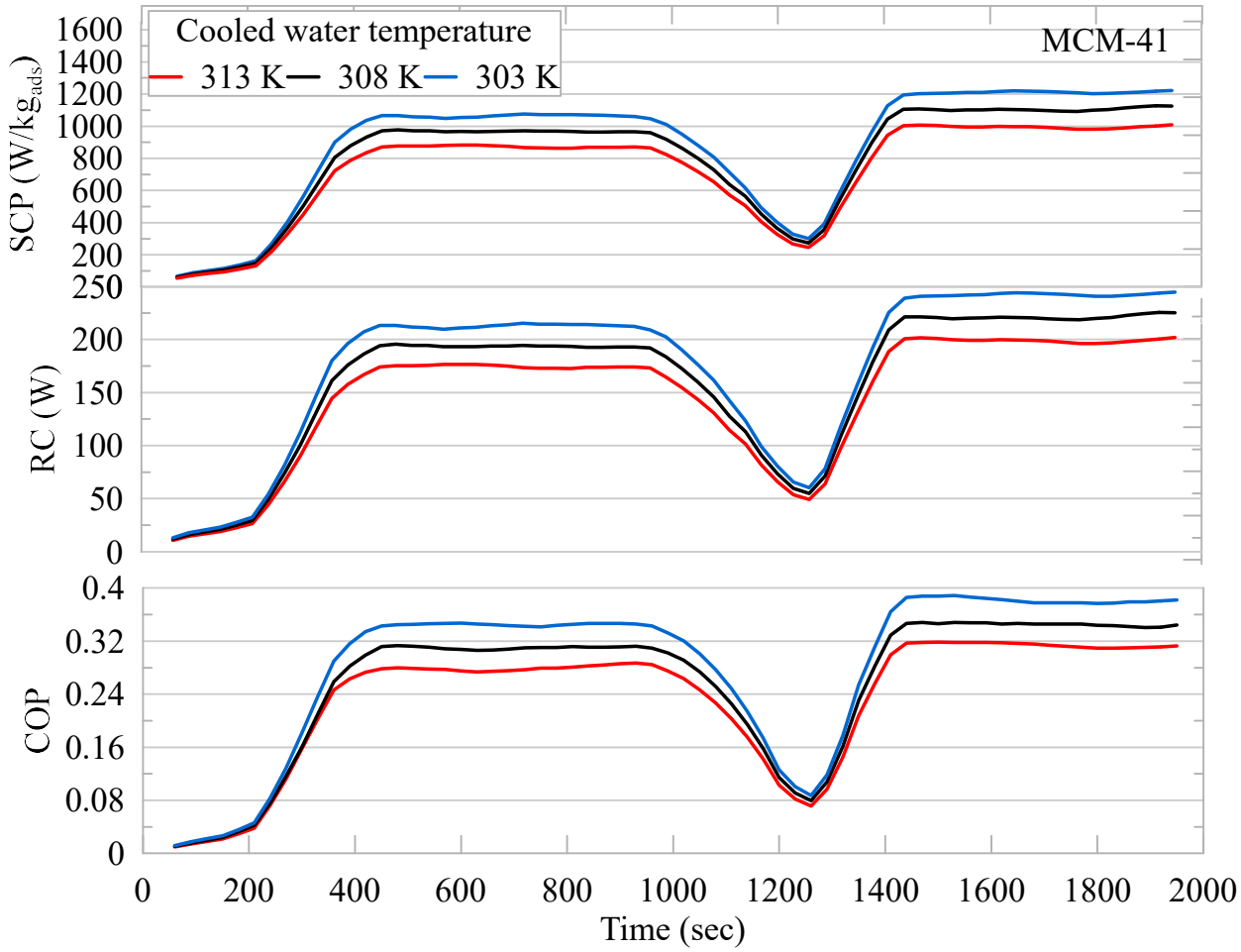

Figure (5.22) Variation of SCP, RC, and COP with time of the two beds ATB at different hot water temperatures for MCM-41.

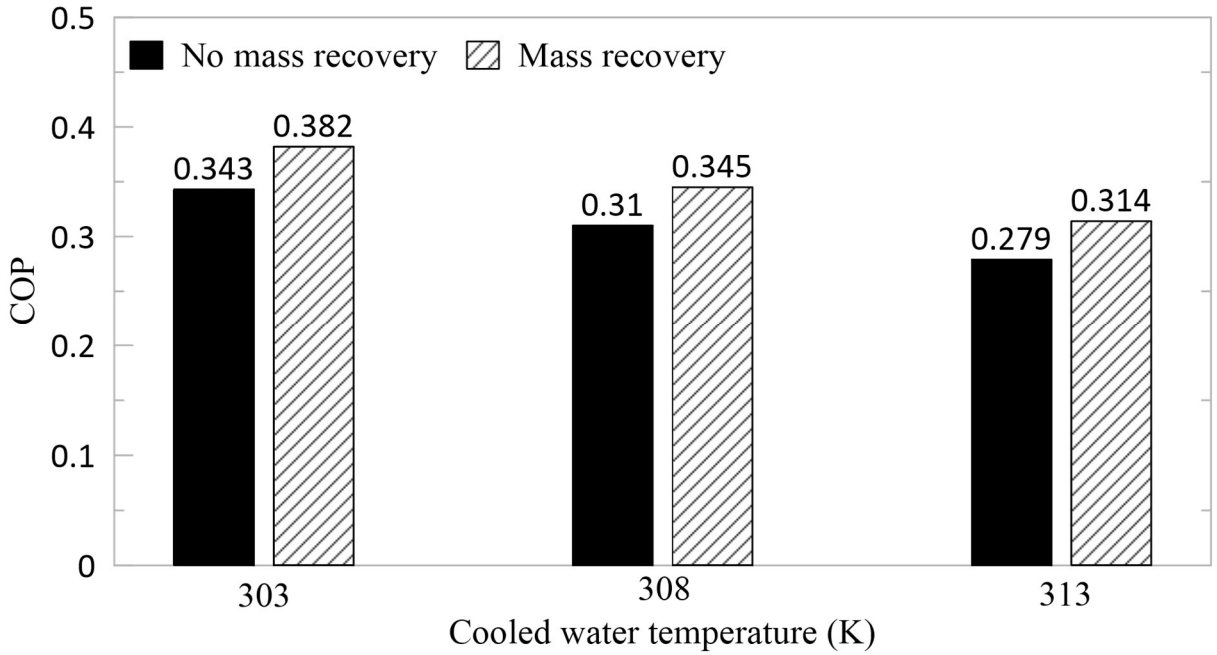

Figure (5.23) Effect of cool water temperature and mass recovery on the cycle COP.

5.3.7 Experimental Results Comparison with Previous Works

The results of the experiment of the uptake of RD-silica gel adsorption in this study have been validated by the previous experimental results by A. L. Tarish [47] and R. H. Mohammed [195], and the uptake of MCM-41 adsorption in this study have been validated by the previous experimental results by Tarish, as depicted in Figure (5.24).

The evaluation of the results has demonstrated a similar trend in the adsorption process, with a deviation range of around 6% and 14% when compared with the outcomes of Tarish [47] and Mohammed [195] for silica gel RD. Additionally, there is a deviation range of about 10% when compared with Tarish [47] results for MCM-41. The comparison was based on a cooled coolant temperature of 308 K.

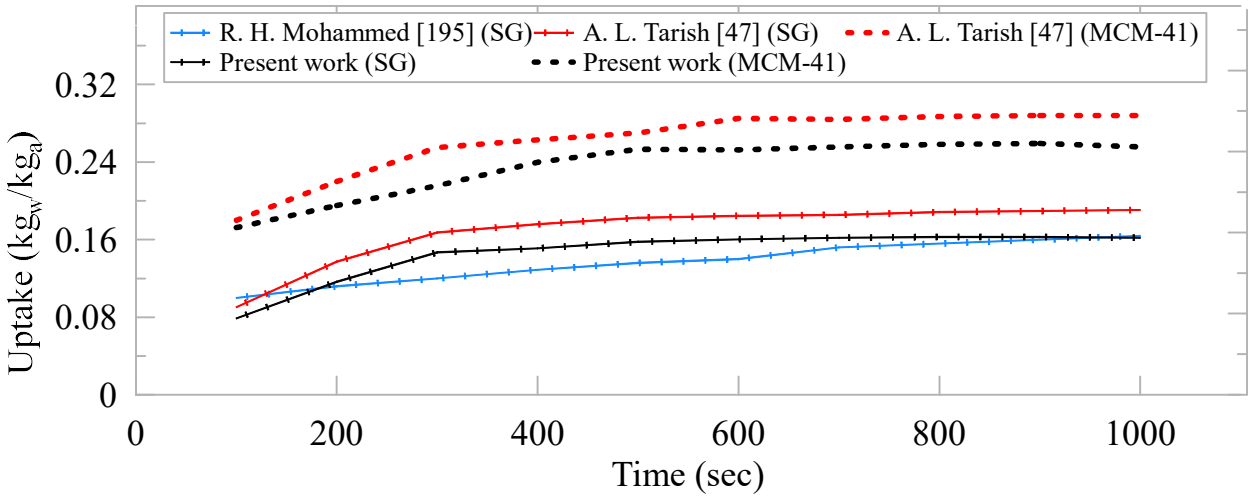

Figure (5.24) Comparison of the present work water uptake with previous works.

5.3.8 COP comparison with previous single-bed ATB

The results of the two beds with mass recovery experiment COP for RD-silica gel and MCM-41 adsorbate materials in this study have been compared with the previous single-bed experimental results by A. L. Tarish [47], as shown in Figure (5.25). The evaluation of the results has demonstrated a similar trend, with an enhancement when using two-bed mass recovery ATB. The COP was improved by 14% and 8.6 % for RD-silica gel and MCM-41, respectively.

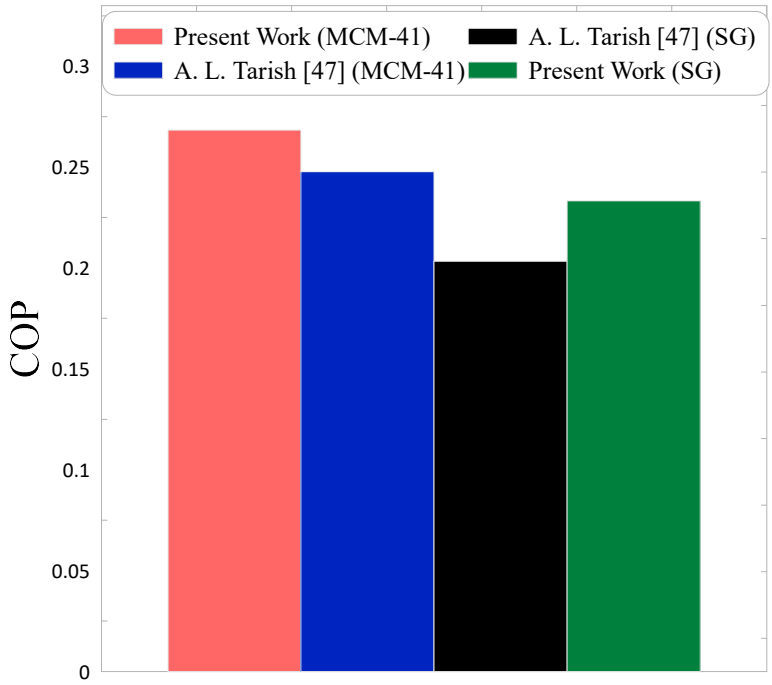

Figure (5.25) Comparison of the present work COP with previous works.

5.4 Heat and Mass Transfer Model (HMTM) for Numerical Results

The Heat and Mass Transfer Model (HMTM) simulation was solved numerically using COMSOL- 6.0 software. The numerical solution aims to predict the refrigerant and coolant flow temperature in the ABU heat exchanger (ABUHE) during the adsorption and desorption processes under various operating conditions. The adsorption working pairs tested in the numerical analyses were silica gel RD adsorbent material and water for comparison and validation of results. Three physics models were used while simulating ABU's adsorption and desorption cycles: porous media, heat transfer, and fluid flow in the HMTM solution approach. ABU's geometry is created symmetrically.

5.4.1 Temperature Distributions at Adsorber Bed Heat Exchanger

The HMTM is utilized to investigate the influence of the hot and cooled water temperature on temperature distribution in ABUHE with working pair silica gel RD/water.

5.4.1.1 Effect of Hot Water Temperature

Figure (5.26) shows the temperature distributions in ABU during the desorption periods at hot water temperatures of 343 K, 353 K, and 363 K, respectively. At the beginning of the desorption period, the temperature of ABU was 308 K. Heat transfer from the hot water to ABU caused temperature gradients in the ABU and consequently raised its temperature from 308K to 340K, 350K, and 360K after 200 seconds of the desorption period. Due to its limited thermal conductivity and low thermal diffusion, the temperature of the solid adsorbent increased gradually over time. It maintained lower than the hot coolant by about 3K.

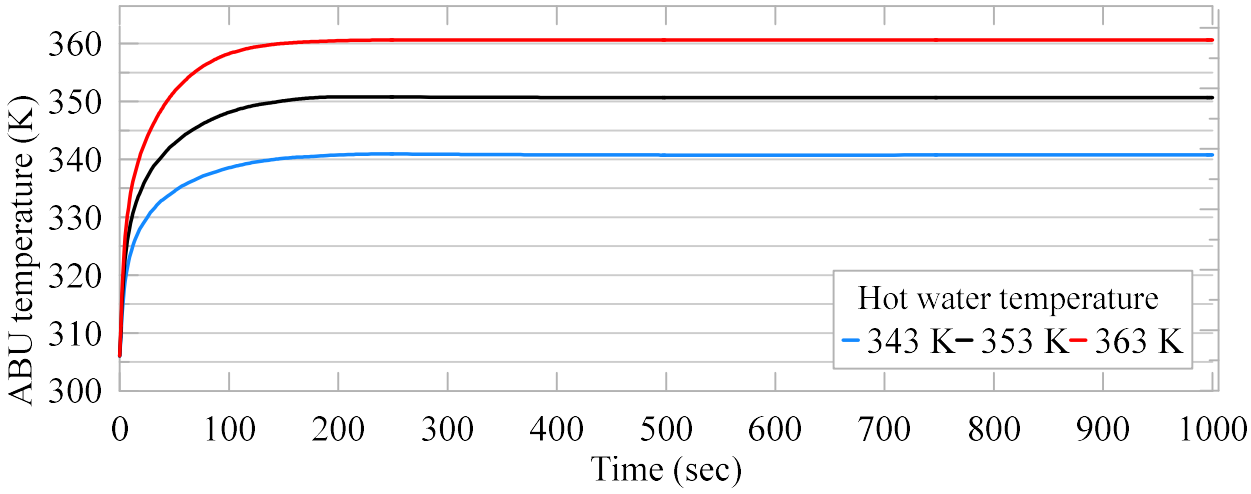

Figure (5.26) Temperature distribution in the ABU at the hot water temperature 343 K, 353 K, and 363 K.

A qualitative three-dimensional assessment of the temperature distributions at different operation times (0, 10, 25, 50, 100, and 200 s) is illustrated in Figure (5.27). The temperature profile indicates the heat transfer characteristics of the system via

the desorption heating bed. The figure shows that the temperature of the adsorption bed, including the heat exchanger and adsorbant, was increased with time because the heat transfer fluid (HTF) inlet temperature is 353 K throughout desorption, while the bed temperature is 308 K.

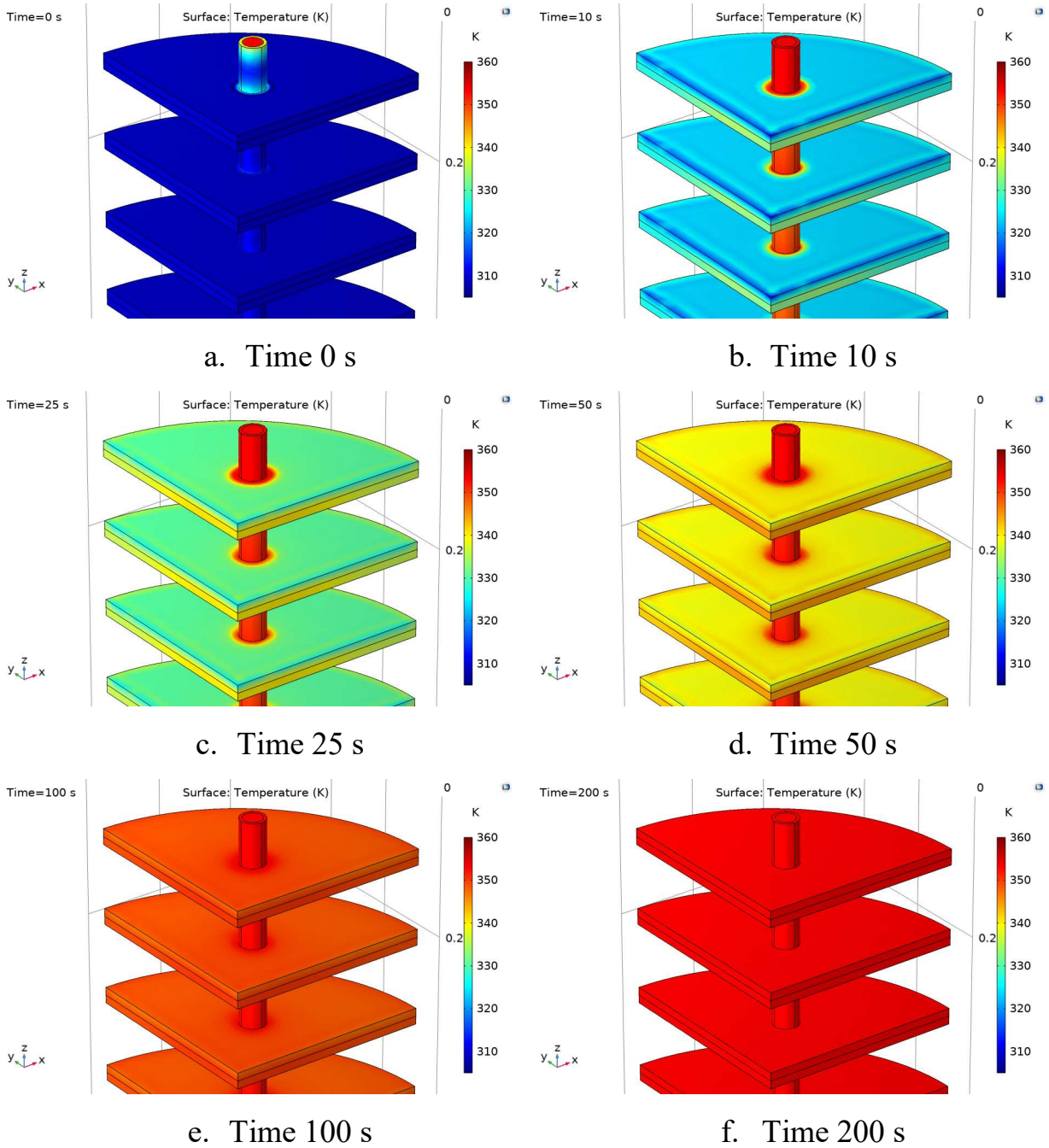

a. Time 0 s b. Time 10 s

c. Time 25 s d. Time 50 s

e. Time 100 s f. Time 200 s

Figure (5.27) Temperature distribution in the ABU at the hot water temperature 353 K.

5.4.1.2 Effect of Cooled Water Temperature

Figure (5.28) depicts the temperature distributions in ABU during the adsorption periods at cooled water temperatures of 303 K, 308 K, and 313 K, respectively. At the beginning of the adsorption period, the temperature of ABU was 353 K. The refrigerant vapor transfers from ECU to ABU at the start of the adsorption process. Due to heat transfer between the cooled coolant and the ABU domain, the ABU temperature dropped from 353K to 303K, 308K, and 313K, as illustrated in the figure. The temperature of the solid adsorbent layer was lowered after 200 s due to an increase in uptake adsorption, but the temperature was maintained higher than the cooled coolant by about 3 K.

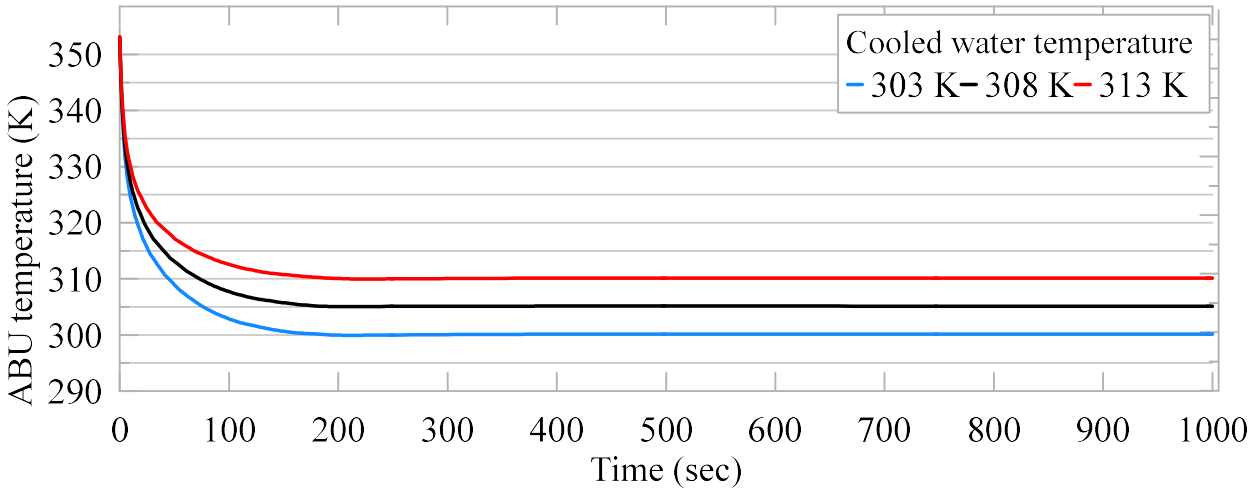

Figure (5.28) Temperature distribution in the ABU at the cooled water temperature 303 K, 308 K, and 313 K.

Figure (5.29) presents a 3-D evaluation of the temperature distributions across different operation times (0, 10, 25, 50, 100, and 200 s). The temperature profile indicates the system's ability to transfer heat through the adsorption cooling bed. The figure shows that the temperature of the adsorption bed, including the heat exchanger and adsorbant, decreased with time because the heat transfer fluid (HTF) inlet

temperature was 308 K throughout adsorption, while the bed temperature was 353 K.

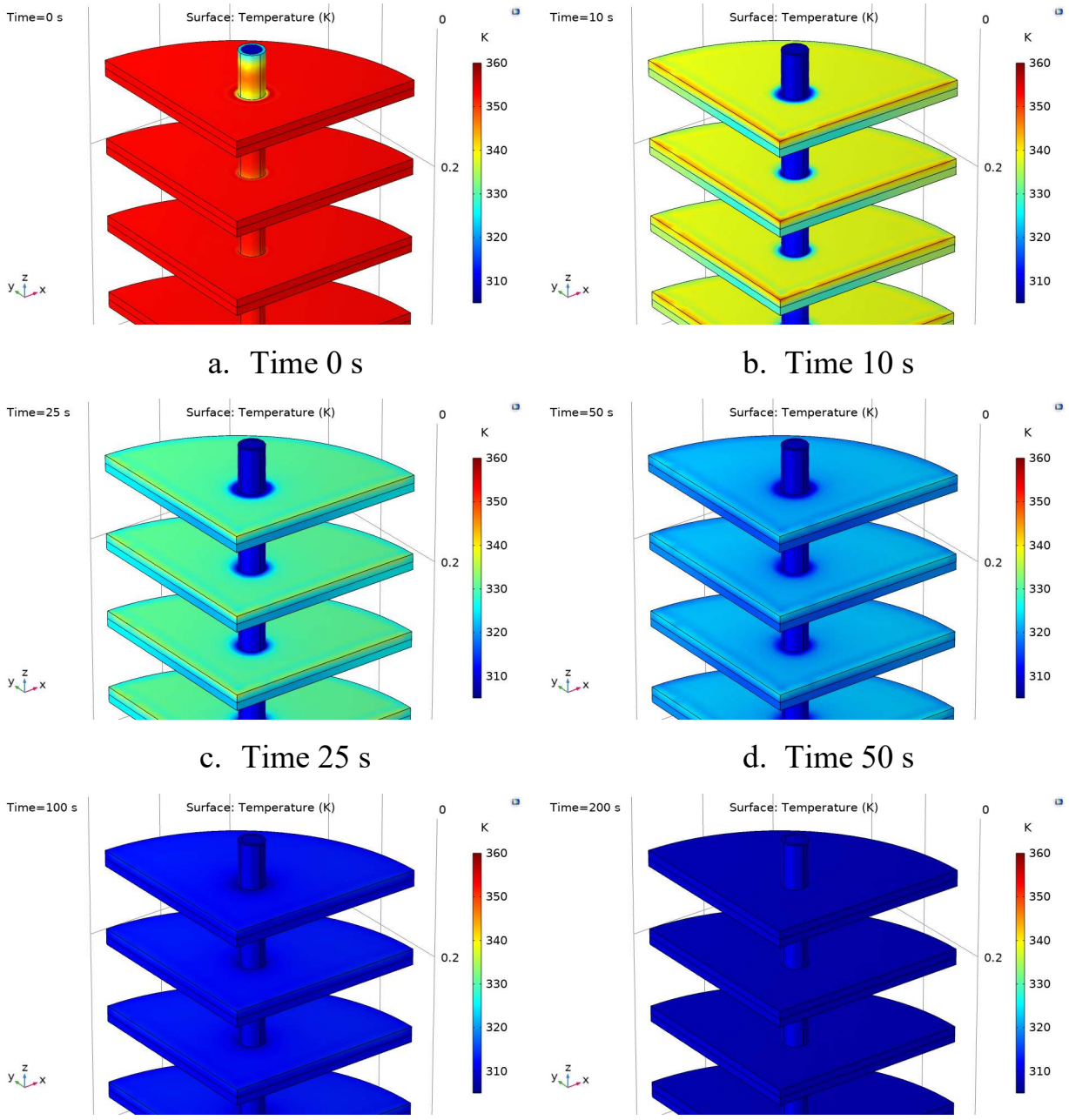

a. Time 0 s b. Time 10 s

c. Time 25 s d. Time 50 s

e. Time 100 s f. Time 200 s

Figure (5.29) Temperature distribution in the ABU at the cooled water temperature 308 K.

5.4.2 Water Uptake Distributions at Adsorber Bed Heat Exchanger

The HMTM analyzes an adsorption cooling bed, which exhibits a finned tube configuration and utilizes a working pair of silica gel / RD and water. It is also used to investigate the influence of hot and cooled water temperatures on water uptake distribution in ABUHE.

5.4.2.1 Effect of Hot Water Temperature

Figure (5.30) shows the adsorbent's water uptake distributions during the adsorption cycle periods at hot water temperatures 343, 353, and 363 K, respectively. At the beginning of the adsorption period, the water uptake of the adsorbent is 0.02 kg_w/kg_{ads}. Heat transfer from adsorbent materials to cooled water at a temperature of 308 K caused an increase in water uptake and consequently raised to 0.23 kg_w/kg_{ads}.

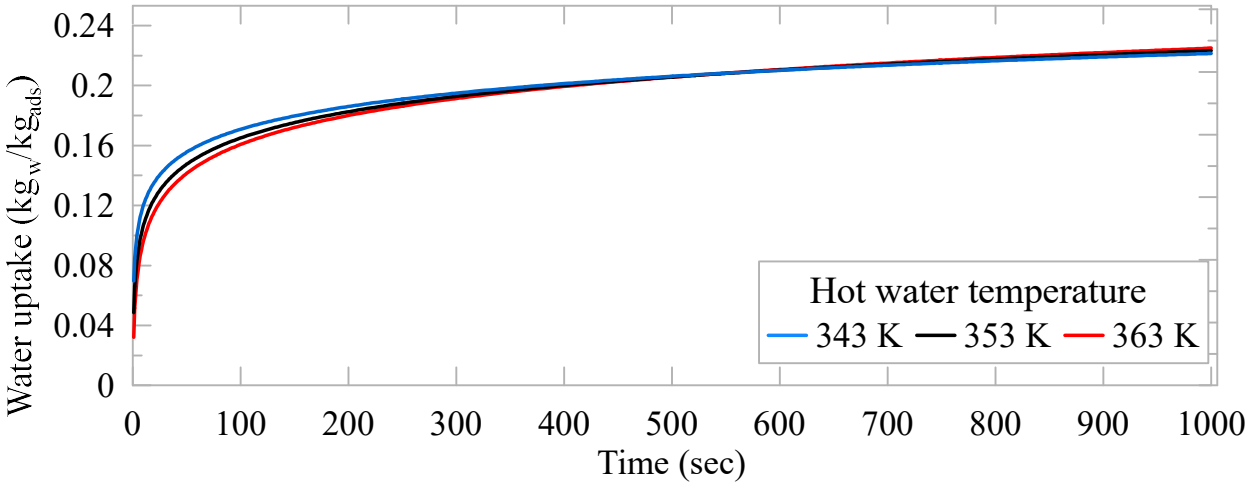

Figure (5.30) Water uptake distribution in the ABU is at the hot water temperature of 343 K, 353 K, and 363 K.

Figure (5.31) presents the three-dimensional evaluation of the water absorption at various time intervals (0, 10, 25, 50, 100, and 200 s). The kinetics of the adsorbed water is slow enough that a time lag occurs between attaining the thermodynamic temperature and setting up the equilibrium. After 200 seconds, the

adsorbent refrigerant bed is nearly completely saturated. The heat transfer fluid (HTF) inlet temperature is 353 K throughout adsorption, while the bed temperature is 308 K.

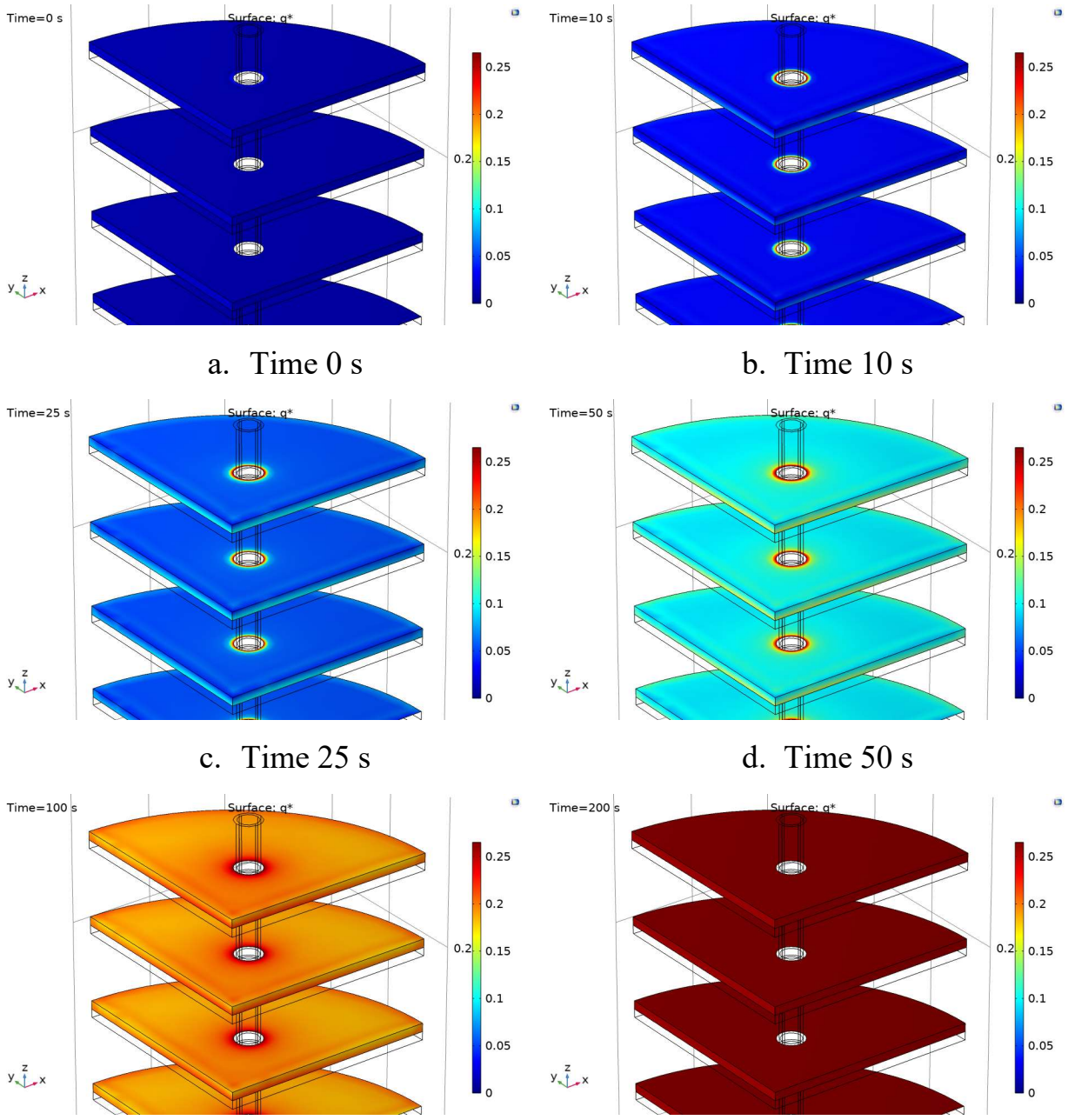

a. Time 0 s b. Time 10 s

c. Time 25 s d. Time 50 s

e. Time 100 s f. Time 200 s

Figure (5.31) Water uptake distribution in the ABU is at the hot water temperature of 343 K.

5.4.2.2 Effect of Cooled Water Temperature

Figure (5.32) depicts the adsorbent's water uptake distributions during the adsorption cycle periods at cooled water temperatures 303, 308, and 313 K, respectively. At the beginning of the adsorption period, the water uptake of the adsorbent was 0.04 kg_w/kg_{ads}. Due to heat transfer between the hot adsorbent at 353 K and cooled water, the water uptake raised from 0.04 kg_w/kg_{ads} to 0.29 kg_w/kg_{ads}, 0.23 $kg_w/kg_{ads,}$ and 0.16 kg_w/kg_{ads} at cooled water temperature 303K, 308K, and 313K respectively.

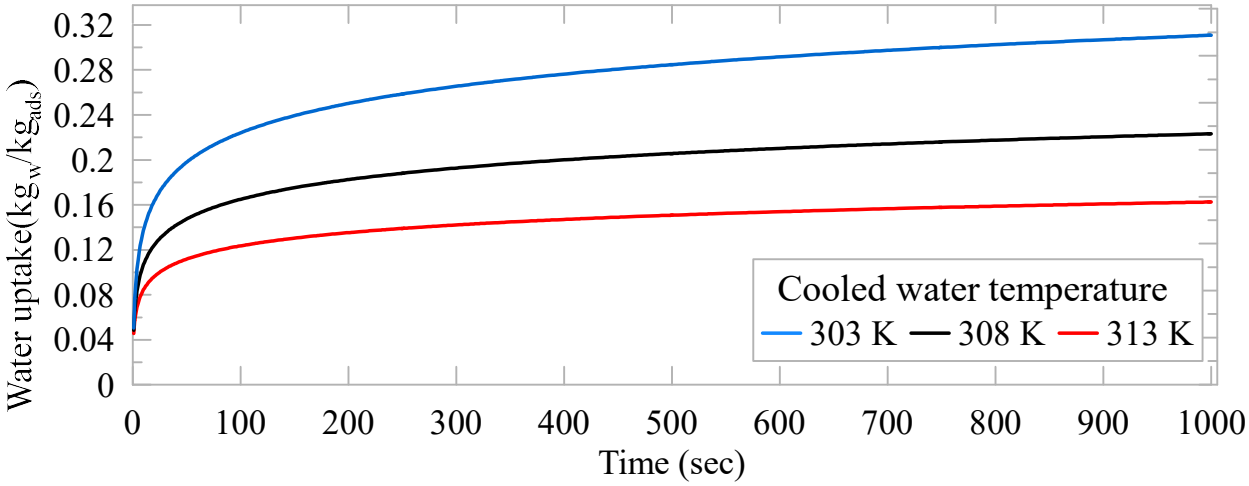

Figure (5.32) Water uptake distribution in the ABU is at the cooled water temperatures 303 K, 308 K, and 313 K.

A qualitative three-dimensional assessment of the water uptake at different operation times (0, 10, 25, 50, 100, and 200 s) is illustrated in Figure (5.33). The heat transfer fluid (HTF) inlet temperature is 303 K throughout adsorption, while the bed temperature is 353 K.

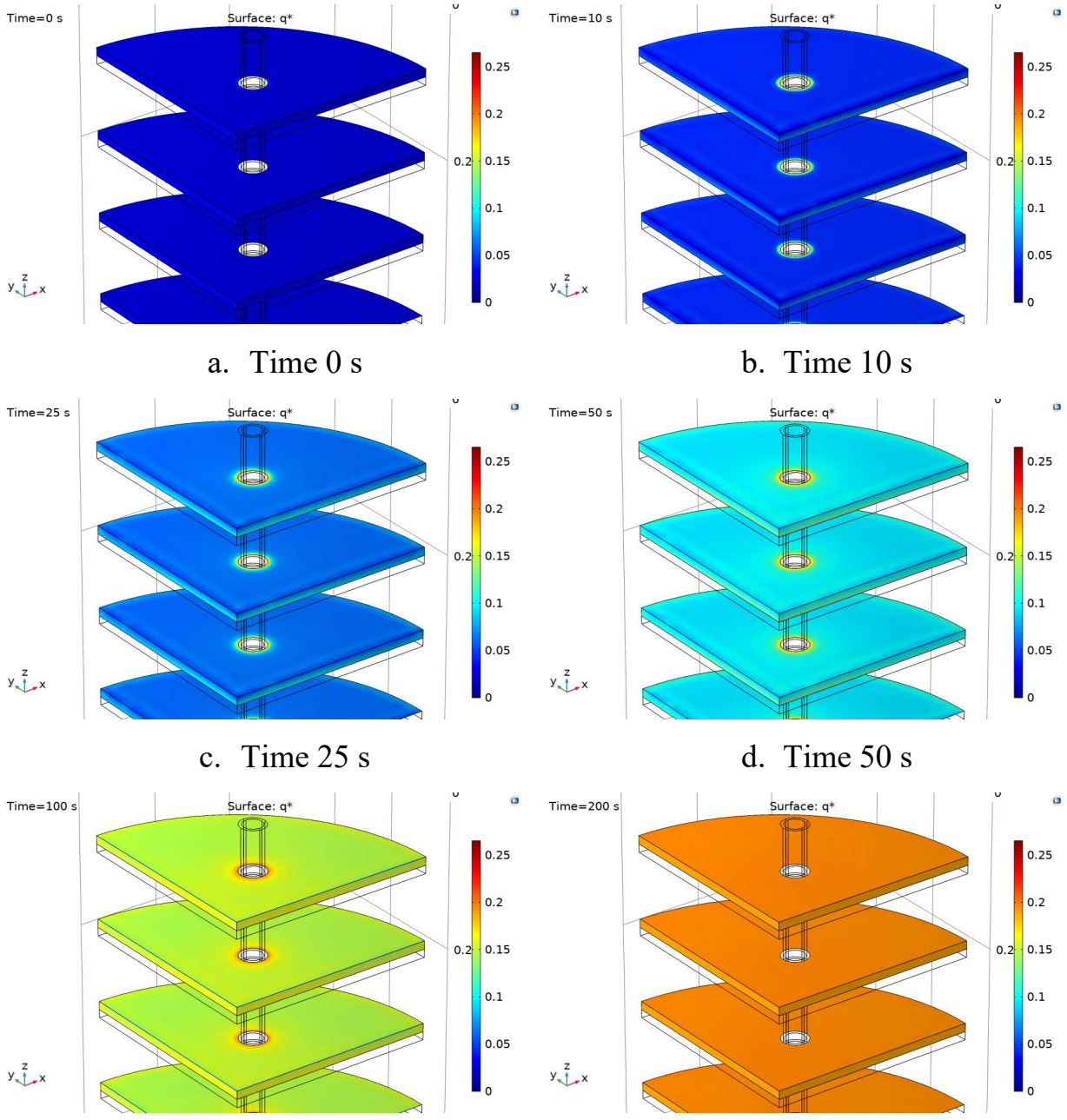

a. Time 0 s b. Time 10 s

c. Time 25 s d. Time 50 s

e. Time 100 s f. Time 200 s

Figure (5.33) Water uptake distribution in the ABU is at the cooled water temperature of 303 K.

5.4.3 Effect of Adsorbent Thickness

The layer thickness of solid adsorbent has an essential effect on ABU performance, so it was studied numerically to determine the optimal layer thickness. During the

adsorption and desorption periods, the impact of variation in the solid adsorbent layer thickness at 2, 4, and 6 mm was shown in Figure (5.34). At the beginning of the adsorption period, the temperature of ABU dropped from 353 K to 308 K after 190, 500, and 800 seconds of the adsorption period for layer thickness at 2mm, 4mm, and 6mm, respectively. Furthermore, the thinner layer can be cooled faster under similar operating conditions than the thicker layers. It can be concluded that, at present design parameters and operating conditions, the optimum layer thickness for achieving an efficient ABU design is 2 mm in the ATB system, which has enhanced the adsorption uptake throughout the adsorption duration and improved the desorption rate during the desorption period.

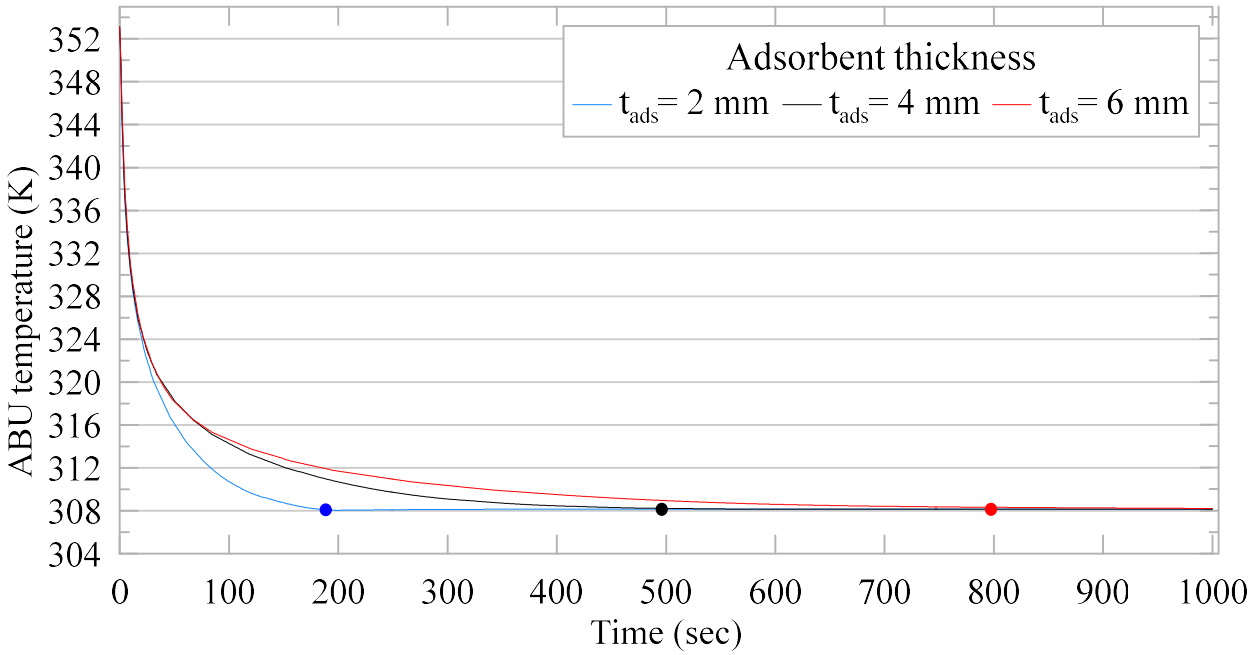

Figure (5.34) Temperature distribution in the ABU at adsorbent layer thicknesses 2 mm, 4 mm, and 6 mm

Figure (5.35) depicts the water uptake distributions in the adsorbent during the adsorption cycle periods at adsorbent layer thicknesses of 2 mm, 4 mm, and 6 mm. Under similar operating conditions with a hot water temperature of 353K and

cooled water temperature of 303K, it can be seen from the figure that water uptake increases as the adsorbent layer thickness decreases. This behavior is because lowering the adsorbent layer thickness improved the heat exchange between the adsorbent's surface and vapor refrigerant, leading to an increase in the adsorption uptake and minimizing the time required by the refrigerant vapor to reach the core of the solid adsorbent particles.

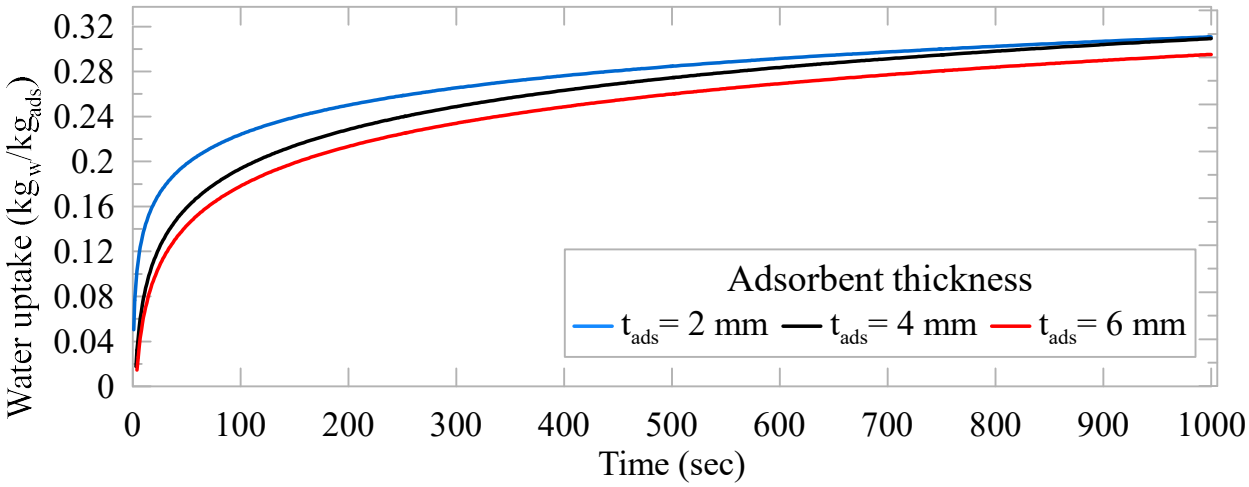

Figure (5.35) water uptake distribution in the ABU at adsorbent layer thicknesses 2 mm, 4 mm, and 6 mm.

5.4.4 Numerical Results Comparison with Other Work

The variation of the bed temperature during the adsorption process with time for the numerical present work is validated with W. Yaïci [184] and B. Shi [151] works results, as shown in Figure (5.36). The results show a temperature drop over the adsorbent bed over time. The average overall error associated with the simulation relative to the result of W. Yaïci [184] is about 0.7%, and the result of B. Shi [151] is about 8%. The comparison was based on an inlet-cooled coolant temperature of 308 K and a driving temperature of 333 K.

The variation of the water uptake during the adsorption process with time for the numerical present work is validated with B. Shi's [151] work results, as shown in Figure (5.37). The average overall error associated with the simulation relative to the result of B. Shi. is about 27 %.

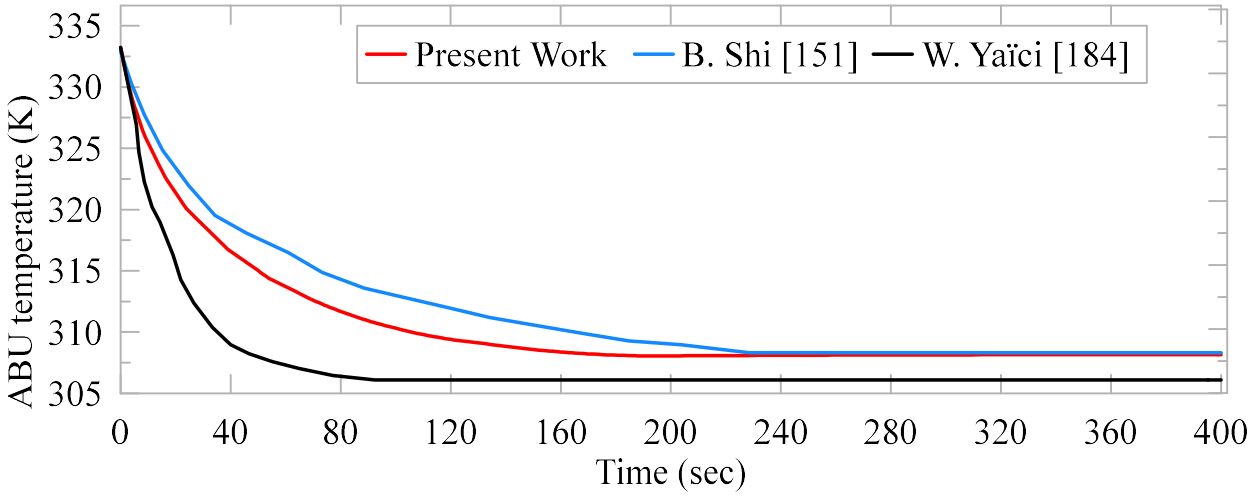

Figure (5.36) Comparison of ABU temperature variation with time between the present Numerical work, B. Shi [151], and W. Yaïci [184] results during the adsorption process for the working pair silica gel RD and water.

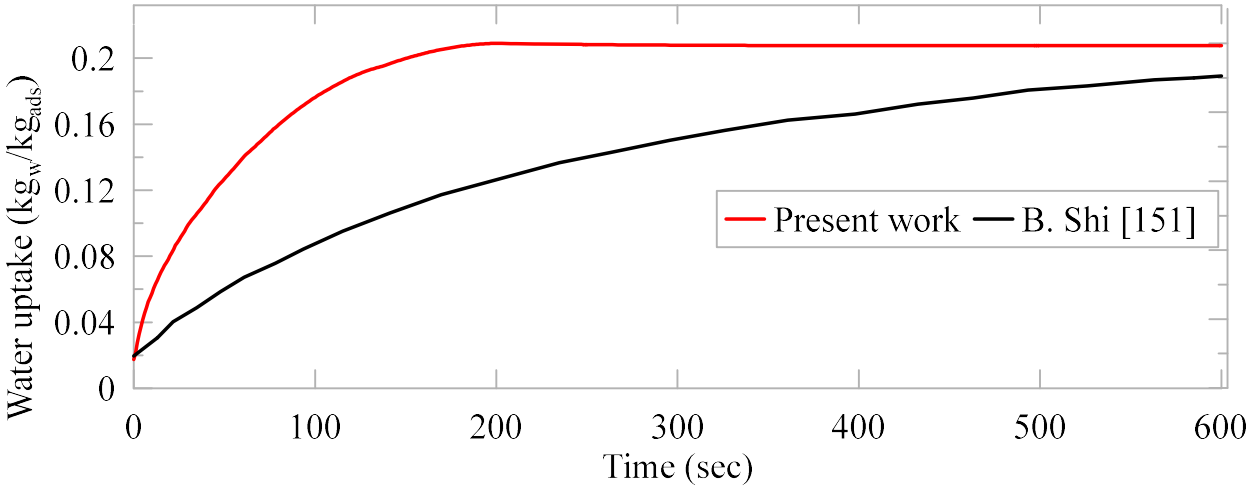

Figure (5.37) Comparison of water uptake variation with time between the present Numerical work and B. Shi [151] result during the adsorption process for the working pair silica gel RD and water.

5.4.5 Theoretical, Numerical, and Experimental Results Validation

The findings of the CMOSOL simulation approach were validated by comparing them with the theoretical and experimental results of the present study. Figure (5.38) depicts the temperature variation with time for ABU throughout the desorption process with a working pair of silica gel RD and water. It can be observed in this figure that there is an acceptable agreement between the results, with deviations of 4% for numerical and theoretical, 7.5% for numerical and experimental, and 10% for theoretical and experimental.

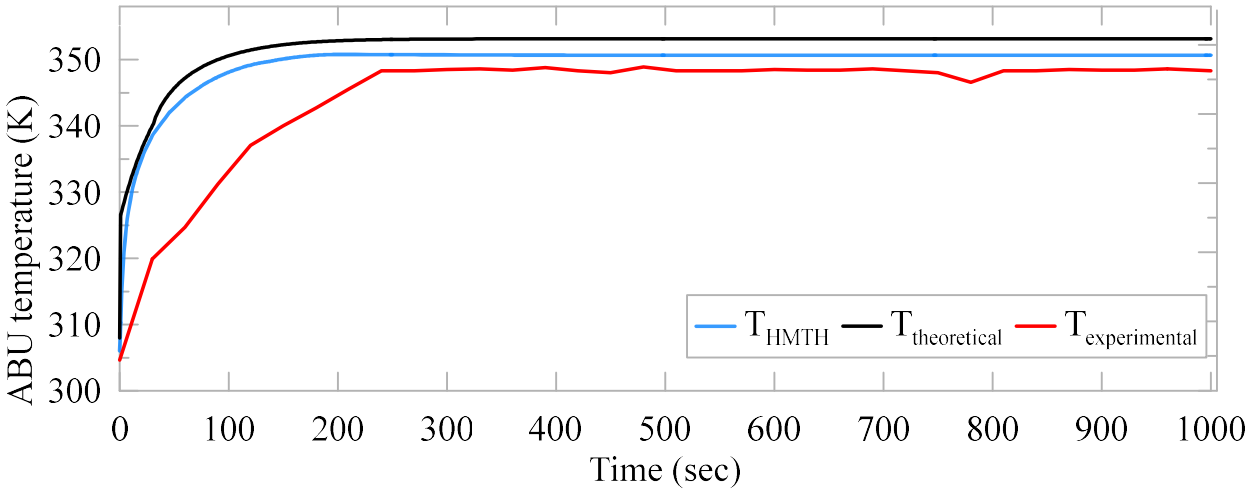

Figure (5.38) Comparison of ABU temperature variation with time between the theoretical, numerical, and experimental results during the desorption process for the working pair silica gel RD and water.

Chapter Six

Conclusions and Recommendations

Chapter Six
Conclusions and Recommendations

6.1 Introduction

The present study has investigated the ATB performance for air conditioning applications experimentally, theoretically, and numerically. A two-bed ATB system with mass recovery technology was investigated and compared with the standard single-bed ATB. The working pairs used in the experimental investigation were silica gel RD and MCM-41/water, and in the theoretical, silica gel RD/water and a new class of working pair MOF-801/water are used. From the experimental, theoretical, and numerical investigations, the following conclusions are derived:

1- The deviation of the present theoretical work compared with A. L. Tarish's [74] work is 4%, while it is 11% for B. B. Saha's work [194].

2- The deviation range in water uptake for the experimental present work is around 6% and 14% when compared with the outcomes of A. L. Tarish [47] and R. H. Mohammed [195] for silica gel RD. Meanwhile, it is 10% compared with A. L. Tarish [47] results for MCM-41.

3- The average overall deviation range in adsorption temperature associated with the present numerical simulation relative to the result of W. Yaïci [194] is about 0.7%, and the result of B. Shi [151] is about 8%.

4- There is an acceptable agreement for temperature results, with deviations of 4% for numerical and theoretical, 7.5% for numerical and experimental, and 10% for theoretical and experimental.

5- The COP of the ATB has been increasing in correlation with cycle time, reaching its peak value of 0.3 and 0.25 for MOF-801 and silica gel, respectively, when the cycle time is set at 1000 s MOF-801.

6- It was observed that COP exhibited a direct proportionality with the flow rate of chilled and cooled water while inversely relating to the flow rate of hot water.

7- It can be deduced that the inlet temperature of the hot coolant exhibited a direct proportion with both refrigeration effect (RE) and SCP while inversely affecting the COP.

8- The COP and RC of the two-bed ATB were improved by 14% and 8% when using mass recovery (60 sec), respectively, compared with the system without mass recovery.

9- The enhancement in SCP, RE, and COP using MCM-41 was 48.5 %, 11.1%, and 10.5 %, respectively, compared with silica gel-RD for the same operation.

10- The temperature of ABU dropped from 353 K to 308 K after 190, 500, and 800 seconds of adsorption period for layer thickness at 2mm, 4mm, and 6mm, respectively. Water uptake increases as adsorbent layer thickness decreases.

6.2 Recommendations for Future Work

Based on the present study investigation, some potential improvements on the ATB system can be recommended for future work as follows:

1- Design a low-cost ATB compact system depending on waste heat sources or solar energy available under Iraqi weather.

2- Conduct a comparative study to investigate the impact of the most influential parameters, such as adsorber bed geometry, adsorbent material type, adsorbent particle diameter, heat exchanger design, and cycle time, on the ATB thermal performance.

3- Utilize a three or four-bed system to obtain continuous refrigeration.

References

References

[1] S. M. Ali and A. Chakraborty, "Adsorption assisted double stage cooling and desalination employing silica gel + water and AQSOA-Z02 + water systems," *Energy Convers Manag*, vol. 117, pp. 193–205, 2016, doi: 10.1016/j.enconman.2016.03.007.

[2] Z. E. Yildirim, "A Study on Isotherm Characteristics of Adsorbent-Adsorbate Pairs Used in Adsorption Heat Pumps," M.Sc. Thesis, Izmir Institute of Technology (Turkey), 2011, [Online]. Available: http://library.iyte.edu.tr/tezler/master/enerjimuh/T000969.pdf

[3] C. Forman, I. K. Muritala, R. Pardemann, and B. Meyer, "Estimating the global waste heat potential," *Renewable and Sustainable Energy Reviews*, vol. 57. Elsevier Ltd, pp. 1568–1579, May 01, 2016. doi: 10.1016/j.rser.2015.12.192.

[4] Zervos, Renewables 2019 Global Status Report, 2019.

[5] H. J. F. Dakkama, "Experimental investigation of MOF adsorption system for ice making, freeze water desalination and cooling applications," Doctoral dissertation, University of Birmingham, 2017, [Online]. Available: http://etheses.bham.ac.uk/id/eprint/7837/

[6] D. Lefebvre, "Thermal Energy Storage Using Adsorption Processes for Solar and Waste Heat Applications: Material Synthesis, Testing and Modeling," M.A.Sc. Thesis, University of Ottawa, 2015, [Online]. Available: https://ruor.uottawa.ca/items/8617cce7-3933-48ca-8a86-c2222ac300d7.

[7] S. K. Henninger *et al.*, "New materials for adsorption heat transformation and storage," *Renew Energy*, vol. 110, pp. 59–68, 2017, doi: 10.1016/j.renene.2016.08.041.

[8] Z. Chen, X. Wang, T. Islamoglu, and O. K. Farha, "Green synthesis of a functionalized zirconium-based metal-organic framework for water and ethanol adsorption," *Inorganics (Basel)*, vol. 7, no. 5, May 2019, doi: 10.3390/inorganics7050056.

[9] I. Ahmed and S. H. Jhung, "Composites of metal-organic frameworks: Preparation and application in adsorption," *Materials Today*, vol. 17, no. 3. Elsevier B.V., pp. 136–146, 2014. doi: 10.1016/j.mattod.2014.03.002.

[10] R. AL-Dadah, S. Mahmoud, E. Elsayed, P. Youssef, and F. Al-Mousawi, "Metal-organic framework materials for adsorption heat pumps," *Energy*, vol. 190, Jan. 2020, doi: 10.1016/j.energy.2019.116356.

[11] X. Xia, M. Cao, Z. Liu, W. Li, and S. Li, "Elucidation of adsorption cooling characteristics of Zr-MOFs: Effects of structure property and working fluids," *Chem Eng Sci*, vol. 204, pp. 48–58, Aug. 2019, doi: 10.1016/j.ces.2019.04.006.

[12] A. H. N. Khalifa, F. M. Hussein, and F. M. Hadi, "Experimental study on two beds adsorption chiller with regeneration," *Mod Appl Sci*, vol. 5, no. 4, pp. 43–52, 2011, doi: 10.5539/mas.v5n4p43.

[13] H. Furukawa *et al.*, "Water adsorption in porous metal-organic frameworks and related materials," *J Am Chem Soc*, vol. 136, no. 11, pp. 4369–4381, Mar. 2014, doi: 10.1021/ja500330a.

[14] A. L. Tarish, A. H. N. Khalifa, and A. J. Hamad, "Methods of Improving the Performance of Adsorption Thermophysical battery based on the Operating Conditions and Structure: A Review," *IOP Conf Ser Mater Sci Eng*, vol. 928, no. 2, 2020, doi: 10.1088/1757-899X/928/2/022040.

[15] P. Goyal, P. Baredar, A. Mittal, and A. R. Siddiqui, "Adsorption refrigeration technology - An overview of theory and its solar energy applications," *Renewable and Sustainable Energy Reviews*, vol. 53. Elsevier Ltd, pp. 1389–1410, Jan. 01, 2016. doi: 10.1016/j.rser.2015.09.027.

[16] K. C. A. Alam, A. Akahira, Y. Hamamoto, A. Akisawa, and T. Kashiwagi, "A four-bed mass recovery adsorption refrigeration cycle driven by low temperature waste/renewable heat source," *Renew Energy*, vol. 29, no. 9, pp. 1461–1475, 2004, doi: 10.1016/j.renene.2004.01.011.

[17] R. Wang, "Adsorption refrigeration research in Shanghai Jiao Tong University," *Renewable and Sustainable Energy Reviews*, vol. 5, no. 1, pp. 1-37, 2001, doi.org/10.1016/S1364-0321(00)00009-5

[18] K. Sumathy, K. H. Yeung, and L. Yong, "Technology development in the solar adsorption refrigeration systems," *Prog Energy Combust Sci*, vol. 29, no. 4, pp. 301–327, 2003, doi: 10.1016/S0360-1285(03)00028-5.

[19] K. M. A. Kabir, K. C. A. Alam, R. A. Rouf, and M. M. A. Sarker, "The effect of mass recovery adsorption cooling cycle to optimize the collector number and time allocation," *AIP Conf Proc*, vol. 1754, 2016, doi: 10.1063/1.4958418.

[20] S. Narayanan, X. Li, S. Yang, I. McKay, H. Kim, and E. N. Wang, "Design and optimization of high performance adsorption-based thermal battery," *ASME 2013 Heat Transfer Summer Conf. Collocated with the ASME 2013 7th Int. Conf. on Energy Sustainability and the ASME 2013 11th Int. Conf. on Fuel Cell Science, Engineering and Technology, HT 2013*, vol. 1, no. July, 2013, doi: 10.1115/HT2013-17472.

[21] S. Narayanan *et al.*, "Thermal battery for portable climate control," *Appl Energy*, vol. 149, pp. 104–116, 2015, doi: 10.1016/j.apenergy.2015.03.101.

[22] M. Tokarev, L. Gordeeva, V. Romannikov, I. Glaznev, and Y. Aristov, "New composite sorbent CaCl2 in mesopores for sorption cooling/heating," *International Journal of Thermal Sciences*, vol. 41, no. 5, pp. 470–474, 2002, doi: 10.1016/S1290-0729(02)01339-X.

[23] Y. Tashiro, M. Kubo, Y. Katsumi, T. Meguro, and K. Komeya, "Assessment of adsorption-desorption characteristics of adsorbents for adsorptive desiccant cooling system," *J Mater Sci*, vol. 39, no. 4, pp. 1315–1319, 2004, doi: 10.1023/B:JMSC.0000013937.11959.6a.

[24] A. Akahira, K. C. A. Alam, Y. Hamamoto, A. Akisawa, and T. Kashiwagi, "Experimental investigation of mass recovery adsorption refrigeration cycle," *International Journal of Refrigeration*, vol. 28, no. 4, pp. 565–572, 2005, doi: 10.1016/j.ijrefrig.2004.10.001.

[25] S. K. Henninger, M. Schicktanz, P. P. C. Hügenell, H. Sievers, and H. M. Henning, "Evaluation of methanol adsorption on activated carbons for thermally driven chillers part I: Thermophysical characterisation," *International Journal of Refrigeration*, vol. 35, no. 3, pp. 543–553, 2012, doi: 10.1016/j.ijrefrig.2011.10.004.

[26] Z. Lu, R. Wang, and Z. Xia, "Experimental analysis of an adsorption air conditioning with micro-porous silica gel-water," *Appl Therm Eng*, vol. 50, no. 1, pp. 1015–1020, 2013, doi: 10.1016/j.applthermaleng.2012.07.041.

[27] S. W. Du, X. H. Li, Z. X. Yuan, C. X. Du, W. C. Wang, and Z. B. Liu, "Performance of solar adsorption refrigeration in system of SAPO-34 and ZSM-5 zeolite," *Solar Energy*, vol. 138, pp. 98–104, 2016, doi: 10.1016/j.solener.2016.09.015.

[28] T. X. Li, J. X. Xu, T. Yan, and R. Z. Wang, "Development of sorption thermal battery for low-grade waste heat recovery and combined cold and heat energy storage," *Energy*, vol. 107, pp. 347–359, 2016, doi: 10.1016/j.energy.2016.03.126.

[29] A. Elsayed, E. Elsayed, R. AL-Dadah, S. Mahmoud, A. Elshaer, and W. Kaialy, "Thermal energy storage using metal–organic framework materials," *Appl Energy*, vol. 186, pp. 509–519, 2017, doi: 10.1016/j.apenergy.2016.03.113.

[30] Q. W. Pan, R. Z. Wang, L. W. Wang, and D. Liu, "Design and experimental study of a silica gel-water adsorption chiller with modular adsorbers," *International Journal of Refrigeration*, vol. 67, pp. 336–344, 2016, doi: 10.1016/j.ijrefrig.2016.03.001.

[31] E. Elsayed, R. Al-Dadah, S. Mahmoud, A. Elsayed, and P. A. Anderson, "Aluminium fumarate and CPO-27(Ni) MOFs: Characterization and thermodynamic analysis for adsorption heat pump applications," *Appl Therm Eng*, vol. 99, pp. 802–812, 2016, doi: 10.1016/j.applthermaleng.2016.01.129.

[32] E. Elsayed, R. AL-Dadah, S. Mahmoud, P. A. Anderson, A. Elsayed, and P. G. Youssef, "CPO-27(Ni), aluminium fumarate and MIL-101(Cr) MOF materials for adsorption water desalination," *Desalination*, vol. 406, pp. 25–36, 2017, doi: 10.1016/j.desal.2016.07.030.

[33] P. J. Vodianitskaia, J. J. Soares, H. Melo, and J. M. Gurgel, "Experimental chiller with silica gel: Adsorption kinetics analysis and performance evaluation," *Energy Convers Manag*, vol. 132, pp. 172–179, 2017, doi: 10.1016/j.enconman.2016.11.028.

[34] Q. W. Pan and R. Z. Wang, "Experimental study on operating features of heat and mass recovery processes in adsorption refrigeration," *Energy*, vol. 135, pp. 361–369, 2017, doi: 10.1016/j.energy.2017.06.131.

[35] S. Narayanan *et al.*, "A thermophysical battery for storage-based climate control," *Appl Energy*, vol. 189, pp. 31–43, 2017, doi: 10.1016/j.apenergy.2016.12.003.

[36] H. J. Dakkama, P. G. Youssef, R. K. Al-Dadah, and S. Mahmoud, "Adsorption ice making and water desalination system using metal organic frameworks/water pair," *Energy Convers Manag*, vol. 142, pp. 53–61, 2017, doi: 10.1016/j.enconman.2017.03.036.

[37] G. Engel, "Sorption cold storage for thermal management of the battery of a hybrid vehicle," *Energy Procedia*, vol. 155, pp. 149–155, 2018, doi: 10.1016/j.egypro.2018.11.060.

[38] E. Kyung, S. Kyum, and J. Sung, "Properties of Mesoporous Silica and MOF by lon Exchange and Salt Impregnation," *Clean Technology*, vol. 24, no. 1, pp. 55–62, 2018.

[39] Z. Lu, "Experimental and simulation analysis of the combined adsorption system driven by 80–140 °C heat source," *Energy Convers Manag*, vol. 184, no. January, pp. 726–734, 2019, doi: 10.1016/j.enconman.2019.01.048.

[40] Q. Pan, J. Peng, H. Wang, H. Sun, and R. Wang, "Experimental investigation of an adsorption air-conditioner using silica gel-water working pair," *Solar Energy*, vol. 185, no. April, pp. 64–71, 2019, doi: 10.1016/j.solener.2019.04.054.

[41] M. M. Abd-Elhady and A. M. Hamed, "Effect of fin design parameters on the performance of a two-bed adsorption chiller," *International Journal of Refrigeration*, vol. 113, pp. 164–173, 2020, doi: 10.1016/j.ijrefrig.2020.01.006.

[42] B. Han and A. Chakraborty, "Adsorption characteristics of methyl-functional ligand MOF-801 and water systems: Adsorption chiller modelling and performances," *Appl Therm Eng*, vol. 175, no. March, p. 115393, 2020, doi: 10.1016/j.applthermaleng.2020.115393.

[43] M. Rezk, M. B. Elsheniti, A. Rezk, and O. A. Elsamni, "Numerical Investigation of Copper Foam Adsorption Beds Packed with MOF- 801 for Space Cooling and Desalination Applications," 13th International Conference on Applied Energy, ICAE 2021.

[44] Y. M. Liu, Z. X. Yuan, X. Wen, and C. X. Du, "Evaluation on performance of solar adsorption cooling of silica gel and SAPO-34 zeolite," *Appl Therm Eng*, vol. 182, no. September 2020, 2021, doi: 10.1016/j.applthermaleng.2020.116019.

[45] M. B. Elsheniti, A. T. Abd El-Hamid, O. A. El- Samni, S. M. Elsherbiny, and E. Elsayed, "Experimental evaluation of a solar two-bed lab-scale adsorption cooling system," *Alexandria Engineering Journal*, vol. 60, no. 3, pp. 2747–2757, 2021, doi: 10.1016/j.aej.2021.01.024.

[46] I. Jahan, T. H. Rupam, M. L. Palash, and B. B. Saha, "Mixed Valance Metal Doped MOF 801 for Adsorption Heat Pumps," Sixth International Conference on Polygeneration – ICP 2021.

[47] A. L. Tarish, A. H. N. Khalifa, and A. J. Hamad, "Impact of the adsorbent materials and adsorber bed design on performance of the adsorption thermophysical battery: Experimental study," *Case Studies in Thermal Engineering*, vol. 31, no. December 2021, p. 101808, 2022, doi: 10.1016/j.csite.2022.101808.

[48] K. H. Yeung and K. Sumathy, "Thermodynamic analysis and optimization of a combined adsorption heating and cooling system," *Int J Energy Res*, vol. 27, no. 15, pp. 1299–1315, 2003, doi: 10.1002/er.944.

[49] A. Akahira, K. C. A. Alam, Y. Hamamoto, A. Akisawa, and T. Kashiwagi, "Mass recovery adsorption refrigeration cycle - Improving cooling capicity," *International Journal of Refrigeration*, vol. 27, no. 3, pp. 225–234, 2004, doi: 10.1016/j.ijrefrig.2003.10.004.

[50] Z. Tamainot-Telto, S. J. Metcalf, R. E. Critoph, Y. Zhong, and R. Thorpe, "Carbon-ammonia pairs for adsorption refrigeration applications: ice making, air conditioning and heat pumping," *International Journal of Refrigeration*, vol. 32, no. 6, pp. 1212–1229, 2009, doi: 10.1016/j.ijrefrig.2009.01.008.

[51] A. Sharafianardakani and M. Bahrami, "A quasi steady state model for adsorption cooling systems: Automotive applications," *ASME 2012 6th International Conference on Energy Sustainability, ES 2012, Collocated with the ASME 2012 10th International Conference on Fuel Cell Science, Engineering and Technology*, no. PARTS A AND B, pp. 1263–1272, 2012, doi: 10.1115/ES2012-91362.

[52] Q. Pan, R. Wang, Z. Lu, and L. Wang, "Thermodynamic analysis and performance simulation of different kinds of mass recovery processes applied in adsorption refrigeration system," *HVAC and R Research*, vol. 20, no. 3, pp. 311–319, 2014, doi: 10.1080/10789669.2014.889512.

[53] A. Sharafian and M. Bahrami, "Critical analysis of thermodynamic cycle modeling of adsorption cooling systems for light-duty vehicle air conditioning applications," *Renewable and Sustainable Energy Reviews*, vol. 48, pp. 857–869, 2015, doi: 10.1016/j.rser.2015.04.055.

[54] P. G. Youssef, R. K. Al-Dadah, S. M. Mahmoud, H. J. Dakkama, and A. Elsayed, "Effect of Evaporator and Condenser Temperatures on the Performance of Adsorption Desalination Cooling Cycle," in *Energy Procedia*, Elsevier Ltd, 2015, pp. 1464–1469. doi: 10.1016/j.egypro.2015.07.263.

[55] I. Solmuş, C. Yamali, C. Yildirim, and K. Bilen, "Transient behavior of a cylindrical adsorbent bed during the adsorption process," *Appl Energy*, vol. 142, pp. 115–124, 2015, doi: 10.1016/j.apenergy.2014.12.080.

[56] A. Allouhi, T. Kousksou, A. Jamil, T. El Rhafiki, Y. Mourad, and Y. Zeraouli, "Optimal working pairs for solar adsorption cooling applications," *Energy*, vol. 79, no. C, pp. 235–247, 2015, doi: 10.1016/j.energy.2014.11.010.

[57] W. Chekirou, N. Boukheit, and A. Karaali, "Heat recovery process in an adsorption refrigeration machine," *Int J Hydrogen Energy*, vol. 41, no. 17, pp. 7146–7157, 2016, doi: 10.1016/j.ijhydene.2016.02.070.

[58] S. Z. Xu, L. W. Wang, and R. Z. Wang, "Thermodynamic analysis of single-stage and multi-stage adsorption refrigeration cycles with activated carbon-ammonia working pair," *Energy Convers Manag*, vol. 117, pp. 31–42, 2016, doi: 10.1016/j.enconman.2016.03.010.

[59] S. M. Ali and A. Chakraborty, "Adsorption assisted double stage cooling and desalination employing silica gel + water and AQSOA-Z02 + water systems," *Energy Convers Manag*, vol. 117, pp. 193–205, 2016, doi: 10.1016/j.enconman.2016.03.007.

[60] F. N. Al-Mousawi, R. Al-Dadah, and S. Mahmoud, "Different bed configurations and time ratios: Performance analysis of low-grade heat driven adsorption system for cooling and electricity," *Energy Convers Manag*, vol. 148, pp. 1028–1040, 2017, doi: 10.1016/j.enconman.2017.06.062.

[61] S. Z. Xu, R. Z. Wang, and L. W. Wang, "Temperature–heat diagram analysis method for heat recovery physical adsorption refrigeration cycle – Taking multi-stage cycle as an example," *International Journal of Refrigeration*, vol. 74, pp. 254–268, 2017, doi: 10.1016/j.ijrefrig.2016.09.021.

[62] R. H. Mohammed, O. Mesalhy, M. L. Elsayed, and L. C. Chow, "Conception d'un nouveau lit compact pour systèmes de refroidissement à adsorption: étude numérique paramétrique," *International Journal of Refrigeration*, vol. 80, pp. 238–251, 2017, doi: 10.1016/j.ijrefrig.2017.04.028.

[63] H. J. Dakkama, A. Elsayed, R. K. Al-dadah, S. M. Mahmoud, and P. Youssef, "Integrated evaporator – condenser cascaded adsorption system for low temperature cooling using different working pairs," *Appl Energy*, vol. 185, pp. 2117–2126, 2017, doi: 10.1016/j.apenergy.2016.01.132.

[64] Q. W. Pan and R. Z. Wang, "Study on operation strategy of a silica gel-water adsorption chiller in solar cooling application," *Solar Energy*, vol. 172, no. September 2017, pp. 24–31, 2018, doi: 10.1016/j.solener.2018.03.062.

[65] L. Q. Zhu *et al.*, "Performance investigation of nanostructured composite surfaces for use in adsorption cooling systems with a mass recovery cycle," *Sci Technol Built Environ*, vol. 24, no. 10, pp. 1084–1103, 2018, doi: 10.1080/23744731.2018.1479613.

[66] Q. Pan, R. Wang, N. Vorayos, and T. Kiatsiriroat, "A novel adsorption heat pump cycle: Cascaded mass recovery cycle," *International Journal of Refrigeration*, vol. 95, pp. 21–27, 2018, doi: 10.1016/j.ijrefrig.2018.08.004.

[67] G. Papakokkinos, J. Castro, J. López, and A. Oliva, "A generalized computational model for the simulation of adsorption packed bed reactors – Parametric study of five reactor geometries for cooling applications," *Appl Energy*, vol. 235, no. June 2018, pp. 409–427, 2019, doi: 10.1016/j.apenergy.2018.10.081.

[68] X. Q. Duong, N. V. Cao, W. S. Lee, and J. D. Chung, "Module integration in an adsorption cooling system," *Appl Therm Eng*, vol. 155, no. March, pp. 508–514, 2019, doi: 10.1016/j.applthermaleng.2019.03.152.

[69] R. Raj and V. Baiju, "Thermodynamic analysis of a solar powered adsorption cooling and desalination system," *Energy Procedia*, vol. 158, pp. 885–891, 2019, doi: 10.1016/j.egypro.2019.01.226.

[70] Y. Jiang, M. H. Bagheri, R. T. Loibl, and S. N. Schiffres, "Thermodynamic limits of adsorption heat pumps: A facile method of comparing adsorption pairs," *Appl Therm Eng*, vol. 160, p. 113906, 2019, doi: 10.1016/j.applthermaleng.2019.113906.

[71] E. Elsayed, R. AL-Dadah, S. Mahmoud, P. Anderson, and A. Elsayed, "Adsorption cooling system employing novel MIL-101(Cr)/CaCl2 composites: Numerical study," *International Journal of Refrigeration*, vol. 107, pp. 246–261, 2019, doi: 10.1016/j.ijrefrig.2019.08.004.

[72] P. Vivekh, D. T. Bui, M. Kumja, M. R. Islam, and K. J. Chua, "Theoretical performance analysis of silica gel and composite polymer desiccant coated heat exchangers based on a CFD approach," *Energy Convers Manag*, vol. 187, no. February, pp. 423–446, 2019, doi: 10.1016/j.enconman.2019.02.093.

[73] A. Amirfakhraei, T. Zarei, and J. Khorshidi, "Advanced heat and mass recovery design in a two bed adsorption desalination system," *Appl Therm Eng*, vol. 198, Nov. 2021, doi: 10.1016/j.applthermaleng.2021.117494.

[74] A. L. Tarish, A. H. N. Khalifa, and A. J. Hamad, "Performance evaluation of adsorption thermophysical battery for air conditioning applications," *Thermal Science and Engineering Progress*, vol. 28, no. September 2021, p. 101060, 2022, doi: 10.1016/j.tsep.2021.101060.

[75] K. C. Leong and Y. Liu, "Numerical modeling of combined heat and mass transfer in the adsorbent bed of a zeolite/water cooling system," *Appl Therm Eng*, vol. 24, no. 16, pp. 2359–2374, 2004, doi: 10.1016/j.applthermaleng.2004.02.014.

[76] Y. Liu and K. C. Leong, "Numerical study of a novel cascading adsorption cycle," *International Journal of Refrigeration*, vol. 29, no. 2, pp. 250–259, 2006, doi: 10.1016/j.ijrefrig.2005.05.008.

[77] J. Y. San and W. M. Lin, "Comparison among three adsorption pairs for using as the working substances in a multi-bed adsorption heat pump," *Appl Therm Eng*, vol. 28, no. 8–9, pp. 988–997, 2008, doi: 10.1016/j.applthermaleng.2007.06.026.

[78] A. S. Uyun, T. Miyazaki, Y. Ueda, and A. Akisawa, "High performance cascading adsorption refrigeration cycle with internal heat recovery driven by a low grade heat source temperature," *Energies (Basel)*, vol. 2, no. 4, pp. 1170–1191, 2009, doi: 10.3390/en20401170.

[79] A. Alahmer, X. Wang, R. Al-Rbaihat, K. C. Amanul Alam, and B. B. Saha, "Performance evaluation of a solar adsorption chiller under different climatic conditions," *Appl Energy*, vol. 175, pp. 293–304, 2016, doi: 10.1016/j.apenergy.2016.05.041.

[80] P. Youssef, S. Mahmoud, R. Al-Dadah, E. Elsayed, and O. El-Samni, "Numerical Investigation of Aluminum Fumarate MOF adsorbent material for adsorption

desalination/cooling application," *Energy Procedia*, vol. 142, pp. 1693–1698, 2017, doi: 10.1016/j.egypro.2017.12.551.

[81] E. Elsayed, R. Al-Dadah, S. Mahmoud, P. Anderson, A. Hassan, and P. Youssef, "Numerical investigation of MIL-101(Cr)/GrO composite performance in adsorption cooling systems," *Energy Procedia*, vol. 142, pp. 4131–4137, 2017, doi: 10.1016/j.egypro.2017.12.336.

[82] M. B. Elsheniti, M. A. Hassab, and A. E. Attia, "Examination of effects of operating and geometric parameters on the performance of a two-bed adsorption chiller," *Appl Therm Eng*, vol. 146, no. September 2018, pp. 674–687, 2019, doi: 10.1016/j.applthermaleng.2018.10.043.

[83] O. Pártl and J. Mikyška, "Numerical modeling of compressible gas flow in zeolite bed and above its surface," *Int J Heat Mass Transf*, vol. 138, pp. 1199–1210, 2019, doi: 10.1016/j.ijheatmasstransfer.2019.04.095.

[84] J. M. Pinheiro, S. Salústio, V. Geraldes, A. A. Valente, and C. M. Silva, "Copper foam coated with CPO-27(Ni) metal–organic framework for adsorption heat pump: Simulation study using OpenFOAM," *Appl Therm Eng*, vol. 178, p. 115498, 2020, doi: 10.1016/j.applthermaleng.2020.115498.

[85] A. Hassan, R. Al-Dadah, S. Mahmoud, H. Fath, E. Hussien, and N. Genidi, "Integration of vacuum multi effect membrane distillation with adsorption/cooling system," *Appl Therm Eng*, vol. 178, p. 115546, 2020, doi: 10.1016/j.applthermaleng.2020.115546.

[86] N. U. Qadir, Z. Y. Xu, Q. W. Pan, S. A. M. Said, R. B. Mansour, and K. Akhtar, "Performance prediction of a two-bed solar-powered adsorption chiller with heat and mass recovery cycles and adaptive cycle time – A first step towards the design of fully autonomous commercial-scale adsorption chillers," *Appl Therm Eng*, vol. 192, no. December 2020, 2021, doi: 10.1016/j.applthermaleng.2021.116950.

[87] T. Miyazaki, A. Akisawa, B. B. Saha, I. I. El-Sharkawy, and A. Chakraborty, "A new cycle time allocation for enhancing the performance of two-bed adsorption chillers," *International Journal of Refrigeration*, vol. 32, no. 5, pp. 846–853, 2009, doi: 10.1016/j.ijrefrig.2008.12.002.

[88] P. G. Youssef, H. Dakkama, S. M. Mahmoud, and R. K. AL-Dadah, "Experimental investigation of adsorption water desalination/cooling system using CPO-27Ni MOF," *Desalination*, vol. 404, pp. 192–199, 2017, doi: 10.1016/j.desal.2016.11.008.

[89] N. Ghilen *et al.*, "Performance Simulation of Two-Bed Adsorption Refrigeration Chiller with Mass Recovery To cite this version : HAL Id : hal-02994585 Fundamentals of Renewable Energy and Applications Performance Simulation of Two-Bed Adsorption Refrigeration Chiller with Ma," pp. 0–7, 2020, doi: 10.4172/20904541.1000229.

[90] H. O. Helaly, M. M. Awad, I. I. El-Sharkawy, and A. M. Hamed, "Theoretical and experimental investigation of the performance of adsorption heat storage system," *Appl*

Therm Eng, vol. 147, no. March 2018, pp. 10–28, 2019, doi: 10.1016/j.applthermaleng.2018.10.059.

[91] J. G. Lee, K. J. Bae, and O. K. Kwon, "Performance investigation of a two-bed type adsorption chiller with various adsorbents," *Energies (Basel)*, vol. 13, no. 10, pp. 1–16, 2020, doi: 10.3390/en13102553.

[92] W. D. Chen and K. J. Chua, "Parameter analysis and energy optimization of a four-bed, two-evaporator adsorption system," *Appl Energy*, vol. 265, no. March, p. 114842, 2020, doi: 10.1016/j.apenergy.2020.114842.

[93] E. Elsayed, M. M. Saleh, R. AL-Dadah, S. Mahmoud, and A. Elsayed, "Aluminium fumarate metal-organic framework coating for adsorption cooling application: Experimental study," *International Journal of Refrigeration*, vol. 130, pp. 288–304, 2021, doi: 10.1016/j.ijrefrig.2021.05.015.

[94] S. Yagnamurthy, D. Rakshit, S. Jain, and B. B. Saha, "Operational envelope and performance enhancement of a two-bed adsorption cooling system," *Appl Therm Eng*, vol. 195, no. June, p. 117181, 2021, doi: 10.1016/j.applthermaleng.2021.117181.

[95] L. Yong and K. Sumathy, "Modeling and simulation of a solar powered two bed adsorption air conditioning system," *Energy Convers Manag*, vol. 45, no. 17, pp. 2761–2775, 2004, doi: 10.1016/j.enconman.2003.12.004.

[96] X. Wang and H. T. Chua, "Two bed silica gel-water adsorption chillers: An effectual lumped parameter model," *International Journal of Refrigeration*, vol. 30, no. 8, pp. 1417–1426, 2007, doi: 10.1016/j.ijrefrig.2007.03.010.

[97] A. Sadeghlu, M. Yari, S. M. S. Mahmoudi, and H. B. Dizaji, "Performance evaluation of Zeolite 13X/CaCl2 two-bed adsorption refrigeration system," *International Journal of Thermal Sciences*, vol. 80, no. 1, pp. 76–82, 2014, doi: 10.1016/j.ijthermalsci.2014.02.001.

[98] S. Mitra, P. Kumar, K. Srinivasan, and P. Dutta, "Performance evaluation of a two-stage silica gel + water adsorption based cooling-cum-desalination system," *International Journal of Refrigeration*, vol. 58, pp. 186–198, 2015, doi: 10.1016/j.ijrefrig.2015.06.018.

[99] B. Shi, R. Al-Dadah, S. Mahmoud, A. Elsayed, and E. Elsayed, "CPO-27(Ni) metal-organic framework based adsorption system for automotive air conditioning," *Appl Therm Eng*, vol. 106, pp. 325–333, 2016, doi: 10.1016/j.applthermaleng.2016.05.109.

[100] A. Alahmer, X. Wang, and K. C. A. Alam, "Dynamic and economic investigation of a solar thermal-driven two-bed adsorption chiller under Perth climatic conditions," *Energies (Basel)*, vol. 13, no. 4, 2020, doi: 10.3390/en13041005.

[101] P. Soni and V. K. Gaba, "Performance analysis of adsorption refrigeration system using silicagel/methanol pair: Experimental & analytical approaches," *Journal of Thermal Engineering*, vol. 7, no. 5, pp. 1079–1089, 2021, doi: 10.18186/thermal.977913.

[102] T. H. Rupam, M. A. Islam, A. Pal, and B. B. Saha, "Adsorption thermodynamics and performance indicators of selective adsorbent/refrigerant pairs," *Appl Therm Eng*, vol. 175, Jul. 2020, doi: 10.1016/j.applthermaleng.2020.115361.

[103] B. B. Saha, A. Akisawa, and T. Kashiwagi, "Thermodynamic Analysis of Adsorption Refrigeration Cycles," IECEC-97 Proceedings of the Thirty-Second Intersociety Energy Conversion Engineering Conference (Cat. No.97CH6203), Honolulu, HI, USA, 1997, pp. 1258-1264 vol.2, doi: 10.1109/IECEC.1997.661949.

[104] J. W. Wu, M. J. Biggs, and E. J. Hu, "Dynamic model for the optimisation of adsorption-based desalination processes," *Appl Therm Eng*, vol. 66, no. 1–2, pp. 464–473, 2014, doi: 10.1016/j.applthermaleng.2014.02.045.

[105] A. Chakraborty, B. B. Saha, S. Koyama, K. C. Ng, and K. Srinivasan, "Adsorption thermodynamics of silica gel-water systems," *J Chem Eng Data*, vol. 54, no. 2, pp. 448–452, Feb. 2009, doi: 10.1021/je800458k.

[106] H. Z. Hassan, "Energy analysis and performance evaluation of the adsorption refrigeration system," *ISRN Mechanical Engineering*, vol. 2013, 2013, doi: 10.1155/2013/704340.

[107] B. Sun and A. Chakraborty, "Thermodynamic frameworks of adsorption kinetics modeling: Dynamic water uptakes on silica gel for adsorption cooling applications," *Energy*, vol. 84, pp. 296–302, May 2015, doi: 10.1016/j.energy.2015.02.101.

[108] M. A. Hadj Ammar, B. Benhaoua, and F. Bouras, "Thermodynamic analysis and performance of an adsorption refrigeration system driven by solar collector," *Appl Therm Eng*, vol. 112, pp. 1289–1296, Feb. 2017, doi: 10.1016/j.applthermaleng.2016.09.119.

[109] S. Singh and S. Dhingra, "Thermal performance of a vapour adsorption refrigeration system: An overview," in *Journal of Physics: Conference Series*, Institute of Physics Publishing, Aug. 2019. doi: 10.1088/1742-6596/1240/1/012024.

[110] M. Sharifzadeh, M. Ghazikhani, and H. Niazmand, "Temporal exergy analysis of adsorption cooling system by developing non-flow exergy function," *Appl Therm Eng*, vol. 139, pp. 409–418, Jul. 2018, doi: 10.1016/j.applthermaleng.2017.12.128.

[111] V. Baiju and C. Muraleedharan, "Exergy Assessment of Single Stage Solar Adsorption Refrigeration System Using ANN," *ISRN Mechanical Engineering*, vol. 2012, pp. 1–10, Sep. 2012, doi: 10.5402/2012/915154.

[112] N. V. Cao and J. D. Chung, "Exergy Analysis of Adsorption Cooling Systems Based on Numerical Simulation," *Energy Technology*, vol. 7, no. 1, pp. 153–166, Jan. 2019, doi: 10.1002/ente.201800414.

[113] M. M. Dubinin, "The potential theory of adsorption of gases and vapors for adsorbents with energetically nonuniform surfaces," *Chemical reviews*, vol. 60, no. 2, p.p 235-241, 1960. doi.org/10.1021/cr60204a006

[114] G. P. Jeppu and T. P. Clement, "A modified Langmuir-Freundlich isotherm model for simulating pH-dependent adsorption effects," *J Contam Hydrol*, vol. 129–130, pp. 46–53, Mar. 2012, doi: 10.1016/j.jconhyd.2011.12.001.

[115] R. Z. Wang, "Adsorption refrigeration research in Shanghai Jiao Tong University," *Renewable & sustainable energy reviews*, vol. 5, no. 1, pp. 1–37, 2001, doi: 10.1016/S1364-0321(00)00009-5.

[116] R. P. Sah, B. Choudhury, R. K. Das, and A. Sur, "An overview of modelling techniques employed for performance simulation of low–grade heat operated adsorption cooling systems," *Renewable and Sustainable Energy Reviews*, vol. 74. Elsevier Ltd, pp. 364–376, 2017. doi: 10.1016/j.rser.2017.02.062.

[117] L. Yong and K. Sumathy, "Review of mathematical investigation on the closed adsorption heat pump and cooling systems," *Renewable and Sustainable Energy Reviews*, vol. 6, no. 4, pp. 305-338, 2002, doi.org/10.1016/S1364-0321(02)00010-2.

[118] Z. Z. Xia, C. J. Chen, J. K. Kiplagat, R. Z. Wang, and J. Q. Hu, "Adsorption equilibrium of water on silica gel," *J Chem Eng Data*, vol. 53, no. 10, pp. 2462–2465, Oct. 2008, doi: 10.1021/je800019u.

[119] H. T. Chua, K. C. Ng, A. Chakraborty, N. M. Oo, and M. A. Othman, "Adsorption characteristics of silica gel + water systems," *J Chem Eng Data*, vol. 47, no. 5, pp. 1177–1181, Sep. 2002, doi: 10.1021/je0255067.

[120] K. Chihara and M. Suzuki, "Air drying by pressure swing adsorption," J. Chem. Eng. Japan, vol. 16, no. 4, pp. 293–299, 1983, doi: 10.1252/jcej.16.293. liquid phase [-]," 1983.

[121] D. A.O, "Langmuir, Freundlich, Temkin and Dubinin–Radushkevich Isotherms Studies of Equilibrium Sorption of Zn 2+ Unto Phosphoric Acid Modified Rice Husk," *IOSR Journal of Applied Chemistry*, vol. 3, no. 1, pp. 38–45, 2012, doi: 10.9790/5736-0313845.

[122] Y. Wang and M. D. LeVan, "Adsorption Equilibrium of Binary Mixtures of Carbon Dioxide and Water Vapor on Zeolites 5A and 13X," *J Chem Eng Data*, vol. 55, no. 9, pp. 3189–3195, Sep. 2010, doi: 10.1021/je100053g.

[123] K. Thu, A. Chakraborty, B. B. Saha, and K. C. Ng, "Thermo-physical properties of silica gel for adsorption desalination cycle," in *Applied Thermal Engineering*, Feb. 2013, pp. 1596–1602. doi: 10.1016/j.applthermaleng.2011.09.038.

[124] A. Kapoor, J. A. Ritter, and R. T. Yang, "On the Dubinin-Radushkevich Equation for Adsorption in Microporous Solids in the Henry's Law Region," Langmuir, 5 vol., no. 4 p.p 1118-1121, 1989, DOI: 10.1021/la00088a043

[125] N. Liu, M. Zhu, H. Wang, and H. Ma, "Adsorption characteristics of Direct Red 23 from aqueous solution by biochar," *J Mol Liq*, vol. 223, pp. 335–342, Nov. 2016, doi: 10.1016/j.molliq.2016.08.061.

[126] J. C. Lou, R. H. Lee, W. H. Chen, C. J. Chang, K. L. Hsu, and J. Y. Han, "Adsorption Kinetics and Thermodynamics of Perchlorate on Carbon Nanotubes in Water," *Journal of Environmental Engineering*, vol. 140, no. 11, Nov. 2014, doi: 10.1061/(asce)ee.1943-7870.0000859.

[127] J. C. Lou, Y. S. Hsu, K. L. Hsu, M. S. Chou, and J. Y. Han, "Comparing the removal of perchlorate when using single-walled carbon nanotubes (SWCNTs) or granular activated carbon: Adsorption kinetics and thermodynamics," *J Environ Sci Health A Tox Hazard Subst Environ Eng*, vol. 49, no. 5, pp. 503–513, Apr. 2014, doi: 10.1080/10934529.2014.859025.

[128] Y. Sen Hsu, J. C. Lou, M. S. Chou, K. L. Hsu, and J. Y. Han, "Characterization of single-walled carbon nanotubes and adsorption of perchlorate in water," *Water Air Soil Pollut*, vol. 226, no. 3, 2015, doi: 10.1007/s11270-015-2330-9.

[129] N. Liu, A. B. Charrua, C. H. Weng, X. Yuan, and F. Ding, "Characterization of biochars derived from agriculture wastes and their adsorptive removal of atrazine from aqueous solution: A comparative study," *Bioresour Technol*, vol. 198, pp. 55–62, Dec. 2015, doi: 10.1016/j.biortech.2015.08.129.

[130] M. I. Khan *et al.*, "Adsorption kinetic, equilibrium and thermodynamic studies of eosin-B onto anion exchange membrane," *Desalination Water Treat*, vol. 155, pp. 84–93, Jul. 2019, doi: 10.5004/dwt.2019.23936.

[131] B. B. Saha, S. Koyama, T. Kashiwagi, A. Akisawa, K. C. Ng, and H. T. Chua, "Waste heat driven dual-mode, multi-stage, multi-bed regenerative adsorption system," *International Journal of Refrigeration*, vol. 26, no. 7, pp. 749–757, Nov. 2003, doi: 10.1016/S0140-7007(03)00074-4.

[132] B. Han and A. Chakraborty, "Adsorption characteristics of methyl-functional ligand MOF-801 and water systems: Adsorption chiller modelling and performances," *Appl Therm Eng*, vol. 175, no. March, p. 115393, 2020, doi: 10.1016/j.applthermaleng.2020.115393.

[133] C. Aharoni and E. C. Tompkins, "Kinetics of Adsorption and Desorption and the Elovich Equation," *Advances in Catalysis*, vol. 21, pp. 1-49, 1970, doi.org/10.1016/S0360-0564(08)60563-5

[134] E. Glueckauf and J. I. Coates, "Theory of chromatography. Part IV. The influence of incomplete equilibrium on the front boundary of chromatograms and on the effectiveness of separation," *Journal of the Chemical Society (Resumed)*, pp. 1315–1321, 1947, doi: 10.1039/jr9470001315.

[135] A. SAKODA and Motoyuki SUZUKI, "Fundamental study on solar powered adsorption cooling system," *Journal of chemical engineering of Japan*, vol. 17, no. 1, p.p 52-57, 1965, doi.org/10.1252/jcej.17.52.

[136] R. H. Mohammed, O. Mesalhy, M. L. Elsayed, M. Su, and L. C. Chow, "Revisiting the adsorption equilibrium equations of silica gel/water for adsorption cooling applications,"

International Journal of Refrigeration, Vol. 86, p.p 40-47, 2017, doi.org/10.1016/j.ijrefrig.2017.10.038

[137] J. Wang and X. Guo, "Adsorption kinetic models: Physical meanings, applications, and solving methods," *Journal of Hazardous Materials*, vol. 390. Elsevier B.V., May 15, 2020. doi: 10.1016/j.jhazmat.2020.122156.

[138] S. Klein and G. Nellis, "Mastering EES," 2012. [Online]. Available: http://fchart.com

[139] A. Akahira, K. C. A. Alam, Y. Hamamoto, A. Akisawa, and T. Kashiwagi, "Mass recovery adsorption refrigeration cycle - Improving cooling capicity," *International Journal of Refrigeration*, vol. 27, no. 3, pp. 225–234, 2004, doi: 10.1016/j.ijrefrig.2003.10.004.

[140] N. Vi Cao, X. Q. Duong, W. S. Lee, M. Y. Park, S. S. Lee, and J. D. Chung, "Exergy analysis of advanced adsorption cooling cycles," *Entropy*, vol. 22, no. 10, pp. 1–13, 2020, doi: 10.3390/e22101082.

[141] Y. Jiang, M. H. Bagheri, R. T. Loibl, and S. N. Schiffres, "Thermodynamic limits of adsorption heat pumps: A facile method of comparing adsorption pairs," *Appl Therm Eng*, vol. 160, p. 113906, 2019, doi: 10.1016/j.applthermaleng.2019.113906.

[142] M. Rezk, M. B. Elsheniti, A. Rezk, and O. A. Elsamni, "Numerical Investigation of Copper Foam Adsorption Beds Packed with MOF- 801 for Space Cooling and Desalination Applications," *13th International Conference on Applied Energy*, ICAE 2021.

[143] A. M. P. Peedikakkal and I. H. Aljundi, "Mixed-Metal Cu-BTC Metal-Organic Frameworks as a Strong Adsorbent for Molecular Hydrogen at Low Temperatures," *ACS Omega*, vol. 5, no. 44, pp. 28493–28499, Nov. 2020, doi: 10.1021/acsomega.0c02810.

[144] O. M. Alduhaish, M. R. Shaik, and S. F. Adil, "Photo-Induced Preparation of Ag@MOF-801 Composite Based Heterogeneous Nanocatalyst for the Production of Biodiesel," *Catalysts*, vol. 12, no. 5, May 2022, doi: 10.3390/catal12050533.

[145] Bergman, Theodore L. Fundamentals of heat and mass transfer. John Wiley & Sons, 2011.

[146] Yunus A. Çengeland and Afshin J. Ghajar, "Heat and Mass Transfer Fundamentals & Applications," McGraw-Hill Education, 2015.

[147] S. H. Seol, K. Nagano, and J. Togawa, "Modeling of adsorption heat pump system based on experimental estimation of heat and mass transfer coefficients," *Appl Therm Eng*, vol. 171, May 2020, doi: 10.1016/j.applthermaleng.2020.115089.

[148] M. L. Ntsoane *et al.*, "Performance evaluation of silica gel-water adsorption based cooling system for mango fruit storage in Sub-Saharan Africa," *Postharvest Biol Technol*, vol. 149, pp. 195–199, Mar. 2019, doi: 10.1016/j.postharvbio.2018.12.004.

[149] A. Fellah, Y. Boukhchana, and A. Ben Brahim, "Quasi-real performances of an irreversible solar absorption refrigeration cycle," *International Journal of Refrigeration*, vol. 100, pp. 21–26, Apr. 2019, doi: 10.1016/j.ijrefrig.2019.01.017.

[150] J. Y. San, "Analysis of the performance of a multi-bed adsorption heat pump using a solid-side resistance model," *Appl Therm Eng*, vol. 26, no. 17–18, pp. 2219–2227, Dec. 2006, doi: 10.1016/j.applthermaleng.2006.03.013.

[151] B. Shi, R. K. Al-Dadah, S. Mahmoud, A. Elsayed, and A. Rezk, "Mathematical and CFD modelling for a rectangular finned tube adsorption bed for automotive cooling system," International Conference on Applied Energy ICAE 2013, Pretoria, South Africa Paper ID: ICAE2013-685.

[152] Rezk A. M., "Theoretical and experimental investigation of silica gel / water adsorption refrigeration systems," Doctoral dissertation, University of Birmingham, 2012.

[153] D. Budiman, A. Rachmat, and Nasruddin, "Peformance cycle analysis of optimum two-bed adsorption chiller," in *AIP Conference Proceedings*, American Institute of Physics Inc., Jan. 2019. doi: 10.1063/1.5086552.

[154] A. Rezk, R. K. Al-Dadah, S. Mahmoud, and A. Elsayed, "Effects of contact resistance and metal additives in finned-tube adsorbent beds on the performance of silica gel/water adsorption chiller," *Appl Therm Eng*, vol. 53, no. 2, pp. 278–284, May 2013, doi: 10.1016/j.applthermaleng.2012.04.008.

[155] S. Mitra, K. Thu, B. B. Saha, and P. Dutta, "Performance evaluation and determination of minimum desorption temperature of a two-stage air cooled silica gel/water adsorption system," *Appl Energy*, vol. 206, pp. 507–518, 2017, doi: 10.1016/j.apenergy.2017.08.198.

[156] Sadik Kakaç, Yaman Yener, and Anchasa Pramuanjaroenkij, *Convective Heat Transfer, Third Edition*, Third. Taylor & Francis Group, LLC, 2014.

[157] A. Bejan and A. D. Kraus, *Heat transfer handbook*. J. Wiley, 2003.

[158] N. V. Cao, X. Q. Duong, W. S. Lee, M. Y. Park, J. D. Chung, and H. Hong, "Effect of heat exchanger materials on the performance of adsorption chiller," *Journal of Mechanical Science and Technology*, vol. 34, no. 5, pp. 2217–2223, May 2020, doi: 10.1007/s12206-020-0443-6.

[159] K. C. A. Alam, B. B. Saha, Y. T. Kang, A. Akisawa, and T. Kashiwagi, "Heat exchanger design effect on the system performance of silica gel adsorption refrigeration systems," *International Journal of Heat and Mass Transfer,* vol 43, no. 24, p.p 4419-4431, 2000, doi.org/10.1016/S0017-9310(00)00072

[160] H. Jawdat Dakkama, "Experimental investigation of mof adsorption system for ice making, freeze water desalination and cooling applications," Doctoral dissertation, University of Birmingham, 2017..

[161] R. Raj and V. Baiju, "Thermodynamic analysis of a solar powered adsorption cooling and desalination system," in *Energy Procedia*, Elsevier Ltd, 2019, pp. 885–891. doi: 10.1016/j.egypro.2019.01.226.

[162] X. Wang and H. T. Chua, "Two bed silica gel-water adsorption chillers: An effectual lumped parameter model," *International Journal of Refrigeration*, vol. 30, no. 8, pp. 1417–1426, Dec. 2007, doi: 10.1016/j.ijrefrig.2007.03.010.

[163] I. I. El-Sharkawy, H. Abdelmeguid, and B. B. Saha, "Towards an optimal performance of adsorption chillers: Reallocation of adsorption/desorption cycle times," *Int J Heat Mass Transf*, vol. 63, pp. 171–182, 2013, doi: 10.1016/j.ijheatmasstransfer.2013.03.076.

[164] D. C. Wang, Z. Z. Xia, J. Y. Wu, R. Z. Wang, H. Zhai, and W. D. Dou, "Study of a novel silica gel-water adsorption chiller. Part I. Design and performance prediction," *International Journal of Refrigeration*, vol. 28, no. 7, pp. 1073–1083, Nov. 2005, doi: 10.1016/j.ijrefrig.2005.03.001.

[165] R. Nikbakhti, X. Wang, and A. Chan, "Performance analysis of an integrated adsorption and absorption refrigeration system," *International Journal of Refrigeration*, vol. 117, pp. 269–283, Sep. 2020, doi: 10.1016/j.ijrefrig.2020.04.019.

[166] K. M. Almohammadi and K. Harby, "Operational conditions optimization of a proposed solar-powered adsorption cooling system: Experimental, modeling, and optimization algorithm techniques," *Energy*, vol. 206, Sep. 2020, doi: 10.1016/j.energy.2020.118007.

[167] S. Bai, T. C. Ho, J. Ha, A. K. An, and C. Y. Tso, "Study of the salinity effects on the cooling and desalination performance of an adsorption cooling cum desalination system with a novel composite adsorbent," *Appl Therm Eng*, vol. 181, Nov. 2020, doi: 10.1016/j.applthermaleng.2020.115879.

[168] A. S. Uyun, A. Akisawa, T. Miyazaki, Y. Ueda, and T. Kashiwagi, "Numerical analysis of an advanced three-bed mass recovery adsorption refrigeration cycle," *Appl Therm Eng*, vol. 29, no. 14–15, pp. 2876–2884, Oct. 2009, doi: 10.1016/j.applthermaleng.2009.02.008.

[169] M. Muttakin, M. A. Islam, K. S. Malik, D. Pahwa, and B. B. Saha, "Study on optimized adsorption chiller employing various heat and mass recovery schemes," *International Journal of Refrigeration*, vol. 126, pp. 222–237, Jun. 2021, doi: 10.1016/j.ijrefrig.2020.12.032.

[170] A. Amirfakhraei, T. Zarei, and J. Khorshidi, "Advanced heat and mass recovery design in a two bed adsorption desalination system," *Appl Therm Eng*, vol. 198, Nov. 2021, doi: 10.1016/j.applthermaleng.2021.117494.

[171] N. Ghilen, S. Gabsi, R. Benelmir, and M. El Ganaoui, "Performance Simulation of Two-Bed Adsorption Refrigeration Chiller with Mass Recovery," *Journal of Fundamentals of Renewable Energy and Applications*, vol. 7, no. 03, p. 3, 2017, doi: 10.4172/2090-4541.1000229ï.

[172] J. P. Holman, *Heat Transfer*, Tenth Edit. New York: McGraw-Hill, 2010.

[173] R. P. Sah, B. Choudhury, and R. K. Das, "Study of a two-bed silica gel–water adsorption chiller: performance analysis," *International Journal of Sustainable Energy*, vol. 37, no. 1, pp. 30–46, Jan. 2018, doi: 10.1080/14786451.2016.1173696.

[174] A. Amirfakhraei, T. Zarei, and J. Khorshidi, "Performance improvement of adsorption desalination system by applying mass and heat recovery processes," *Thermal Science and Engineering Progress*, vol. 18, Aug. 2020, doi: 10.1016/j.tsep.2020.100516.

[175] M. Z. I. Khan, B. B. Saha, K. C. A. Alam, A. Akisawa, and T. Kashiwagi, "Study on solar/waste heat driven multi-bed adsorption chiller with mass recovery," *Renew Energy*, vol. 32, no. 3, pp. 365–381, Mar. 2007, doi: 10.1016/j.renene.2006.02.003.

[176] A. Akahira, K. C. A. Alam, Y. Hamamoto, A. Akisawa, and T. Kashiwagi, "Experimental investigation of mass recovery adsorption refrigeration cycle," *International Journal of Refrigeration*, vol. 28, no. 4, pp. 565–572, Jun. 2005, doi: 10.1016/j.ijrefrig.2004.10.001.

[177] Y. Liu and K. C. Leong, "Numerical study of a novel cascading adsorption cycle," *International Journal of Refrigeration*, vol. 29, no. 2, pp. 250–259, Mar. 2006, doi: 10.1016/j.ijrefrig.2005.05.008.

[178] A. el Fadar, A. Mimet, and M. Pérez-García, "Modelling and performance study of a continuous adsorption refrigeration system driven by parabolic trough solar collector," *Solar Energy*, vol. 83, no. 6, pp. 850–861, Jun. 2009, doi: 10.1016/j.solener.2008.12.003.

[179] R. H. Mohammed, O. Mesalhy, M. L. Elsayed, and L. C. Chow, "Performance enhancement of adsorption beds with silica-gel particles packed in aluminum foams," *International Journal of Refrigeration*, vol. 104, pp. 201–212, Aug. 2019, doi: 10.1016/j.ijrefrig.2019.03.013.

[180] L. Zhi Zhang and L. Wang, "Effects of coupled heat and mass transfers in adsorbent on the performance of a waste heat adsorption cooling unit," Applied Thermal Engineering, vol. 19, no. 2, p.p 195-215, 1999, doi.org/10.1016/S1359-4311(98)00023-4

[181] B. S. P Neuman, "Theoretical Derivation of Darcy's Law," Acta mechanica, vol. 25, p.p 153-170, 1977, doi.org/10.1007/BF01376989

[182] S. Whitaker, "Flow in Porous Media I: A Theoretical Derivation of Darcy's Law," Transport in porous media, vol. 1, pp.3-25, 1986, doi.org/10.1007/BF01036523.

[183] W. A. Hall, "An Analytical Derivation of the Darcy Equation," Eos, Transactions American Geophysical Union, vol. 37, no. 2, pp. 185-188, 1956. https://doi.org/10.1029/TR037i002p00185

[184] W. Yaïci and E. Entchev, "Coupled unsteady computational fluid dynamics with heat and mass transfer analysis of a solar/heat-powered adsorption cooling system for use in buildings," *Int J Heat Mass Transf*, vol. 144, pp. 1–17, 2019, doi: 10.1016/j.ijheatmasstransfer.2019.118648.

[185] I. Solmuş, D. Andrew, C. Yamali, and D. Baker, "A two-energy equation model for dynamic heat and mass transfer in an adsorbent bed using silica gel/water pair," *Int J Heat Mass Transf*, vol. 55, no. 19–20, pp. 5275–5288, Sep. 2012, doi: 10.1016/j.ijheatmasstransfer.2012.05.036.

[186] R. H. Mohammed, O. Mesalhy, M. L. Elsayed, S. Hou, M. Su, and L. C. Chow, "Physical properties and adsorption kinetics of silica-gel/water for adsorption chillers," *Appl Therm Eng*, vol. 137, pp. 368–376, 2018, doi: 10.1016/j.applthermaleng.2018.03.088.

[187] M. A. Islam, A. Pal, and B. B. Saha, "Experimental study on thermophysical and porous properties of silica gels," *International Journal of Refrigeration*, vol. 110, pp. 277–285, 2020, doi: 10.1016/j.ijrefrig.2019.10.027.

[188] H. Chen, J. Ding, W. Wang, X. Wei, and J. Lu, "Water adsorption characteristics of MCM-41 post-modified by Al grafting and cations doping: equilibrium and kinetics study," *Adsorption*, vol. 23, no. 1, pp. 113–120, Jan. 2017, doi: 10.1007/s10450-016-9829-2.

[189] X. S. Zhao and G. Q. Lu, "Modification of MCM-41 by Surface Silylation with Trimethylchlorosilane and Adsorption Study," *The Journal of Physical Chemistry B*, vol. 102, no. 9, pp. 1556-1561, 1998, doi.org/10.1021/jp972788m.

[190] S. C. Chang, S. Y. Chien, C. L. Chen, and C. K. Chen, "Analyzing adsorption characteristics of CO 2 , N 2 and H 2 O in MCM-41 silica by molecular simulation," *Appl Surf Sci*, vol. 331, pp. 225–233, Mar. 2015, doi: 10.1016/j.apsusc.2015.01.084.

[191] H. W. Coleman, W. Glenn. Steele, and H. W. Coleman, *Experimentation, validation, and uncertainty analysis for engineers*. John Wiley & Sons, 2009.

[192] A. R. M. Rezk and R. K. Al-Dadah, "Physical and operating conditions effects on silica gel/water adsorption chiller performance," *Appl Energy*, vol. 89, no. 1, pp. 142–149, 2012, doi: 10.1016/j.apenergy.2010.11.021.

[193] W. S. Chang, C. C. Wang, and C. C. Shieh, "Experimental study of a solid adsorption cooling system using flat-tube heat exchangers as adsorption bed," *Appl Therm Eng*, vol. 27, no. 13, pp. 2195–2199, Sep. 2007, doi: 10.1016/j.applthermaleng.2005.07.022.

[194] B. B. Saha, E. C. Boelman, and T. Kashiwagij, "Computational analysis of an advanced adsorption-refrigeration cycle," *Energy*, vol. 20, no. 10, pp. 983-994, 1995, doi.org/10.1016/0360-5442(95)00047-K.

[195] R. H. Mohammed, O. Mesalhy, M. L. Elsayed, and L. C. Chow, "Scaling analysis of heat and mass transfer processes in an adsorption packed bed," *International Journal of Thermal Sciences*, vol. 133, no. May, pp. 82–89, 2018, doi: 10.1016/j.ijthermalsci.2018.07.017.

Appendices

Appendix A: Thermal resistances analysis using Engineering Equation solver (EES) software.

Thermal design of ABU in adsorption process

```
"Inner heat transfer coefficient"
function a(x,d_i,e)
if (x<2400) then
    t=46/x
else
    t=1/sqrt(-1.8*ln((6.9/x)+(((e/d_i)/3.6)^1.11)))
endif
a=t
end;
function r(x,f,pr)
if (x<2300) then
delta=3.66
else
delta=((f/8)*(x-1000)*pr)/(1+(12.7*((f/8)^0.5)*(pr^(2/3)-1)))
endif
r=delta
end;
f=a((4*m/(pi*d_i*mu_w)),d_i,e)
Nus=r((4*m/(pi*d_i*mu_w)),f,pr)
Nus=(h_i*1000*d_i)/k_w
T_av=30 [C]
d_i=0.00482 [m]
d_o=0.00635 [m]
e=0.0015*10^(-3) [m]
m=0.5 [kg/s]
l_t=0.264 [m]
Av=0.5 [-]
Ac=0.4 [-]
d_f=0.1 [m]
D_ads=0.000348 [m]
t_ads=0.002 [m]
k_ads=0.2 [W/mK]
A_i=pi*d_i*L_t  {m^2}
A_o=pi*d_o*L_t  {m^2}
mu_w=Viscosity(Water,T=T_av,x=0)
cp_w=Cp(Water,T=T_av,x=0)
k_w=Conductivity(Water,T=T_av,x=0)
pr=(mu_w*cp_w*1000)/k_w
k_t=Conductivity(Copper, T=T_av)
k_f=k_t
R_conv=1/(h_i*A_i)
R_cond=ln(d_o/d_i)/(2*pi*k_t*l_t)
R_contact=1/((1/l_t)*(Ac*(2*k_t*k_ads)/(k_t+K_ads))+(Av*k_f))
```

```
R_cont1=R_contact/A_fin
A_fin=12*(pi/4)*(d_f^2)
R_cont2=R_contact/(pi*d_o*t_ads)
R_rad=t_ads/(A_fin*k_ads)
R_axi=ln(d_f/d_ads)/(2*pi*k_ads*d_f)
R1=R_cont1+R_rad
R2=R_cont2+R_axi
R3=(R1+R2)/(R1*R2)
R_t=R_conv+R_cond+R3
U=1000/R_t
```

Table (A-1) thermal resistance results of ABU in adsorption process

Parameter	Definition	Value	Unit
h_i	Average heat transfer coefficient for inlet water	603.6	W/m^2K
R_{conv}	Convective thermal resistance at tube internal surface	0.4144	K/W
R_{cond}	Conduction thermal resistance of the tube wall	0.0004196	K/W
$R_{contact}$	Contact thermal resistance	0.005034	m^2K/W
R_{cont1}	Contact thermal resistance between outer tube and adsorbent	0.641	K/W
R_{cont2}	Contact thermal resistance between fin and adsorbent	126.2	K/W
R_{rad}	Radial thermal resistance between solid adsorbent	1.273	K/W
R_{axi}	Axial thermal resistance between solid adsorbent	45.05	K/W
$U_{ABU,ads}$	Overall heat transfer coefficient for ABU in adsorption process	1060	W/m^2K

Thermal design of ABU in desorption process

```
"Inner heat transfer coefficient"
function a(x,d_i,e)
if (x<2400) then
    t=46/x
else
    t=1/sqrt(-1.8*ln((6.9/x)+(((e/d_i)/3.6)^1.11)))
endif
a=t
end;
function r(x,f,pr)
if (x<2300) then
delta=3.66
else
delta=((f/8)*(x-1000)*pr)/(1+(12.7*((f/8)^0.5)*(pr^(2/3)-1)))
endif
r=delta
end;
f=a((4*m/(pi*d_i*mu_w)),d_i,e)
Nus=r((4*m/(pi*d_i*mu_w)),f,pr)
Nus=(h_i*1000*d_i)/k_w
```

T_av=90 [C]
d_i=0.00482 [m]
d_o=0.00635 [m]
e=0.0015*10^(-3) [m]
m=0.5 [kg/s]
l_t=0.264 [m]
Av=0.5 [-]
Ac=0.4 [-]
d_f=0.1 [m]
D_ads=0.000348 [m]
t_ads=0.002 [m]
k_ads=0.2 [W/mK]
A_i=pi*d_i*L_t {m^2}
A_o=pi*d_o*L_t {m^2}
mu_w=Viscosity(Water,T=T_av,x=0)
cp_w=Cp(Water,T=T_av,x=0)
k_w=Conductivity(Water,T=T_av,x=0)
pr=(mu_w*cp_w*1000)/k_w
k_t=Conductivity(Copper, T=T_av)
k_f=k_t
R_conv=1/(h_i*A_i)
R_cond=ln(d_o/d_i)/(2*pi*k_t*l_t)
R_contact=1/((1/l_t)*(Ac*(2*k_t*k_ads)/(k_t+K_ads))+(Av*k_f))
R_cont1=R_contact/A_fin
A_fin=12*(pi/4)*(d_f^2)
R_cont2=R_contact/(pi*d_o*t_ads)
R_rad=t_ads/(A_fin*k_ads)
R_axi=ln(d_f/d_ads)/(2*pi*k_ads*d_f)
R1=R_cont1+R_rad
R2=R_cont2+R_axi
R3=(R1+R2)/(R1*R2)
R_t=R_conv+R_cond+R3
U=1000/R_t

Table (A-2) thermal resistance results of ABU in desorption process

Parameter	Definition	Value	Unit
h_i	Average heat transfer coefficient for inlet water	1487	W/m^2K
R_{conv}	Convective thermal resistance at tube internal surface	0.1682	K/W
R_{cond}	Conduction thermal resistance of the tube wall	0.0004228	K/W
$R_{contact}$	Contact thermal resistance	0.005072	m^2K/W
R_{cont1}	Contact thermal resistance between outer tube and adsorbent	0.6458	K/W
R_{cont2}	Contact thermal resistance between fin and adsorbent	127.1	K/W
R_{rad}	Radial thermal resistance between solid adsorbent	1.273	K/W
R_{axi}	Axial thermal resistance between solid adsorbent	45.05	K/W
$U_{ABU,des}$	Overall heat transfer coefficient for ABU in desorption process	1438	W/m^2K

Thermal design of ECU in evaporation process

```
"Inner heat transfer coefficient"
function a(x,d_i,e)
if (x<2400) then
    t=46/x
else
    t=1/sqrt(-1.8*ln((6.9/x)+(((e/d_i)/3.6)^1.11)))
endif
a=t
end;
function r(x,f,pr)
if (x<2300) then
delta=3.66
else
delta=((f/8)*(x-1000)*pr)/(1+(12.7*((f/8)^0.5)*(pr^(2/3)-1)))
endif
r=delta
end;
f=a((4*m/(pi*0.004*mu_w)),0.004,e)
Nus=r((4*m/(pi*0.004*mu_w)),f,pr)
Nus=(h_i*1000*0.004)/k_w
T_av=15 [C]
d_i=0.0132 [m]
d_o=0.0158 [m]
e=0.0015*10^(-3) [m]
m=0.5 [kg/s]
l_t=2[m]
pr=(mu_w*cp_w*1000)/k_w
mu_w=Viscosity(Water,T=T_av,x=0)
cp_w=Cp(Water,T=T_av,x=0)
k_w=Conductivity(Water,T=T_av,x=0)
k_t=Conductivity(Copper, T=T_av)
hfg=Enthalpy_vaporization(Water,T=T_av)
rho_liq=Density(Water,T=T_av,x=0)
rho_vap=Density(Water,T=T_av,x=1)
sigma=SurfaceTension(Water,T=T_av)
R_conv_i=A_o/(h_i*A_i)
A_i=pi*d_i*l_t
R_cond=A_o*ln(d_o/d_i)/(2*pi*k_t*l_t)

"Outer heat transfer coefficient"
h_o=((mu_w*hfg)/DT)*(((9.81*rho_liq-rho_vap)/sigma)^0.5)*(Ja/(cf*pr))^3
cf=0.015
Ja=(cp_w*DT)/hfg
DT=5
R_conv_o=A_o/(h_o*A_o)
```

A_o=pi*d_o*l_t
U=1000/(R_conv_i+R_conv_o+R_cond)

Table (A-3) thermal resistance results of ECU in evaporation process

Parameter	Definition	Value	Unit
h_i	Average heat transfer coefficient for inlet water	2167	W/m^2K
$R_{conv,i}$	Convective thermal resistance at tube internal surface	0.0005523	K/W
h_o	Average heat transfer coefficient for outlet refrigerant	1.64	W/m^2K
$R_{conv,o}$	Convective thermal resistance at tube outer surface	0.6098	K/W
R_{cond}	Conduction thermal resistance of the tube wall	$3.61 *10^{-6}$	K/W
$U_{ECU, evap}$	Overall heat transfer coefficient for ABU in desorption process	1638	W/m^2K
A_{ECU}	Heat exchanger area	0.09927	m^2

Thermal design of ECU in condensation process

"Inner heat transfer coefficient"
function a(x,d_i,e)
if (x<2400) then
    t=46/x
else
    t=1/sqrt(-1.8*ln((6.9/x)+(((e/d_i)/3.6)^1.11)))
endif
a=t
end;
function r(x,f,pr)
if (x<2300) then
delta=3.66
else
delta=((f/8)*(x-1000)*pr)/(1+(12.7*((f/8)^0.5)*(pr^(2/3)-1)))
endif
r=delta
end;
f=a((4*m/(pi*0.004*mu_w)),0.004,e)
Nus=r((4*m/(pi*0.004*mu_w)),f,pr)
Nus=(h_i*1000*0.004)/k_w
mu_w=Viscosity(Water,T=T_av,x=0)
cp_w=Cp(Water,T=T_av,x=0)
k_w=Conductivity(Water,T=T_av,x=0)
k_t=Conductivity(Copper, T=T_av)
hfg=Enthalpy_vaporization(Water,T=T_av)
rho_liq=Density(Water,T=T_av,x=0)
rho_vap=Density(Water,T=T_av,x=1)
cp_vap=Cp(Water,T=T_av,x=1)
hfg_c=hfg+(0.8*cp_vap*(T_sat-T_m))
pr=(mu_w*cp_w*1000)/k_w
T_av=35 [C]

d_i=0.0134 [m]
d_o=0.0158 [m]
e=0.0015*10^(-3) [-]
m=0.5 [kg/s]
l_t=2 [m]
N_t=5 [-]
T_m=T_av
T_sat=T_sat(Water,P=p)
p=5 [pa]
R_conv_i=1/(h_i*A_i)
A_i=pi*d_i*l_t
R_cond=ln(d_o/d_i)/(2*pi*k_t*l_t)
"outer heat transfer coefficient"
h_o=0.729*((9.81*rho_liq*(rho_liq-rho_vap)*k_w^3*hfg_c)/(N_t*mu_w*(T_m-T_sat)*d_o))^(0.25)
R_conv_o=1/(h_o*A_o)
A_o=pi*d_o*l_t
U=1000/(R_conv_i+R_conv_o+R_cond)

Table (A-4) thermal resistance results of ECU in condensation process

Parameter	Definition	Value	Unit
h_i	Average heat transfer coefficient for inlet water	963	W/m^2K
$R_{conv,i}$	Convective thermal resistance at tube internal surface	0.01233	K/W
h_o	Average heat transfer coefficient for outlet refrigerant	1880	W/m^2K
$R_{conv,o}$	Convective thermal resistance at tube outer surface	0.005358	K/W
R_{cond}	Conduction thermal resistance of the tube wall	$3.31 *10^{-6}$	K/W
$U_{ECU, evap}$	Overall heat transfer coefficient for ABU in desorption process	5642	W/m^2K
A_{ECU}	Heat exchanger area	0.09927	m^2

Appendix B : Preliminary Design for Heat Exchange using EES software

```
"Design of ABU"
N_f=12
d_f=0.1 [m]
t_f=0.002[m]
S=0.02 [m]
do_t=0.0063 [m]
di_t=0.00482 [m]
N_t=4
t_ads=0.002 [m]
h_ads=2760 [kJ/kg]
rho_cu=Density(copper, T=25)
rho_sg=761 [kg/m^3]
rho_FAM02=650 [kg/m^3]
rho_Z13X=730 [kg/m^3]
rho_MOF801=1400 [kg/m^3]
c_cu=Cp(Copper, T=25)
c_sg=0.924 [KJ/kgK]
c_FAM02=0.822 [KJ/kgK]
c_MOF801=0.76 [KJ/kgK]
c_Z13X=0.836 [KJ/kgK]
A_fin=(pi/4)*(d_f^2)
V_fin=A_fin*t_f
L_HX=N_f*(S+t_f)
A_ABU=N_f*(((2*A_fin)-
(N_t*(pi/4)*do_t^2))+(pi*d_f*t_f)+(N_t*p
i*do_t*s))
M_fin=N_f*V_fin*rho_cu
M_t=N_t*pi*(((do_t^2)-
(di_t)^2)/4)*L_HX*rho_cu
M_ABU=M_fin+M_t
M_sg=(N_f-1)*A_fin*t_ads*rho_sg
M_FAM02=(N_f-
1)*A_fin*t_ads*rho_FAM02
M_Z13X=(N_f-
1)*A_fin*t_ads*rho_Z13X
M_MOF801=(N_f-
1)*A_fin*t_ads*rho_MOF801
HCR_sg=(M_sg*c_sg)/(M_ABU*c_cu)
HCR_FAM02=(M_FAM02*c_FAM02)/(M_AB
U*c_cu)
HCR_MOF801=(M_MOF801*c_MOF801)/(M_
ABU*c_cu)
HCR_Z13X=(M_Z13X*c_Z13X)/(M_ABU*c_c
u)
t_1=30
t_c=35
t_e=5
t_3=85
"heat of adsorbent"
Q_adsorbent=m_sg*c_sg*(t_3-t_1)  "kJ"
"heat of ABU"
Q_HX=m_ABU*c_cu*(t_3-t_1) "kJ"
"heat of adsorption"
Q_adsorption= m_sg*0.05*h_ads
"heat of refrigerante"
Q_ref=(m_sg*0.4*4.2*(50-
T_1))+(m_sg*0.5*(0.4)*4.2*(t_3-50))
"total heat"
Q_t=(Q_adsorbent+Q_HX+Q_adsorption+Q_ref
)
"condenser"
m_w_c=0.05*m_sg/1000
hfg_c=Enthalpy_vaporization(Water,T=T_c)
Q_cond=m_w_c*hfg_c
"evaporator"
hfg_e=Enthalpy_vaporization(Water,T=T_e)
Q_evap=m_w_c*hfg_e

"Mass and surface area of ECU heat exchanger"
d_o_ECU=0.01585 [m]
d_i_ECU=0.013411 [m]
L_ECU=2 [m]
M_ECU=pi*((d_o_ECU^2-
d_i_ECU^2)/4)*L_ECU*rho_cu
A_ECU=pi*d_o_ECU*L_ECU
```

Appendix C: Model built in Simulink for the two-bed adsorption thermophysical battery system

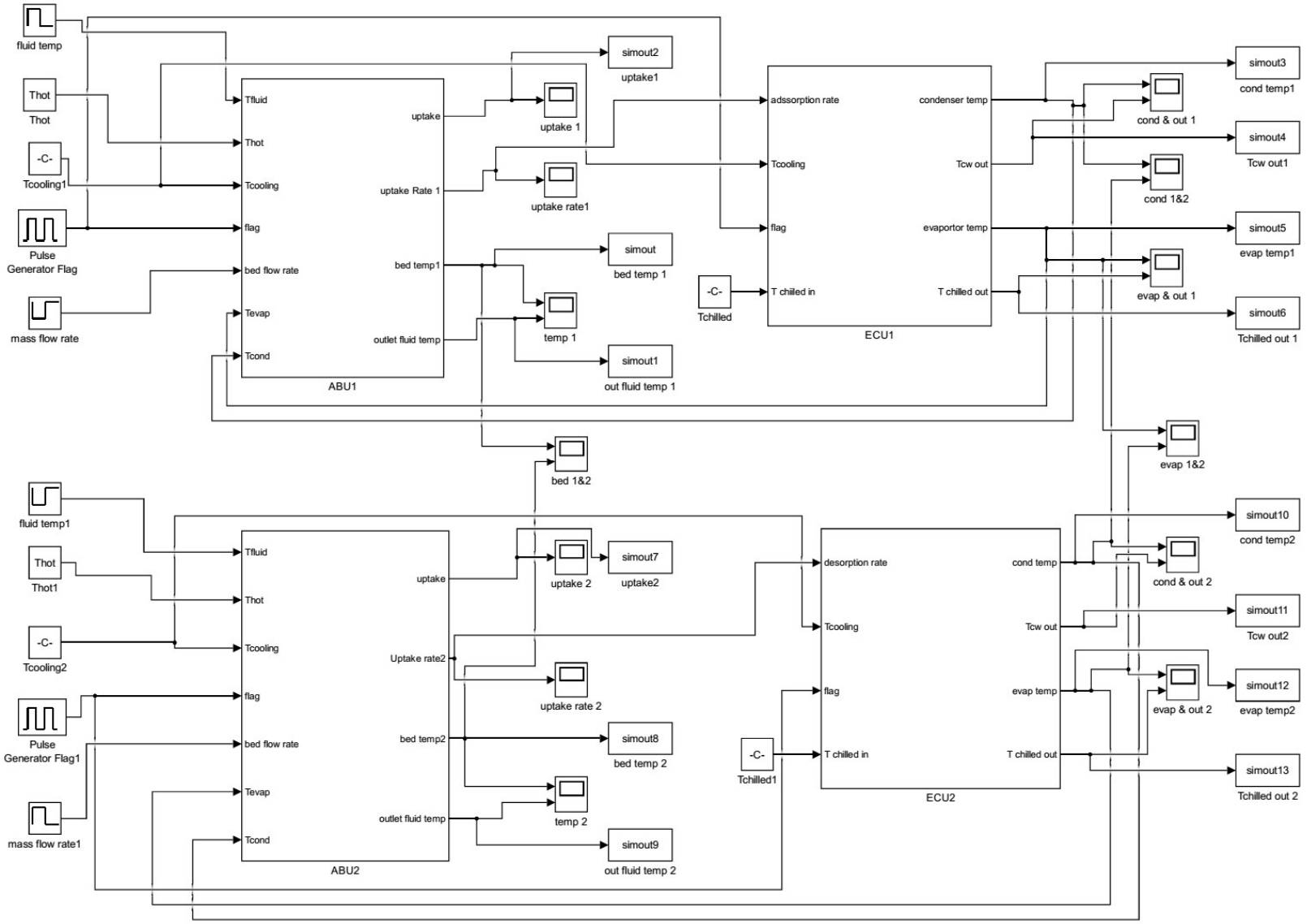

ABU

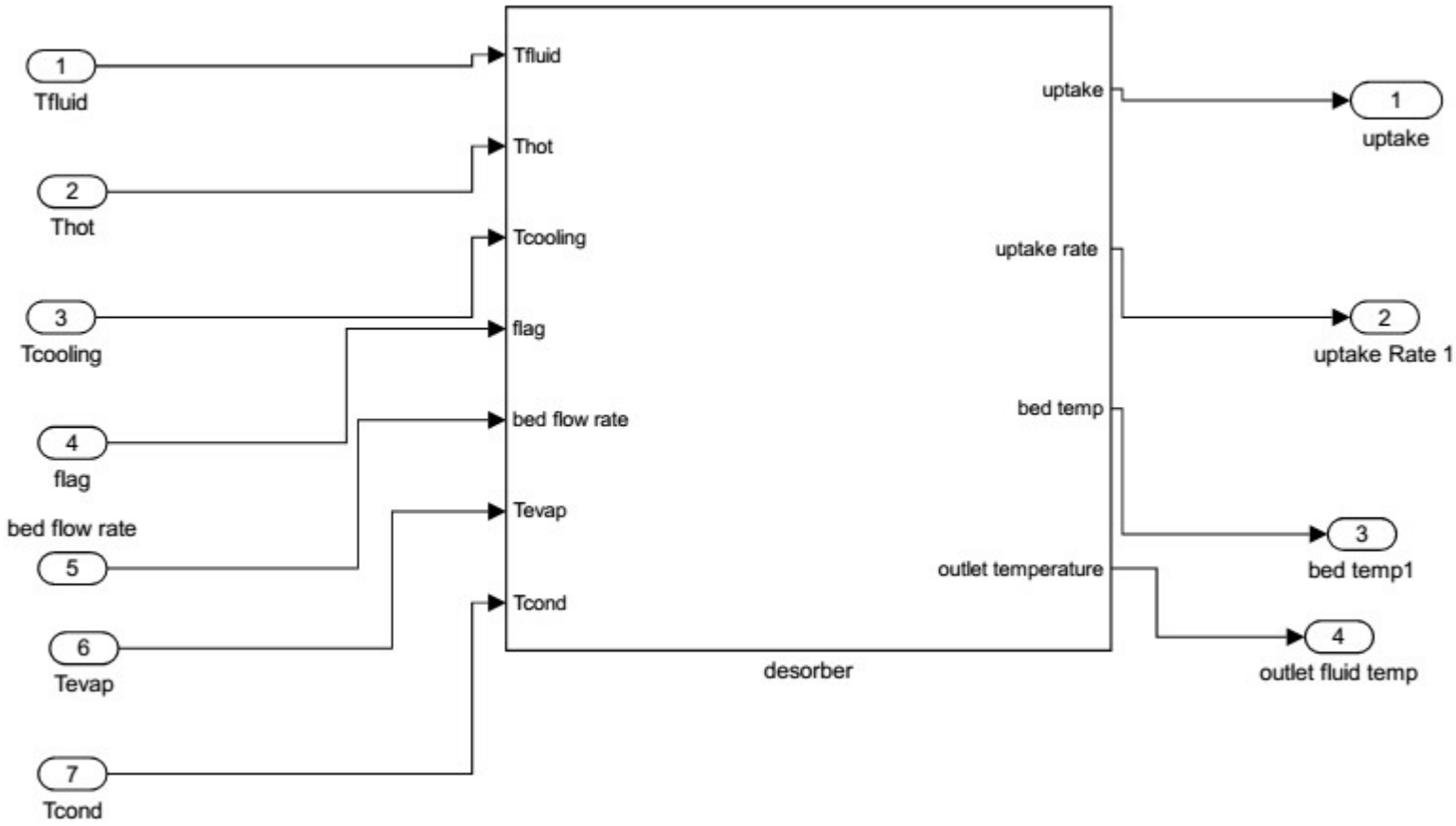
1
Tfluid
2
Thot
3
Tcooling
4
flag
bed flow rate
5
6
Tevap
7
Tcond
Tfluid
Thot
Tcooling
flag
bed flow rate
Tevap
Tcond
desorber
uptake
uptake rate
bed temp
outlet temperature
1
uptake
2
uptake Rate 1
3
bed temp1
4
outlet fluid temp

Desorber

```
function [UA_bed1, bed_capacity_term, adsorption_heat_term]
= bedterms(dxdt,uptake,flag,UA_bed)
Ma= 10;             % adsorbent mass
Cpa= 0.924;         %specific heat of adsorbent
Cpcu= 0.386;        % copper specific heat
Cw=4.186;           % specific heat of water
McuHex=1.811;        %  copper tube  mass
Q_ads=2760;     % heat of adsorption Kj/Kg
bed_capacity_term=(Ma*(Cpa+Cw*uptake)+Cpcu*McuHex);
adsorption_heat_term= flag*Q_ads*Ma*dxdt;
```

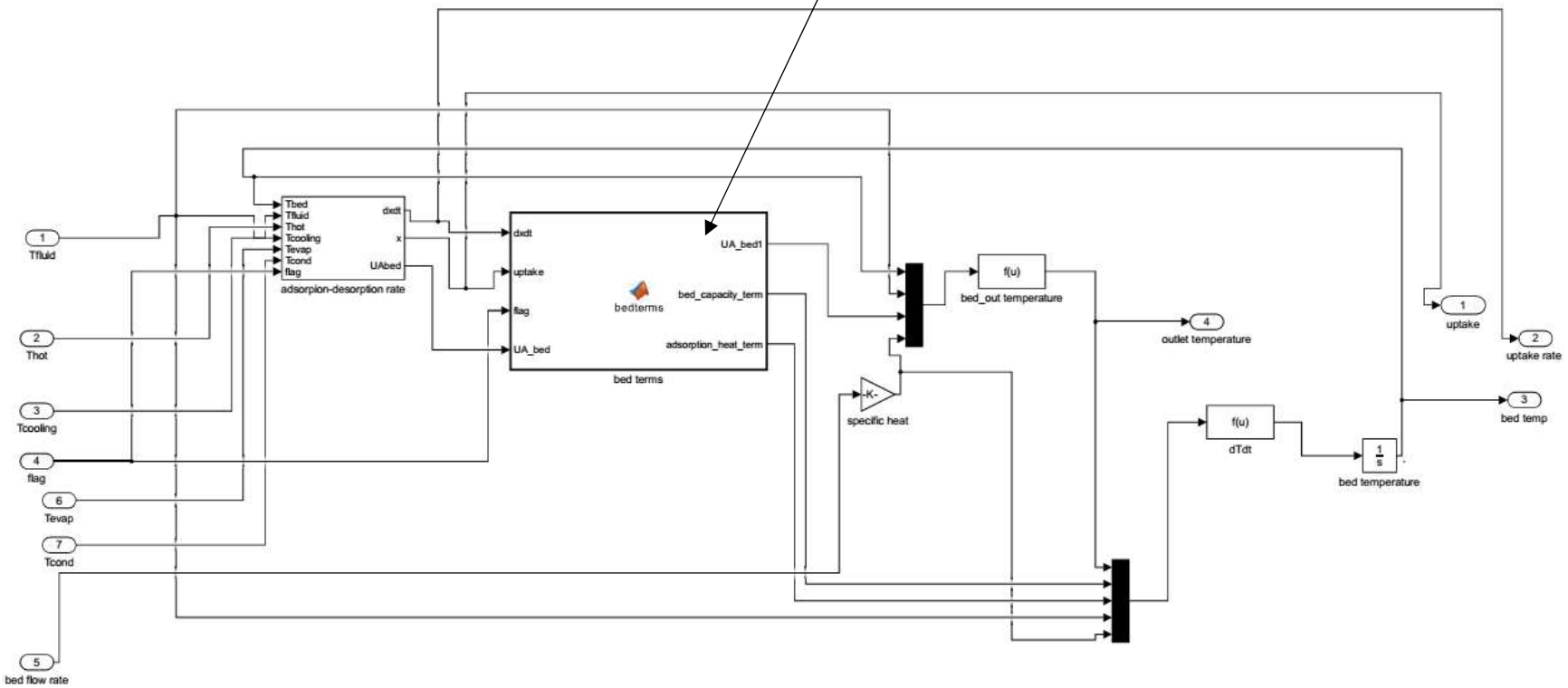

Adsorption – desorption rate

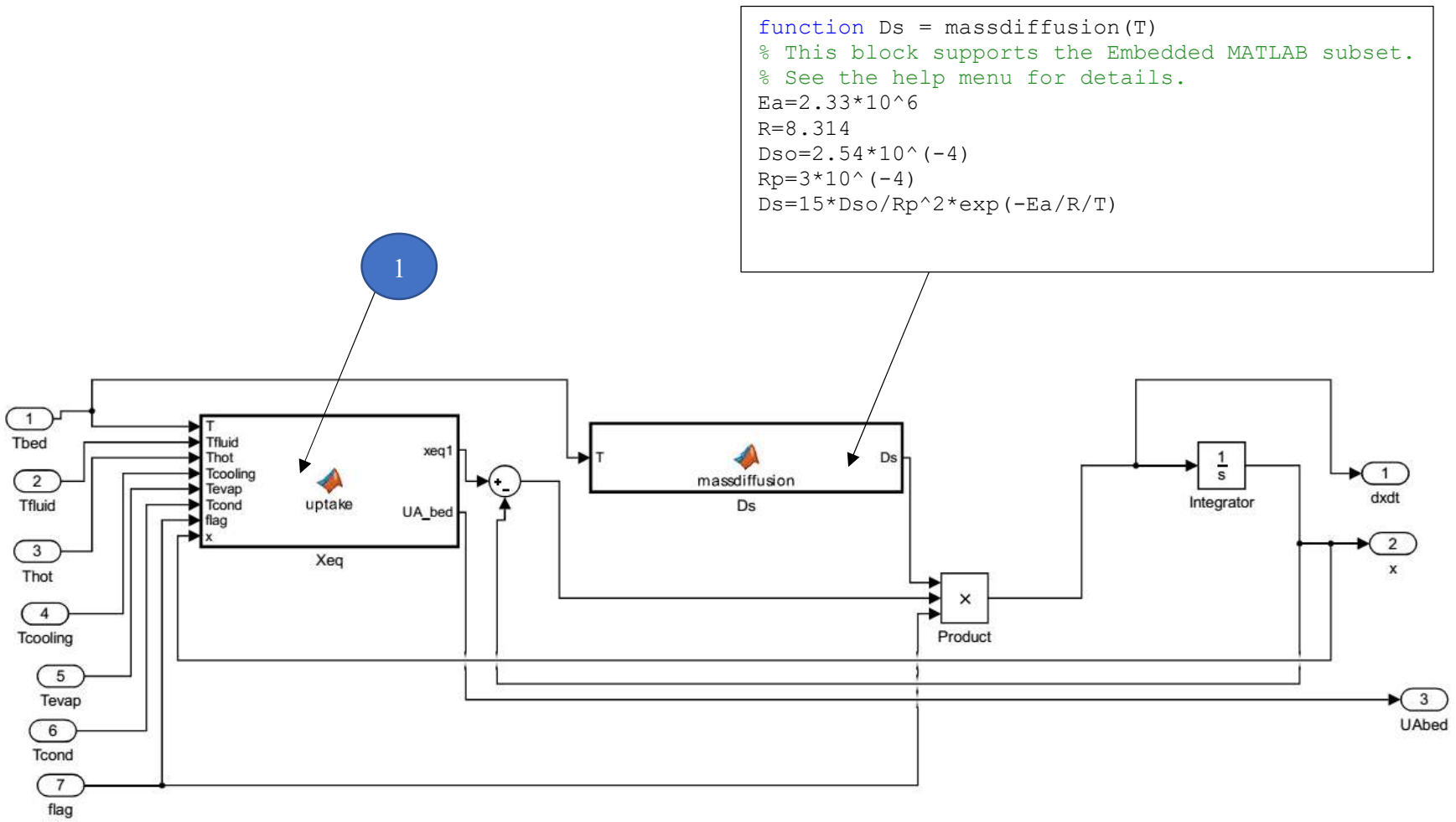

1

```
function [xeq1,UA_bed]=uptake(T,Tfluid,Thot,Tcooling,Tevap,Tcond,flag,x)
% This block supports the Embedded MATLAB subset.
% See the help menu for details.

if(Tfluid==Tcooling)
UA_bed=1060/1000  %kW/K
else
UA_bed= 1438/1000%kW/K
end

A0=-6.5314; A1=0.72452E-1; A2=-0.23951E-3; A3=0.25493E-6;
B0=-15.587; B1=0.15915; B2=-0.50612E-3; B3=0.53290E-6;
A=A0+(A1*(T))+(A2*(T)^2)+(A3*(T)^3);
B=B0+(B1*(T))+(B2*(T)^2)+(B3*(T)^3);
%preheating-precooling

%adsorption

if (Tfluid==Tcooling && flag==1)
P=2874.21 - 30.0056*Tevap + 0.0749237*Tevap*Tevap + 0.000196524*Tevap^3 - 0.00000114235*Tevap^4 + 1.37231E-
09*Tevap^5  % units are in KPa
Ps=2874.21 - 30.0056*T + 0.0749237*T^2 + 0.000196524*T^3 - 0.00000114235*T^4 + 1.37231E-09*T^5   % units
are in KPa
xeq1=A*(P/Ps)^B;

 %desorption

elseif(Tfluid==Thot && flag==1)
P=2874.21 - 30.0056*Tcond + 0.0749237*Tcond^2 + 0.000196524*Tcond^3 - 0.00000114235*Tcond^4 + 1.37231E-
09*Tcond^5   % units are in KPa  % units are in KPa
Ps=2874.21 - 30.0056*T + 0.0749237*T^2 + 0.000196524*T^3 - 0.00000114235*T^4 + 1.37231E-09*T^5   % units
are in KPa
xeq1=A*(P/Ps)^B;

else
    xeq1=x
end
```

From EES

ECU

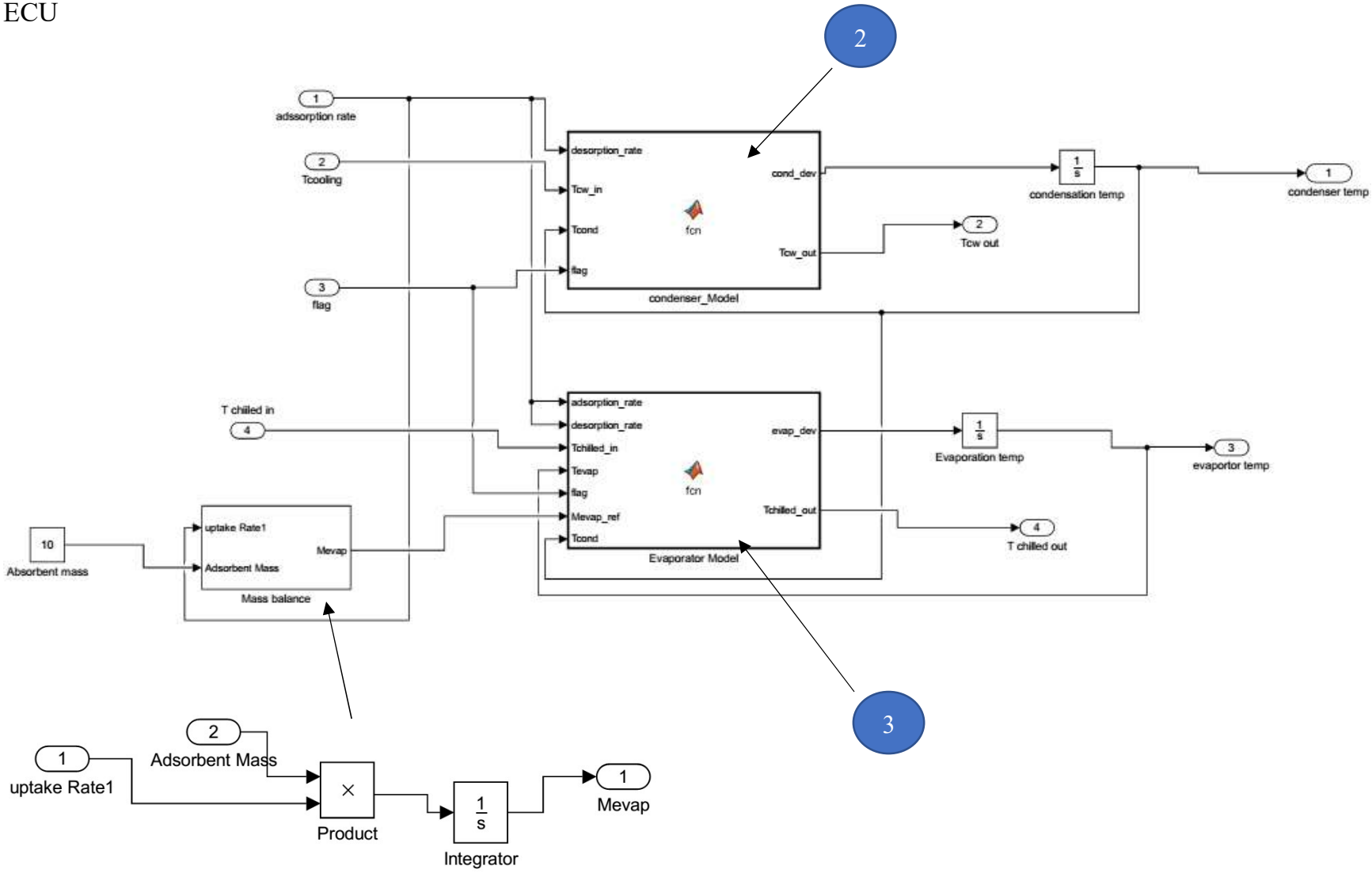
2
1
adssorption rate
2
Tcooling
3
flag
desorption_rate
Tcw_in
Tcond
flag
cond_dev
fcn
Tcw_out
condenser_Model
1/s
condensation temp
1
condenser temp
2
Tcw out
T chilled in
4
adsorption_rate
desorption_rate
Tchilled_in
Tevap
flag
Mevap_ref
Tcond
evap_dev
fcn
Tchilled_out
Evaporator Model
1/s
Evaporation temp
3
evaportor temp
4
T chilled out
10
Absorbent mass
uptake Rate1
Adsorbent Mass
Mevap
Mass balance
3
1
uptake Rate1
2
Adsorbent Mass
×
Product
1/s
Integrator
1
Mevap

2

```
function [cond_dev,Tcw_out] = fcn(desorption_rate,Tcw_in,Tcond, flag)

Mcond_ref= 1        % water charge in the condenser
Cp_w=4.18 % water sepcific heat
Cp_steam=1.8
Mcond=1.004      % copper tubes mass in the condenser
cpCu=0.386    % copper
hfg=2418   % kJ/kg
Ma= 10       % adsorbent mass _kg
UA_cond=5642/1000     % kJ/kg
m_dotcw=0.6   % kg/s
condenser_capacity=Mcond_ref*Cp_w+Mcond*cpCu
desorption1= -flag*hfg*Ma*desorption_rate-flag*Cp_steam*(Tcond)*Ma*desorption_rate
Tcw_out=Tcond+(Tcw_in-Tcond)*exp(-UA_cond/(m_dotcw*Cp_w))
waterloadterm=-m_dotcw*Cp_w*(Tcw_out-Tcw_in)
cond_dev=(desorption1+waterloadterm)/condenser_capacity
```

3

```
function  [evap_dev,Tchilled_out]  =  fcn(adsorption_rate,desorption_rate,Tchilled_in,Tevap,  flag,Mevap_ref,
Tcond)
Cp_w=4.18 % water sepcific heat
Mevap=1.004      % copper tubes mass in the evaporator
cpCu=0.386    % copper
hfg=2283   % kJ/kg
cp_steam=1.8
Ma= 10       % adsorbent mass _kg
UA_evap=1638/1000     % kJ/kg
m_dotchilled=0.1   % kg/s
evap_capacity=Mevap_ref*Cp_w+Mevap*cpCu
adsorptionterm=-flag*hfg*Ma*adsorption_rate-flag*cp_steam*Ma*Tevap*adsorption_rate
Tchilled_out=Tevap+(Tchilled_in-Tevap)*exp(-UA_evap/(m_dotchilled*Cp_w))
waterloadterm=-m_dotchilled*Cp_w*(Tchilled_out-Tchilled_in)
desorptionterm=-flag*Cp_w*(Tcond)*Ma*desorption_rate
evap_dev=(adsorptionterm+waterloadterm+desorptionterm)/evap_capacity
```

Appendix D: Calibrations and Uncertainty

Temperature Calibrations

To get accurate data, all thermocouples measured were calibrated versus mercury thermometers using conventional techniques before being put in the experimental setup. The thermocouples and mercury thermometers were placed in a container filled with water. The temperature of the water was gradually raised by using an electrical water heater. Figures (D.1) to (D.14) show the thermocouples and mercury thermometers that were measured and the uncertainties that were obtained. The uncertainties of the measurement variables have been determined as illustrated in Table (D-1).

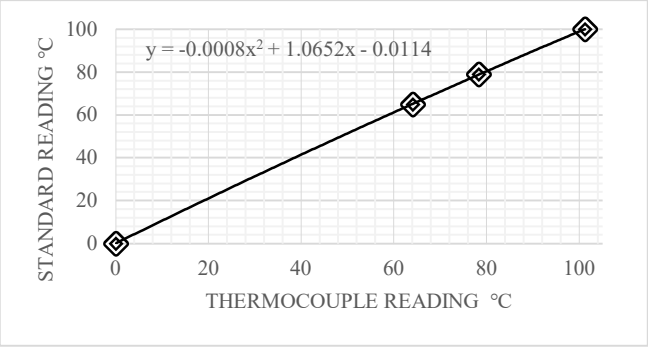

Figure (D.1) Temperature calibration (T1).

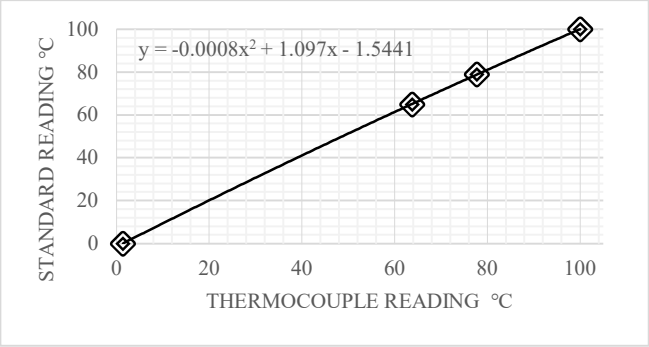

Figure (D.2) Temperature calibration (T2).

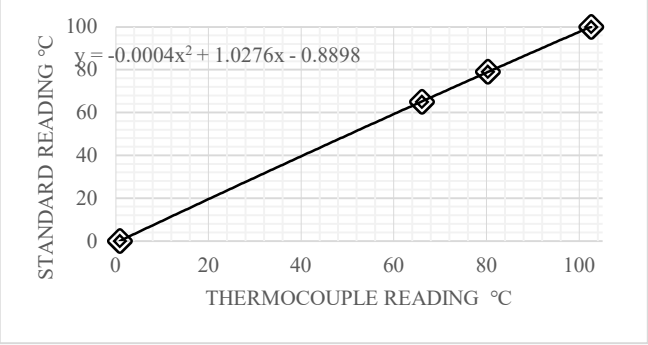

Figure (D.3) Temperature calibration (T3).

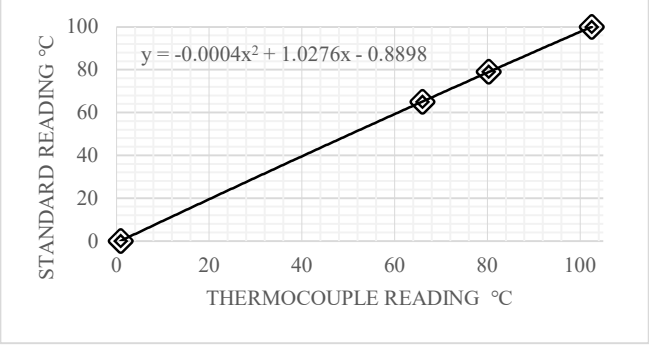

Figure (D.4) Temperature calibration (T4).

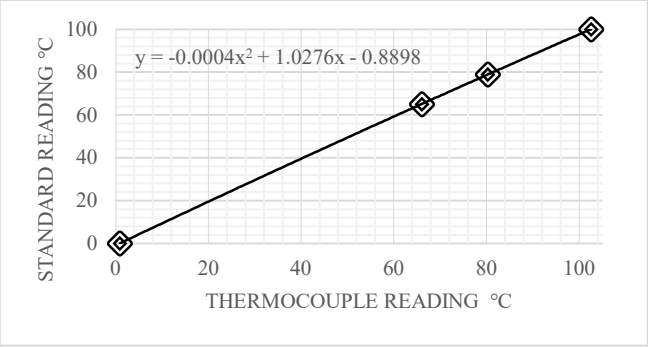

Figure (D.5) Temperature calibration (T5).

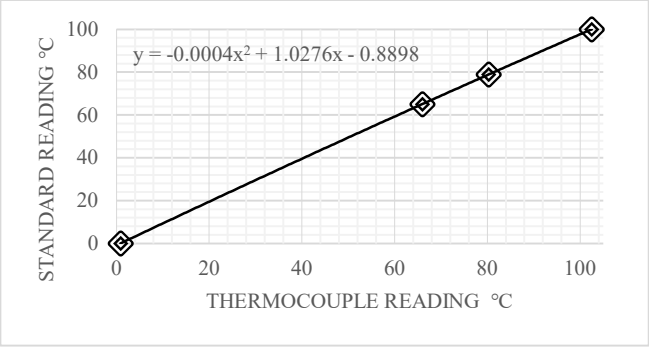

Figure (D.6) Temperature calibration (T6).

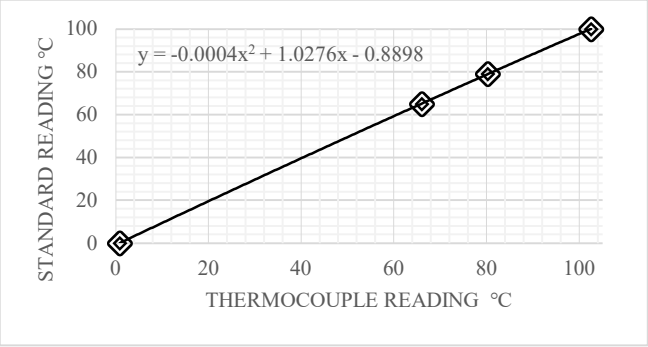

Figure (D.7) Temperature calibration (T7).

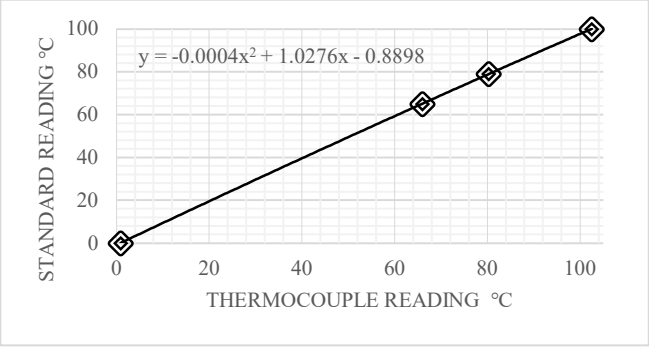

Figure (D.8) Temperature calibration (T8).

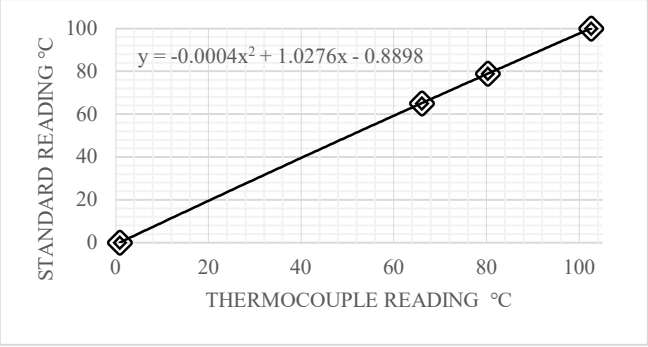

Figure (D.9) Temperature calibration (T9).

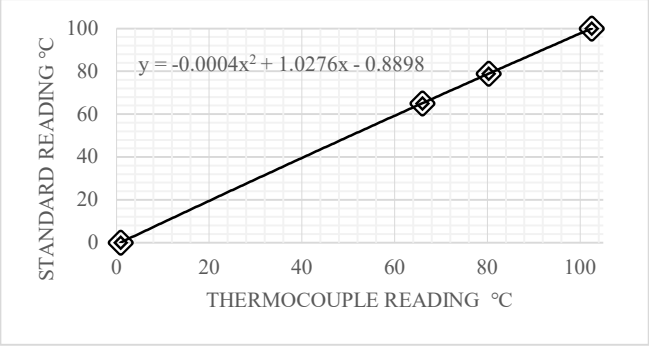

Figure (D.10) Temperature calibration (T10).

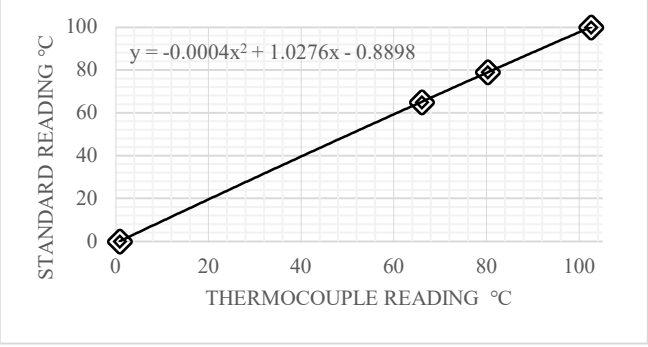

Figure (D.11) Temperature calibration (T11).

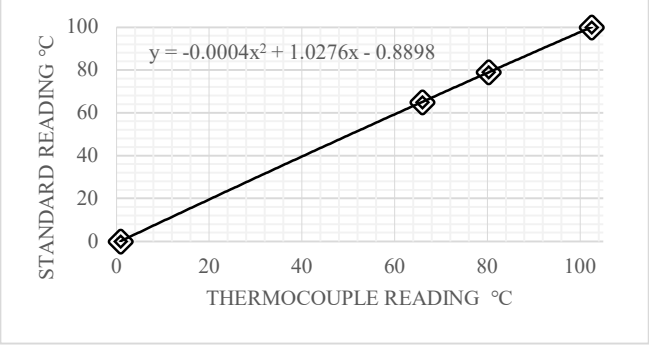

Figure (D.12) Temperature calibration (T12).

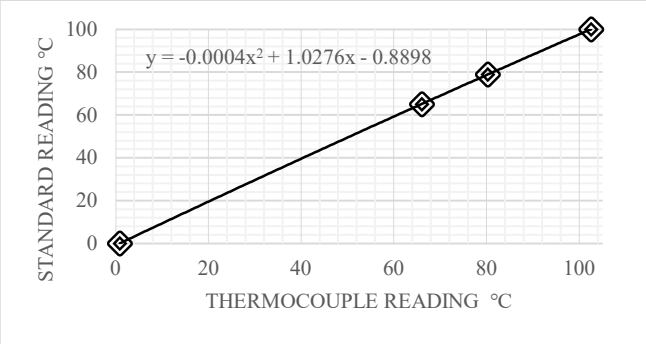

Figure (D.13) Temperature calibration (T13).

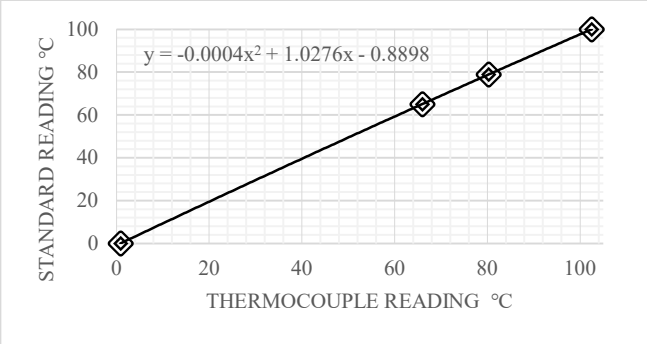

Figure (D.14) Temperature calibration (T14).

Table (D.1) Absolute accuracy of measurements

Variables	Accuracy
T_1= inside ABU_1	± 0.2563
T_2= inside ABU_2	± 0.3526
T_3=inlet water to ABU_1 heat exchanger.	± 0.1168
T_4=outlet water from ABU_1 heat exchanger.	± 0.1058
T_5=inlet water to ABU_2 heat exchanger.	± 0.3025
T_6=outlet water from ABU_2 heat exchanger.	± 0.2098
T_7= ECU_1 vapor temperature	± 0.1895
T_8= ECU_1 liquid temperature	± 0.3256
T_9= ECU_2 vapor temperature	± 0.2856
T_{10}= ECU_2 liquid temperature	± 0.2796
T_{11}=inlet water to ECU_1 heat exchanger.	± 0.3658
T_{12}=outlet water from ECU_1 heat exchanger.	± 0.3025
T_{13}=inlet water to ECU_2 heat exchanger.	± 0.1065
T_{14}=outlet water from ECU_2 heat exchanger.	± 0.1135

Uncertainty Propagation

The uncertainty of experimental measurements can be estimated by taking a sample and obtaining the confidence interval. During the design stages of the experiments, the uncertainty was estimated from the characteristics of the instrument and the data acquisition system resolution. The Root Sum Square (RSS) technique for uncertainty

propagation assumes that the measurements are normally distributed quantities that are uncorrelated and also that there are no systematic errors in the measurements. The uncertainty of measurement variables was analyzed using Engineering Equation Solver (EES) software.

Unit Settings: SI K kPa kJ mass deg

Variable±Uncertainty	Partial derivative	% of uncertainty
$COP = 0.2471 \pm 0.008764$		
$m_{chw} = 0.5 \pm 0.01$ [LPM]	$\partial COP / \partial m_{chw} = 0.4941$	31.79 %
$m_{cw} = 1 \pm 0.01$ [LPM]	$\partial COP / \partial m_{cw} = 6.776E-18$	0.00 %
$m_{hw} = 1 \pm 0.01$ [LPM]	$\partial COP / \partial m_{hw} = -0.1017$	1.35 %
$M_{sg} = 175 \pm 2$ [gram]	$\partial COP / \partial M_{sg} = 0$	0.00 %
$P_{ABU1} = 5.5 \pm 0.01$ [kPa]	$\partial COP / \partial P_{ABU1} = 0$	0.00 %
$P_{ABU2} = 1.5 \pm 0.01$ [kPa]	$\partial COP / \partial P_{ABU2} = 0$	0.00 %
$P_{ECU1} = 5.5 \pm 0.01$ [kPa]	$\partial COP / \partial P_{ECU1} = 0$	0.00 %
$P_{ECU2} = 1.5 \pm 0.01$ [kPa]	$\partial COP / \partial P_{ECU2} = 0$	0.00 %
$T_{ABU1} = 350 \pm 0.2536$ [K]	$\partial COP / \partial T_{ABU1} = 0$	0.00 %
$T_{ABU2} = 309 \pm 0.3526$ [K]	$\partial COP / \partial T_{ABU2} = 0$	0.00 %
$T_{chw,in} = 288 \pm 0.1065$ [K]	$\partial COP / \partial T_{chw,in} = 0.04118$	25.04 %
$T_{chw,out} = 282 \pm 0.1135$ [K]	$\partial COP / \partial T_{chw,out} = -0.04118$	28.44 %
$T_{cw,in} = 304 \pm 0.3025$ [K]	$\partial COP / \partial T_{cw,in} = -8.960E-20$	0.00 %
$T_{cw,out} = 311 \pm 0.2098$ [K]	$\partial COP / \partial T_{cw,out} = 0$	0.00 %
$T_{ECU1} = 305 \pm 0.3256$ [K]	$\partial COP / \partial T_{ECU1} = 0$	0.00 %
$T_{ECU2} = 290 \pm 0.2856$ [K]	$\partial COP / \partial T_{ECU2} = 0$	0.00 %
$T_{hw,in} = 353 \pm 0.1168$ [K]	$\partial COP / \partial T_{hw,in} = -0.02035$	7.35 %
$T_{hw,out} = 348 \pm 0.1058$ [K]	$\partial COP / \partial T_{hw,out} = 0.02035$	6.03 %
$Q_H = 850 \pm 11.57$		
$m_{chw} = 0.5 \pm 0.01$ [LPM]	$\partial Q_H / \partial m_{chw} = 0$	0.00 %
$m_{cw} = 1 \pm 0.01$ [LPM]	$\partial Q_H / \partial m_{cw} = 0$	0.00 %
$m_{hw} = 1 \pm 0.01$ [LPM]	$\partial Q_H / \partial m_{hw} = 350$	9.15 %
$M_{sg} = 175 \pm 2$ [gram]	$\partial Q_H / \partial M_{sg} = 0$	0.00 %
$P_{ABU1} = 5.5 \pm 0.01$ [kPa]	$\partial Q_H / \partial P_{ABU1} = 0$	0.00 %
$P_{ABU2} = 1.5 \pm 0.01$ [kPa]	$\partial Q_H / \partial P_{ABU2} = 0$	0.00 %

P_{ABU2} = 1.5±0.01 [kPa]	$\partial Q_H / \partial P_{ABU2}$ = 0	0.00 %
P_{ECU1} = 5.5±0.01 [kPa]	$\partial Q_H / \partial P_{ECU1}$ = 0	0.00 %
P_{ECU2} = 1.5±0.01 [kPa]	$\partial Q_H / \partial P_{ECU2}$ = 0	0.00 %
T_{ABU1} = 350±0.2536 [K]	$\partial Q_H / \partial T_{ABU1}$ = 0	0.00 %
T_{ABU2} = 309±0.3526 [K]	$\partial Q_H / \partial T_{ABU2}$ = 0	0.00 %
$T_{chw,in}$ = 288±0.1065 [K]	$\partial Q_H / \partial T_{chw,in}$ = 0	0.00 %
$T_{chw,out}$ = 282±0.1135 [K]	$\partial Q_H / \partial T_{chw,out}$ = 0	0.00 %
$T_{cw,in}$ = 304±0.3025 [K]	$\partial Q_H / \partial T_{cw,in}$ = 0	0.00 %
$T_{cw,out}$ = 311±0.2098 [K]	$\partial Q_H / \partial T_{cw,out}$ = 0	0.00 %
T_{ECU1} = 305±0.3256 [K]	$\partial Q_H / \partial T_{ECU1}$ = 0	0.00 %
T_{ECU2} = 290±0.2856 [K]	$\partial Q_H / \partial T_{ECU2}$ = 0	0.00 %
$T_{hw,in}$ = 353±0.1168 [K]	$\partial Q_H / \partial T_{hw,in}$ = 70	49.91 %
$T_{hw,out}$ = 348±0.1058 [K]	$\partial Q_H / \partial T_{hw,out}$ = -70	40.95 %

RE = 210±6.879

m_{chw} = 0.5±0.01 [LPM]	$\partial RE / \partial m_{chw}$ = 420	37.28 %
m_{cw} = 1±0.01 [LPM]	$\partial RE / \partial m_{cw}$ = 0	0.00 %
m_{hw} = 1±0.01 [LPM]	$\partial RE / \partial m_{hw}$ = 0	0.00 %
M_{sg} = 175±2 [gram]	$\partial RE / \partial M_{sg}$ = 0	0.00 %
P_{ABU1} = 5.5±0.01 [kPa]	$\partial RE / \partial P_{ABU1}$ = 0	0.00 %
P_{ABU2} = 1.5±0.01 [kPa]	$\partial RE / \partial P_{ABU2}$ = 0	0.00 %
P_{ECU1} = 5.5±0.01 [kPa]	$\partial RE / \partial P_{ECU1}$ = 0	0.00 %
P_{ECU2} = 1.5±0.01 [kPa]	$\partial RE / \partial P_{ECU2}$ = 0	0.00 %
T_{ABU1} = 350±0.2536 [K]	$\partial RE / \partial T_{ABU1}$ = 0	0.00 %
T_{ABU2} = 309±0.3526 [K]	$\partial RE / \partial T_{ABU2}$ = 0	0.00 %
$T_{chw,in}$ = 288±0.1065 [K]	$\partial RE / \partial T_{chw,in}$ = 35	29.37 %
$T_{chw,out}$ = 282±0.1135 [K]	$\partial RE / \partial T_{chw,out}$ = -35	33.35 %
$T_{cw,in}$ = 304±0.3025 [K]	$\partial RE / \partial T_{cw,in}$ = 0	0.00 %
$T_{cw,out}$ = 311±0.2098 [K]	$\partial RE / \partial T_{cw,out}$ = 0	0.00 %

$T_{cw,out}$ = 311±0.2098 [K]	$\partial RE/\partial T_{cw,out}$ = 0	0.00 %
T_{ECU1} = 305±0.3256 [K]	$\partial RE/\partial T_{ECU1}$ = 0	0.00 %
T_{ECU2} = 290±0.2856 [K]	$\partial RE/\partial T_{ECU2}$ = 0	0.00 %
$T_{hw,in}$ = 353±0.1168 [K]	$\partial RE/\partial T_{hw,in}$ = 0	0.00 %
$T_{hw,out}$ = 348±0.1058 [K]	$\partial RE/\partial T_{hw,out}$ = 0	0.00 %

SCP = 600±20.82

m_{chw} = 0.5±0.01 [LPM]	$\partial SCP/\partial m_{chw}$ = 1200	33.24 %
m_{cw} = 1±0.01 [LPM]	$\partial SCP/\partial m_{cw}$ = -1.110E-14	0.00 %
m_{hw} = 1±0.01 [LPM]	$\partial SCP/\partial m_{hw}$ = 0	0.00 %
M_{sg} = 175±2 [gram]	$\partial SCP/\partial M_{sg}$ = -3.429	10.85 %
P_{ABU1} = 5.5±0.01 [kPa]	$\partial SCP/\partial P_{ABU1}$ = 1.110E-14	0.00 %
P_{ABU2} = 1.5±0.01 [kPa]	$\partial SCP/\partial P_{ABU2}$ = 0	0.00 %
P_{ECU1} = 5.5±0.01 [kPa]	$\partial SCP/\partial P_{ECU1}$ = 0	0.00 %
P_{ECU2} = 1.5±0.01 [kPa]	$\partial SCP/\partial P_{ECU2}$ = 0	0.00 %
T_{ABU1} = 350±0.2536 [K]	$\partial SCP/\partial T_{ABU1}$ = 0	0.00 %
T_{ABU2} = 309±0.3526 [K]	$\partial SCP/\partial T_{ABU2}$ = 0	0.00 %
$T_{chw,in}$ = 288±0.1065 [K]	$\partial SCP/\partial T_{chw,in}$ = 100	26.18 %
$T_{chw,out}$ = 282±0.1135 [K]	$\partial SCP/\partial T_{chw,out}$ = -100	29.73 %
$T_{cw,in}$ = 304±0.3025 [K]	$\partial SCP/\partial T_{cw,in}$ = 0	0.00 %
$T_{cw,out}$ = 311±0.2098 [K]	$\partial SCP/\partial T_{cw,out}$ = 0	0.00 %
T_{ECU1} = 305±0.3256 [K]	$\partial SCP/\partial T_{ECU1}$ = 0	0.00 %
T_{ECU2} = 290±0.2856 [K]	$\partial SCP/\partial T_{ECU2}$ = 0	0.00 %
$T_{hw,in}$ = 353±0.1168 [K]	$\partial SCP/\partial T_{hw,in}$ = 0	0.00 %
$T_{hw,out}$ = 348±0.1058 [K]	$\partial SCP/\partial T_{hw,out}$ = 0	0.00 %

Flow-meter Calibrations

Table (D.2) Mass flow rate calibration for hot and cooled water flow rate

flow rate		Flow-meter 1 (hot water flow rate)				Flow-meter 2 (cooled water flow rate)			
Flow meter reading (LPM)	Flow meter reading $\dot{m}_F$ (kg/s)	Wight (kg)	time (s)	$_A\dot{m}$ (kg/s)	Error % $(\frac{\dot{m}_F-\dot{m}_A}{\dot{m}_F})$	Wight (kg)	time (s)	$_A\dot{m}$ (kg/s)	Error % $(\frac{\dot{m}_F-\dot{m}_A}{\dot{m}_F})$
0.5	0.0083333	1	125	0.008	4	1	126	0.007937	4.761905
1	0.0166667	1	64.52	0.015499	7.005579665	1	66	0.015152	9.090909
1.5	0.025	1	42	0.02381	4.761904762	1	44.2	0.022624	9.502262
2	0.0333333	1	33	0.030303	9.090909091	1	33.2	0.03012	9.638554
2.5	0.0416667	1	26	0.038462	7.692307692	1	25.1	0.039841	4.38247
3	0.05	1	21	0.047619	4.761904762	1	21.7	0.046083	7.834101
3.5	0.0583333	1	19	0.052632	9.77443609	1	18.5	0.054054	7.335907
4	0.0666667	1	16	0.0625	6.25	1	15.2	0.065789	1.315789

Table (D.3) Mass flow rate calibration chilled and condensing water flow rate

flow rate		Flow-meter 3 (chilled water flow rate)				Flow-meter 4 (condensing water flow rate)			
Flow meter reading (LPM)	Flow meter reading $\dot{m}_F$ (kg/s)	Wight (kg)	time (s)	$\dot{m}_A$ (kg/s)	Error % $(\frac{\dot{m}_F-\dot{m}_A}{\dot{m}_F})$	Wight (kg)	time (s)	$\dot{m}_A$ (kg/s)	Error % $(\frac{\dot{m}_F-\dot{m}_A}{\dot{m}_F})$
0.5	0.0083333	1	124.5	0.008032	3.614458	1	125.5	0.007968	4.38247
1	0.0166667	1	65.2	0.015337	7.97546	1	64.8	0.015432	7.407407
1.5	0.025	1	43.5	0.022989	8.045977	1	42.1	0.023753	4.988124
2	0.0333333	1	33.1	0.030211	9.365559	1	32.1	0.031153	6.542056
2.5	0.0416667	1	25.4	0.03937	5.511811	1	24.6	0.04065	2.439024
3	0.05	1	20.6	0.048544	2.912621	1	22.1	0.045249	9.502262
3.5	0.0583333	1	18.8	0.053191	8.81459	1	18.4	0.054348	6.832298
4	0.0666667	1	15.8	0.063291	5.063291	1	15.6	0.064103	3.846154

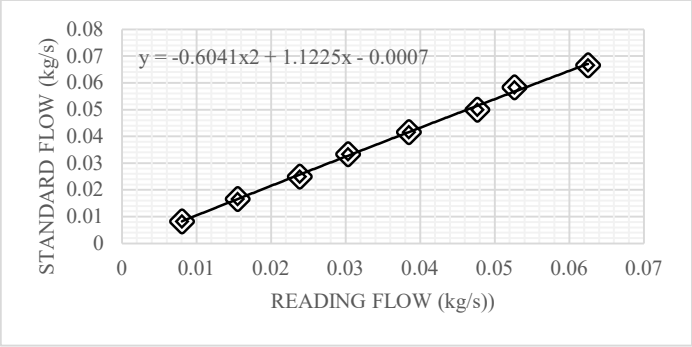

Figure (D.15) Flowmeter 1 calibration (hot water flow rate).

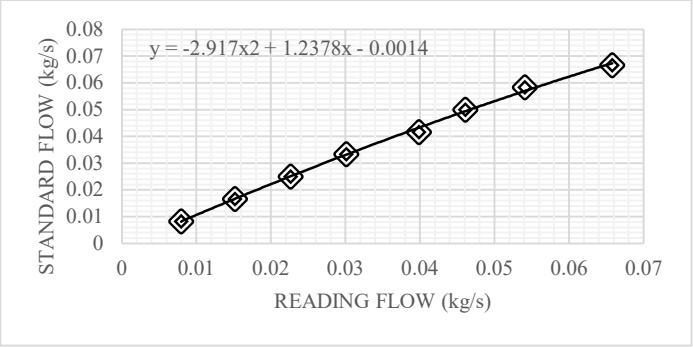

Figure (D.16) Flowmeter 2 calibration (cooled water flow rate).

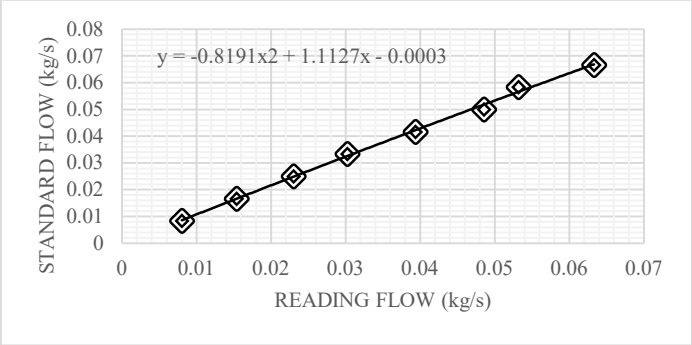

Figure (D.17) Flowmeter 3 calibration (chilled water flow rate).

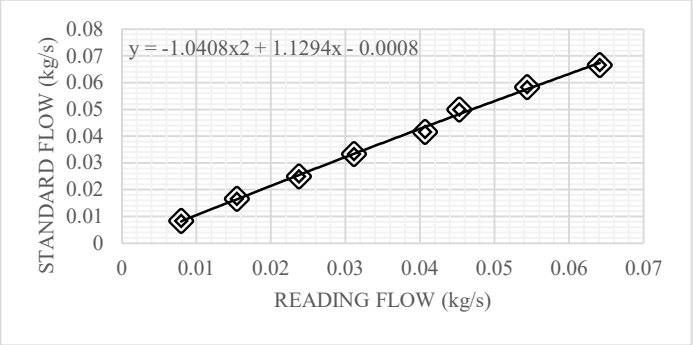

Figure (D.18) Flowmeter 4 calibration (condensing water flow rate).

Appendix E: Arduino coding

```
void setup() {
pinMode(7, OUTPUT);
pinMode(6, OUTPUT);
pinMode(5, OUTPUT);
pinMode(4, OUTPUT);
pinMode(3, OUTPUT);
pinMode(2, OUTPUT);}
int rest=60000;
void loop() {
 digitalWrite(7, LOW);
 digitalWrite(6, LOW);
 digitalWrite(5, LOW);
 digitalWrite(4, HIGH);
 digitalWrite(3, LOW);
 digitalWrite(2, LOW);
delay(250000);                        // wait for a second
 digitalWrite(7, HIGH);
 digitalWrite(6, LOW);
 digitalWrite(5, LOW);
 digitalWrite(4, HIGH);
 digitalWrite(3, HIGH);
 digitalWrite(2, HIGH);
delay(750000-rest);                        // wait for a second
 digitalWrite(7, LOW);
 digitalWrite(6, LOW);
 digitalWrite(5, LOW);
 digitalWrite(4, LOW);
 digitalWrite(3, LOW);
 digitalWrite(2, LOW);
delay(rest);
 digitalWrite(7, LOW);
 digitalWrite(6, LOW);
 digitalWrite(5, HIGH);
 digitalWrite(4, LOW);
 digitalWrite(3, LOW);
 digitalWrite(2, LOW);
delay(250000);
 digitalWrite(7, LOW);
 digitalWrite(6, HIGH);
 digitalWrite(5, HIGH);
 digitalWrite(4, LOW);
 digitalWrite(3, HIGH);
 digitalWrite(2, HIGH);
delay(750000);}
```

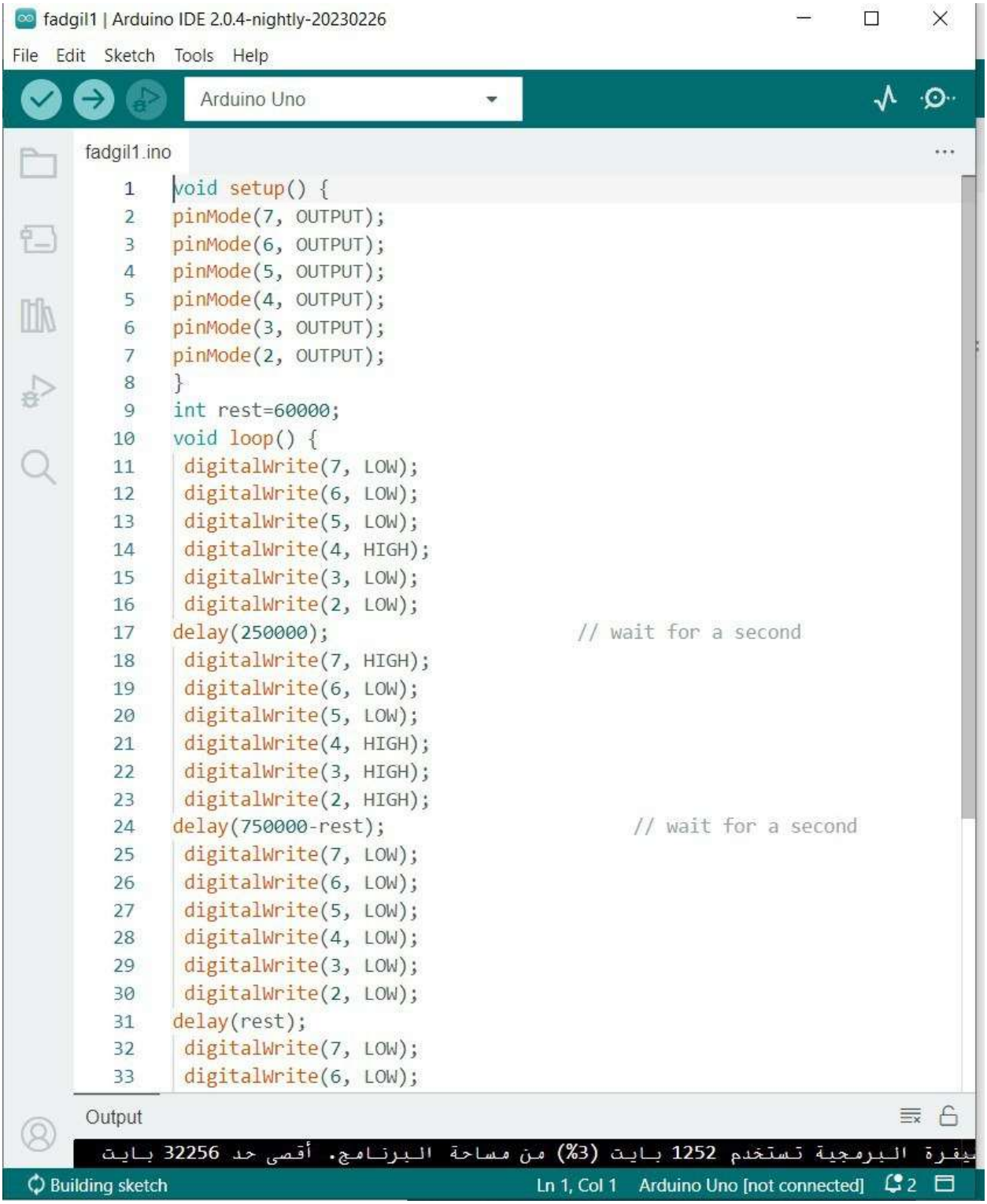
fadgil1 | Arduino IDE 2.0.4-nightly-20230226
File Edit Sketch Tools Help
Arduino Uno
fadgil1.ino
1 void setup() {
2 pinMode(7, OUTPUT);
3 pinMode(6, OUTPUT);
4 pinMode(5, OUTPUT);
5 pinMode(4, OUTPUT);
6 pinMode(3, OUTPUT);
7 pinMode(2, OUTPUT);
8 }
9 int rest=60000;
10 void loop() {
11 digitalWrite(7, LOW);
12 digitalWrite(6, LOW);
13 digitalWrite(5, LOW);
14 digitalWrite(4, HIGH);
15 digitalWrite(3, LOW);
16 digitalWrite(2, LOW);
17 delay(250000); // wait for a second
18 digitalWrite(7, HIGH);
19 digitalWrite(6, LOW);
20 digitalWrite(5, LOW);
21 digitalWrite(4, HIGH);
22 digitalWrite(3, HIGH);
23 digitalWrite(2, HIGH);
24 delay(750000-rest); // wait for a second
25 digitalWrite(7, LOW);
26 digitalWrite(6, LOW);
27 digitalWrite(5, LOW);
28 digitalWrite(4, LOW);
29 digitalWrite(3, LOW);
30 digitalWrite(2, LOW);
31 delay(rest);
32 digitalWrite(7, LOW);
33 digitalWrite(6, LOW);
Output
Building sketch
Ln 1, Col 1 Arduino Uno [not connected]

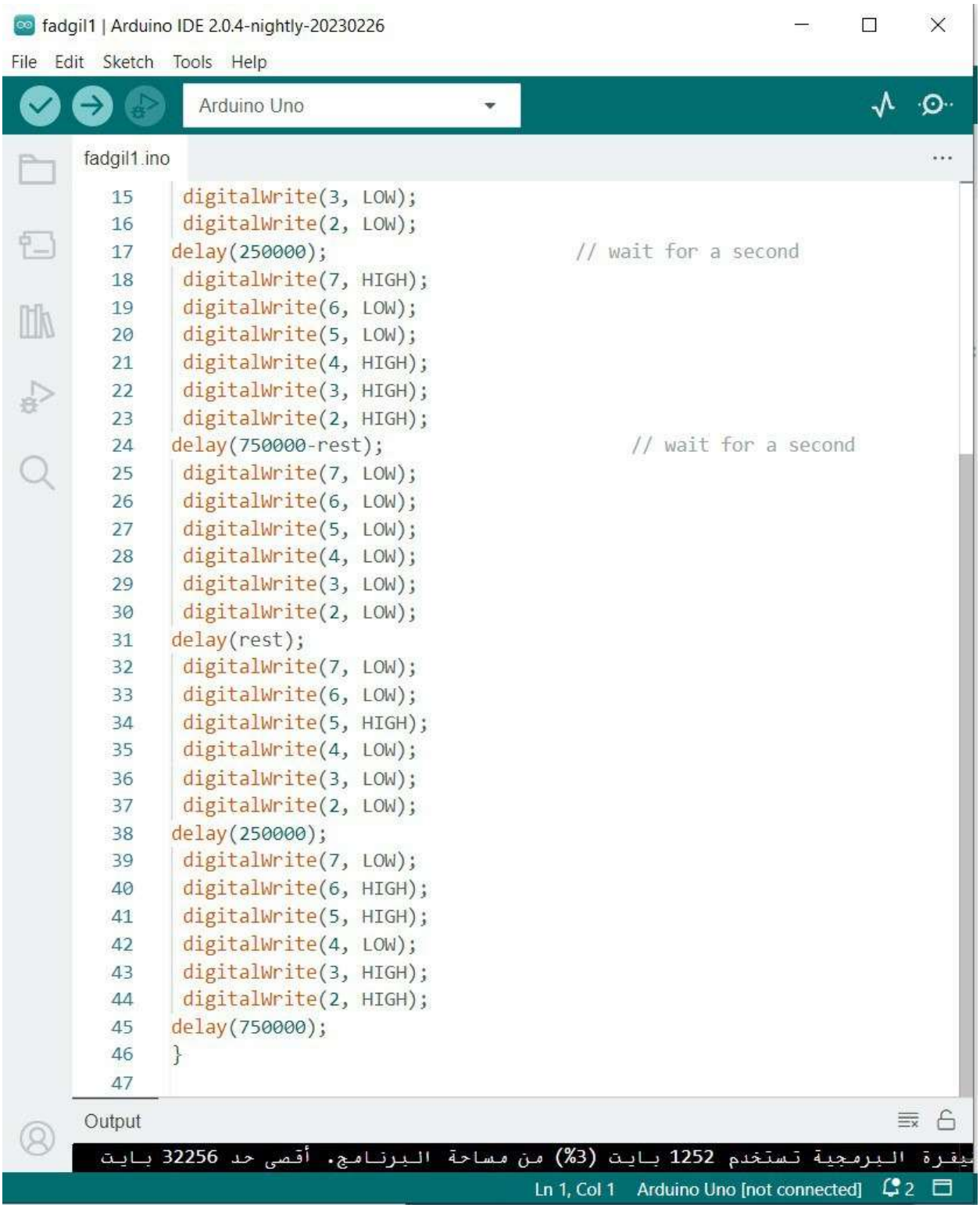
fadgil1 | Arduino IDE 2.0.4-nightly-20230226
File Edit Sketch Tools Help
Arduino Uno
fadgil1.ino
15 digitalWrite(3, LOW);
16 digitalWrite(2, LOW);
17 delay(250000); // wait for a second
18 digitalWrite(7, HIGH);
19 digitalWrite(6, LOW);
20 digitalWrite(5, LOW);
21 digitalWrite(4, HIGH);
22 digitalWrite(3, HIGH);
23 digitalWrite(2, HIGH);
24 delay(750000-rest); // wait for a second
25 digitalWrite(7, LOW);
26 digitalWrite(6, LOW);
27 digitalWrite(5, LOW);
28 digitalWrite(4, LOW);
29 digitalWrite(3, LOW);
30 digitalWrite(2, LOW);
31 delay(rest);
32 digitalWrite(7, LOW);
33 digitalWrite(6, LOW);
34 digitalWrite(5, HIGH);
35 digitalWrite(4, LOW);
36 digitalWrite(3, LOW);
37 digitalWrite(2, LOW);
38 delay(250000);
39 digitalWrite(7, LOW);
40 digitalWrite(6, HIGH);
41 digitalWrite(5, HIGH);
42 digitalWrite(4, LOW);
43 digitalWrite(3, HIGH);
44 digitalWrite(2, HIGH);
45 delay(750000);
46 }
47
Output
Ln 1, Col 1 Arduino Uno [not connected] 2

Publication List

No.	Paper title	Journal
1	Numerical analysis of two-bed adsorption thermophysical battery	Applied Thermal Engineering 236 (2024) 121847
2	Experimental investigation of two-bed adsorption thermophysical battery with mass recovery technology	Energy Conversion and Management 309 (2024) 118460
3	Intermittent and Continuous Adsorption Refrigeration Systems Techniques: A Review	The Fourth International Conference on Sustainable Engineering Techniques, AIP

Applied Thermal Engineering 236 (2024) 121847

Contents lists available at ScienceDirect

Applied Thermal Engineering

journal homepage: www.elsevier.com/locate/apthermeng

Research Paper

Numerical analysis of two-bed adsorption thermophysical battery

Fadhil Abdulrazaq Kareem [a,b,*], Abdul Hadi N. Khalifa [a], Ahmed J. Hamad [a]

[a] Middle Technical University, Technical Engineering College, Baghdad, Iraq
[b] Middle Technical University, Institute of Technology, Baghdad, Iraq

ARTICLE INFO

Keywords:
Adsorption
Thermophysical battery
Silica gel
Adsorption bed unit
MATLAB simulink
Uptake and offtake

ABSTRACT

Air conditioning systems powered by waste energy sources, such as solar-driven adsorption air conditioning systems, hold significant importance. The present study delves into the performance assessment of a silica gel-based adsorption thermophysical battery (ATB) under varying operational conditions. Advanced cycles featuring a two-bed configuration have been devised to enable semi-continuous operation and refrigeration. This novel design presents a compact ATB that integrates the evaporator and condenser within a single heat exchanger, referred to as the Evaporator-Condenser Unit (ECU), thereby reducing the overall size and cost of the ATB system. The operating and design characteristics of the two-bed adsorption system were thoroughly explored using a theoretical model developed through MATLAB software. Evaluations were conducted on various performance metrics of the ATB, encompassing the coefficient of performance (COP), cooling capacity, specific cooling power, adsorption isotherm, and kinetics. A theoretical approach was formulated using the lumped parameter (LPM) and modified Freundlich adsorption equations. It can be deduced that the inlet temperature of the hot coolant exhibited a direct proportion with both refrigeration effect (RE) and specific cooling power (SCP) while inversely affecting the coefficient of performance (COP). A decrease in coolant temperature from 313 to 303 K resulted in a noteworthy 13.4 %. Furthermore, it was observed that COP exhibited a direct proportionality with the flow rate of chilled and cooled water while inversely relating to the flow rate of hot water.

1. Introduction

In many developing countries with limited access to electricity, there is a growing interest in cooling and heating demand. According to the International Institution of Refrigeration (IIR), refrigeration and air conditioning applications consume roughly 15 % of total electrical power usage [1]. Refrigeration and air conditioning systems are divided into two categories based on their energy source: mechanical and thermal. Mechanical energy is used in the automatic system, while the thermally driven system operates with thermal energy sources. Using fuels to generate power to drive up the automated system would contribute to further environmental problems. Therefore, the current circumstance calls for developing a thermally driven cooling and heating system using waste heat or renewable energy sources. Examples of thermally driven cooling and heating systems are absorption and adsorption systems [2]. The solar adsorption system with a cooling capacity of 528 kW was deployed in an Indian government building. As well as in 2018, Fahrenheit (a German company) successfully installed several innovative adsorption units in numerous countries, such as Germany, Austria, Netherlands, Spain, and Saudi Arabia [3]. The adsorption system is significant for various applications, including thermal batteries, dehumidification, and water delivery. The adsorption systems have advantages: Low power requirements, low-temperature heat sources, simplicity of use, minimal noise and vibration, no crystallization, an environmentally friendly operating refrigerant, and an extended service life [4]. The process of the adsorption systems depended on the waste heat from any source to produce cooling and heating without harmful environmental impact. Furthermore, the adsorption systems employ natural working fluids and adsorbent materials with low global warming and no ozone depletion potential. The evaluation of the adsorption cooling and heating system depends directly on the amount of water vapor uptake of the adsorbent material, which is affected by the relative pressure and the temperature of the adsorption beds.

On the other hand, the adsorption system has problems such as high requirements for the vacuum in the condenser, lower coefficient of performance (COP) and specific cooling power (SCP), and intermittent operation. Over the last few years, there has been a rise in interest in investigating adsorption cooling systems. As a result, alternative procedures involving thermal recovery, mass recovery, single-stage, multi-

* Corresponding author.
E-mail addresses: fadhiljua91@yahoo.com (F.A. Kareem), ahaddi58@gmail.com (A.H.N. Khalifa), ahmed.elhamad@yahoo.com (A.J. Hamad).

https://doi.org/10.1016/j.applthermaleng.2023.121847
Received 7 August 2023; Received in revised form 25 September 2023; Accepted 23 October 2023
Available online 26 October 2023

Energy Conversion and Management 309 (2024) 118460

Contents lists available at ScienceDirect

Energy Conversion and Management

journal homepage: www.elsevier.com/locate/enconman

Research Paper

Experimental investigation of two-bed adsorption thermophysical battery with mass recovery technology

Fadhil Abdulrazaq Kareem [a,b], Ahmed J. Hamad [a], Abdul Hadi N. Khalifa [a]

[a] Middle Technical University, Technical Engineering College – Baghdad, Iraq
[b] Middle Technical University, Institute of Technology - Baghdad, Iraq

ARTICLE INFO

Keywords:
Two beds
Mass recovery
Adsorption thermophysical battery
Experimental study
Continuous cycle
Adsorption refrigeration

ABSTRACT

This paper developed a novel semi-continuous two-bed Adsorption Thermophysical Battery (ATB), utilizing silica gel RD/water as the adsorption pair. The Absorber Bed Unit (ABU) was designed and manufactured using finned tubes, while the condenser and evaporator are incorporated under a single Evaporator-Condenser Unit (ECU). The study investigated the impact of mass recovery, hot and cooled water temperature, and the chilled, cooled, and hot water flow rate on the system performance. The results of the study revealed that the ATB with mass recovery demonstrated a higher Coefficient of Performance (COP) and Refrigeration Capacity (RC) in comparison to the system without mass recovery. The average COP for the cycles with and without mass recovery were 0.228 and 0.2, respectively. The present study determined that the most favorable duration for mass recovery was 60 s. A substantial reduction in the COP can be observed as the hot and cooled water temperature increases. Also, the COP of the ATB was found to be directly related to the flow rates of chilled and cooled water but not to the flow rates of hot water. In addition, the COP of the two-bed ATB with mass recovery was improved by 14 % compared with the single-bed ATB. Finally, the adsorption uptake rose by 24 % when the cooled temperature was decreased from 313 K to 303 K.

1. Introduction

There is a growing interest in waste heat-powered air refrigeration systems in many developing nations with low electrical accessibility. The adsorption system's primary benefit is utilizing a thermal energy source, particularly waste heat. Adsorption systems employ low-temperature sources, typically 60–120 °C, to produce a cooling effect. This approach effectively harnesses the waste heat energy derived from solar, hot exhaust gas, and geothermal energy while eliminating potential environmental hazards [1]. Recently, there has been a growing interest in investigating adsorption system techniques. Consequently, research is currently being carried out to explore other approaches involving thermal recovery, mass recovery, single-stage and multi-bed designs, and various adsorbent materials. This investigation aims to enhance the COP and Specific Cooling Power (SCP) of the ATB [2,3].

The adsorption system is known by several names, including refrigeration, cooling, chiller, and solar cooling adsorption, all of which differ in operating principle from the ATB. The ATB uses the mechanisms of thermal energy storage by discharging at desorption/condensation and charging at adsorption/evaporation. The ATB outperforms the adsorption system in the unit's overall size, adsorber bed number, heat source, evaporator and condenser number size, cost, and adsorbent mass. However, the ATB cycle is considered intermittent due to the lack of cooling during the heating and desorption. Several factors can make ATB more economically viable compared to other refrigeration systems. These factors include enhancing system performance, minimizing the cost of adsorption components, designing standard adsorption systems for both structure and process and improving overall system efficiency [4].

A semi-continuous refrigeration cycle using adsorption technology requires a minimum of two adsorbent beds. This ensures that at least one bed is always in the cooling and adsorption stage, thus maintaining a semi-continuous refrigeration process. The two-bed operating system is typically employed when the ideal desorption and adsorption times are the same. Both the adsorption and desorption processes can take a reasonable amount of time as a half-cycle duration. Implementing a multi-bed system becomes a viable solution when there is a significant difference between the optimal adsorption time and desorption time. Utilizing the three-bed system is a viable option when the ideal duration for adsorption is twice as long as the ideal duration for desorption. In

E-mail addresses: fadhiljua91@yahoo.com (F.A. Kareem), ahmed.elhamad@yahoo.com (A.J. Hamad), ahaddi58@gmail.com (A.H.N. Khalifa).

https://doi.org/10.1016/j.enconman.2024.118460
Received 24 February 2024; Received in revised form 26 March 2024; Accepted 18 April 2024

Intermittent and Continuous Adsorption Refrigeration Systems Techniques: A Review

Fadhil Abdulrazzaq Kareem[1,2, a)], Abdul Hadi N. Khalifa[1, b)], and Ahmed J. Hamad[1,c)]

[1] *Middle Technical University, Technical Engineering College – Baghdad, Power Mechanics Engineering Department, Baghdad, Iraq*
[2] *Middle Technical University, Institute of Technology-Baghdad, Baghdad, Iraq*

[a)] Corresponding author: fadhiljua91@yahoo.com
[b)] ahaddi58@yahoo.com
[c)] ahmed.elhamad@mtu.edu.iq

Abstract. In recent decades, adsorption refrigeration systems (ARS) are becoming increasingly popular as one type of environmentally friendly refrigeration system that uses low-grade thermal energy. However, because of its low specific cooling power (SCP) and performance coefficient (COP) compared with the traditional refrigeration systems, it has not been widely commercialized. The present research reviews several methods for improving the SCP and COP of ARS. Several topics related to the performance improvement of the adsorption refrigeration system have been covered such as two-bed ARS, heat recovery, mass recovery, heat and mass recovery, and cascade ARS. This literature review can help the researchers to understand the performance improvement methods for the multi-bed ARS leading to; high COP, lower cost, and shorter charging and discharging cycles times for ARS. Based on the literature review, it can be concluded that raising the temperature of the regeneration and evaporation leads to raising the COP of ARS, whereas raising the condensation temperature lowers the COP. The COP of ARS was about 0.28, 0.26, and 0.25 for MCM-41, silica gel-RD, and silica gel-blue, respectively. The mass recovery cycle enhances the SCP and COP over the traditional cascade cycle. The COP decreases with the increase in the time of the mass recovery. Finally, the heat recovery cycle is suitable for air-conditioning applications.

INTRODUCTION

Global energy consumption is rising quickly, as is the need for cooling, refrigeration, and comfort air conditioning. It has been discovered that cooling requirements are closely associated with people's living standards. According to estimates from the International Institute of Refrigeration in Paris, different refrigeration and air-conditioning operations utilize around 15% of the world's total power production, and households and commercial buildings use about 45% of their total energy for air-conditioning systems. These issues may be solved by heat-driven refrigeration cycles. use of solar energy and low-grade waste heat, such as industrial waste heat and engine exhaust, etc. In 1848, Faraday's laboratory created adsorption-based refrigeration. Between 1940 and 1945, a calcium chloride/ammonia ARS driven by steam at 100°C was used for food storage on a train from London to Liverpool, UK.[1]. The operation of ARS is similar to that of a typical vapor compression system, except that in this case, thermal compressors that operate with heat input are used in place of the traditional compressors. So obviating the requirement for electrical energy to carry out the mechanical procedure. The behavior of an adsorption cooling system is determined by the adsorption/desorption parameters of the specific adsorbent/refrigerant pair [2]. As shown in Fig. 1, the major components of ARS are adsorption heat exchanger, condenser, expansion device, and evaporator.

The basic adsorption cycle comprises four thermodynamic processes as shown in Fig. 2:

i- Heating and pressurization
ii- Heating, desorption, and condensation

الخلاصة
بطارية الامتزاز الحرارية (ATB) تمثل بديل مستدام لانظمة التبريد الانظغاطية التي تعمل على الطاقة الكهربائية , في مجال تقنية التبريد والتجميد. الهدف الرئيسي من هذه الدراسة هو تقييم أداء النموذج الرياضي لمنظومة (ATB) المتكونة من وعائين للامتزاز تحت ظروف تشغيل مختلفة. تمت دراسة منظومة (ATB) نظريا وعدديا وعمليا.
في الجزء النظري، تم حل معادلات Lumped Parameter Predicting Model (LPM), modified Freundlich adsorption, and kinetic equilibrium equations لتقييم أداء منظومة (ATB) التي تعمل على ازواج الامتزاز Metal-Organic Frameworks adsorbent (MOF-801) مع الماء والسليكا جل نوع RD مع الماء. حيث تم استخدام برنامج MATLAB-19 وبرنامج حل المعادلات الهندسية (EES) لحل المعادلات المذكورة سابقا لدراسة اداء المنظومة.
في الجزء العملي، تم تصنيع ودراسة منظومة (ATB) متكونة من وعائين للامتزاز (ABU) لغرض الحصول على تبريد شبه مستمر, وكذلك استخدام تقنية استرداد الكتلة لغرض تحسين معامل اداء المنظومة (COP) وتحسين طاقة التبريد النوعية (SCP). تم تصنيع وعائين للامتزاز (ABU) بقطر 24 سم وارتفاع 30 سم , حيث يمكن كل منهما العمل اما امتزاز او انتزاز. بالإضافة إلى ذلك، تم دمج المبخر والمكثف في مبادل حراري واحد يسمى وحدة المبخر-المكثف (ECU)، حيث تم تصنيع مبادلين (ECU) بأبعاد 22 سم في الطول و 14 سم في العرض و 12 سم في الارتفاع. أدت عملية الدمج وتصنيع مبادل واحد (ECU) الى تقليل الحجم الكلي للمنظومة وكذلك تقليل كلفة التصنيع. تم دراسة أداء منظومة (ATB) التي تعمل على ازواج الامتزاز Mobil Composition of Matter (MCM-41) مع الماء والسليكا جل نوع RD مع الماء.
اما في الجزء العددي، تم التعامل مع حل نموذج التوازن الحراري ثلاثي الأبعاد باستخدام برنامج COMSOL-6 لتحليل توزيع الحرارة والكتلة داخل وعاء الامتزاز.
توصلت النتائج النظرية إلى أن (COP) لمنظومة (ATB) عند استخدام (MOF 801) يتفوق على السيليكا جل بنسبة 20 % عند ضبط وقت الدورة على 1000 ثانية. كذلك، تم تحسين (COP) و (SCP) لبطارية الامتزاز الحرارية بنسبة 25 % و 39 % على التوالي لمادة (MOF 801) مقارنةً بالسيلكا جل عند استخدام كتلة المادة الممتزة 10 كجم. تم ملاحظة انخفاض في قيمة (COP) للمنظومة بنسبة 31.6 % عند زيادة درجة حرارة الماء الساخن من 343 إلى 363 كلفن, وايضا تم ملاحظة زيادة في قيمة (COP) للمنظومة بنسبة 5 % عند انخفاض درجة حرارة الماء البارد من 313 إلى 303 كلفن عند استخدام (MOF 801). وكذلك تم استنتاج ان قيمة (COP) تتناسب طرديا مع معدل تدفق الماء البارد وعسيا مع معدل تدفق الماء الساخن.
أضهرت النتائج العملية تحسن في مقدار(COP) و (RC) لبطارية الامتزاز الحرارية ذات الوعائين بمقدار 14 % و 8 % عند استخدام تقنية استرداد الكتلة مقارنةً بالنظام بدونها وكان افضل مدة لتطبيق تقنية استرادا الكتلة هي 60 ثانية. وكذلك بينت النتائج تفوق لزوج الامتزاز (MCM-41) مع الماء بنسبة 11.1 % لـ (RC) و 10.5 % لـ (COP) مقارنةً بزوج الامتزاز سيليكا جل RD في نفس ظروف التشغيل.
أخيرًا، أظهرت النتائج العددية أن درجة حرارة وعاء الامتزاز زادت تدريجيًا أثناء عملية discharging وانخفضت تدريجيًا أثناء عملية charging مع مرور الوقت. وكذلك اوضحت النتائج ان توزيع درجة الحرارة و uptake للمادة الممتزة عندما يكون سمك الطبقة 2 ملم افضل من سمك 4 او 6 ملم .

جمهورية العراق

وزارة التعليم العالي والبحث العلمي

الجامعة التقنية الوسطى

الكلية التقنية الهندسية– بغداد

تحسين أداء نظام البطارية الحرارية المدمجة لتطبيقات التجميد

رسالة مقدمة
إلى مجلس الكلية التقنية الهندسية- بغداد وهي جزء من
متطلبات نيل شهادة دكتوراه فلسفة في اختصاص
هندسة الحراريات

من قبل الطالب
فاضل عبدالرزاق كريم
بكالوريوس هندسة 2012
ماجستير هندسة الحراريات 2015

أشراف

د. عبدالهادي نعمة خليفة
أستاذ

د. احمد جاسم حمد
أستاذ

نيسان 2024 شوال 1445